SPATIOTEMPORAL DELIVERY OF COMPLEMENTARY PROTEINS FOR REPAIR OF THE INFARCTED MYOCARDIUM

by

Hassan Kassem Awada

Bachelor of Science in Engineering, The University of Michigan, 2010

Submitted to the Graduate Faculty of

Swanson School of Engineering in partial fulfillment

of the requirements for the degree of

Ph.D. Bioengineering

University of Pittsburgh

2016

UNIVERSITY OF PITTSBURGH

SWANSON SCHOOL OF ENGINEERING

This dissertation was presented

by

Hassan Kassem Awada

It was defended on

March 22, 2016

and approved by

Sanjeev G. Shroff, Ph.D., Professor and Chair, Department of Bioengineering

Donna B. Stolz, Ph.D., Associate Professor, Department of Cell Biology

Kang Kim, Ph.D., Associate Professor, Department of Medicine

Shilpa Sant, Ph.D., Assistant Professor, Department of Pharmaceutical Sciences

Dissertation Director: Yadong Wang, Ph.D., Professor, Department of Bioengineering

SPATIOTEMPORAL DELIVERY OF COMPLEMENTARY PROTEINS FOR REPAIR OF THE INFARCTED MYOCARDIUM

Hassan Kassem Awada, Ph.D.

University of Pittsburgh, 2016

Ischemic heart disease is a leading cause of morbidity and mortality worldwide. After the onset of myocardial infarction, multiple pathologies develop and progress the disease towards heart failure. Pathologies such as ischemia, inflammation, cardiomyocyte death, ventricular remodeling and dilation, and interstitial fibrosis, develop and involve the signaling of many proteins. Therapeutic proteins can play important roles in limiting or countering pathological changes after infarction. However, they typically have low retention rate and short half-lives in vivo in their free form and can benefit from the advantages offered by controlled release systems to overcome their challenges. Protein-based therapies can be more effective when concerns such as spatiotemporal presentation, bioactivity, and retention are addressed. We tested the efficacy of controlled delivery of different combinations of cardiac-implicated proteins such as VEGF, HGF, PDGF, FGF-2, IL-10, TIMP-3, and SDF-1α. The controlled delivery of an optimal combination of proteins per their physiologic spatiotemporal cues to the infarcted myocardium holds great potential to repair and regenerate the damaged heart muscle. To address this issue, we developed a spatiotemporal delivery vehicle comprised of fibrin gel and heparin-based coacervates. Proteins that should be released relatively quickly are embedded in the fibrin gel, while proteins that should be released over a longer period are embedded in the coacervate and distributed in the same gel. This dissertation describes the process of developing the fibrin gel-coacervate composite for spatiotemporal delivery of therapeutic proteins and

demonstrates its potential in triggering a significant cardiac repair process. It explores the ability of the coacervate to co-release different proteins, the development of the fibrin gel-coacervate system to achieve sequential delivery of different proteins, and the optimization of protein combinations and doses, paving the way for a potential comprehensive strategy to treat myocardial infarction.

TABLE OF CONTENTS

LIST OF TABLES

LIST OF FIGURES

PREFACE

I would like to express my sincere gratitude and thanks to my advisor, Dr. Yadong Wang, for guiding me throughout my Ph.D. journey, and for enabling a great environment and lab culture to conduct graduate biomedical research. I also would like to thank my thesis committee: Dr. Sanjeev Shroff, Dr. Donna Stolz, Dr. Kang Kim, and Dr. Shilpa Sant for their valuable and insightful feedback and suggestions for my thesis. In addition, I would like to thank and acknowledge Dr. Kevin Hitchens and Lesley Foley for their contribution in performing cardiac MRI, Dr. Noah Johnson for his peer mentorship, Zhouguang Wang for his contribution in performing western blot experiments and analysis, Mintai Hwang for his contribution in creating schematics, and Lou Johnson for his contribution in design of experiments statistical analysis.

Lastly, my deepest gratitude and love goes to my wife, Zahraa Koussan, for inspiring, supporting, and encouraging me all along the way, and keeping my morale high every single day. I also thank my dear family and my family-in-law for their continuous support. Additionally, I send a heartfelt and sincere tribute to my late father, Kassem Awada, who would have been very proud and happy to see me reach this point in education and life. To my father, my wife, my family, my first coming child and daughter Layla, and all my loved ones, I dedicate this Ph.D. dissertation.

1.0 INTRODUCTION

Note: Most of the introductory chapter was published as a review article in Biomaterials Journal. H.K. Awada, Y. Wang. 2016. "Towards Comprehensive Cardiac Repair and Regeneration after Myocardial Infarction: Aspects to Consider and Proteins to Deliver". Biomaterials 82: 94-112.

Cardiovascular diseases (CVD) can be very costly and burdensome to society economically, socially, and psychologically. CVD account for 32% of deaths in the United States (US). Myocardial infarction (MI), commonly known as heart attack, is a major CVD that is responsible for significant morbidity and mortality, causing an estimated 7.3 million deaths per year worldwide [1]. According to the American Heart Association, 720,000 Americans experience new and recurrent heart attacks each year. Approximately, 15% of those experiencing an MI in a given year die because of it. In 2010, the direct and indirect cost of heart disease was approximately $205 billion in the US [2].

Heart transplantation is the most effective treatment for chronic heart failure (CHF) patients. However, this option is very limited due to the lack of heart donors, highly invasive and complex surgical procedures, and significant cost. Reperfusion methods of the blocked coronary artery through percutaneous coronary intervention (PCI), coronary bypass surgery, and anti-thrombotic therapy are considered the standard of care for MI patients. In addition, angiotensin-converting enzyme (ACE) inhibitors and β-blockers are commonly used in the clinic to prevent adverse cardiac remodeling. Although these treatment methods lead to

significant reductions in restenosis and improve lifestyles and long-term survival, the incidence of MI and heart-related mortality have not significantly changed [3, 4]. The conventional medical treatments have reached their practical limits and are not able to regenerate the damaged cardiac tissue and restore heart function. Also, not all patients are eligible for these kinds of interventions. Therefore, the development of alternative MI treatment therapies is paramount.

MI occurs as a result of an occlusion in one of the two main coronary arteries branching into the heart walls. The occlusion is usually due to coronary atherosclerosis and thrombosis that lead to heart muscle damage and likely progression to heart failure (**Figure 1**). As a result of the ischemia, many changes occur at the molecular, cellular, and tissue levels of the myocardium. Hypoxia, death of cardiomyocytes, inflammation, ventricular dilation and adverse remodeling, tissue necrosis, interstitial fibrosis, and contractile dysfunction are some of the main features that may present themselves during progression from MI to CHF [5, 6]. The next subsections will present overviews on these different pathological aspects of MI and the therapeutic interventions that have been explored to counter them in the last 15 years. We focus on proteins as potential therapies to repair and regenerate damaged cardiac tissue. We also focus on the complexity of tissue regeneration and repair processes providing reasoning for more comprehensive therapies. Finally, we discuss the importance of using controlled release systems to overcome the limitations of protein therapy.

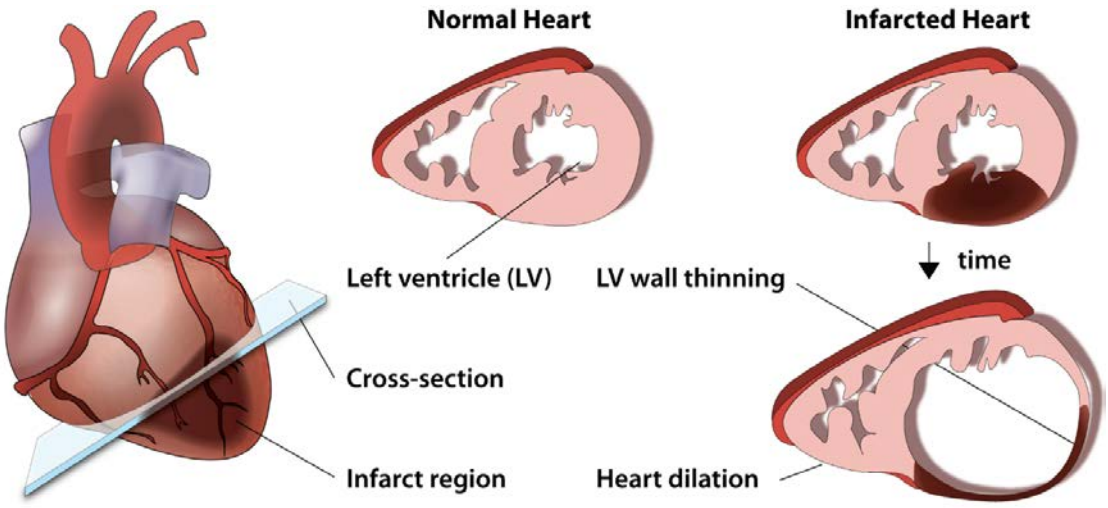

Figure 1. Myocardial Infarction (MI) causes severe damage and adverse remodeling in the left ventricle (LV) myocardium, leading over time to LV wall thinning and dilation and ultimately progressing to contractile dysfunction and heart failure.

1.1 PATHOLOGICAL ASPECTS OF MI AND CORRESPONDING THERAPEUTIC INTERVENTIONS

Over the last 15 years, many experimental studies provided evidence of the adult heart's limited potential to regenerate and repair, motivating tests of new therapies [7-10]. Many of these attempted to overcome the limitations imposed by the endogenous biological system in order to achieve healing rather than scarring of the heart after MI. The full elucidation of the mechanisms of MI pathologies can help design more effective therapies. Therapeutic strategies, therefore, should take into account the different aspects of MI pathologies, and find solutions for the most critical or the complete set of impairments using more comprehensive well-designed approaches. In this subsection, we describe various pathological changes after MI and proteins that may reverse or counter these changes (**Table 1**).

Table 1. Therapeutic proteins of interest with cardiac functions. Certain proteins should be either promoted or antagonized after MI to induce proper cardiac repair and regeneration.

Protein	Acronym	Main cardiac functions	References
Insulin-like growth factor-I	IGF-I	Anti-apoptotic; promote stem cell growth and differentiation	[27], [79], [122], [129]
Hypoxia-inducible factor-1α	HIF-1α	Trigger release of angiogenic GFs and nitric oxide	[12], [16-18]
Transforming growth factor-β	TGF-β	Upregulate fibroblast proliferation, migration, and differentiation; trigger myofibroblast activation	[164], [166], [168], [203]
Sonic hedgehog	Shh	Induce cardiac morphogenesis; anti-apoptotic	[20], [86]
Fibroblast growth factor-1	FGF-1	Initiation of angiogenesis; stimulate cardiomyocyte proliferation	[18], [20], [108], [225]
Fibroblast growth factor-2	FGF-2	Initiation of angiogenesis; upregulate proliferation, migration, and survival of endothelial cells; induce chemotaxis; anti-apoptotic	[16-18], [20], [22], [88]
Vascular endothelial growth factor-A	VEGF-A	Initiation of angiogenesis; upregulate proliferation, migration, and survival of endothelial cells ; trigger nitric oxide release	[16-20]
Platelet-derived growth factor-BB	PDGF-BB	Upregulate proliferation and chemotaxis of pericytes; promote neovessel maturation; anti-apoptotic	[17], [27], [38], [249]
Angiopoietin-1	Ang-1	Promote stabilization of endothelial cell-pericyte interactions and vessel maturation	[37], [40]
Angiopoietin-2	Ang-2	Promote destabilization of endothelial cell-pericyte interactions and vessel extravasation	[37], [40]
Hepatocyte growth factor	HGF	Angiogenic, anti-apoptotic; chemotactic on stem cells	[29], [30], [122], [215]
Granulocyte colony-stimulating factor	G-CSF	Chemotactic for stem cells; anti-apoptotic; angiogenic	[28], [80], [121]
Stromal cell-derived factor-1α	SDF-1α	Chemotactic for stem cells; angiogenic	[31], [32], [85], [117], [216]
Erythropoietin	EPO	Chemotactic for stem cells; angiogenic; anti-apoptotic	[81-84], [124], [213]
Thymosin-β4	Thymosin-β4	Chemotactic for stem cells; angiogenic	[27], [123]
Neuregulin-1	NRG-1	Induce cardiomyocyte proliferation; anti-apoptotic	[104-107]
Matrix metalloproteinase-2	MMP-2	Promote ECM degradation by catalyzing the proteolysis of ECM proteins	[60], [131], [141]
Matrix metalloproteinase-9	MMP-9	Promote ECM degradation by catalyzing the proteolysis of ECM proteins	[60], [131], [141]
Tissue inhibitor of metalloproteinases-1	TIMP-1	Inhibit MMP activity and ECM degradation; anti-apoptotic	[88], [148], [150]
Tissue inhibitor of metalloproteinases-3	TIMP-3	Inhibit MMP activity and ECM degradation; anti-apoptotic; anti-inflammatory	[88], [140], [147], [149], [150], [177]
Interleukin-10	IL-10	Anti-inflammatory; anti-apoptotic	[66], [67]
Interleukin-1β	IL-1β	Pro-inflammatory; induce MMP activity	[55], [139], [164]
Interleukin-6	IL-6	Pro-inflammatory; upregulate fibroblast proliferation; induce MMP activity	[55], [164]
Tumor necrosis factor-α	TNF-α	Pro-inflammatory; pro-apoptotic; trigger myofibroblast activation; induce MMP activity	[55], [62], [63], [139]
Monocyte chemoattractant protein-1	MCP-1	Pro-inflammatory; angiogenic; chemoattractant	[26], [61], [128]
Relaxin	Relaxin	Vasodilatory; anti-fibrotic; angiogenic; anti-inflammatory	[53]

1.1.1 Heart ischemia

1.1.1.1 *Ischemic damage and importance of proper vasculature*

The heart vasculature ensures the metabolic and structural homeostases of the heart. Proper perfusion provided by blood vessels is crucial for the growth and survival of cardiomyocytes [11]. For instance, improved activation of hypoxia response pathways by stabilizing hypoxia inducible factor (HIF)1-α in endothelial cells (ECs) leads to increased cardiomyocyte survival, improved LV systolic function, and reduced scar size [12]. The deficiency of laminin-α4, an abundant extracellular matrix (ECM) protein in the basement membrane of myocardial blood vessels, leads to myocyte hypoxia and necrosis, and ultimately heart failure [13]. Moreover, the interaction between ECs and cardiomyocytes offers increased protection for the myocytes through nitric oxide (NO)-dependent mechanisms and regulate myocyte contractility after an ischemic insult [14, 15]. Inadequate perfusion of the heart muscle can contribute to an irreversible myocardial hibernation and decrease of contractile function [11]. Hence, therapeutic angiogenesis that aims to form new blood vessels from pre-existing ones might contribute to the repair of the infarcted myocardium [16].

1.1.1.2 *Angiogenesis mechanisms and proangiogenic therapies*

The hypoxic conditions activate angiogenic growth factors (GFs) that cause pericytes to detach from bloods vessels, allowing the loosening of cell-cell junctions and the migration, proliferation, and differentiation of ECs. Differentiated endothelial tip and stalk cells elongate the sprouting neovessels and form vessel lumens. As two neovessels fuse, blood perfusion can be initiated. Maturation and stabilization follow through the recruitment of pericytes to wrap around the growing neovessels [17]. Angiogenesis is a complex, tightly regulated process that

requires the cooperation of different cells, GFs, ECM, and signaling molecules (**Figure 2**). Spatial and temporal cues are important to ensure an adequate angiogenic outcome.

Vascular endothelial GF (VEGF) and basic fibroblast GF (FGF-2) are key initiators of angiogenesis. VEGF is an endothelial-specific factor that stimulates the proliferation, migration, and survival of ECs. It is upregulated in response to hypoxia by HIF1-α signaling more than any other angiogenic factor [17, 18]. Additionally, VEGF induces the production of NO, a critical vasodilator, and promotes vascular permeability [19]. VEGF-mediated angiogenesis demonstrated therapeutic benefit in many ischemic heart disease animal models [20, 21]. FGF-2 induces proliferation and migration of ECs and smooth muscle cells (SMCs), induces ECs to physically organize into tube-like structures, and triggers angiogenesis [16, 18, 20]. Additionally, FGF-2 promotes survival of ECs, SMCs, and cardiomyocytes [22]. FGF-2 upregulates the expression of VEGF and vice versa [23, 24]. Moreover, FGF-2 increases the expression of other proangiogenic molecules such as hepatocyte GF (HGF), monocyte chemoattractant protein-1 (MCP-1), and platelet-derived GF receptor (PDGFR) on vascular SMCs [25, 26]. Administration of FGF-2 at the infarcted myocardium improves revascularization and cardiac contractility and reduces infarct size [3, 20, 27]. Other proteins that also improve angiogenesis include FGF-1, HGF, granulocyte colony-stimulating factor (G-CSF), sonic hedgehog (Shh), erythropoietin (EPO), and stromal cell-derived factor 1-alpha (SDF-1α) (**Table 1**) [18, 20, 27, 28]. For example, HGF induces proliferation and migration of ECs, acts in synergy with VEGF, and improves heart function after MI through angiogenesis [29, 30]. SDF-1α might contribute to angiogenesis not by direct actions on ECs, but by recruiting endothelial progenitor cells (EPCs) and inducing other angiogenic factors such as VEGF [31, 32]. Some single GF applications, namely VEGF and FGF-2, reached clinical trials,

but showed only modest to little benefit in inducing proper revascularization and treating MI patients [20, 33, 34]. Possible reasons behind the limited therapeutic benefit seen in patients include rapid diffusion, large doses, and short half-lives of bolus injections of GFs and the minor attention paid to the spatiotemporal and physiologic presence of different GFs during angiogenesis.

1.1.1.3 *Importance of temporal cues in therapeutic angiogenesis*

The involvement of many signals, GFs, ECM components, and different cell types in the process of angiogenesis suggests that relying on a single factor might not be enough (**Figure 2**). It has been shown that VEGF or FGF-2 alone can lead to the formation of aberrant and leaky vessels that might regress quickly [35, 36]. Angiopoietin (Ang)-2 destabilizes blood vessels by weakening the interactions between ECs and pericytes [37]. Platelet-derived GF (PDGF) and Ang-1 are involved in stabilizing neovessels. PDGF triggers the recruitment of SMCs that cover the newly formed vessels, thus improving their functionality and reducing the possibility of regression and leakiness [38]. VEGF was shown to be a negative regulator of PDGF that inhibits its signaling and recruitment of pericytes. VEGF activates its receptor VEGFR-2, which complexes with PDGFR-β to block its signal transduction [39]. In contrast to Ang-2, Ang-1 strengthens the interactions between ECs and pericytes [37]. Approaches that sequentially delivered early angiogenic factors such as FGF-2, VEGF, and Ang-2 followed by late factors such as PDGF and Ang-1 demonstrate a more robust angiogenesis process and mature neovasculature than single factors [40-43]. Therefore, therapies that aim to form mature vasculature in ischemic tissues should take into account the proper time to administer GFs and limit any potential antagonism between different GFs (**Figure 2**).

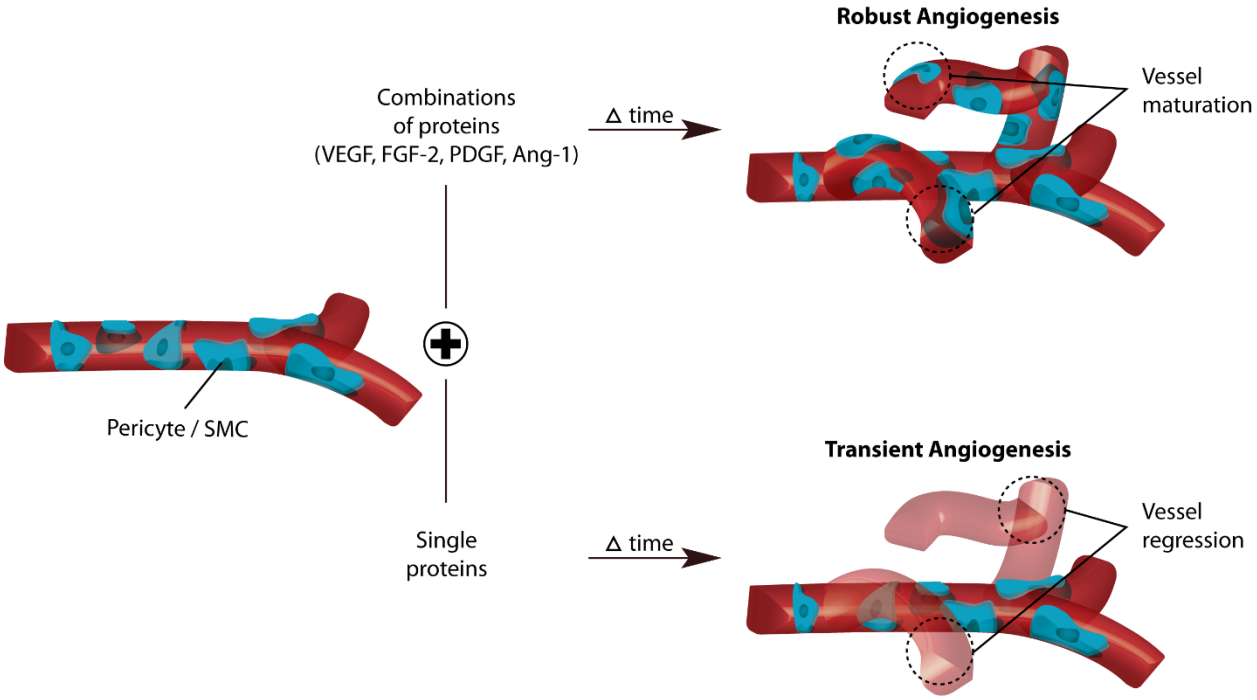

Figure 2. Fate of angiogenesis induced by combination or single protein therapies. A combination therapy that employs proteins involved in triggering angiogenesis (i.e. VEGF, FGF-2) in combination with proteins involved in stabilizing new blood vessels by pericytes (i.e. PDGF, ANG1), is more likely to induce a robust angiogenesis process forming mature and stable vasculature. Single protein therapies might lead to a transient angiogenesis process with new blood vessels prone to regression due to lack of stability and maturity provided by pericytes.

1.1.1.4 *Role of vasodilation*

Nitric Oxide (NO) is a potent vasodilator that helps regulate blood vessel tone and cardiac function [44]. It has been shown that reduced endothelial NO after MI contributes to pathophysiology and heart failure [45]. It is involved in the tissue response to ischemia and improves angiogenesis through HIF1-α and VEGF-mediated mechanisms [16]. Loss of function models targeting nitric oxide synthase (NOS) enzymes can lead to pathological consequences for vascular function [46, 47]. Mice lacking NOS show reduced LV function and increased adverse remodeling after MI [48, 49]. It has been reported that specific NOS1 overexpression in

cardiomyocytes reduces infarct size and oxidative stress and improves cardiac function after infarction [50]. NOS3 can help recruit EPCs, induce neovascularization, and limit LV remodeling and dysfunction after infarction [44, 51]. Improving the bioavailability of endothelial NO after MI using statin treatment leads to increased angiogenesis and EPC mobilization and reduces fibrosis and cardiac dysfunction [52].

Relaxin is another molecule with potent vasodilation properties and can affect cardiac remodeling [53]. It has also been shown to have anti-inflammatory, anti-fibrotic, and angiogenic effects, all considered beneficial to treat MI patients. Relaxin exerts its effects on the cardiovascular system by binding to relaxin family peptide receptor 1 (RXFP1) and triggering intracellular signaling pathways that induce cyclic adenosine monophosphate (cAMP) production, NO signaling, tyrosine kinases, and others. Clinical trials of relaxin suggest it has important cardioprotective roles and can relieve symptoms of acute heart failure [53].

1.1.2 Inflammatory response

1.1.2.1 *Effects of inflammation after MI*

Inflammatory cells such as neutrophils and monocytes rush into the ischemic heart in the early stages after MI triggering a strong inflammatory response. The therapeutic targeting of the inflammatory response after MI has been met with controversy mainly because the presence of inflammatory cells acts as a double-edged sword. Inflammatory cells can promote beneficial effects such as inducing angiogenesis by monocytes secreting proangiogenic factors and phagocytosis of dead cells and their cellular debris. However, they can also have detrimental effects on cell survival and cause tissue damage, infarct expansion, and LV dilation [54, 55]. Neutrophils produce large amount of reactive oxygen species (ROS) and elastase which cause

cell apoptosis and elastin degradation [55, 56]. In addition, they can reduce the proangiogenic effects of progenitor cells and bolster ischemic conditions [57, 58]. A limited presence of neutrophils is necessary to initiate the inflammatory response. Macrophages are also strong regulators of post-infarction events such as angiogenesis and scar formation. Macrophage activation can lead to two major distinct phenotypes: M1 and M2. M1 macrophages promote further inflammation and ECM degradation, while M2 macrophages contribute to anti-inflammation, angiogenesis, and ECM reconstruction [59]. Therefore, specific reduction in the levels of specific inflammatory mediators might show a therapeutic benefit after MI.

1.1.2.2 *Implicated proteins and anti-inflammatory therapy*

Pro-inflammatory cytokines such as interleukin (IL)-1β, tumor necrosis factor (TNF)-α, IL-6, and IL-1 levels are elevated in the infarct zone and activate matrix metalloproteinases (MMPs), which degrade the ECM (**Table 1**) [55]. For example, leukocyte-derived MMP-9 deletion protects the ischemic heart from LV dilation and cardiac rupture, but also disrupts angiogenesis [60]. LV dilation and inflammatory response are significantly attenuated in IL-1 and MCP-1 knockout mouse models, but not infarct size [61]. TNF-α upregulates in heart failure, promotes invasion of inflammatory cells to the ischemic myocardium, induces MMP production, triggers cell apoptosis, and exacerbates adverse LV remodeling [62, 63]. Transforming GF (TGF)-β can deactivate macrophages, downregulate pro-inflammatory cytokines, and promote ECM preservation [61]. Tissue inhibitor of MMPS (TIMP)-3 inhibits TNF-α-converting enzyme (TACE), the enzyme activator of TNF-α [64]. Other studies suggest a cytoprotective role of TNF-α in preventing myocyte apoptosis after MI [65]. Ultimately, clinical trials using TNF inhibitors were unsuccessful [33]. This might suggest pleiotropic actions of some cytokines such as TNF-α or that the failed outcome might be as a result of toxic effects due to high doses

used. IL-10 is an anti-inflammatory cytokine that inhibits the production of pro-inflammatory cytokines. IL-10 can induce TIMP-1 production by mononuclear cells which may help in reducing ECM degradation by MMPs [54]. Treating the infarcted heart with IL-10 can improve ejection fraction and angiogenesis, and reduce infarct size, fibrosis, and cardiomyocyte death [66, 67]. In contrast, a knockout study reported that IL-10 does not have a critical role in LV remodeling [68]. Decreasing the neutrophil invasion after ischemia through the inhibition of CCAAT/enhancer binding protein (C/EBP) pathway results in less fibrosis and improves cardiac function [69].

It seems logical that quenching the inflammatory response completely will not yield the desired functional benefits for the injured heart, because clearing dead cells from the infarct area helps reduce tissue necrosis and damage. It appears imperative that a tightly regulated inflammatory response, both temporally and spatially, should be available for a limited time after MI. Therefore, the goal of anti-inflammation therapy should not be a complete suppression of the post-infarction inflammatory response, but rather to properly modulate it in order to reduce the potentially dangerous consequences of uncontrolled activity. Because the MI inflammatory response activates both detrimental and protective signaling pathways, it is crucial for therapeutic strategies to respond to the pathophysiologic complexity of the infarct environment and optimize dose and spatiotemporal profiles of applied agents in order to achieve a successful outcome.

1.1.3 Myocardial cell death and strategies to improve myocardium viability

A human LV contains up to 4 billion cardiomyocytes. In a few hours, an MI can kill 25% of them [70]. The intense inflammatory reaction, ischemic conditions, adverse remodeling, LV

dilation, and infarct expansion put millions of surviving cardiomyocytes at risk of death through apoptosis or necrosis (**Figure 3**). The immediate generation of ROS after ischemia, mainly by inflammatory cells, induces apoptosis among myocytes [71]. This massive death of myocytes sets into motion a cascade of events that lead to the replacement of damaged tissue with a scar. Scar tissue reduces the ability of the LV to contract and pump blood efficiently, thus markedly reducing overall cardiac function.

1.1.3.1 *Cell apoptosis mechanisms and anti-apoptotic therapy*

Apoptosis is characterized by cell shrinkage, fragmentation of intracellular structures, and phagocytosis into neighbor cells [72]. The balance between pro-apoptotic proteins such as Bax, Bak and Bid, and anti-apoptotic proteins such as Bcl-2 and Bcl-x_L is essential to determine a cell's survival or death after an apoptotic signal (**Figure 3**). In the post-MI environment, elevated expression levels of Fas receptor, an apoptosis mediator, were reported [73]. In addition, increased activation of caspases, the key executioner proteins of cell apoptosis, and increased ratio of Bax to Bcl-2 have been linked to cardiomyocyte apoptosis [74, 75]. The activation of the PI3K/Akt and Ras-Raf-MEK-ERK pathways inhibits apoptosis and imparts cardioprotective effects (**Figure 3**) [76-78].

Insulin-like GF (IGF)-I and HGF can activate the PI3K/Akt pathway, enhance cell survival, and reduce cardiomyocyte apoptosis resulting in improved heart function [79]. G-CSF is another chemokine that prevents apoptosis of myocytes and inhibits the decrease in levels of Bcl-2 and Bcl-x_L forced under oxidative stress conditions [80]. EPO has demonstrated anti-apoptotic activities in many studies [81-83]. In a rat MI model, EPO upregulated Bcl-2 and downregulated Bax, which led to improvements in the heart hemodynamic function [84]. FGF-2, Shh, SDF-1α, Thymosin-β4, PDGF-BB, IL-33, and TIMP-1 can also reduce cardiomyocyte

apoptosis and improve overall cardiac function after MI (**Table 1**) [27, 85-88]. Targeting of specific miRNAs has also been recently investigated to prevent cardiomyocyte death [89, 90]. Additionally, β-blockers demonstrate anti-apoptotic actions that ameliorate ischemic effects [91].

Cardiomyocyte apoptosis is detected during all phases after MI and not only in the infarct zone, but also extends to the viable myocardium in remote noninfarcted region [75, 92]. This suggests that apoptosis could be responsible for a significant amount of myocyte death from the onset of MI injury and throughout the progression to heart failure. It is therefore crucial to design anti-apoptotic therapeutic interventions that counter cell death following MI.

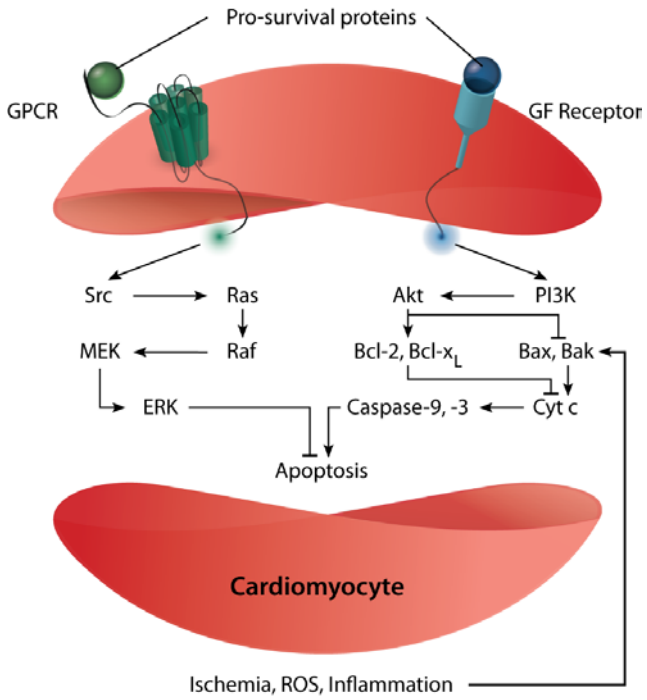

Figure 3. Ischemia, reactive oxygen species (ROS), and inflammation can trigger pro-apoptotic protein signaling (Bax, Bak) and inhibit anti-apoptotic protein signaling (Bcl-2, Bcl-xL) within cardiomyocytes leading to release of cytochrome c and activation of caspases causing apoptosis. Pro-survival proteins that bind to their respective receptors on the myocyte surface can trigger PI3K/Akt and Ras-Raf-MEK-ERK pathways anti-apoptotic molecular pathways to prevent cell death.

1.1.3.2 *Cardiomyocyte proliferation*

The view that adult mammalian cardiomyocytes lose their regenerative capacity shortly after birth has been long-held. The rarity of primary myocardial tumors, the limited recovery after myocardial injury, and the difficulty to stimulate proliferation in mature adult cardiomyocytes, all support the view of the heart as an organ with effectively no regenerative capacity [93]. However, recent findings contested the notion that cardiomyogenesis in adult hearts doesn't occur and proved that new cardiomyocytes can arise to replace old or dead ones even though the turnover rate is very low [9, 10, 94, 95]. The controversy about the origin of new cardiomyocytes persists. Do these new myocytes result from the division of pre-exiting ones or are they a result of differentiation of resident or recruited progenitor cells? It seems there is evidence for both origins and mechanisms, but possibly with different extents of contribution. In this subsection, we focus on factors that promote proliferation of existing cardiomyocytes; and in the next subsection we focus on cardiomyogenic differentiation of progenitor cells.

There have been several attempts to induce cell cycle reentry for cardiomyocytes by removing inhibitors such as p27 or triggering activators such as cyclinD1 and E2F2 [96, 97]. Activating the Hippo signaling pathway increases cardiomyocyte proliferation postnatally in mice [98, 99]. Moreover, regulation of the expression of certain miRNAs can affect cardiomyocyte proliferation and heart function [100, 101]. Periostin, an ECM protein, was shown to stimulate a cardiomyocyte subpopulation to reenter the cell cycle and proliferate. Periostin treatment improved cardiac function and angiogenesis, and reduced fibrosis and infarct size after MI in rodents [102]. However, another study reported no increase in cardiomyocyte proliferation after periostin treatment [103]. Another protein, neuregulin (NRG)-1, has recently shown ability to stimulate survival, differentiation, and proliferation of

cardiomyocytes through ErbB2 and ErbB4 [104]. In a cardiomyopathy model, NRG-1 administration improved cardiac function and survival; and when combined with ACE inhibitor therapy, the effects were additive [105]. Another study demonstrated that NRG-1 therapy reduces infarct size and improves cardiac function due to proliferation of a small subpopulation of existing adult mouse cardiomyocytes rather than an increased differentiation of resident or recruited progenitor cells or decreased cardiomyocyte apoptosis [106]. Ongoing human clinical trials suggest promising results of NRG-1 therapy on increasing ejection fraction of heart patients [107]. FGF-1 administration, in conjunction with p38 inhibition, can induce cardiomyocyte proliferation, improve angiogenesis and cardiac function, and reduce scarring and wall thinning [108].

The formation of new cardiomyocytes happens at a low rate even with the highest estimates, and therefore remains inadequate for the full replacement of lost myocardial tissue after infarction. It is thus important for therapies that aim to repair infarcted myocardiums to be designed with a broader focus than just aiming to boost the cardiomyocyte turnover with either mechanism. In addition, protein therapies that focus on cardiomyocyte proliferation need to consider the duration of the signal required to trigger significant cardiomyocyte mitosis. They also need to be localized and selective for myocytes, so as to prevent any potential tumor formation in remote tissues.

1.1.3.3 *Stem/progenitor cell homing and differentiation*

The envisioned goal of having stem/progenitor cells in the injury site after MI, whether transplanted or recruited by chemokines, is to differentiate into functional cardiomyocytes to replace the lost ones and improve cardiac performance. Genetic fate mapping provides evidence that some endogenous progenitor cells undergo myogenic differentiation after MI and give rise

to new cardiomyocytes [94, 109-111]. Cardiosphere-derived cells (CDCs) have been suggested to express a cardiomyocyte phenotype and electrically couple to surrounding cardiomyocytes [112]. Other studies provided evidence suggesting that most progenitor cells being investigated in cell therapies do not differentiate into cardiomyocytes, but rather might improve heart function via paracrine signaling that activates repair and regeneration pathways [94, 113-115]. Regardless of the mechanisms that progenitor cells undertake in the infarcted region, it seems there is a consensus that they result in benefits at the tissue and functional levels, which explains why many cell therapies have reached the clinical trials stage [7, 8, 116].

Many molecules play important roles in the repair of the myocardium by recruiting stem/progenitor cells to the injury site. Mobilizing endogenous progenitors might compensate for the low retention and survival of exogenous transplanted cells. SDF-1α is a powerful chemokine that can mobilize EPCs, hematopoietic stem cells (HSC), mesenchymal stem cells (MSCs), and cardiac stem cells (CSCs) to the infarct zone [85]. Recruitment of one or more kinds of progenitor cells to the heart by SDF-1α promotes beneficial effects after MI, possibly through enhancing angiogenesis and myocyte survival and differentiation [85, 117-119]. G-CSF induces proliferation and mobilization of stem cells to the infarcted myocardium [27, 28]. It exerts beneficial effects on heart function after MI [120, 121]. Clinical trials using G-CSF have not been as promising possibly due to patient ages or timing of administration, but research on G-CSF therapy continues [28]. In addition, HGF has been reported to be chemotactic on CSCs and to improve cardiac function after MI when applied alongside IGF-I [122]. Establishing an IGF-I gradient at the infarct border zone enhances the recruitment of endogenous CSCs and improvement in myocardial regeneration [122]. Moreover, Thymosin-β4 can induce the mobilization of adult epicardial progenitor cells and coronary vasculogenesis and angiogenesis

[123]. EPO has also been suggested to mobilize endothelial progenitors [124], with positive effects on cardiac function in heart disease patients [125, 126]. More recently, prostaglandin E2, an endogenous fatty acid derivative, was reported to recruit CSCs and potentially regulate their differentiation to cardiomyocytes after infarction [127]. Other mobilizers of stem cells to the ischemic myocardium include MCP-1, MCP-3, stem cell factor (SCF), VEGF, and nerve GF (NGF) (**Table 1**) [128]. As for differentiation, IGF-I is suggested to induce the differentiation of CSCs into myocytes and contribute to the recovery of heart function and structure after infarction [129]. FGF-2 has also been suggested to differentiate resident CSCs into functional cardiomyocytes in vitro [130].

The ideal route for recruited endogenous or transplanted adult progenitor cells in the infarcted myocardium is to differentiate into cells of cardiac lineages, including cardiomyocytes, vascular endothelial, and mural cells, and become properly integrated into the tissue to replace the lost dead cells. However, although these progenitors' ability to differentiate is still controversial, their variable but widely-accepted therapeutic benefit after MI, likely through paracrine activities, is a testimony to their importance in advancing cardiac repair after infarction. The identity of the most efficient progenitor cells needed after MI and a suitable strategy to improve their presence in the infarct zone are still matters of debate and extensive investigation.

1.1.4 ECM degradation and ventricular remodeling

1.1.4.1 *ECM structure and imbalance after MI*

MI results in an adverse remodeling process in the cardiac muscle manifesting clinically by LV dilation and heart pump dysfunction ultimately progressing to heart failure [5, 6]. The

remodeling process brings about major alterations in the structure of the ECM. Serving as the base that provides structural stability, contractile force transmission, and correct cardiomyocyte geometry, the ECM composition and orientation are strictly regulated in a healthy myocardium mainly by MMPs and their endogenous inhibitors, the TIMPs (**Figure 4**) [131]. The imbalance in the MMP/TIMP ratio contributes to the abnormal remodeling of the ECM post MI.

The appropriate presence of important structural proteins in the ECM, collagen and elastin, allows the optimal transmission of contractile force (**Figure 4**). Approximately 85% of the myocardial collagen is type I and 11% is type III. Type I collagen fibrils have very high tensile strength and provide resistance to deformation, while type III collagen fibrils are more distensible and provide resilience. The extent of collagen fibril maturation through crosslinking helps determine ventricular compliance. On the other hand, elastic fibers allow passive recoil in the myocardium after stretching [131, 132].

After an ischemic insult, the profile of collagen changes at different phases of cardiac remodeling and the region within the myocardium. For instance, during the initial phase, collagen is degraded in the infarct region; however in later stages, abnormal collagen synthesis, orientation, and crosslinking in the infarct region and then in remote noninfarct areas lead to fibrosis and further pathological remodeling [132]. Collagen has a long half-life and a slow turnover compared to other proteins [133]; thereby ECM replacement after degradation will also be slow, which places the myocardium at increased vulnerability for adverse remodeling after MI.

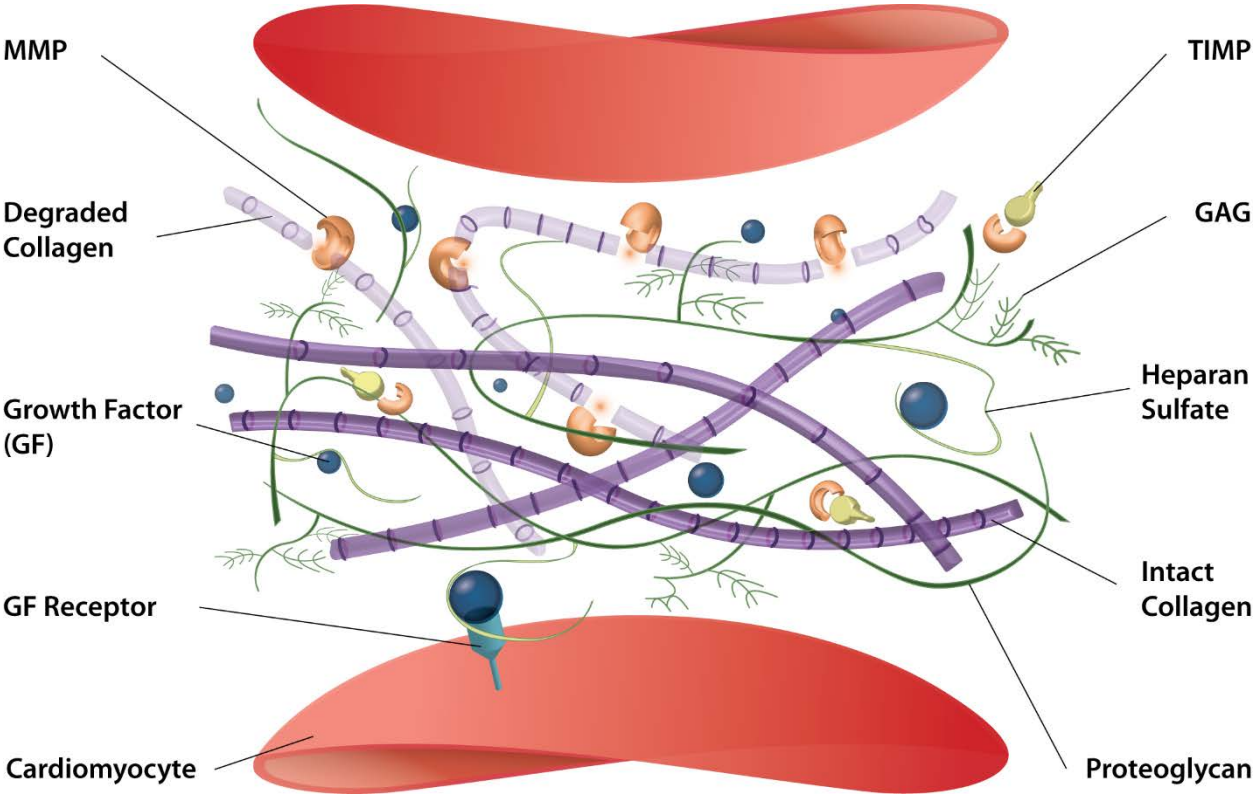

Figure 4. The myocardial extracellular matrix (ECM) serves as the base that connects cardiomyocytes, provides structural stability, and enables the transmission of chemical signals and contractile forces. The ECM contains structural proteins such as collagen and elastin, proteoglycans such as heparan sulfate, and adhesive glycoproteins such as fibronection and laminin. The ECM composition and orientation are strictly regulated in a healthy myocardium mainly by matrix metalloproteinases (MMPs) and their endogenous inhibitors, the tissue inhibitors of metalloproteinases (TIMPs). TIMPs can help reduce early ECM degradation after MI alongside GFs involved in promoting cell survival, cardiomyogenesis, and angiogenesis.

1.1.4.2 *Implicated proteins in adverse remodeling*

Many MMPs have been implicated in cardiovascular diseases. During cardiac remodeling, MMPs are released by different cells including cardiac fibroblasts, cardiomyocytes, vascular cells, and inflammatory cells [134, 135]. MMPs are usually activated by serine proteases and other MMPs through the cleavage of a propeptide in the amino terminus [136]. The functions of

MMPs after infarction are complex and could involve both positive and negative effects, because multiple molecular pathways are involved and can regulate distinct and overlapping processes including angiogenesis, wound healing, ECM homeostasis, proliferation, and apoptosis [137, 138]. MMP activity can be regulated by transcriptional and post-translational factors such as TNF-α, IL-1β, TGF-β, other MMPs, oxidative stress, and mechanical stretch [139]. Additionally, MMP activity can be regulated by TIMPs which prevent MMP access to its substrates by binding to the MMP's catalytic domain; however affinities differ (**Figure 4**) [136, 140].

After MI, a significant increase in MMP activity leads to an imbalance in the MMP/TIMP ratio favoring the degradation of the myocardial ECM over deposition. MMP-2 and MMP-9 have been implicated in early ECM degradation [141] and in advancing contractile dysfunction by degrading cardiac proteins such as myosin heavy chain, myosin light chain-1, troponin I, and α-actinin [131]. MMP-7 null mice show improved survival after MI [142]. Fibrosis and LV dilation are reduced when MMP-9 was deleted [143]. Knocking out MMP-2 or MMP-9 in mice protects them from cardiac rupture post infarction [60, 144]. However, healing and angiogenesis are impaired in the long term indicating different effects temporally and spatially [60].

1.1.4.3 *Therapeutic interventions to alter ECM remodeling*

The inhibition of NF-κB by IκB leads to a reduction in MMP-2 and MMP-9 expression, thereby reducing LV dilation after MI [145]. TIMP-4 null mice show increased LV dysfunction, fibrosis, hypertrophy, and MMP activity [146]. Deficiencies of TIMP-1 or TIMP-3 in mice can lead to increased LV remodeling, dilation, and dysfunction after MI [147-150]. Cell-based TIMP-3 gene delivery improves cardiac function [151]. TIMP-1 or TIMP-3-based therapies are

able to improve ejection fraction and reduce MMP-2 activity and apoptosis in the ischemic myocardium of rats [88]. Greater functional improvement and preservation of elastic fibers are observed in TIMP-3-treated group, possibly because TIMP-3 is ECM-bound, giving it a greater advantage in protecting the myocardial ECM [152]. ACE inhibitors, β-blockers, and statins have also been suggested as anti-remodeling agents that reduce MMP activity and ECM degradation after MI [153-155].

MMP/TIMP-based therapies need to be applied soon after MI because excessive ECM degradation can accelerate adverse remodeling and result in wall thinning and cardiac rupture. On the other hand, some therapies might also need to focus on preventing excessive ECM deposition which could promote fibrosis that spreads in the later stages after MI and extends from infarct to noninfarct zones leading to LV stiffness and contractile dysfunction [156]. ECM homeostasis is urgently needed to be restored in the post-MI environment, with therapies preventing ECM degradation favored early on in infarct region, while therapies preventing excessive ECM deposition may be beneficial at the later stages in noninfarct regions. While a few-fold increase in collagen above normal levels in the myocardium can cause ventricular stiffness and moderate malfunction [157], only a slight collagen level decrease below normal can lead to detrimental effects including dilation, rupture, and adverse remodeling [60, 140, 158]. So, determining which MMPs and/or MMP functions to inhibit, the optimal timing of intervention, the optimal dose of therapeutic agents, and the myocardium regions to be treated are all essential parameters to achieve a successful cardiac repair and ECM homeostasis.

1.1.5 Fibrosis

1.1.5.1 *Role of cardiac fibroblasts and myofibroblasts*

Cardiac fibroblasts make up 50-70% of the cells within the myocardium while only occupying a quarter of the tissue volume [159]. They synthesize ECM components, regulate their turnover and maintain homeostasis through MMPs and TIMPs, and help transport mechanical and chemical signals [159]. After MI injury, many fibroblasts differentiate into their activated form, myofibroblasts, under the actions of mechanical stress and different chemical stimuli such as TGF-β [131, 160]. Myofibroblasts express α-smooth muscle actin (α-SMA) and are not normally found in healthy adult hearts. They are attracted to the infarct region and participate in the remodeling process by producing collagen and other proteins that form a matrix and replace dead cardiomyocytes [131, 159]. This increased collagen deposition ultimately leads to interstitial fibrosis and the formation of the myocardial scar in the infarct area [160]. Using connexins, myofibroblasts form gap junctions with each other and cardiomyocytes [161]. Being nonexcitable cells, the myofibroblasts, lying between cardiomyocytes and expanding the ECM, will create gaps between the myocytes which may result in impulse conductivity problems such as arrhythmias [162, 163].

1.1.5.2 *Implicated proteins and anti-fibrotic therapy*

Myofibroblasts are activated by different proteins and cytokines such as TGF-β, Angiotensin-II, and TNF-α (**Table 1**). In the cardiac tissue, TGF-β stimulates proliferation, migration, and differentiation of fibroblasts into myofibroblasts, thereby considered the top regulator of the fibrotic response after MI [164]. Antagonizing TGF-β in the early stage after MI might exacerbate ECM degradation and promote LV dilation [165], while antagonizing it in the late

stage might be more beneficial to prevent fibrosis and adverse remodeling in noninfarct regions. The administration of c-Ski, an endogenous inhibitor of TGF-β, helps inhibit fibroblast differentiation into myofibroblasts, which might limit fibrosis and adverse remodeling after MI [166]. IL-6 promotes fibroblast proliferation, but reduces collagen synthesis and induces MMP secretion. IL-1β and TNF-α inhibit fibroblast proliferation and collagen synthesis and increase MMP levels [164]. Recent studies have suggested an important role for the WNT/Frizzled (FZD) pathway in regulating myofibroblast migration and differentiation [167-169]. The administration of an FZD receptor antagonist improves cardiac function after MI [169]. Angiotensin-II induces fibroblast proliferation and differentiation, with ACE and angiotensin-II receptors being expressed actively by myofibroblasts after MI [170]. ACE inhibitors have been part of the standard of care for heart patients for a long time, as they are associated with reducing TGF-β levels and fibrosis [171, 172]. The β-adrenergic sympathetic system is an important regulator of cardiac function and because of the massive loss of cardiomyocytes after MI, the system's activity increases with β2-adrenoceptor receptors dominating cardiac fibroblasts [164]. B-blockers have been shown to inhibit fibroblast proliferation [173]. Also, relaxin reduces fibroblast differentiation and proliferation, thereby preventing cardiac fibrosis [53]. Statins such as simvastatin can suppress human myofibroblast proliferation [174]. Simvastatin was also shown to reduce fibroblast α-SMA expression and that effect is abolished with TGF-β administration [175].

The fibrotic tissue that develops in the infarct area also expands to the noninfarct regions of the left and right ventricles driven by the excess collagen deposition accompanied by distorted crosslinking of collagen fibers [176]. This results in reduced compliance and increased stiffness of the heart muscle, thus leading to CHF [160]. Some studies argue in favor of some

myofibroblast presence stressing on their roles as providers of contractile force across the ECM and wound-healing mediators [88, 177]. Therefore, it is important for anti-fibrotic therapies to be employed in late stages and prioritize the prevention of ECM deposition and fibrosis in noninfarct regions. This brings to attention the importance of optimizing doses and spatiotemporality of injected agents, because early excessive degradation of the ECM and suppression of collagen synthesis in the infarct region can contribute to LV dilation and possible rupture. The right balance is needed for proper repair and functional recovery.

1.1.5.3 *Reprogramming cardiac fibroblasts into myocytes*

Because replacing millions of lost cardiomyocytes is a difficult task and in order to counter the negative effects of interstitial fibrosis, the idea of turning a portion of endogenous cardiac fibroblasts into functional cardiomyocytes is quite intriguing. Recently, a new therapeutic approach that aims to reprogram and convert fibroblasts into cardiomyocyte-like cells emerged [9, 178]. The introduction of combinations of cardiac transcription factors to fibroblasts such as GATA4, Mef2c, Tbx5, HAND2 and/or microRNAs such as miR-1, miR-133, miR-208, miR-499 has shown potential to activate cardiac gene expression and directly convert fibroblasts from different sources into cardiomyocyte-like cells [179-182]. Additionally, blocking JAK/ STAT and WNT signaling pathways has been suggested to generate cardiomyocytes from fibroblasts [183]. However the reprogramming efficiency remains low.

In infarcted mouse hearts, gene delivery of combinations of the above-mentioned transcription factors led to the generation of myocytes from endogenous cardiac fibroblasts, which seemed to integrate and form gap junctions with pre-existing myocytes after several weeks. This therapeutic intervention in turn reduced infarct scar size and improved heart function [182, 184]. It is possible that other cell types within the heart such as progenitor cells

and ECs might undergo reprogramming to adopt myocyte-like phenotypes. Introducing VEGF alongside cardiac transcription factors was found to enhance heart function and reduce fibrosis more than the transcription factors alone, showing that revascularization mediated by VEGF can improve the survival of cardiomyocytes, new and preexisting, and add to the overall therapeutic benefit [184]. Using lentiviruses, the introduction of relevant miRNAs to infarcted mouse hearts led to the reprogramming of cardiac fibroblasts into cardiomyocytes [181].

It is important to develop the necessary tools that can increase the yield and efficacy of cell reprogramming. For instance, reprogrammed cells would be more beneficial if they were able to proliferate and couple electromechanically with the preexisting myocytes as well, in order to preserve proper contractile and conductive function. However, cell reprogramming should be performed under tight controls, so that abnormalities like cardiac arrhythmias do not develop. Also, specific targeting of cardiac fibroblasts with reprogramming factors is important so that off-target fibroblasts will not be affected. Deeper understanding of the molecular mechanisms underlying cell reprogramming would help advance the therapeutic approaches based on this new technology.

1.1.6 Electrical conduction abnormalities after MI

Proper electrical conduction is necessary for optimal cardiac output. Calcium plays an important role in the contractile function of the heart. Following an action potential, the rush of calcium into the cytosol of a cardiomyocyte via its respective channels induces adenosine triphosphate (ATP) hydrolysis, which in turn drives the interaction between actin and myosin and causes the cardiomyocytes to contract [185]. It has been reported that patients with dilated cardiomyopathy show an impaired uptake of calcium, thus compromising the heart’s contractile function [186,

187]. The ischemic environment causes oxidative stress and elevation of intracellular calcium levels that affect the survival and function of cardiomyocytes [188, 189]. Therapeutic interventions could benefit from the use of calcium channel blockers which block the cardiomyocyte L-type calcium channels to reduce excessiveness in the heart's contraction and conduction velocity [190].

1.2 PROTEINS AND PROTEIN-BASED THERAPIES: IMPORTANCE AND ADVANTAGES

1.2.1 Physiological roles of proteins and the microenvironment

Proteins including GFs, morphogens, hormones, cytokines, chemokines, antibodies, transcription factors, and enzymes are very important in cell signaling, function, and behavior (**Table 1**). Proteins transmit signals that trigger various cellular processes between cells of same and different types, their ECM, and between different tissues and organs. Identifying the target cells is important because distinct types of cells can have different responses to the same protein. Equally important is the determination of the proteins of interest in the process of tissue regeneration (**Table 1**). Proteins can initiate different processes such as proliferation, migration, differentiation, apoptosis, growth, and adhesion by binding to their specific receptors expressed by the target cells. This receptor binding can almost exclusively occur when proteins are in their soluble form having been secreted by cells or released from the ECM by enzymes and proteases.

1.2.1.1 *Role of protein concentration and gradient formation*

The effects exerted by proteins depend on their concentration in the cellular microenvironment, thereby influencing the expression of their receptors and the levels of other proteins, whose secretion and effects can be either antagonized or promoted [191]. For example, depending on the concentration of VEGF in the microenvironment, angiogenesis can be inadequate, normal, or aberrant and excessive [192]. Different cellular effects of HGF have been observed depending on its concentration, level of activation, and receptor expression [79]. A threshold concentration of TGF-β can change the molecular signal from growth to apoptosis [193]. Also, the concentrations of signaling proteins and the expression of their receptors are time-dependent and change at different stages of repair and regeneration. There are temporal differences in the presence of certain proteins and the expression of their receptors during events such as angiogenesis, inflammation, cardiac remodeling, and bone repair suggesting their physiological roles might be limited to certain stages.

The formation of a protein gradient enables the cells to detect directional and spatial cues, so as to respond to the protein signal. The diffusion rate, receptor binding, size, half-life, ECM affinity, and secretion or inhibition of a protein are all factors that determine the formation of a gradient and its steepness [194-196]. It was demonstrated that cells can modify their receptors through endocytosis and reorient itself towards the direction of a chemoattractant [197, 198]. This directed migration of cells requires a concentration gradient to effectively guide the cells towards the target site, and the threshold of the concentration gradient might differ from one chemoattractant to another depending on the signaling cascades it activates. For instance, NGF can stimulate extracellular-signal-regulated kinases (ERK) activity at 30% lower concentration threshold than epidermal GF (EGF) [199]. The direction of axonal growth can be

affected by different chemical gradients of NGF and laminin [196]. A density gradient of Arg-Gly-Asp (RGD)-containing peptides can direct the alignment of fibroblasts [200].

1.2.1.2 *Effect of biomechanics and architecture on protein behavior*

The ECM is comprised of architectural, mechanical, and molecular components responsible for the structural integrity of tissues and transfer of information and signals between cells, tissues, and organs (Fig. 5). The signaling cascades can be triggered to activate cellular processes and regulate cell behavior by the binding of ECM proteins and polysaccharides to integrins on the cell surface [131]. ECM glycosaminoglycans (GAG) such as heparan sulfate contribute to the formation of protein gradients by facilitating the interaction between GFs such as VEGF and FGF and their receptors (Fig. 5). This prolongs the duration of GF signaling by protecting them from proteolytic degradation, thus rendering their actions on processes like proliferation, migration, and differentiation more effective [201].

The mechanics of the ECM influenced by traction forces, shear stresses, fluid flows, and others can affect the behavior of cells and tissues and how they respond to protein signals [202]. Abnormal matrix synthesis or degradation can have dire consequences on the cells of a mechanically stressed tissue. Mechanical forces can induce the release of proteins and work in conjunction with them to remodel the ECM or affect cell behavior. For instance, fibroblast differentiation into myofibroblasts needs both TGF-β and mechanical stress [203]. Vascular SMCs are triggered to express various differentiation markers in response to the cyclic stretching of arterial walls [204]. Cells in a constrained collagen matrix generate different contractile forces depending on the stimulation of different GFs, while their responses are similar in a floating collagen matrix [205, 206]. In cases of laminar, pulsatile, and steady blood flow, resultant shear stresses modulate endothelial cell function, phenotype, gene and protein

expression in a different way than when the flow is disturbed [204]. The mechanics of the microenvironment help determine the fate of cells when stimulated by proteins, including apoptosis, growth, differentiation, migration, and contraction. Cell behavior is also dependent on the structural organization of the ECM. It has been shown that interactions between cells, ECM, and signaling proteins can differ between two-dimensional (2D) and three-dimensional (3D) architectures [207]. Cells in a 3D microenvironment enjoy the ability to spread, attach, cluster ligands, change integrin and receptor expression, and perform chemokinesis or chemotaxis more effectively.

Therefore, the process of tissue repair and regeneration depends in a collective fashion on a complex network of signaling proteins that are present in specified concentrations and spatiotemporal gradients in the wider context of the ECM microenvironment with its mechanics and architecture. All of these parameters and aspects are crucial when designing therapeutic strategies to treat cardiovascular diseases.

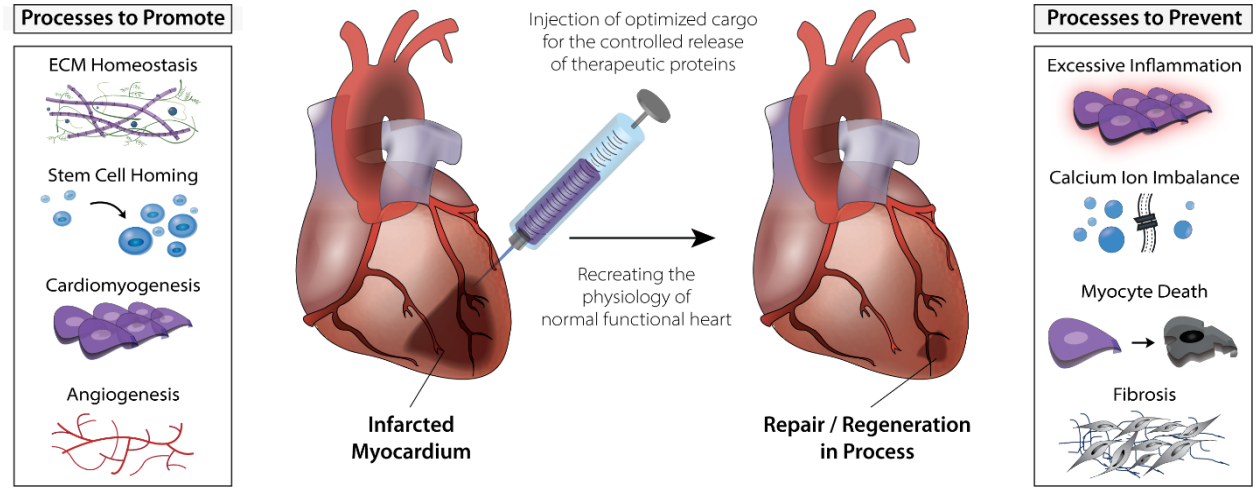

Figure 5. Repair and regeneration of the infarcted myocardium can be driven by delivery of proteins that address MI pathologies. To treat MI, a therapy needs to promote ECM homeostasis, stem cell homing, cardiomyogenesis, and angiogenesis, and prevent excessive inflammation, calcium imbalance, cardiomyocyte death, and fibrosis. Processes needed to be promoted or prevented after MI can have temporal differences. Some such as ECM homeostasis and calcium balance need to happen early on, while others such as fibrosis prevention should happen later. Injecting a protein delivery system carrying specific proteins of interest and delivering them per their physiologic cues offers the potential to trigger repair and regeneration signaling cascades leading to the restoration of a functional myocardium.

1.2.2 Advantages and challenges of protein-based therapy

Exogenous proteins can be produced at high yields in a cost-effective manner with the aid of recombinant DNA and phage display technologies. Proteins can also be stabilized for relatively long periods, thus offering off-the-shelf availability. Additionally, protein administration can be potentially regulated spatially and temporally with specific doses used. Moreover, protein therapies offer the advantage for enhanced targeted interventions with the ability to elucidate mechanisms of action and regulatory molecular pathways involved [20, 33, 208]. The exogenous administration of therapeutic proteins can be utilized to supplement inadequate

endogenous levels or replace defective proteins. They can also be used to upregulate or downregulate other molecules or to trigger certain cellular processes and activate specific molecular pathways (**Figure 5**).

Because proteins play a central role in the process of tissue repair and regeneration, strategies to exogenously administer proteins of interest that have the potential to repair and restore normal function are continuously developed and improved (**Table 1**). No protein therapy has made it to the cardiovascular market and achieved clinical use yet [33]. Therapies that were dependent on bolus administration of proteins showed some efficacy in improving the function of ischemic hearts in animal models [20, 27]. However, in clinical trials, such method of administration proved ineffective and results were generally disappointing. For instance, VEGF, FGF-2, HGF, EPO, GM-CSF, and NRG-1 therapies did not demonstrate consistently significant improvements in revascularization and myocardial function compared to placebo in Phase I and II clinical trials, despite being tolerable and reasonably safe at different doses used [8, 20, 28, 34]. This is likely due to the drawbacks of bolus injections and the use of single proteins to repair tissues that likely require the complex signals and cooperation of many proteins. Proteins, administered by bolus injections, have poor retention at the target tissue because they are diluted and diffuse away quickly. In addition, soluble proteins are highly unstable and typically have short half-lives because they are prone to proteolytic degradation and enzymatic deactivation. High doses are often needed to induce small therapeutic benefit, and such high systemic levels of proteins can be potentially toxic [208].

Thus, in order to make a breakthrough in the field of protein-based therapy for cardiac regeneration, it is logical to use multiple proteins that have different functions to address different challenges (**Table 1**). Equally important is the use of controlled delivery systems that

can present these proteins in a bioactive form spatiotemporally per their physiological cues. Such presentation allows, as close as possible, the recapitulation of the natural microenvironment of a healthy functional heart. Developing such sophisticated strategies might yield a comprehensive cardiac repair and regeneration process for MI patients (**Figure 5**).

1.3 CONTROLLED RELEASE SYSTEMS: IMPORTANCE AND POTENTIAL IN CARDIAC REPAIR

1.3.1 Development and characterization of properties

Controlled release systems provide an exciting potential to overcome the challenges posed by bolus administration of proteins for cardiac repair after MI. These systems can be designed to protect, control, sustain, and localize the delivery of proteins to the ischemic heart muscle (**Figure 6, 7**). In addition to the potential protein-mediated therapeutic benefits, some delivery systems are based on biomaterials that can also provide mechanical support and reduce adverse LV remodeling [209]. The main challenges that face the development of effective delivery systems include the optimal combination of proteins and the ability to control their concentration and spatiotemporal gradients upon delivery. Ideally, a controlled delivery vehicle would serve as a depot that provides physiological cues of crucial proteins needed for proper tissue regeneration, thus assuming the essential role of the ECM in protection, stabilization, regulation of activity, control of concentration, and spatial translocation of proteins within the myocardium (**Figure 6, 7**).

Biomaterials used in the development of controlled release systems can be natural or synthetic polymers. Natural polymers include fibrin, collagen, gelatin, alginate, chitosan, hyaluronic acid, heparin, and others [20, 210]. These natural materials are appealing because they can be easily recognized by the natural microenvironment, thereby reducing potential immunogenicity or toxicity. In addition, they can be degraded by endogenous enzymes. However, their mass production can be costly and the modification of their mechanical and chemical properties can be challenging. On the other hand, synthetic polymers include poly(lactic-co-glycolic acid) (PLGA), polyethylene glycol (PEG), polycaprolactone (PCL), poly-L-lactide (PLLA), and others [20, 210]. These synthetic materials offer the advantage of easier tailoring of material properties to fit the specialized needs of biomedical applications. Moreover, synthetic materials can be typically produced in a cost-effective fashion and in large quantities. Major challenges to the successful and effective use of synthetic materials include biocompatibility and biodegradability. They need to be non-toxic and tolerated by the immune system. The material should completely degrade and resorb into the body or excrete from the body. They may also need to mimic the behavior of natural materials in strength, compliance, stiffness, porosity, among other properties (**Figure 6**).

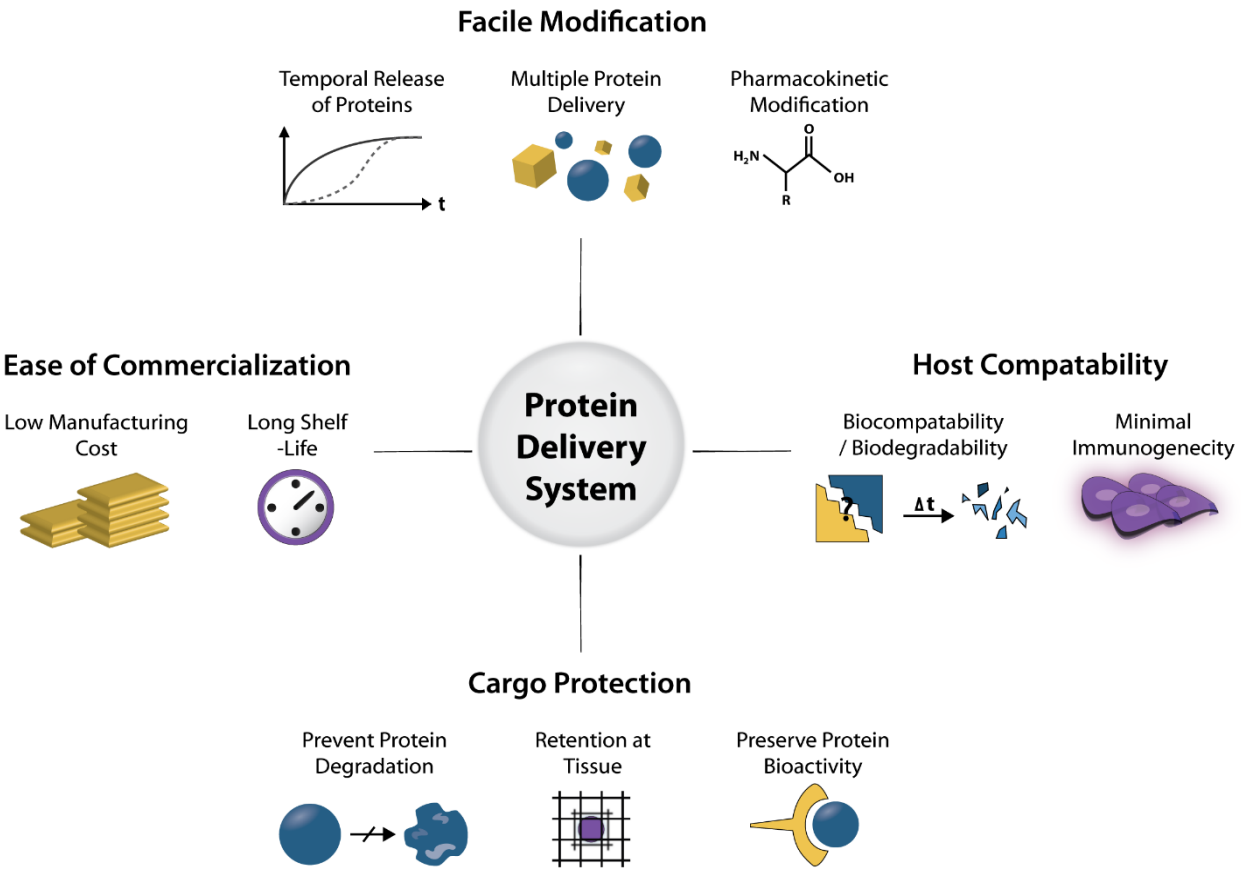

Figure 6. Desirable properties of an effective protein delivery system. Practically, it may be difficult to satisfy all of the desirable properties and a balance has to be made based on cost and resources.

There are various methods for protein encapsulation in a delivery vehicle, which ultimately determine the release rate of these proteins (**Figure 8**). Physical entrapment requires the mixing of proteins with polymers before they gel or solidify. The crosslinking density and structural stability of the polymeric network determine the encapsulation efficiency and release of the protein via diffusion and/or degradation mechanisms depending on the size of the protein relative to pore sizes of the matrix [211]. Proteins can be immobilized to the matrix using electrostatic interactions, ionic and hydrogen bonds, and covalent attachment (**Figure 7**). These methods can employ macromolecules and polymers such as heparin, heparan sulfate, hyaluronic acid, PEG, MMP linkers, and functional groups such as carboxyl, amino, and hydroxyl groups

[195, 208]. Some encapsulation methods include steps of leaching, use of organic solvents, processing at high temperatures, freeze-drying, and chemical modification which can be harmful to the stability and bioactivity of the proteins [208]. Therefore, it is essential to employ techniques that prevent potential denaturation and deactivation of proteins, so that they can perform their intended activity upon release from the delivery system (**Figure 6, 7**). By modifying polymerization conditions, composition, stoichiometry, functional groups, and other tunable parameters, natural and synthetic polymers can form different kinds of injectable matrices for the controlled delivery of proteins that can be implemented in cardiac repair strategies (**Figure 6, 7**). Different kinds of release profiles can be achieved depending on the type and property of a delivery vehicle (**Figure 8**). Injectable delivery platforms such as hydrogels, micro- and nanoparticles, coacervates, peptide nanofibers, and liposomes are discussed in the next sections (**Figure 7**).

1.3.2 Hydrogels

Hydrogels are made through physical or chemical crosslinking of polymers to create hydrophilic networks swollen by water (**Figure 7**) [3]. They are often biocompatible, can be made to have soft tissue-like elasticity and permeability. Certain hydrogels can be injected into the body through minimally invasive techniques. The water content of hydrogels can help reduce interfacial tension with other tissue fluids allowing gas permeation and small compound diffusion. They typically have burst releases of embedded proteins and can sustain their release for short periods (**Figure 8**). Gaining a better control over the release kinetics and the tailoring of hydrogel mechanical and chemical properties are areas of continued investigation. For instance, the mechanical properties of hydrogels based on natural materials can be enhanced by

conjugating inhibitors or crosslinkers that reduce hydrolysis. Immobilizing affinity groups on hydrogels can strengthen their binding of proteins and prolonging their release. Moreover, biodegradability of synthetic hydrogels can be improved by introducing proteolytic sequences in their synthesis, while injectability can arise through crosslinks triggered by in vivo stimuli. Gelatin and chitosan hydrogels have been used to deliver proteins such as FGF-2 and EPO to induce revascularization and cardiac repair [212, 213]. Fibrin gels have been utilized to release angiogenic factors and increase the formation of microvessels [214]. Collagen gels containing TIMP-1 and TIMP-3 can improve cardiac function and reduce adverse remodeling after infarction [88]. Alginate hydrogels have been used for sequential delivery of proteins such as IGF-1 followed by HGF or VEGF followed by PDGF to improve ischemic heart function [41, 215]. Recently, hyaluronic acid-based hydrogel loaded with SDF-1α and angiogenic peptide Ac-SDKP was delivered to the infarcted myocardium improving ejection fraction, stem cell recruitment, and angiogenesis [216]. The delivery of TIMP-3 using a hyaluronic acid hydrogel improves ejection fraction and reduces ventricular dilation, LV wall stress, MMP activity, inflammation, and infarct size in a porcine model [177]. An ECM-derived hydrogel releasing an engineered HGF fragment demonstrated cardiomyocyte protection and downregulation of pro-fibrotic markers in vitro, and improved cardiac function and angiogenesis in vivo [217]. PEG-based hydrogels have been used to treat infarcted hearts and deliver single or multiple proteins such as VEGF, HGF, and IGF-1 which reduced scar burden and enhanced heart function [218-220].

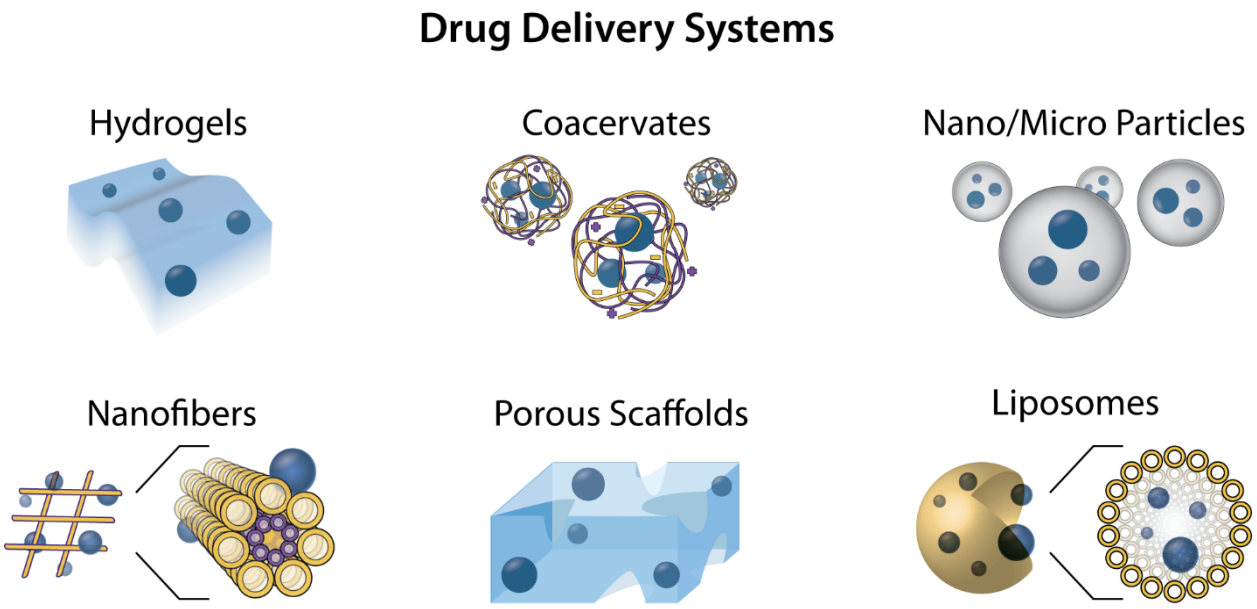

Figure 7. Commonly used and developed drug delivery systems include hydrogels, nano/micro particles, coacervates, self-assembled nanofibers, porous scaffolds, and liposomes. The structural, mechanical, and chemical properties of these systems can be modified to control the release kinetics of cargo.

1.3.3 Micro- and nanoparticles

Micro- and nanoparticles are injectable small particles often produced from polymers, functionalized to target specific injury sites, and control the release of embedded bioactive molecules like proteins which can be dissolved within, entrapped, encapsulated, or adsorbed (**Figure 7**). Because of their small size, micro- and nanoparticles are injectable and can diffuse and accumulate in different tissues. The particle size also plays an important role in the release rate of encapsulated proteins because of changing surface-to-volume ratios and the ability of cells to endocytose them (**Figure 8**) [221]. The loading of proteins into micro- and nanoparticles usually requires the use of relatively harsh conditions and organic solvents that put the proteins at risk of denaturation and loss of bioactivity [208]. Such conditions prompted

the utilization of surfactants, carrier proteins, and sugars as stabilizers during the process of protein encapsulation in a bid to minimize potential loss of protein bioactivity [222]. PLGA is one polymer that has shown a lot of potential in controlled delivery because of its high biocompatibility and safety. It is also FDA-approved for various medical applications. PLGA microparticles have been used to release SDF-1α, thus increasing the extent of stem cell recruitment in vitro [223]. Delivering VEGF to the ischemic heart using PLGA microparticles induces angiogenesis and reduces LV wall thinning and adverse remodeling [224]. In another study by the same group, these microparticles are used to co-deliver FGF-1 and NRG-1 to the heart after MI which improved cardiac function, revascularization, cardiomyocyte proliferation, progenitor cell homing, and reduced infarct size and fibrosis [225]. IGF-1 delivered by PLGA nanoparticles can significantly improve Akt activation and ejection fraction and reduce apoptosis and infarct size in mice hearts [226]. Heat shock protein 27 (HSP27)-loaded PLGA microparticles inside an alginate hydrogel improved cardiac cell protection under hypoxia [227]. PLGA microparticles loaded with milrinone have also been used to improve ejection fraction and reduce inflammation in a rodent MI model [228]. Micro- and nanoparticles based on other biomaterials such as porous silicon, silica, lecithin, pluronic, and dextran have been recently investigated for delivery of proteins to repair the infarcted myocardium [229-232].

1.3.4 Coacervates

Complex coacervates are a new class of drug delivery vehicles [233]. They can be formed by the mixing of oppositely charged polyelectrolytes resulting in aggregates of colloidal droplets held together by electrostatic attractive forces and apart from the surrounding liquid (**Figure 7**) [234-236]. The coacervation process leads to phase-separation of a polymer-rich liquid phase

from a polymer-poor one. Only recently, the investigation of coacervates as drug delivery vehicles started with the advancement of this field. Particularly interesting features of coacervates include their ability to load molecules with high capacity and self-assemble in aqueous solutions without the need for organic solvents, thereby evading the risk of denaturing loaded proteins [235-237]. Once proteins, drugs, or small molecules are embedded within the coacervate, they become protected from the proteolytic and enzymatic degradation, thus maintaining their bioactivity and sustaining their release (**Figure 8**) [235]. The coacervate droplets exist in dynamic equilibrium, thus reducing their likelihood of aggregation in response to ionic concentration or temperature changes in their environment. The small size of coacervates, on the order of nanometers, allows them to be injectable through fine gauge needles. The stability of ionic coacervates is an area that needs improvement, especially for a systemic delivery route when blood carries the coacervate [234, 235]. Even though coacervates have only been utilized in drug delivery applications for a relatively short time, they have shown many advantages over conventional methods of protein delivery which calls for the continued experimentation of coacervates in tissue engineering applications.

Elastin-like polypeptides (ELPs) are one of the coacervate systems recently explored for drug delivery [238]. ELPs are recombinant proteins made to mimic the hydrophobic domains of tropoelastin which undergo a coacervation process above their tunable transition temperature. ELP fusion proteins have been designed to increase retention at the target tissue. For example, interleukin-1 receptor antagonist (IL-1RA) has been fused with ELP, and was found to mitigate different arthritis-type conditions and reduce cartilage degeneration in the knee joint after injury [239]. ELPs have also been employed to develop nanocarriers for cancer treatment. The

anticancer drug placitaxel (PTX) was conjugated to ELPs and found to accumulate more in tumors than free PTX showing better tumor regression in mice prostates [240].

Another coacervate system utilizes the complexation between polycations and heparin to control the release of heparin-binding GFs [235, 236]. The use of heparin in delivery systems advantageously imitates the native signaling environment involving ECM proteoglycans, ligands, and cell receptors. Heparin is allowed to bind to the GFs first, and then a synthetic polycation is added at specific stoichiometric ratios to induce the charged-based phase separation resulting in the formation of GF-loaded coacervates. This type of coacervate has been used to induce wound healing, therapeutic angiogenesis, and cardiac repair [86, 241-243]. FGF-2 coacervate was effective in inducing angiogenesis, reducing fibrosis and myocardial scarring, and improving contractile function in a mouse MI model [241]. Shh coacervate has been shown to improve cardioprotection, vascularization, and heart function in rodents after MI [86, 244].

1.3.5 Other delivery systems

A few other delivery systems have been utilized in protein delivery to the ischemic heart (**Figure 7**). Lipid-based vehicles have been developed for use in cardiac repair, however challenges posed by liposomes such as instability and interaction with circulating lipoproteins are still being addressed [232, 245]. Anti-P-selectin-conjugated liposomes loaded with VEGF were delivered to the infarcted myocardium leading to an improved systolic function and fractional shortening [246]. Self-assembled peptides, formed by alternating hydrophilic and hydrophobic domains of oligopeptides, are another platform used for delivery of proteins

(**Figure 7**) [247]. They have been used to deliver IGF-1, PDGF-BB, FGF-2, VEGF, and others to improve cardiac function post infarction [248-251].

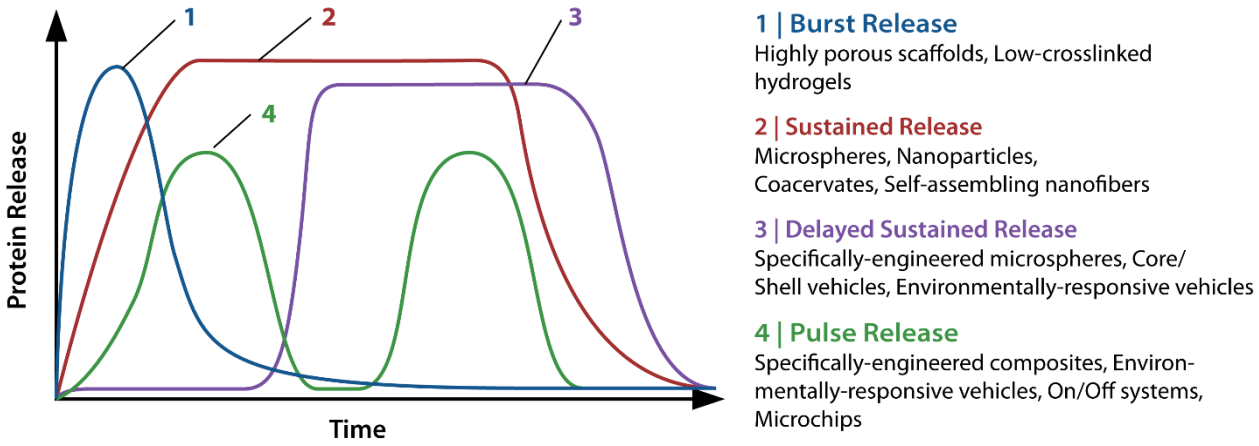

Figure 8. Different release profiles can be attained by different controlled release systems. The rate and style of release over a certain period can be controlled by changing the design and chemical and mechanical properties of the delivery vehicle.

1.3.6 A clinical and market perspective on protein delivery systems

Following the limited success of protein-based therapies in the clinic, there has been a rising interest in the development of more effective methods of administering proteins to the target tissues. Commercially marketed protein-containing products such as Regranex and InFUSE have not been fully adopted in regenerative medicine because of safety and efficacy concerns. Much testing and validation need to be performed before successful adoption of protein delivery systems in the market. In particular, in vivo studies are necessary to develop appropriate administration methods and demonstrate safety and efficacy of the encapsulated proteins in inducing the desired response. Proving safety, scalability, reproducibility, ease of manufacturing, cost-effectiveness, biocompatibility, and biodegradability are all factors that can help push controlled release systems past clinical trials and pave the road towards full adoption

in the clinics. There is a long way to go and many hurdles to overcome, but the potential market for therapeutic proteins for the heart is just beginning to open up and has a huge growth potential. This motivates many researchers to improve the controlled protein delivery field and race to clinical success.

1.4 THE POTENTIAL OF POLYCATION:HEPARIN COACERVATE IN TISSUE REPAIR AND REGENERATION

Drug delivery systems can gain a new level of effectiveness when they are designed to mimic the physiologic microenvironment as much as possible. Heparin-based coacervates are one example of such biomimetic systems (**Figure 7, 9**) [236, 237, 242, 252]. A complex coacervate can be formed by the electrostatic interactions between polycations and polyanions leading to phase separation (**Figure 9**). Heparin-based coacervates take into account the essential role of the ECM in protection and translocation of GFs within tissues. Heparin, the most negative natural polymer in the body, binds over 400 proteins and peptides, many of which have important biological functions [253]. By employing heparin, these coacervates imitate the signaling methods of the native environment that involve ECM proteoglycans, ligands, and cell receptors. The inspiration in the design of our coacervate came from the stable, ternary complex formed by heparin, fibroblast growth factor (FGF), and its cell receptor FGFR, whereby heparin facilitates their association [236]. We decided to create a simplistic mimic of the heparin-binding domain of FGFR. The heparin-binding domain of many proteins contains residues such as lysine and arginine, which are important for inter-molecular interaction and downstream signaling [253]. So, we conjugated the most basic amino acid, Arginine, to a hydrolyzable

backbone of ethylene glycol and aspartic acid resulting in the formation of a synthetic polycation, a polycation poly(ethylene arginyl aspartate diglyceride) (PEAD) (**Figure 9A**) [235]. PEAD bears 2 cationic groups (amine and guanidine) per repeating unit and thus interacts strongly with polyanions such as heparin (**Figure 9**). To form the coacervate, we allow the protein and heparin to bind and then add PEAD which induces phase separation that can be macroscopically seen as a turbid solution indicating the neutralization of the charge. In our coacervate system, heparin is non-covalently immobilized within the complex by electrostatic interactions, which can guarantee the preservation of its natural bioactivity. The polycation PEAD was designed specifically for protein delivery [235]. It is biodegradable with minimal cytotoxicity [237].

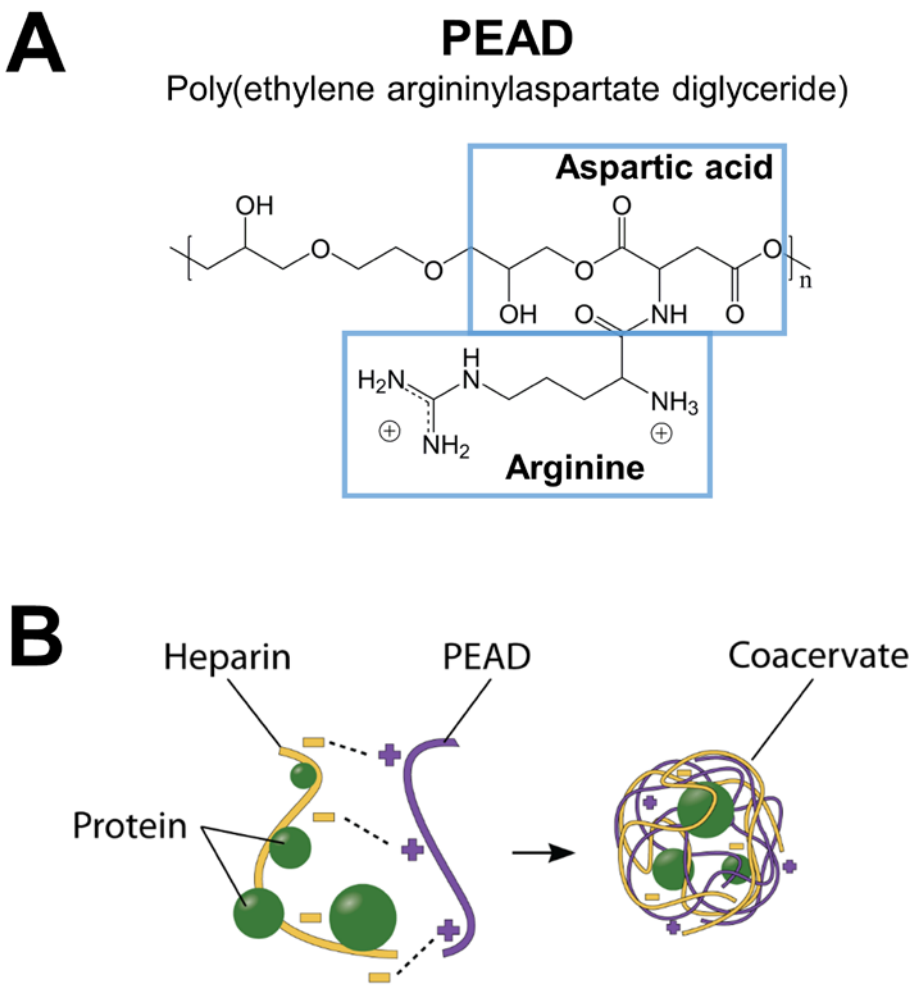

Figure 9. (A) Chemical structure of the polycation PEAD. PEAD has a hydrolyzable backbone of ethylene glycol and aspartic acid and bears 2 cationic groups per repeating unit, located on its arginine. (B) The natural polyanion heparin and heparin-binding proteins can form a complex, which upon mixing with PEAD leads to the formation of a protein-loaded coacervate complex based on electrostatic interactions.

Heparin-based coacervates are able to encapsulate proteins with high efficiency, protect them from proteolytic degradation, prolong their bioactivity, and sustain their release over time (**Figure 9**) [235, 236, 242]. There are a number of ways to control the formation of coacervates and their release kinetics such as altering the molecular weights of the polyelectrolytes, their charge density, the stoichiometric ratio of positively- and negatively-charged polymers, pH, salt concentration, and others [234-236, 252]. Our group has utilized the coacervation process

between a PEAD and heparin to control the delivery of proteins for various biomedical applications such as therapeutic angiogenesis, wound healing, cardiac repair, and bone regeneration [233].

The administration of heparin-binding epidermal growth factor (HB-EGF)-loaded coacervates to full-thickness excisional normal and diabetic mouse wounds led to fast wound closure compared to free HB-EGF by improving re-epithelialization, angiogenesis, keratinocyte, and angiogenesis [243]. FGF-2 coacervate triggered comprehensive angiogenesis in a subcutaneous model, increasing the formation of mature and stable vasculature that participates in blood circulation [242]. BMP-2 coacervate enhanced the osteogenic effect of muscle-derived stem cells by increasing their differentiation and ectopic bone formation [254]. In regards to cardiac repair, FGF-2 coacervate improved cardiac function and angiogenesis, and reduced inflammation, fibrosis, and cardiomyocyte death after MI injury [241]. In addition, Shh coacervate was shown to protect cardiomyocytes from apoptosis and induce important GF signaling in vitro, and improve vascularization and heart function in rats after MI [86, 244].

1.5 CONCLUSIONS AND FUTURE DIRECTIONS

Current treatments only defer further cardiac damage and dysfunction rather than restore the normal function of the heart. Given the limited potential of the adult mammalian heart to repair and regenerate on its own after MI, and the identification of favorable proteins that are able to induce cardiac protection, repair, and regeneration, protein therapeutics remain a hopeful, feasible, and effective path for future treatments of ischemic heart disease, even though the road towards clinical translation is still filled with obstacles (**Figure 5, 10**).

Further understanding and elucidation of molecular mechanisms of myocardial tissue repair and regeneration will contribute to the development of more effective treatment strategies (**Figure 10**). Working on multiple aspects such as revascularization, remodeling prevention, and cardiomyogenesis is posed to be a more promising approach towards full recovery and comprehensive regeneration of the infarcted myocardium than single-focus approaches (**Figure 5, 10**). Therefore, the decision on which proteins to combine to address many of the aspects discussed in this chapter is important. Additionally, the ability to design therapeutic strategies that can mimic the natural regenerative microenvironment is a key determinant of successful repair process after MI (**Figure 6, 7**).

The notion of recapitulating the physiology of the heart environment can be facilitated and potentially achieved through the utilization of efficient, targeted, biocompatible, and tightly controlled protein delivery systems that can support the bioactivity, stability, and retention of released proteins at the target site (**Figure 6, 7**). Proteins are not meant to be available at any time or any place during the repair process. Delivery and release kinetics of proteins need to be tightly regulated spatially and temporally, so that their physiological concentrations, gradient formations, and biological cues are optimal for preservation and regeneration of the myocardium. Because hundreds of millions of cardiomyocytes are lost after an ischemic insult, it is extremely hard to replace such a vast amount of lost tissue. Many researchers support the idea of combination therapy that combine the use of cell and protein therapies. Such an approach needs to clearly identify the source and quantity of cells to use. If the cells become fully differentiated into functional adult cardiomyocytes that are electromechanically coupled with the rest of the heart muscle, it will be a powerful way to regenerate the damaged heart.

The complexity of biological systems makes it difficult to integrate all the aspects of tissue repair and regeneration. Systems biology approaches can potentially help combine massive experimental data with computational modeling to design highly effective strategies. The physiology and pathology of the heart are intrinsically complex, thus it is indispensable to design strategies that can yield substantial therapeutic benefit and pave the way to full clinical adoption in the cardiovascular market (**Figure 5, 10**).

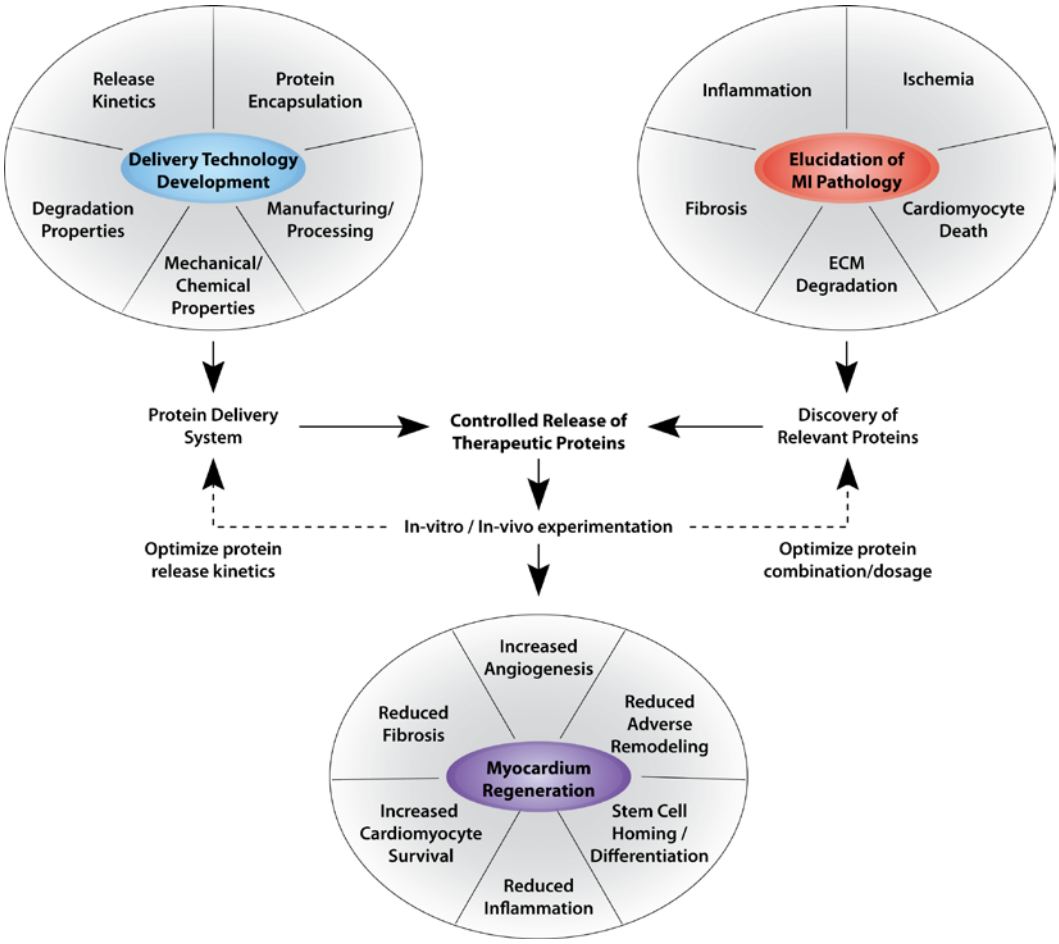

Figure 10. Schematic of a protein therapy design. An effective therapy requires the elucidation of the pathological changes after MI, leading to the identification of involved proteins. It is also essential to develop a proper delivery technology that can encapsulate proteins of interest and deliver them in a physiologic manner. The optimized strategy can potentially counter or reverse the pathological progression and trigger the repair and regeneration mechanisms in the heart.

1.6 SPECIFIC AIMS

The central hypothesis of this research is that controlled protein delivery using a vehicle, capable of sequential release of proteins necessary at different stages of the repair process, can trigger significant tissue repair and regeneration in the clinically-relevant context of treating myocardial infarction (MI). Our preliminary results, previous publications, and the current literature demonstrate the therapeutic potential of many proteins in cardiac repair (**Table 1**). The desired controlled release patterns were achieved using our heparin-based coacervates in combination with fibrin gel. Towards our central hypothesis, I tested the efficacy of controlled delivery of combinations of therapeutic proteins with roles in cardiac function, VEGF, HGF, PDGF, FGF-2, IL-10, TIMP-3, and SDF-1α, using in vitro assays and an in vivo rat MI model. This dissertation is outlined in the following three Specific Aims:

Specific Aim 1: Characterize the ability of the heparin-based coacervate to co-release proteins and evaluate its efficacy using angiogenic in vitro assays. The heparin-based coacervate was tested for its ability to co-release VEGF and HGF. The protein-loaded coacervates were characterized for their charge, size, and morphology. The stimulatory effects of combining these two proteins and controlling their delivery were evaluated on endothelial cell proliferation and tube formation using in vitro assays.

Specific Aim 2: Design a delivery vehicle to achieve sequential release of proteins and evaluate its efficacy in stimulating therapeutic angiogenesis in vitro and in an in vivo rat myocardial infarction model. To achieve sequential release of VEGF, an early-stage angiogenic factor, followed by PDGF, a late-stage angiogenic factor, I tested embedding VEGF in fibrin gel, while embedding PDGF inside heparin-based coacervates and distributing them inside the same gel. The efficacy of sequential release was tested on cell proliferation and

microvasculature formation in vitro. In vivo testing followed using a rat MI model to evaluate the effect of sequentially-released VEGF and PDGF on cardiac function, angiogenesis, cardiomyocyte survival, inflammation, and fibrosis at 4 weeks after MI.

<u>Specific Aim 3:</u> Optimize a combination of complementary proteins for cardiac repair using factorial design of experiment (DOE) and evaluate the efficacy of the optimized combination using the sequential release system in a rat myocardial infarction model. I chose a combination of four proteins with relatively distinct cardiac functions, FGF-2, IL-10, SDF-1α, and TIMP-3, to be tested for their potential in cardiac repair. I embedded TIMP-3 and IL-10 in fibrin gel, while embedding FGF-2 and SDF-1α inside heparin-based coacervates and distributing them inside the same gel. The combination and doses of proteins were first optimized based on their improvement of cardiac function utilizing a statistical fractional factorial design. Using a rat MI model, the efficacy of the optimized combination was then tested on cardiac function, myocardial strain levels, left ventricle dilation and wall thinning, angiogenesis, cardiomyocyte survival, inflammation, stem cell homing, fibrosis, matrix metalloproteinases activity, survival molecular pathways, and protein level signaling at 2 and/or 8 weeks after MI.

2.0 DUAL DELIVERY OF VEGF AND HGF TO TRIGGER STRONG ANGIOGENIC RESPONSES

Note: The research work of chapter 2 was published in Macromolceular Bioscience Journal. H.K. Awada, N.R. Johnson, Y. Wang. 2014. "Dual delivery of vascular endothelial growth factor and hepatocyte growth factor coacervate displays strong angiogenic effects". Macromolecular Bioscience 14: 679-686.

Controlled delivery of multiple growth factors (GFs) holds great potential for the clinical treatment of ischemic diseases and might be more therapeutically effective to reestablish vasculature than the provision of a single GF. Vascular endothelial GF (VEGF) and hepatocyte GF (HGF) are two potent angiogenic factors. However, due to rapid degradation and dilution in the body, their clinical potential will rely on an effective mode of delivery. We have developed a coacervate, comprised of heparin and a biodegradable polycation, which protects GFs from proteolysis and potentiates their bioactivities. Here we show that the coacervate incorporates VEGF and HGF and sustains their release for at least 3 weeks. We confirm their strong angiogenic effects on endothelial cell proliferation and tube formation in vitro. Furthermore, we demonstrate that coacervate-based dual delivery of these factors has stronger effects than free application of both factors and individual GF delivery.

2.1 INTRODUCTION

Harnessing the body's ability to regenerate damaged tissues and enhance functional recovery presents an exciting and challenging opportunity for growth factor (GF) therapy. The regenerative microenvironment is influenced by the interactions between cells, the extracellular matrix (ECM), and signaling molecules. GFs, chemokines, and cytokines can trigger endogenous repair mechanisms by providing the appropriate signals for cells to proliferate, migrate, differentiate, or apoptose [208, 255, 256]. Although the delivery of a single GF has shown promise in the treatment of some diseases, many conditions require a more complex approach [195, 257]. Co-delivery of multiple GFs may be paramount to successful therapeutic angiogenesis for ischemic tissues such as infarcted myocardiums and chronic wounds. According to the Angiogenesis Foundation, at least 314 million patients in Western nations could benefit from some form of pro-angiogenic therapy [258]. Vascular endothelial GF (VEGF) and hepatocyte GF (HGF) are potent stimulators of angiogenesis and play important roles in promoting endothelial cell growth, proliferation, migration, differentiation, and survival [259-264]. Several studies have demonstrated that the combination of VEGF and HGF in free-form triggers an angiogenic response that is stronger than either GF alone [265-268]. This underscores the complexity of the neovascularization process and the need to develop therapies which adequately address this complexity.

The efficacy of GF therapy hinges on a delivery system that can appropriately maintain their bioactivity and bioavailability [208, 255]. Effective delivery vehicles may achieve this by protecting the GFs from proteolytic degradation and controlling their spatiotemporal release, while also avoiding side effects from high GF concentrations systemically or at unwanted distal locations [191, 195, 208, 255]. Concentrating efforts on the development of delivery systems

with the capability of delivering GFs in a time-dependent and dose-dependent fashion might be the key to obtaining sufficient tissue development [195]. We have previously described a new class of controlled release vehicles: an injectable polyvalent coacervate formed by a polycation, poly(ethylene arginyl aspartate diglyceride) (PEAD), and heparin that can control the release of heparin-binding GFs [235, 237]. More than 400 human proteins bind heparin, many of which are important for healthy vasculature and tissue regeneration [253]. The coacervate is biodegradable, has excellent biocompatibility, and can enhance the bioactivity of the GFs [86, 235, 241-243]. The objective of this study was to characterize the ability of the heparin-based coacervate to co-release VEGF and HGF and examine the effect of their dual release on human endothelial cell (EC) proliferation and tube formation. This is the first study to investigate the ability of heparin-based coacervates at multiple GF release. We hypothesized that co-delivery of VEGF and HGF would yield stronger and more robust angiogenic effects than those of the individual GF coacervates and the co-administration of free GFs.

2.2 MATERIALS AND METHODS

2.2.1 Characterization of VEGF and HGF coacervates

2.2.1.1 *Zeta potential and dynamic light scattering (DLS) measurements*

PEAD was synthesized as previously described [235, 237]. Heparin (Scientific Protein Labs, Waunakee, WI) and PEAD were each dissolved at 10mg/ml in deionized (DI) water and filter-sterilized at 0.22μm. Heparin was initially combined with either $VEGF_{165}$ or HGF (Peprotech, Rocky Hill, NJ) or both at 100:1 mass ratio of heparin:GF to ensure that the solution was

saturated with heparin to bind all the available GFs. Solutions were then titrated with PEAD to obtain different PEAD:heparin:GF mass ratios. The solution was diluted with DI water to a total of 750µl before zeta potential was measured with a Zetasizer Nano ZS90 (Malvern, Worcestershire, UK). Results were reported as a mean with standard deviation for 25 measurements. The same instrument was used to determine the hydrodynamic diameters of PEAD:heparin (mass ratio 5:1), heparin:VEGF (100:1), PEAD:heparin:VEGF (500:100:1), heparin:HGF (100:1), and PEAD:heparin:HGF (500:100:1) by dynamic light scattering (DLS). Results were reported as a mean with polydispersity index (PDI) for 25 measurements. PDI in the area of light scattering is used to describe the width of the particle size distribution.

2.2.1.2 *Fluorescent imaging of the coacervate*

PEAD solution was mixed with rhodamine-labeled heparin at the previously optimized 5:1 PEAD:heparin mass ratio [235]. The coacervate was centrifuged at 12,100g for 10 minutes to form a pellet. The supernatant was aspirated to remove unbound heparin and the pellet was resuspended in DI water and added to a 96-well plate for fluorescent imaging (Eclipse Ti; Nikon, Tokyo, Japan).

2.2.1.3 *Scanning electron microscopy (SEM)*

Samples were prepared with PEAD:heparin mass ratio 5:1 for blank coacervate and PEAD:heparin:GF mass ratio 500:100:1 for VEGF or HGF coacervates. The complex was dropped on an aluminum stub, lyophilized, gold sputter-coated, and examined by SEM (JSM-6335F field emission SEM; JEOL, Peabody, MA).

2.2.2 Growth factor loading efficiency and release assay

The release profiles of VEGF and HGF were determined by sandwich ELISA. VEGF+HGF coacervates (n=3) were formed using 200ng of each GF combined with heparin followed by PEAD at 500:100:1 mass ratio of PEAD:heparin:GF in 200µl of DI water. Solution was centrifuged at 12,100g for 10 minutes to pellet the coacervate. The supernatant was collected and stored, and pellet was resuspended in DI water. The samples were incubated at 37°C. The first collection (Day 0) was used to determine the loading efficiency. The same centrifugation and supernatant collection procedure was repeated on days 1, 3, 7, 14, and 21. Sandwich ELISA was performed to detect the amount of released GF in the supernatants according to the instructions of VEGF ELISA kit (Peprotech, Rocky Hill, NJ) or HGF ELISA kit (R&D Systems, Minneapolis, MN). After the addition of sulfuric acid stop solution, the absorbance at 450/540nm was recorded by a SynergyMX plate reader (Biotek, Winooski, VT). Standard solutions (n=3) that contained 200ng of each of free VEGF and HGF in 200µl of DI water were prepared to create standard curves and determine total release.

2.2.3 Endothelial proliferation and live cell count assays

Similar culture conditions were used for cell proliferation and live cell count assays. Passage 6 human umbilical vein endothelial cells (HUVEC) (ATCC, Manassas, VA) were labeled with Calcein AM (Molecular Probes, Eugene, OR) for 2 hours before seeding 10^4 cells in 100µl EGM-2 media (Lonza, Walkersville, MD) per well in a 96-well plate. Six hours after seeding, group-specific media was added and 8 groups were tested (n=3 wells/group): basal media, blank coacervate, free HGF, free VEGF, free VEGF+HGF, HGF coacervate, VEGF coacervate, and VEGF+HGF coacervates. Each GF was added at a final 30ng/ml concentration.

For the BrdU cell proliferation assay (Millipore, Billerica, MA), the plate was incubated at 37°C for 16 hours, then 20µl of BrdU label was added to each well and incubated for 4 hours. The proliferation assay protocol was then followed according to the kit's instruction manual. After the addition of the stop solution, the absorbance at 450/540nm was recorded by a SynergyMX plate reader and normalized to the basal media control.

For the live cell count assay, the plate was incubated at 37°C for 3 days, then cells were observed using a fluorescence microscope. Cell number was determined by manually counting the cells in a 0.67mm^2 field in the center of the well (n=3 wells/group). Fluorescent images of cells were taken of 4mm^2 fields.

2.2.4 Endothelial tube formation assay

Fibrin gels were prepared for a three-dimensional (3D) cell culture environment as previously described [269]. Briefly, 6mg/ml bovine fibrinogen (Sigma-Aldrich, St. Louis, MO) was dissolved in EGM-2 media, added in 150µl volumes per well of a 24-well plate, activated with 150µl of 0.1mg/ml thrombin solution (Sigma-Aldrich, St. Louis, MO) in EGM-2, swirled gently to mix and solidified at 37°C. Passage 5 HUVEC were labeled with Calcein AM for 2 hours, then 1.5x10^5 cells were seeded on top of each gel in 1ml EGM-2 media and incubated at 37°C overnight. After confluent cell monolayers formed next day on top of each gel, media was removed and 300µl group-specific fibrin gels were overlaid and solidified as before, followed by 1ml EGM-2 media on top. Group-specific additions to top gels included 8 groups: basal media, blank coacervate, free VEGF, free HGF, free VEGF+HGF, VEGF coacervate, HGF coacervate, and VEGF+HGF coacervates. In all groups, the dose of VEGF or HGF was 250ng. After culturing for 3 days, media was removed and wells were imaged with a fluorescence

microscope. An endothelial tube was defined as a straight cellular extension joining two cell masses or branch points [269]. Tube number, lengths, and thicknesses were measured as angiogenic indices [269-271]. Using NIS-Elements AR imaging software (Nikon, Tokyo, Japan), endothelial tubes were manually counted and quantified in length and thickness in a $0.67mm^2$ field in the center of each well (n=3 wells/group).

2.2.5 Statistical analysis

GraphPad Prism 5.0 statistical software (La Jolla, CA) was used for statistical analysis. One-way ANOVA followed by the post-hoc Tukey's comparison test was used to analyze the data for bioactivity assays. Data is presented as mean ± standard deviations (SD). Statistical significance was set at $p<0.05$.

2.3 RESULTS AND DISCUSSION

2.3.1 VEGF and HGF coacervates characterization

The zeta potential of the strongly negative solution of heparin:GF (100:1 mass ratio) turned more positive as it was titrated with the polycation PEAD (**Figure 11A**). At 100:100:1 mass ratio of PEAD:heparin:GF, VEGF coacervate and HGF coacervate had negative zeta potentials of approximately -52mV and -42mV, respectively. Zeta potentials approached neutrality at a mass ratio of approximately 500:100:1 with high turbidity in the solution, regardless of the GF used (-0.9mV for VEGF, and -1.8mV for HGF). As more PEAD was added, the zeta potential reached a positive plateau of 22mV for VEGF coacervate and 17mV for HGF coacervate at

1000:100:1 mass ratio (**Figure 11A**). Previously we reported that a 5:1 mass ratio of PEAD:heparin produced a neutral coacervate [235]. Our results indicate that a small amount of GFs does not have a significant effect on zeta potential. Therefore, for the rest of this study, we used a PEAD:heparin:GF mass ratio of 500:100:1 to achieve maximal coacervation.

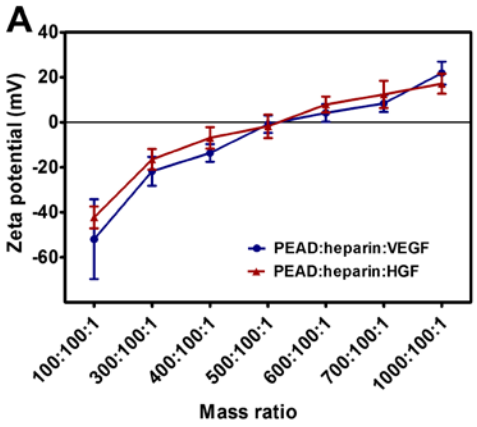

B

Structure	Diameter (nm)	PDI
PEAD:heparin	425.2	0.01
Heparin:VEGF	139.8	0.36
PEAD:heparin:VEGF	476.1	0.33
Heparin:HGF	147.3	0.44
PEAD:heparin:HGF	460.6	0.33

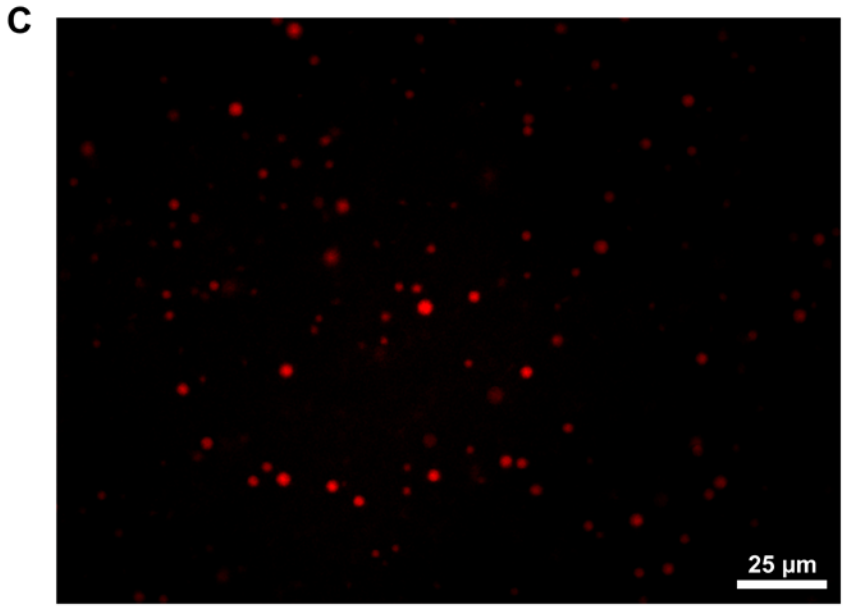

Figure 11. (A) Zeta potentials of VEGF and HGF coacervates were measured at different mass ratios of PEAD:heparin:GF by titrating negative heparin:GF solutions with positive PEAD. Coacervates approached neutrality at 500:100:1. (B) DLS measurements show the hydrodynamic diameters of heparin:GF, PEAD:heparin, and PEAD:heparin:GF particles. (C) Spherical droplets of rhodamine-labeled blank coacervates were imaged by fluorescence microscope showing variable sizes. Scale bar=25µm.

DLS measurements showed significant increases in hydrodynamic diameters upon addition of PEAD to heparin:GF complexes. The blank coacervate had a hydrodynamic diameter of 425nm. VEGF coacervate and HGF coacervate had diameters of 476nm and 461nm, respectively; demonstrating a small increase in size possibly due to GF addition (**Figure 11B**). Fluorescent imaging of a blank coacervate using rhodamine-labeled heparin revealed thousands of spherical liquid droplets that are sub-micron in size and can aggregate over time to create larger coacervate droplets (**Figure 11C**). SEM images revealed the morphology of VEGF coacervate and HGF coacervate to be mainly composed of ribbon-like structures with globular beads of various sizes (**Figure 12**). There were no apparent morphological differences between blank coacervates and GF-loaded coacervates (**Figure 12**). This suggests that the ribbon-like structures are likely generated from PEAD while the globular bead structures originate from heparin, as was deduced from our previous characterization of the coacervate [235].

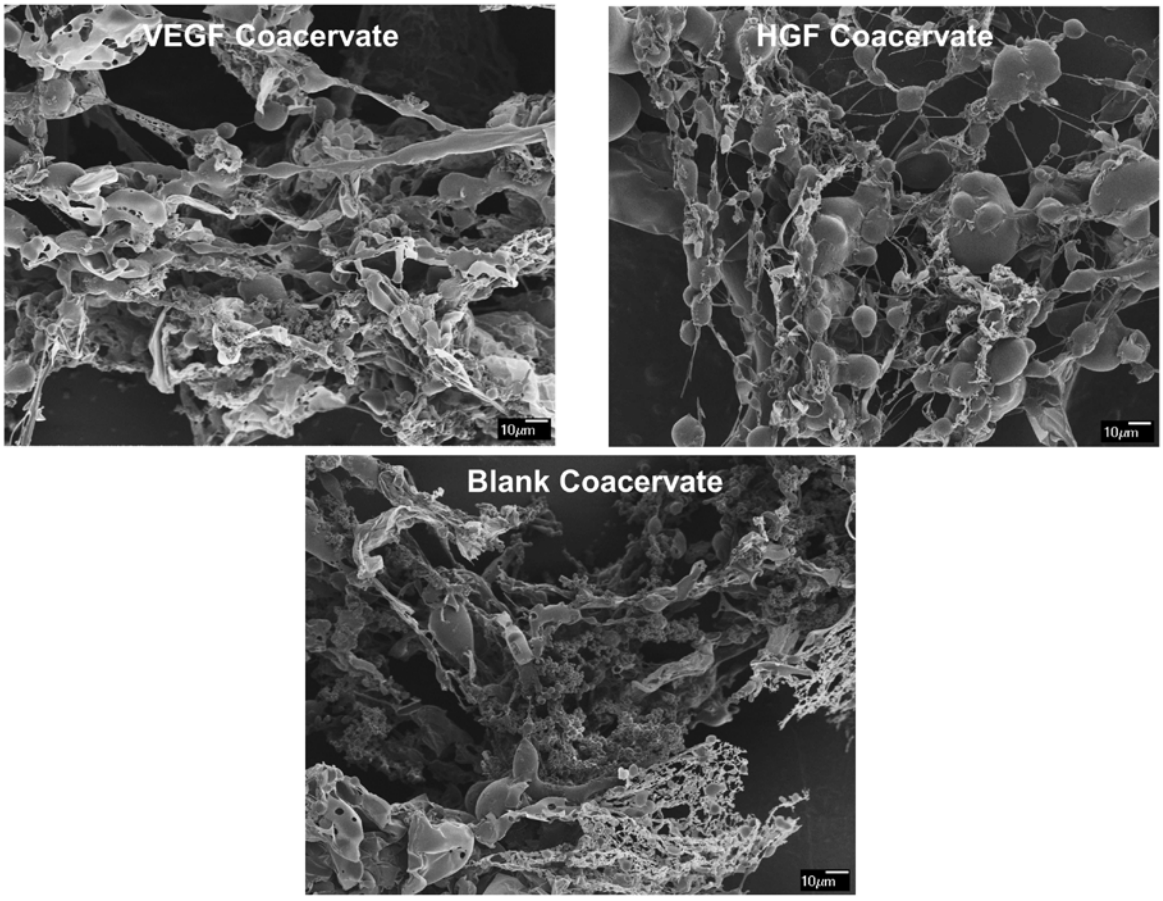

Figure 12. SEM images at low magnification (500X) show the ribbon-like structures and globular domains of blank coacervate, VEGF coacervate, and HGF coacervate.

2.3.2 Coacervate loading and release of VEGF and HGF

We studied the GF release kinetics from the coacervate by detecting the amount of released VEGF and HGF in the supernatant after pelleting the coacervate solution. The loading efficiency of VEGF was approximately 99%. The VEGF release profile showed a relatively small initial burst of 6% by 1 day. After 3 days, the release became nearly linear and resulted in a total release of approximately 35% by 21 days (**Figure 13**). The loading efficiency of HGF was approximately 98%. The HGF release profile also showed a relatively small initial burst of 5% by 1 day. After 3 days, the release became nearly linear and resulted in a total release of

approximately 27% by 21 days (**Figure 13**). Our results suggest a significant impact of the heparin-binding affinity of each GF on release rate. HGF, with a strong heparin-binding affinity (Dissociation constant K_d= 12nM), released slower from the coacervate than VEGF which has a relatively weaker heparin-binding affinity (K_d= 165nM) [272]. However, the release rate of any GF can also be influenced by the hydrolytic degradation of PEAD, degradation of the coacervate components by enzymes such as esterases and heparinases, and dissociation of the complex in an ionic environment. Therefore, the release rate is expected to be faster in vivo where such conditions might be prevalent.

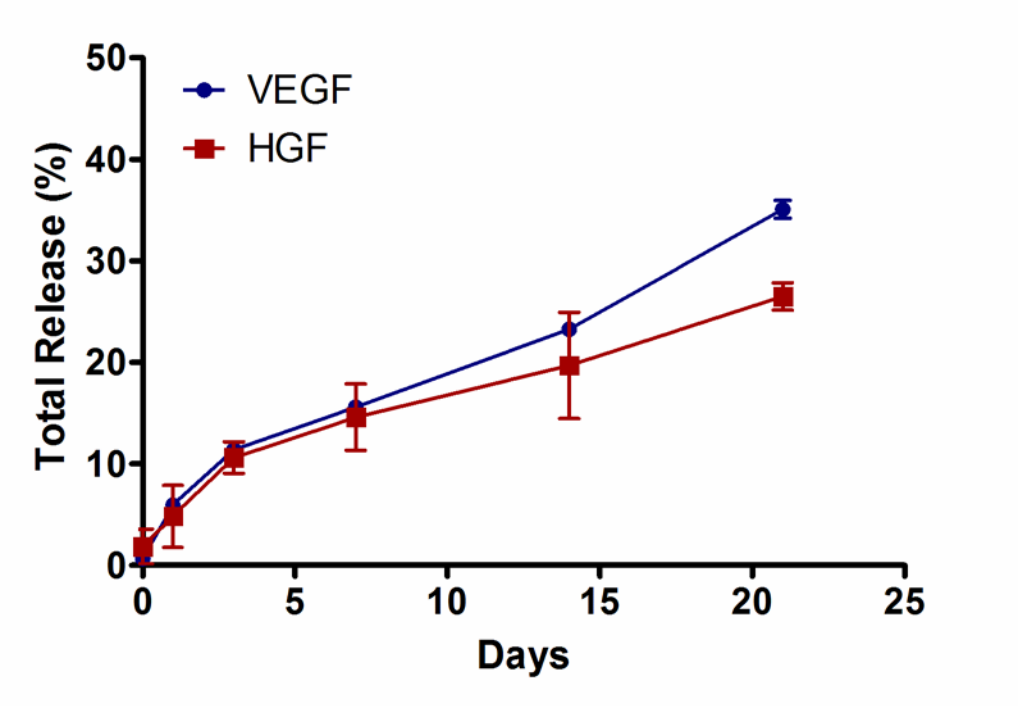

Figure 13. Sustained in vitro release of VEGF and HGF from the heparin-based coacervate. Approximately 35% of VEGF and 27% of HGF amounts were released by 3 weeks. Data are presented as means ± SD (n=3).

Without effective controlled release systems, GFs tend to diffuse away from the target sites, degrade quickly, lose their bioactivities, and are potentially harmful when injected at high

concentrations [208]. Current protein delivery systems including hydrogels, polymeric microspheres, and peptide nanofibers face a number of challenges [255]. For example, the formation of poly(lactic-co-glycolic acid) (PLGA) microspheres requires organic solvents which may compromise the bioactivity of the loaded GF [273]. Some hydrogels, on the other hand, face challenges to control the GF release kinetics and result in large initial burst releases [274]. Peptide nanofibers are expensive to synthesize which may be a roadblock to clinical translation [249]. In addition, all of these types of delivery vehicles often have relatively low GF loading efficiencies.

The coacervate delivery system was developed to overcome challenges faced by other delivery approaches. The coacervate was used in this study to simultaneously release VEGF and HGF. The coacervate release kinetics can be controlled by changing some parameters such as the molecular weight of PEAD and/or heparin, the charge density of PEAD, and the [PEAD:heparin] mass ratio. The coacervate preserves the native properties and function of heparin through the ionic interactions with PEAD without covalent cross-linking to the delivery matrix. Intact heparin supports a high GF loading efficiency and preservation of GF bioactivity, and the phase-separation induced by coacervation helps localize the GFs to the target tissues [235, 236, 242]. Finally, the coacervate is injectable and therefore can be easily utilized in a clinical setting.

2.3.3 VEGF+HGF coacervates display strong angiogenic effects

VEGF is an established promoter of blood vessel formation and remains the main driver of angiogenesis [275]. However, the administration of VEGF alone might lead to the formation of immature, leaky, and unstable neovessels [264]. The utility of VEGF is also restricted by a dose

limit, which could lead to undesirable side effects if surpassed [276, 277]. Additional factors are therefore necessary to trigger a more robust angiogenesis process. HGF is another potent angiogenic factor that stimulates endothelial cell proliferation and migration, and can induce endogenous expression of VEGF [259, 263, 278]. In addition, HGF has demonstrated chemotactic and anti-apoptotic activities on different cell types [279].

It has been shown that the combination of VEGF and HGF results in a more robust angiogenic response in vitro and in vivo than either factor alone [265-268, 280]. A combined gene therapy of VEGF and HGF amplified the activation of ERK1/2 signaling pathway in vitro, involved in cell survival and proliferation, and increased perfusion in a hindlimb ischemia mouse model compared to single plasmid injection [280]. Another study concluded that combining VEGF and HGF promoted endothelial cell survival and tubulogenesis in collagen gels with enhanced expression of anti-apoptotic genes Bcl-2 and A1 [268]. Although these studies demonstrate the benefit of VEGF and HGF combination therapy, their clinical potential might be limited because bolus and systemic injections of free-form GFs tend to have low efficacy. A study that displayed the capability to release VEGF and HGF simultaneously and sequentially, using poly(trimethylene carbonate) based photo-cross-linked elastomers, did not evaluate any angiogenic effects of the two factors together or compare their bioactivity results to free GF administration [281]. Therefore, we were prompted in this study to investigate the potential benefit of coacervate-based dual delivery of VEGF and HGF on angiogenic applications.

To investigate the effects of controlled release of VEGF and HGF on endothelial proliferation, we applied each GF separately or together, and in free-form or delivered by the coacervate to cell cultures and detected levels of administered BrdU, which is a thymidine

analog that incorporates into newly synthesized DNA strands of actively proliferating cells. One day after application, both GFs together in free-form significantly induced higher proliferation ($p<0.05$) compared to each GF alone, which showed little effect compared to control ($p>0.05$) (**Figure 14A**). Each GF alone delivered by the coacervate also significantly stimulated proliferation ($p<0.01$) compared to each GF alone in free-form. Finally, coacervate delivery of both GFs together significantly induced higher proliferation ($p<0.01$) compared to all other groups (**Figure 14A**).

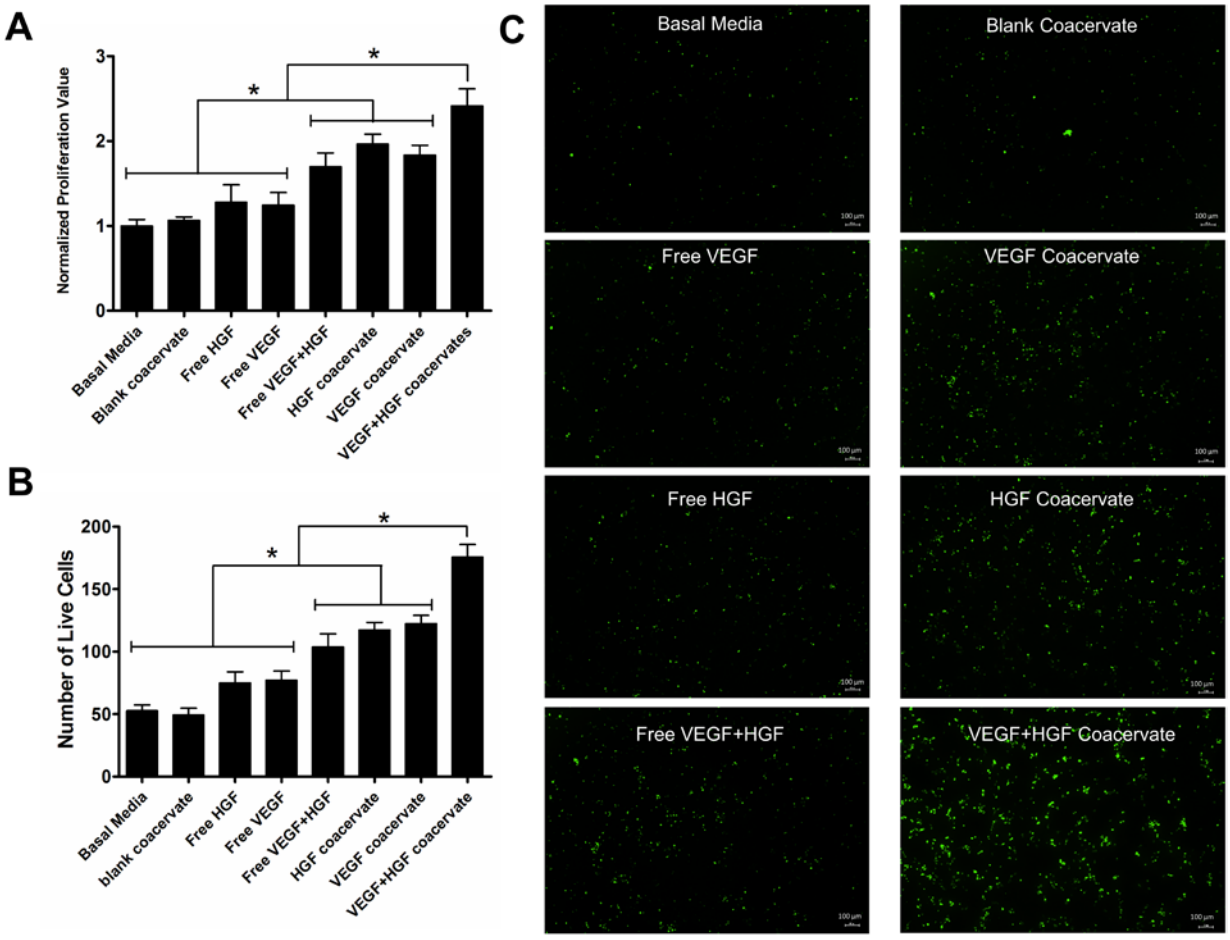

Figure 14. Endothelial cell proliferation and live cell count assays. Treatment groups with 30ng/ml concentration for each of VEGF or HGF were applied to cell culture wells with seeded HUVEC. (A) One day after incubation, BrdU cell proliferation assay was performed and absorbance was recorded (n=3 wells/group). Data is presented as a fold-change from the basal media (n=3 wells/group). (B) **Live endothelial cell number was quantified after 3 days incubation in 0.67mm^2 fields in the center of wells (n=3 wells/group).** (C) **Microscope fluorescent images of calcein-stained HUVEC in 4mm^2 fields. Bars indicate means ± SD. * p value <0.05.**

To verify that cell proliferation continued beyond 1 day and that the cells were still viable, we used Calcein staining after 3 days culture and counted the number of live ECs. The results were similar to that of the proliferation assay with combined VEGF and HGF showing significantly more live cells ($p<0.05$) compared to each GF alone, and coacervate delivery of

both factors inducing significantly higher viability ($p<0.001$) than all groups (**Figure 14B,C**). These results show the benefit of dual delivery of VEGF and HGF using the coacervate on endothelial cell proliferation, a key process in angiogenesis.

To investigate the tubulogenesis potential of coacervate delivery of HGF and VEGF, we performed an established HUVEC tube formation assay within fibrin gels [269, 282]. This 3D angiogenesis assay better preserves the vessel architecture and represents a closer mimicking of in vivo events than 2D models [282, 283]. After 3 days of culture, no significant tube formation was observed in the basal media or blank coacervate control groups (**Figure 15A**). VEGF and HGF each induced tube formation which was improved with coacervate delivery compared to free-form application, and their coacervate dual delivery induced the most well-interconnected, thick endothelial tubes (**Figure 15A**).

Both GFs applied together in free-form significantly increased EC tube number ($p<0.05$) and thickness ($p<0.05$) compared to each GF alone. Each GF alone delivered by the coacervate significantly increased the EC tube number ($p<0.05$) and thickness ($p<0.01$) compared to each GF alone in free-form**.** More importantly, coacervate delivery of both GFs administered together significantly increased EC tube number ($p<0.05$) and thickness ($p<0.01$) compared to all groups (**Figure 15B,C**). Although combining VEGF and HGF induced more and thicker tubes in both free-form and using the coacervate, this combination interestingly did not have a significant effect on tube length ($p>0.05$) compared to delivery of each GF alone. However, the coacervate groups did induce significantly longer tubes ($p<0.01$) than their corresponding free-form groups (**Figure 15D**).

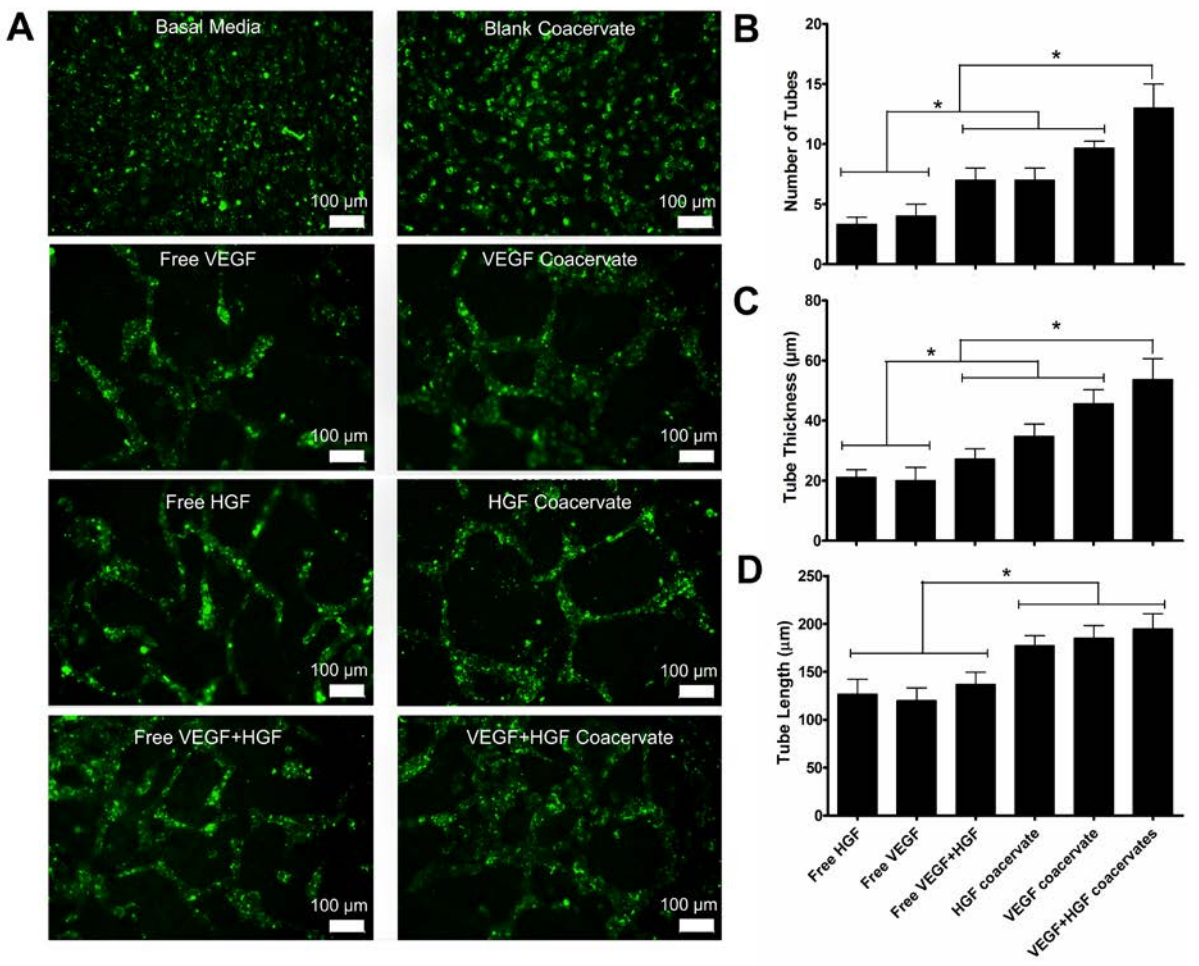

Figure 15. Endothelial tube formation assay between fibrin gels. HUVEC were seeded on bottom gel and specific treatment groups (n=3 wells/group) were added to top gel and incubated for 3 days. (A) Microscope fluorescent images of calcein-stained endothelial tubes formed in different groups. (B) Number of endothelial tubes, (C) tube thickness, and (D) tube length were quantified by microscope imaging analysis software in 0.67 mm^2 fields at center of wells. Bars indicate means ± SD. * p value < 0.05.

As it has been previously reported, our results confirm the stronger angiogenic effects of VEGF and HGF when applied together to promote angiogenesis [265-268, 280]. A gene expression profiling study demonstrated that there exists distinct signal transduction pathways for VEGF and HGF in vascular endothelial cells with little overlap between the genes regulated by each [284]. This could serve as an explanation to the synergism between VEGF and HGF

leading to beneficial effects that exceed the application of each alone. Additionally, we demonstrated in this study that controlled dual delivery of the two factors using a polycation:heparin coacervate does not impede the cooperation between the two GFs, but rather enhances it compared to free-form GF application. In the design of the coacervate platform, we were inspired by the stable ternary complex formed by heparin, fibroblast growth factor, and its cell receptor, whereby heparin facilitates their association [236, 285]. We mimicked the heparin-binding domain of fibroblast growth factor receptor (FGFR) which contains many basic amino acids to create the synthetic polycation PEAD. Utilizing heparin in its native conformation facilitates the GF-receptor interaction and likely results in the improved angiogenic effects demonstrated in this study. As we have demonstrated with other heparin-binding GFs, the coacervate serves as an effective delivery vehicle for VEGF and HGF. The coacervate sustained their release for at least 3 weeks, localized their actions, and potentiated their bioactivities compared to free-form GFs. This study also validated the use of this delivery platform for sustained delivery of multiple factors, motivating future investigations of other GF combinations and simultaneous and sequential delivery of multiple proteins.

2.4 CONCLUSIONS

Many ischemic tissues cannot recover their normal functions and structure without proper vascular support. Angiogenesis is a complicated process which involves the signaling of many proteins. Therefore, regulating the local availability of different GFs can prove a powerful tool in controlling tissue regeneration. The coacervate may serve as an effective system to deliver GFs either individually or in combinations. In this study, the coacervate displayed its ability to

load VEGF and HGF with high efficiency and sustain their release for at least 3 weeks. Combining VEGF and HGF yielded strong angiogenic effects, shown by endothelial cell proliferation and tube formation assays. More importantly, we demonstrated that coacervate-based dual delivery of these factors had more profound angiogenic effects than free GFs and controlled delivery of each GF alone, suggesting the potential benefit of this approach for therapeutic angiogenesis in vivo.

3.0 SEQUENTIAL DELIVERY OF VEGF AND PDGF TO PROMOTE THERAPEUTIC ANGIOGENESIS AND HEART FUNCTION AFTER MI

Note: The research work of chapter 3 was published in the Journal of Controlled Release. H.K. Awada, N.R. Johnson, Y. Wang. 2015. "Sequential delivery of angiogenic growth factors improves revascularization and heart function after myocardial infarction". Journal of Controlled Release 207:7-17.

Treatment of ischemia through therapeutic angiogenesis still faces significant challenges. Growth factor (GF)-based therapies can be more effective when concerns such as GF spatiotemporal presentation, bioactivity, bioavailability, and localization are addressed. During angiogenesis, vascular endothelial GF (VEGF) is important at an early stage to initiate neovessel formation, while platelet-derived GF (PDGF) is needed later to stabilize the neovessels. The spatiotemporal delivery of multiple bioactive GFs involved in angiogenesis, in a close mimic to physiological cues, holds great potential to treat ischemic diseases. To achieve sequential release of VEGF and PDGF, we embedded VEGF in fibrin gel and PDGF in a heparin-based coacervate that is distributed in the same fibrin gel. In vitro, we show the benefits of this controlled delivery approach on cell proliferation, chemotaxis, and microvessel formation. A myocardial infarction (MI) rat model demonstrated the effectiveness of this delivery system in improving cardiac function, angiogenesis, cardiomyocyte survival, and

reducing ventricular wall thinning, fibrosis, and inflammation in the infarct zone 4 weeks after MI. Collectively, our results suggest that this delivery approach mitigated the injury caused by MI and may serve as a new therapy to treat ischemic hearts.

3.1 INTRODUCTION

Ischemic heart disease is a leading cause of morbidity and mortality in the United States. In 2010, the estimated direct and indirect cost of heart disease was approximately $200 billion. In that year, myocardial infarction (MI) was prevalent in 7.6 million Americans. Approximately, 15% of the people who experience a heart attack (MI) in a given year will die of it [2]. During MI, insufficient blood supply to a region of the heart muscle (infarct zone) leads to cell death and pathological remodeling which often progresses to heart failure over time [5]. Therapeutic angiogenesis aims to restore blood flow to the affected ischemic heart muscle by new blood vessel formation from existing vasculature [16, 27, 286]. Revascularization by pro-angiogenic therapies has so far failed to provide satisfactory outcomes in clinical trials [20, 287, 288]. Bolus injections of single growth factors (GFs) usually lead to limited efficacy because of loss of bioactivity, missing critical signals in the cascade of events that lead to stable angiogenesis, among others. An effective angiogenesis-based therapy can be developed when a comprehensive understanding of angiogenic mechanisms becomes available [256, 288]. Repair and regeneration strategies should focus on utilizing the GFs that play vital roles in the process of angiogenesis, as well as the need to administer them spatiotemporally and in bioactive conformations [20, 195, 208, 255, 287].

Many studies have shown that GFs such as fibroblast GF-2 (FGF-2), vascular endothelial GF (VEGF), angiopoietin-2 (Ang-2) are key factors in triggering angiogenesis, but these factors alone may result in leaky and immature blood vessels that are susceptible to early regression [35, 36]. Other GFs such as platelet-derived GF (PDGF) and angiopoietin-1 (Ang-1) help stabilize neovessels [289, 290]. Among potential angiogenic candidates, VEGF and PDGF are promising due to their potency, specificity, and cardioprotective roles [17, 20, 27, 249]. VEGF, an endothelial-specific factor, triggers the process through endothelial cell (EC) sprouting, proliferation, migration, and lumen formation, and is thus primarily needed in the first few days of angiogenesis [17, 291, 292]. After lumenal formation, mural cells are recruited by PDGF to cover the neovessels and provide stabilization; therefore PDGF is required at a later stage of angiogenesis to prevent vessel regression or the formation of aberrant and leaky vessels [17, 289]. It has been shown that early-stage angiogenic factors can have antagonistic effects on late-stage factors and vice versa, when present simultaneously [39, 40, 43]. Therefore, it appears imperative to sequentially administer these two GFs to imitate their physiological presence during angiogenesis.

To control the spatiotemporal cues and protect the bioactivity of VEGF and PDGF, we developed a controlled delivery system composed of fibrin gel and a recently developed biocompatible heparin-based coacervate that we characterized in previous reports [235, 293]. Fibrin gel, formed through the polymerization of fibrinogen by thrombin, is commercially available and has been used for protein and cell delivery [210]. Complex coacervates are formed by mixing oppositely charged polyelectrolytes resulting in spherical droplets of organic molecules held together noncovalently and apart from the surrounding liquid and have shown potential in sustained protein delivery [233, 294]. VEGF was embedded into the fibrin gel,

while PDGF was loaded into the coacervate then embedded into the gel (**Figure 16A**). The coacervate was used to sustain the release of PDGF. This system provided rapid release of VEGF followed by slower and sustained release of PDGF from a single injection. Here we report the effects of sequentially delivered VEGF and PDGF on revascularization and heart function after MI in rats.

3.2 MATERIALS AND METHODS

3.2.1 Release assays of VEGF and PDGF

Poly(ethylene argininylaspartate diglyceride) (PEAD) was synthesized as previously described [237]. The release assays (n=3) were performed using 100ng of $VEGF_{165}$ and 100ng of PDGF-BB (PeproTech, Rocky Hill, NJ). All solutions were prepared in 0.9% saline. For the release assay of both factors from the coacervate, PDGF or VEGF coacervates were made by mixing 1µl of 100ng/µl of the GF with 1µl of 10mg/ml heparin first (Scientific Protein Labs, Waunakee, WI), then with 5µl of 10mg/ml of PEAD, at PEAD:heparin:GF mass ratio of 500:100:1, creating 7µl coacervate solution for each GF. Solution was diluted up to 100µl.

For the release assay of the two GFs from the fibrin gel-coacervate composite, the composite was made by mixing 83µl of 20mg/ml fibrinogen solution (Sigma-Aldrich, St. Louis, MO) containing 100ng of unbound VEGF with 7µl of PDGF coacervate solution (as described above), 5µl of 1mg/ml aprotonin solution (Sigma-Aldrich, St. Louis, MO), and lastly adding 5µl of 1mg/ml thrombin solution (Sigma-Aldrich, St. Louis, MO). A 100µl of 0.9% saline was deposited on top of the composite gel.

For both release assays at 1h, solutions were centrifuged at 12,100g for 10 min and supernatant was aspirated and stored at -80°C to detect amount of released GFs by ELISA kits (PeproTech, Rocky Hill, NJ). A fresh 100µl of 0.9% saline solution was deposited on top and the procedure was repeated at 16h, 1, 4, 7, 14, and 21 days. The samples were incubated at 37°C. After ELISA procedure was performed, the absorbance at 450/540 nm was measured by a SynergyMX plate reader (Biotek, Winooski, VT). Standard solutions (n=3) that contained 100ng of each of free VEGF and PDGF in 100µl of 0.9% saline were prepared to create standard curves and determine total release.

3.2.2 Smooth muscle cell chemotaxis assay

Chemotactic media was prepared as 500µl MCDB-131+10% fetal bovine serum (FBS) per well in a 24-well plate with group-specific addition of saline (basal media), empty vehicle, or 100ng free PDGF or in the coacervate. Culture inserts of 8µm pore size (BD Falcon, Franklin Lakes, NJ) were placed in each well and 10^4 isolated baboon smooth muscle cells (SMCs) were pipetted into the insert in 200µl basal media and plate was incubated at 37°C. After 12h, cells remaining inside the insert were removed from the upper surface of the membrane with a cotton swab. Cells that had migrated to the lower surface of the membrane were then fixed in methanol for 15 min. Cells were incubated for 15 min in the dark with PicoGreen fluorescent dye from Quant-iT PicoGreen dsDNA Kit (Molecular Probes, Eugene, OR), diluted 200-fold to working concentration in DPBS. Cells were imaged with a fluorescent microscope (Eclipse Ti; Nikon, Tokyo, Japan) and images were taken in the center of each well and counted manually (n=3 wells/group).

3.2.3 Endothelial and smooth muscle cells proliferation assays

Human umbilical vein endothelial cells (HUVEC) (ATCC, Manassas, VA) or isolated baboon SMCs were seeded at 10^4 cells per well in a 96-well plate and cultured in EGM-2 media (Lonza, Walkersville, MD) or MCDB131+0.2% FBS media, respectively. Group-specific additions (n=3 wells/group) were made to media with GF concentrations at 20ng/ml per well for SMCs and 25ng/ml of each GF per well for HUVEC. The plates were incubated for 48 h at 37°C. 20µl of pre-prepared BrdU label was then added for 4 h and the proliferation assays were performed according to kit's instructions (Millipore, Temecula, CA). The absorbance at 450/540nm was measured by a SynergyMX plate reader. Absorbance proliferation values were normalized to the average basal media value (n=3 wells/group). The endothelial proliferation assay compared the 4 groups: basal media, empty vehicle, Free VEGF+PDGF, and sequentially delivered VEGF+PDGF. The SMC proliferation assay compared the 4 groups: basal media, empty vehicle, free PDGF, and PDGF coacervate.

3.2.4 Ex vivo rat aortic ring assay

Thoracic rat aortae (n=3 per group) were dissected according to established protocols [295, 296], cleaned from fibro-adipose tissue, and cut into approximately 1.5mm ring segments. Rings were serum-starved overnight in serum-free endothelial basal medium (EBM). Next day, fibrin gels were made by dissolving 6mg/ml bovine fibrinogen (Sigma-Aldrich, St. Louis, MO) in EGM-2 media, added in 150µl volumes per well of a 24-well plate, activated with 150µl of 0.1mg/ml thrombin solution (Sigma-Aldrich, St. Louis, MO) in EGM-2, swirled gently to mix and solidified at 37°C. The aortic rings were embedded in the center of the 3D fibrin matrix

(one per well) that contained different treatment groups (GF dose of 250ng) with luminal axis perpendicular to the bottom of the well in a 24-well plate. 500µL of EBM was placed on top of gel and plate was incubated at 37°C for 6 days. Rings were then imaged using brightfield (BF) microscopy and quantified in terms of microvasculature sprouting area (n=3 wells/group). The aortic ring assay compared the 4 groups: basal media, empty vehicle, free VEGF+PDGF, and sequentially delivered VEGF+PDGF.

3.2.5 Rat acute myocardial infarction model

University of Pittsburgh Institutional Animal Care and Use Committee (IACUC) approval was obtained prior to beginning all animal studies. MI and injections were performed as previously described [297]. Briefly, 6-7 week old (175-225g) male Sprague-Dawley rats (Charles River Labs, Wilmington, MA) were anesthetized first then maintained with 2% isoflurane at 0.3L/min (Butler Schein, Dublin, OH), intubated, and connected to a mechanical ventilator to support breathing during surgery. The body temperature was maintained at 37°C by a hot pad. The ventral side was shaved and a small incision was made through the skin. Forceps, scissors, and q-tips were used to dissect through the skin, muscles, and ribs. Once the heart was visible, the pericardium was torn. MI was induced by permanent ligation of the left anterior descending (LAD) coronary artery using a 6-0 polypropylene suture (Ethicon, Bridgewater, NJ). Infarct was confirmed by macroscopic observation of a change in color from bright red to light pink in the area below the ligation suture. Five minutes after the induction of MI, different treatment and control solutions were injected intramyocardially at 3 equidistant points around the infarct zone

using a 31 gauge needle (BD, Franklin Lakes, NJ). Groups included: saline, empty vehicle, free VEGF+PDGF, or sequentially delivered VEGF+PDGF.

The saline group (n=7) underwent the surgery in which MI was induced and 100µl of 0.9% sterile saline was injected around the infarct region. The empty group (n=7) underwent the surgery in which MI was induced and 100µl of empty fibrin gel-coacervate composite was injected around the infarct region. The free VEGF+PDGF group (n=7) underwent the surgery in which MI was induced and 100µl of 0.9% sterile saline containing 1.5µg each of free VEGF and PDGF was injected around the infarct region. The sequentially delivered VEGF+PDGF (n=7) underwent the surgery in which MI was induced and 100µl of fibrin gel-coacervate composite loaded with the GFs was injected around the infarct region.

The GF-loaded fibrin gel-coacervate composite was prepared as follows: PDGF coacervate was made by mixing 1.5µl of 1µg/µl of PDGF (1.5µg dose) with 3µl of 5mg/ml heparin first, then with 3µl of 25mg/ml of PEAD, at PEAD:heparin:PDGF mass ratio of 50:10:1, creating 7.5µl PDGF coacervate solution, which was added to 82.5µl of 20mg/ml fibrinogen solution containing 1.5µg VEGF, and then 5µl of 1mg/ml aprotonin was added (Sigma-Aldrich, St. Louis, MO). Lastly, 5µl of 1.5mg/ml thrombin (Sigma-Aldrich, St. Louis, MO) was added and the total solution was injected shortly before gelation occurred, approximately 40 seconds after mixing (**Figure 16A**). All solutions were prepared in 0.9% sterile saline. The chest was closed and the rat was allowed to recover. At multiple time points, rats were imaged using echocardiography. At 4 weeks after MI, animals were sacrificed and hearts were harvested for histological and immunohistochemical evaluations.

3.2.6 Echocardiography

Echocardiography was performed 2 days before surgery (baseline) and at 2, 14, and 28 days post-MI surgery to evaluate cardiac function. Rats (n=7 per group) were anesthetized then maintained with 1-1.5% isoflurane gas throughout the echocardiographic study. Rats were placed in the supine position, immobilized on a heated stage equipped with echocardiography, and the hair in the abdomen was removed. The body temperature was maintained at 37°C. Short-axis videos of the left ventricle (LV) by B-mode were obtained using a high-resolution in vivo small animal imaging system (Vevo 2100, Visual Sonics, Ontario, Canada) equipped with a high-frequency linear probe (MS400, 30 MHz) (FUJIFILM VisualSonics, Canada). End-systolic (ESA) and end-diastolic (EDA) areas were measured using NIH ImageJ and fractional area change (FAC) was calculated as: [(EDA-ESA)/EDA]×100%. Percent improvements of one group over another were calculated as the difference between the % drops in FAC values of the first and second groups divided by the higher % drop of the two groups.

3.2.7 Histological analysis

At 4 weeks post-infarction, rats were sacrificed by injecting 2ml of saturated potassium chloride (KCl) solution (Sigma Aldrich, St. Louis, MO) in the LV to arrest the heart in diastole. Hearts were harvested and frozen in O.C.T compound (Fisher Healthcare, Houston, TX). Specimens were sectioned at 6μm thickness from apex to the ligation level with 500μm intervals. Sections were fixed in 2-4% paraformaldehyde (fisher Scientific, Fair Lawn, NJ) prior to all staining procedures.

Hematoxylin and eosin (H&E) staining was performed for general evaluation. H&E stained slides were randomly selected (n=5-6 per group) and the ventricular wall thickness in the infarct zone was measured near the mid-section level of the infarct tissue using NIS Elements AR imaging software (Nikon Instruments, Melville, NY).

For assessment of fibrosis, picrosirius red staining was used to stain collagen fibers and imaged under polarized light. The fraction area of collagen deposition in the infarct region was measured by NIS Elements AR software near the mid-section level of the infarct tissue (n=5-6 per group). An object count tool was used to include RGB pixels specific to the stained collagen fibers in the infarct area by defining a proper threshold value.

3.2.8 Immunohistochemical analysis

For evaluation of inflammation, a mouse anti-rat CD68 (1:100, Millipore, Temecula CA), a pan-macrophage marker, was used followed by an Alexa fluor 594 goat anti-mouse antibody (1:200, Invitrogen, Carlsbad, CA). Slides were counterstained with 4',6-diamidino-2-phenylindole (DAPI) (Invitrogen, Carlsbad, CA). For quantification near the mid-section level of the infarct tissue, CD68-positive cells were counted in two opposite regions of the infarct border zone, averaged, and reported per mm^2 areas (n=4-5 per group).

For evaluation of angiogenesis, ECs were detected by a rabbit polyclonal von Willebrand factor (vWF) antibody (1:200, US Abcam, Cambridge, MA) followed by an Alexa fluor 594 goat anti-rabbit antibody (1:200). Mural cells were detected by a FITC-conjugated anti-α-smooth muscle actin (α-SMA) monoclonal antibody (1:500, Sigma Aldrich, St. Louis, MO). Slides were last counterstained with DAPI. For quantification near the mid-section level of the infarct tissue, vWF-positive vessels (defined as those with lumen) and α-SMA-positive

vessels were counted in two opposite regions of the infarct border zone, averaged, and reported per mm^2 areas (n=4-5 rats per group).

For evaluation of cardiac muscle viability, a mouse anti-rat cardiac troponin I (cTnI) antibody (1:200, US Abcam, Cambridge, MA) followed by an Alexa fluor 488 goat anti-mouse antibody (1:200, Invitrogen, Carlsbad, CA). Slides were counterstained with DAPI. The fraction area of viable cardiac muscle in the infarct region was measured by NIS Elements AR software near the mid-section level of the infarct tissue (n=4-5 per group). An object count tool was used to include RGB pixels specific to the stained viable cardiac muscle in the infarct area by defining a proper threshold value.

3.2.9 Statistical analysis

Results are presented as means ± standard deviations (SD). GraphPad Prism 5.0 software (La Jolla, CA) was used for statistical analysis. Statistical differences between groups were analyzed by one-way ANOVA (multiple groups) or two-way repeated ANOVA (repeated echocardiographic measurements) with 95% confidence interval. Bonferroni multiple comparison test was performed for ANOVA post-hoc analysis. Statistical significance was set at $p<0.05$.

3.3 RESULTS

3.3.1 Fibrin gel-coacervate system achieves sequential delivery

Previously, we studied VEGF release from the coacervate which was relatively slow likely because of its mid-range affinity for heparin (Dissociation constant k_d=165nM) [272, 293]. With a weaker heparin-binding affinity (k_d=752nM), PDGF release from the coacervate occurs faster than for VEGF (**Appendix A**) [298]. A proper therapeutic angiogenesis process needs a sequential release of VEGF first followed by PDGF. Therefore, the coacervate alone was not enough to achieve sequential release (**Appendix A**). In order to obtain faster VEGF release, we embedded it in a fibrin gel without loading it into the coacervate. We then loaded PDGF in the coacervate and embedded it in the same fibrin gel to sustain its release (**Figure 16A**). The loading efficiencies were 87% for VEGF and 97% for PDGF as observed 1 hour after loading. Approximately 44% of the VEGF released by day 1, while only 14% of PDGF released during the same period (**Figure 16B**). Having a significant release of VEGF by day 1 might prove beneficial for angiogenesis and heart function after MI [299]. This delivery system achieved sequential release kinetics, where 95% of VEGF was released by 1 week and only 40% of PDGF, which continued to release up to 75% after 3 weeks (**Figure 16B**). The in vivo release rate can be further influenced by fibrinolysis, hydrolytic degradation of the PEAD polycation, enzymatic degradation by esterases and heparinases, and dissociation of the coacervate in an ionic environment. Thus, in vivo release is expected to be faster. Overall, the release kinetics attained with the fibrin gel-coacervate delivery vehicle may enhance the formation of neovasculature based on the physiological roles of VEGF and PDGF during angiogenesis [17, 289].

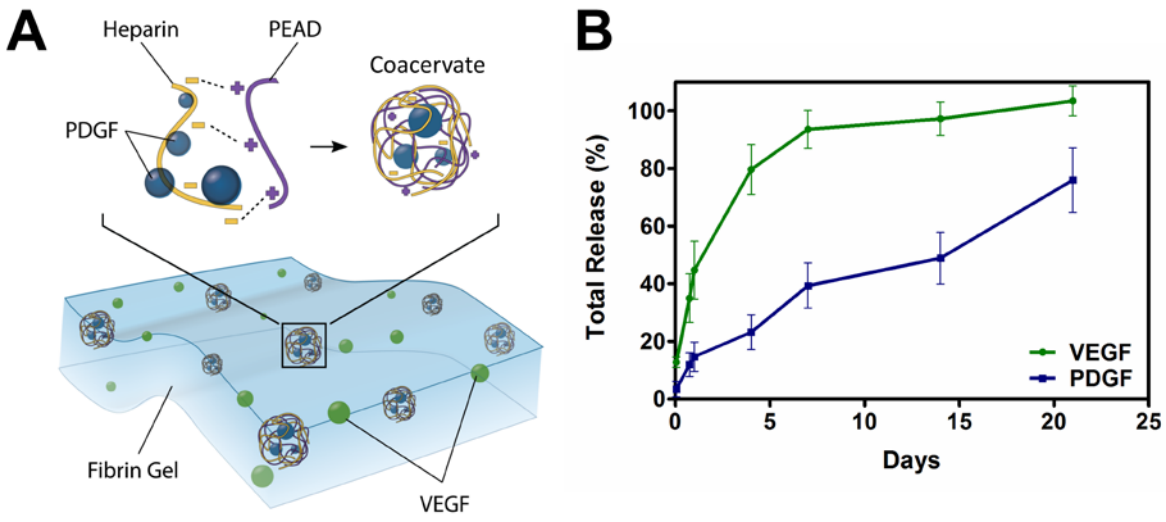

Figure 16. (A) The delivery system was comprised of a fibrin gel embedding VEGF and PDGF-loaded coacervates. The coacervate was formed through electrostatic interactions by combining PDGF with heparin then with PEAD polycation. (B) The delivery system described achieved sequential quick release of VEGF followed by a sustained release of PDGF. Data are presented as means ± SD (n=3 per group).

3.3.2 PDGF coacervate induces SMC chemotaxis and proliferation

We reported previously on VEGF bioactivity in free form and using the coacervate [293]. Here, we evaluated the effect of PDGF released from the coacervate on SMC migration using a porous cell culture inserts. Free PDGF induced significantly more SMC migration compared to controls ($p<0.001$), however the same dose of PDGF delivered by the coacervate had the greatest chemotactic effect compared to all groups ($p<0.001$) (**Figure 17A,B**). The empty vehicle was also demonstrated to be inert with no effect on cell migration compared to basal media alone.

We also tested the effect of coacervate-released PDGF on SMC proliferation using a BrdU assay. BrdU is a thymidine analog that incorporates into newly synthesized DNA strands

of actively proliferating cells. Again, we observed no significant effect of the empty vehicle compared to basal media control. Both free PDGF and PDGF coacervate induced significant SMC proliferation compared to control groups ($p<0.01$). However, PDGF coacervate also increased cell proliferation compared to free PDGF ($p<0.01$) (**Figure 17C**). Collectively, these results demonstrate that PDGF released from the coacervate is highly bioactive and can stimulate proliferation and migration of SMCs in vitro.

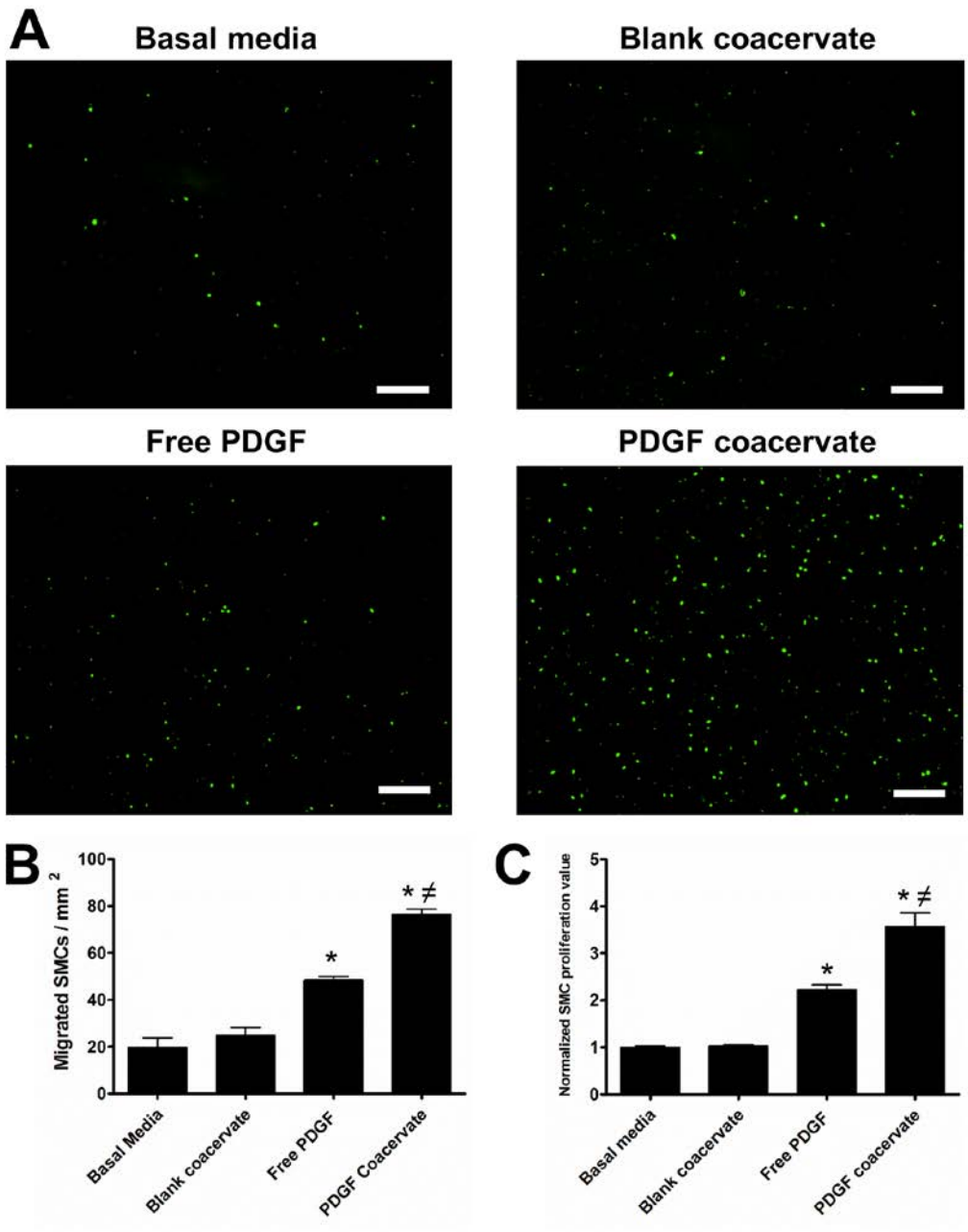

Figure 17. (A) After 12h, images show more migrated SMC through the cell culture insert membrane towards PDGF coacervate compared to other groups. Scale bar=250µm. (B) **Although free PDGF significantly induced migration compared to control, it was less than PDGF coacervate which significantly enhanced migration compared to all other groups.** (C) **After 48h, free PDGF induced significantly more SMC proliferation than controls, while PDGF coacervate induced significantly more proliferation than all groups. Data are presented as means ± SD (n=3 per group). * p<0.05 vs basal media. ≠ p<0.05 vs free PDGF.**

3.3.3 Sequential delivery improves endothelial proliferation and vessel sprouting

In order to evaluate the potential benefit of sequential release of VEGF and PDGF, we performed EC proliferation and aortic ring vessel sprouting assays. We hypothesized that high initial PDGF concentrations would reduce the effect of VEGF on ECs. Free VEGF+PDGF induced significantly more proliferation than basal media ($p<0.01$), but not more than empty vehicle ($p>0.05$), which showed no difference compared to basal media. However, sequentially delivered VEGF+PDGF induced significantly more proliferation than both controls and free GFs ($p<0.001$) (**Figure 18A**).

In the aortic ring assay, free VEGF+PDGF induced significantly more microvessel outgrowth and greater sprouting area from ring segments compared to basal media ($p<0.01$), but not to empty vehicle ($p>0.05$). In contrast, sequential delivery showed significantly larger sprouting area than all groups ($p<0.001$) (**Figure 18B,C**). Taken together, these experiments suggest that PDGF has some antagonistic effect on VEGF-mediated angiogenic responses in vitro which can be avoided by a sequential delivery approach.

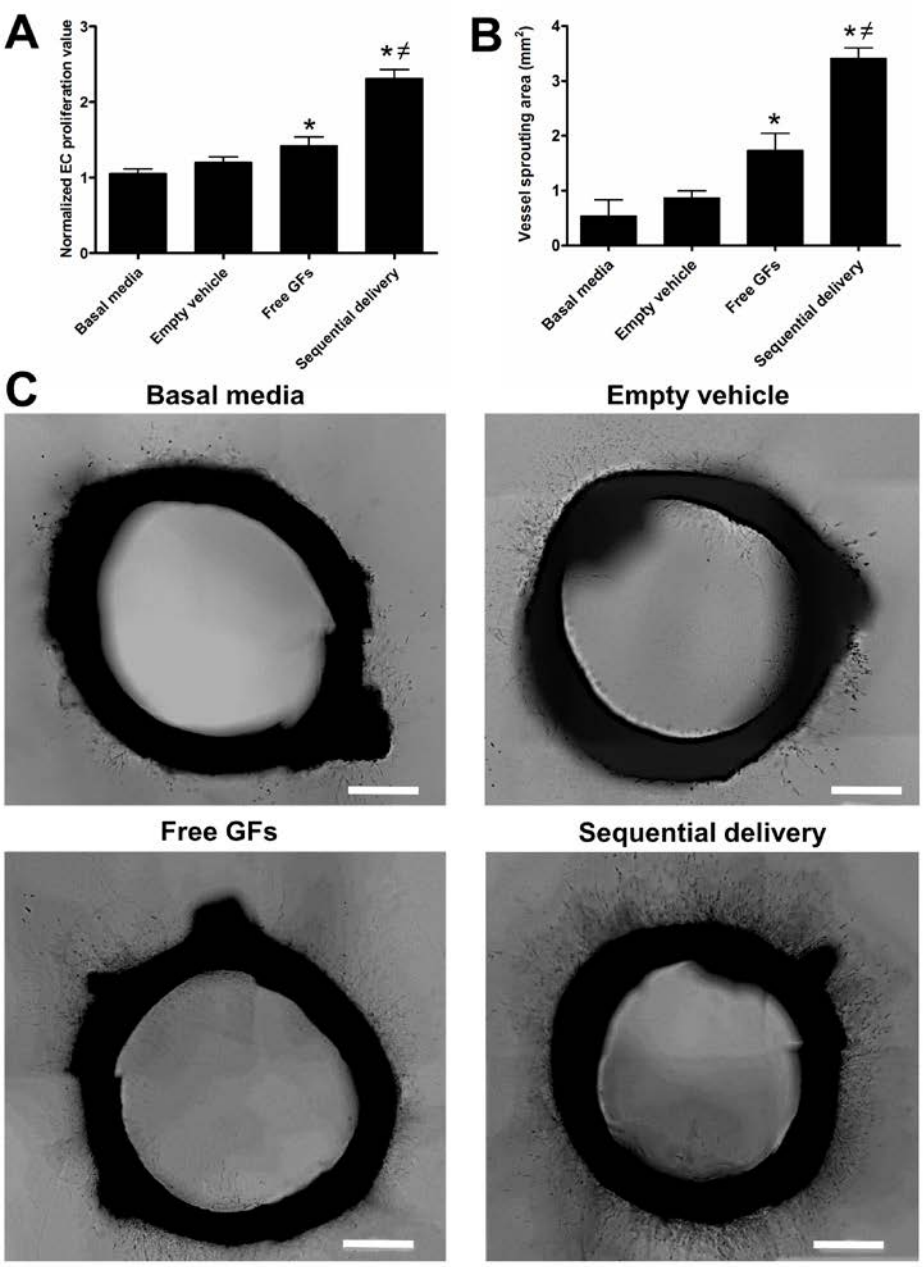

Figure 18. After 48h, free VEGF+PDGF induced significantly more endothelial proliferation than basal media, while sequential delivery of VEGF and PDGF induced significantly more proliferation than all groups. (B) After 6 days, rat aortic ring assay shows that free VEGF+PDGF induced significantly larger microvasculature sprouting area than basal media. Sequential delivery induced significantly larger sprouting areas compared to all groups. (C) Representative images show microvasculature formation around rat aortic rings, with more sprouting observed in the sequential delivery group. Data are presented as means ± SD (n=3 per group). * p<0.05 vs basal media. ≠ p<0.05 vs free GFs. Scale bar=500μm.

3.3.4 Sequential delivery of VEGF and PDGF improves overall cardiac function

We next evaluated the in vivo effect of sequential delivery in a rat MI model comparing saline, empty vehicle, free VEGF+PDGF, and sequentially delivered VEGF+PDGF. We evaluated changes in LV contractility using 2-D echocardiography and reported heart function as fractional area change (FAC). ESA and EDA values were statistically similar for all groups ($p>0.05$) suggesting little to no effect on ventricular dilation over the time period evaluated (**Figure 19A,B**).

MI induction was confirmed by a significant drop in FAC 2 days after infarction (**Figure 19C**). No significant differences were found between groups at baseline or at day 2 ($p>0.05$). At 2 weeks, sequential delivery group showed a significant improvement in cardiac function compared to all other groups ($p<0.001$) (**Figure 19C**). No significant differences were found between saline, empty vehicle, and free GFs values at 2 weeks ($p>0.05$). At 4 weeks, FAC declined slightly for all groups, but sequential delivery group maintained its improvement in cardiac function with a significantly higher FAC compared to all groups ($p<0.001$). FAC values were approximately 30% for saline, 32% for empty vehicle, 34% for free GFs groups, and 44% for sequential delivery (**Figure 19C**). The sequential delivery value represented a 66% improvement over saline at 4 weeks, a slight decline from 68% at 2 weeks. The ability of sequential delivery to improve and maintain the cardiac function 4 weeks after MI stresses the importance of spatiotemporal presentation towards the effectiveness of VEGF and PDGF.

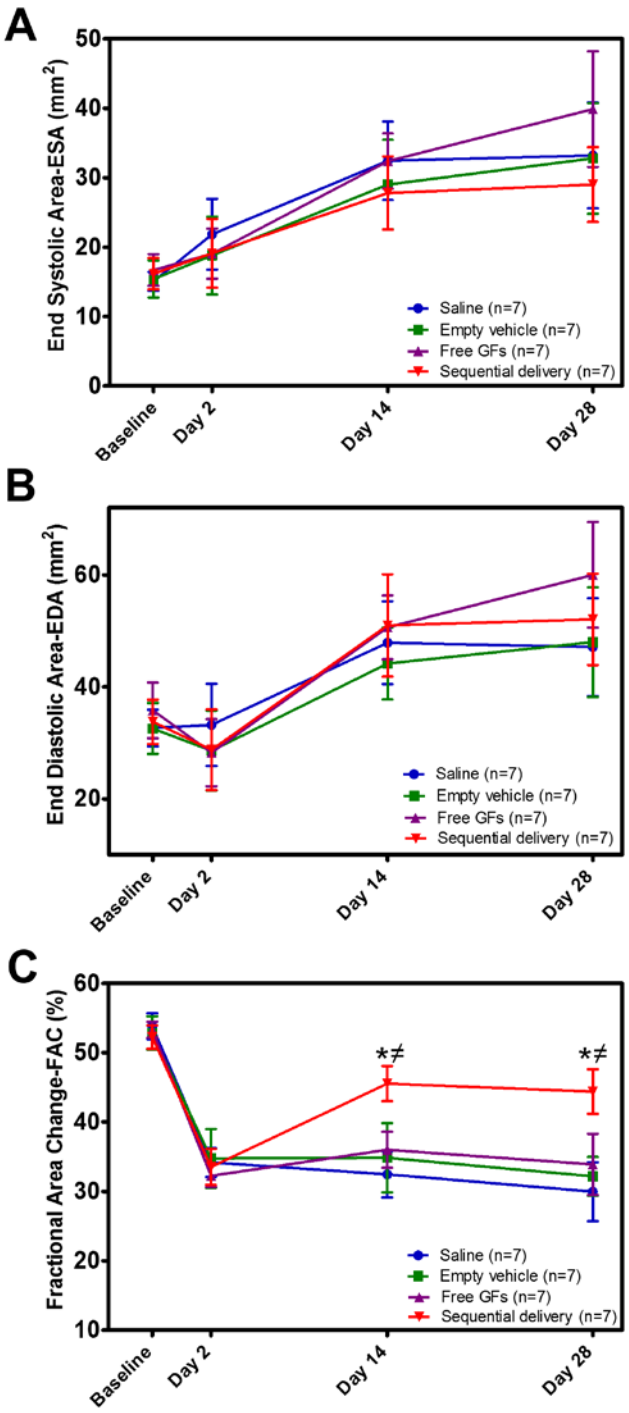

Figure 19. (A) End-systolic area (ESA) and (B) End-diastolic area (EDA) showed no statistical difference between groups during the evaluated period(C) Fractional area change (FAC) reflected a significantly improved cardiac contractility at 2 wks and maintained at 4 wks in the sequential delivery group compared to all groups. Data are presented as means ± SD (n=7 per group). * $p<0.05$ vs saline. ≠ $p<0.05$ vs free GFs.

3.3.5 Sequential delivery reduces ventricular wall thinning and fibrosis in the infarcted myocardium

After evaluation of overall cardiac function, we performed investigations at the tissue level using histology and immunohistochemistry. At 4 weeks, H&E stained tissue showed increased granulated scar tissue areas with significantly thinner LV walls in the infarct region in saline, empty vehicle, and free GFs groups with no statistical differences in wall thicknesses between them ($p>0.05$). In contrast, sequential delivery showed significantly thicker LV walls compared to all groups ($p<0.01$) with less scar tissue and granulation replacing normal cardiac muscle (**Figure 20A,B**). This demonstrates the benefit of our therapy in preserving the ventricular wall structure.

The extent of fibrosis was assessed using picrosirius red staining. Collagen deposition was quantified and found to be significantly less in the sequential delivery group ($p<0.05$) compared to all other groups which contained dense deposition of fibrillar collagen along the LV wall and extended to the infarct border zone (**Figure 20C,D**). The area fractions of collagen deposition were approximately 36% for saline, 32% for empty vehicle, 31% for free GFs, and 19% for sequential delivery (**Figure 20C**). The reduced fibrosis and LV wall thinning due to sequential delivery of VEGF and PDGF is likely a contributing factor to the enhanced cardiac contractility since less fibrotic tissue reduces the stiffening of the ventricular walls and the extent of cardiac remodeling that occurs after MI [300].

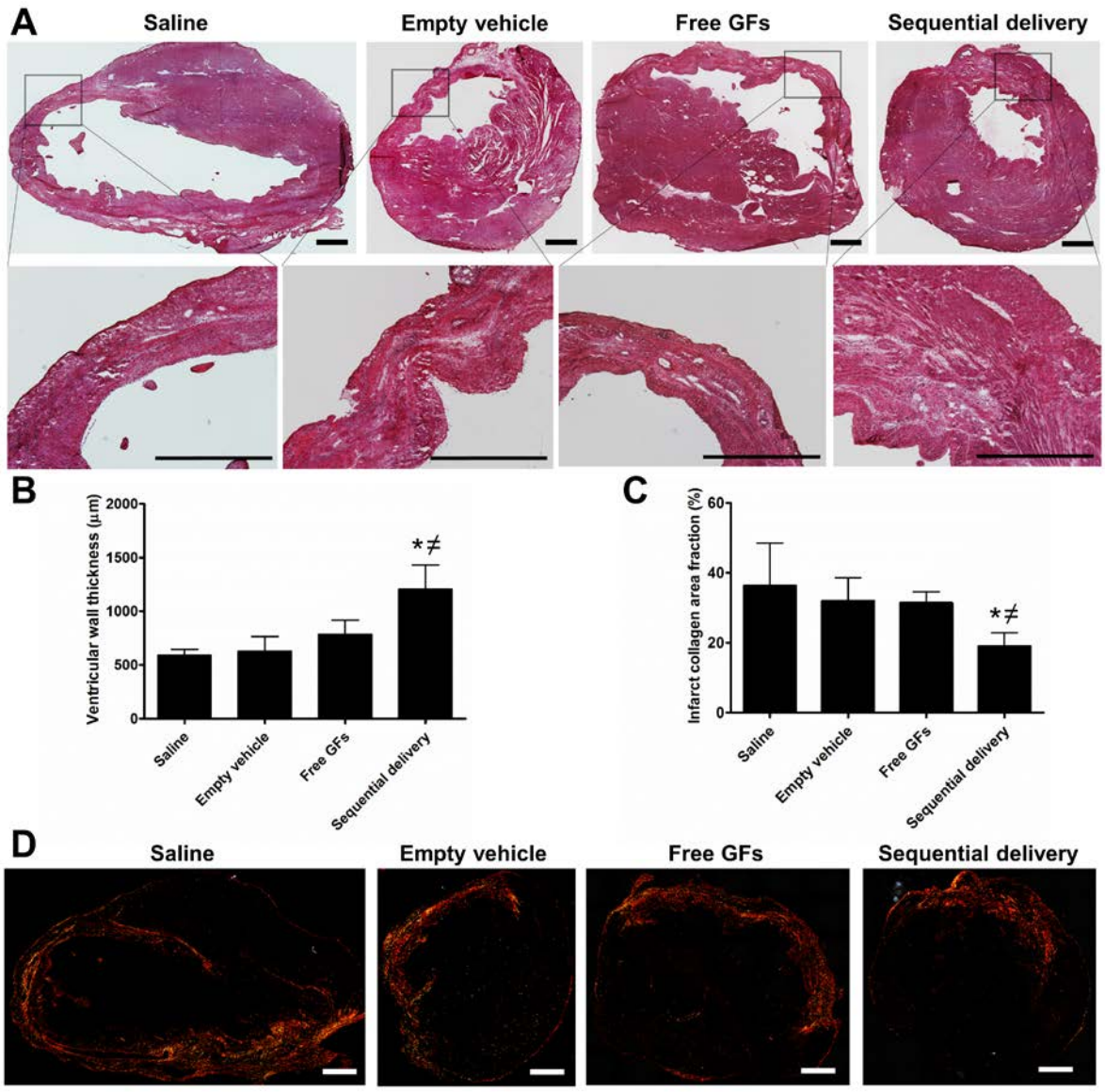

Figure 20. (A) At 4 weeks, H&E staining showed ventricular wall thinning with damaged cardiac muscle surrounded by scar tissue in saline, empty vehicle, and free GFs groups. However, these damages were apparently alleviated in the sequential delivery group. Scale bar=1000µm. Quantitative analysis showed (B) **significantly reduced ventricular wall thinning and** (C) **significantly reduced fibrosis in the sequential delivery group compared to all groups.** (D) **At 4 weeks, picrosirius red staining images show the dense collagen deposition areas along the LV wall and infarct zone in saline, empty vehicle, and free GFs groups. Collagen deposition was significantly reduced in the sequential delivery group. Data are presented as means ± SD (n=5-6 per group). * $p<0.05$ vs saline. ≠ $p<0.05$ vs free GFs. Scale bar=1000µm.**

3.3.6 Sequential delivery provides persistent angiogenesis in the infarcted myocardium

Restoring blood flow to the infarcted myocardium through robust angiogenesis is key to tissue regeneration and functional recovery. To investigate the development of mature and stable vasculature in the borderzone of the infarct region, we stained for the EC marker vWF and pericyte marker α-SMA (**Figure 21A**). In addition to being an EC marker, vWF is a marker of cell homeostasis and can be used to evaluate the functionality of new blood vessels [301]. After 4 weeks, free VEGF+PDGF group showed a significantly higher number of vWF-positive vessels ($p<0.05$) in comparison to saline and empty vehicle groups which showed only few vessels in the borderzone zone (**Figure 21A,B**). In contrast, sequential delivery showed an increase in vWF-positive vessels that was significantly higher than all groups ($p<0.001$). This suggests that sequential release of VEGF and PDGF helped improve the formation of neovessels with increased functionality.

The stability and maturity of new vasculature and prevention of its regression is very important for successful ischemic tissue repair. The goal of therapeutic angiogenesis is therefore to produce neovasculature that is not transient but rather is long-term, stable, mature, and robust. To examine the maturity of neovessels, we stained for α-SMA to detect pericytes associated with newly formed vWF-positive vessels (**Figure 21A**). Few α-SMA-vWF-positive vessels were found in saline, empty vehicle, and free GFs groups with no statistical difference among them ($p>0.05$). On the other hand, sequential delivery showed significantly more α-SMA-vWF-positive vessels than all groups ($p<0.001$) likely due to the recruitment of pericytes by PDGF released in a sustained manner by the fibrin gel-coacervate delivery system (**Figure 21A,C**). These results indicate the formation of stable and mature neovessels including capillaries and arterioles that are likely involved in tissue perfusion. This robust angiogenesis

process is seemingly a key factor in the observed improvement of cardiac contractility at the functional level.

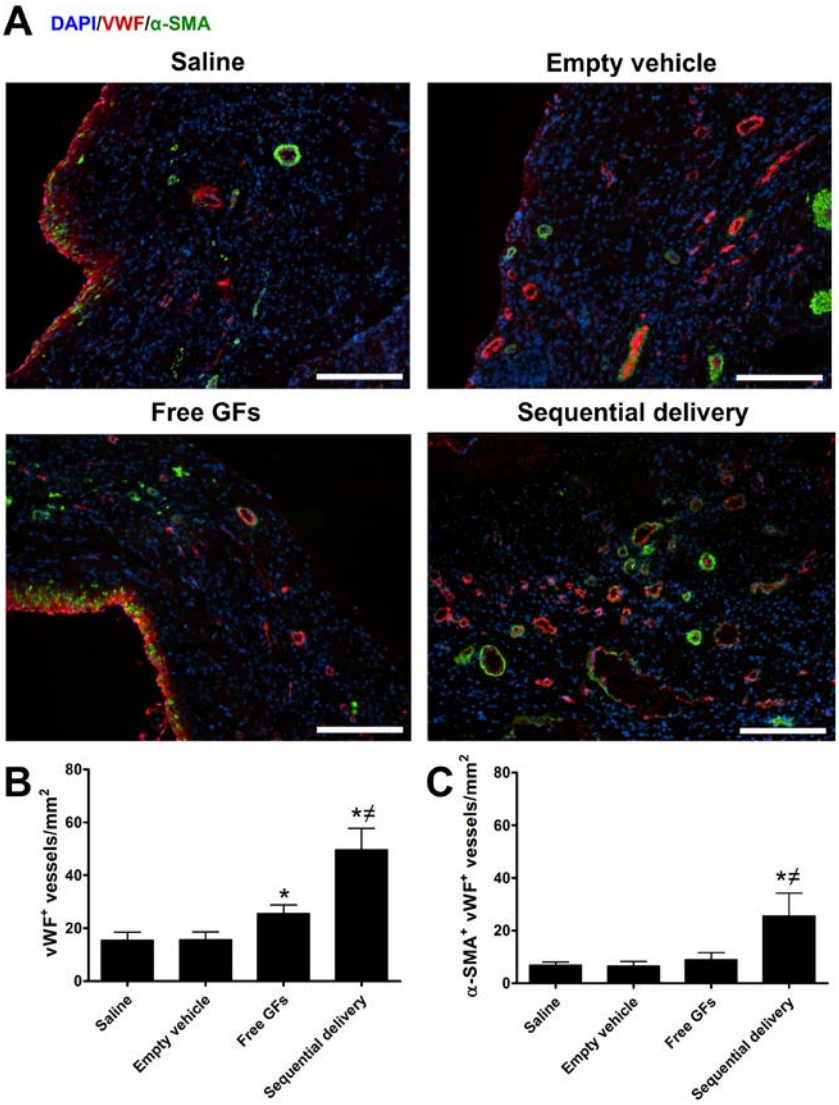

Figure 21. (A) Representative images show co-staining of vWF (red) and α-SMA (green) that reflect the level of neovessel formation, their functionality and maturity, with noticeable improved angiogenesis in the sequential delivery group at 4 weeks. Scale bar=200μm. (B) **Saline and empty vehicle groups show few vWF-positive vessels. While free GFs induced significantly more vWF-positive vessels than controls, sequential delivery induced significantly more than all groups. (C) Sequential delivery induced significantly more α-SMA-vWF-positive vessels than all groups. Data are presented as means ± SD (n=4-5 per group). * p<0.05 vs saline. ≠ p<0.05 vs free GFs.**

3.3.7 Sequential delivery maintains cardiac viability in the infarcted myocardium

Cardiomyocyte survival is essential to maintain proper contractile function of the LV after MI. The viability of the cardiac muscle in the infarcted myocardium was examined by staining for cardiomyocyte marker cTnI (**Figure 22A**). At 4 weeks, saline, empty vehicle, and free GFs groups showed reduced cardiomyocyte survival in the infarct region with cTnI-positive area fractions of approximately 31%, 29%, and 27%, respectively (**Figure 22A,B**). There was no statistical differences noted among the three groups ($p>0.05$). In contrast, sequential delivery showed a significantly higher cTnI-positive area fraction of 56% in the infarct region compared to all groups ($p<0.05$) suggesting better viability and preservation of the cardiac myofibers which help in the improvement of overall cardiac function (**Figure 22A,B**).

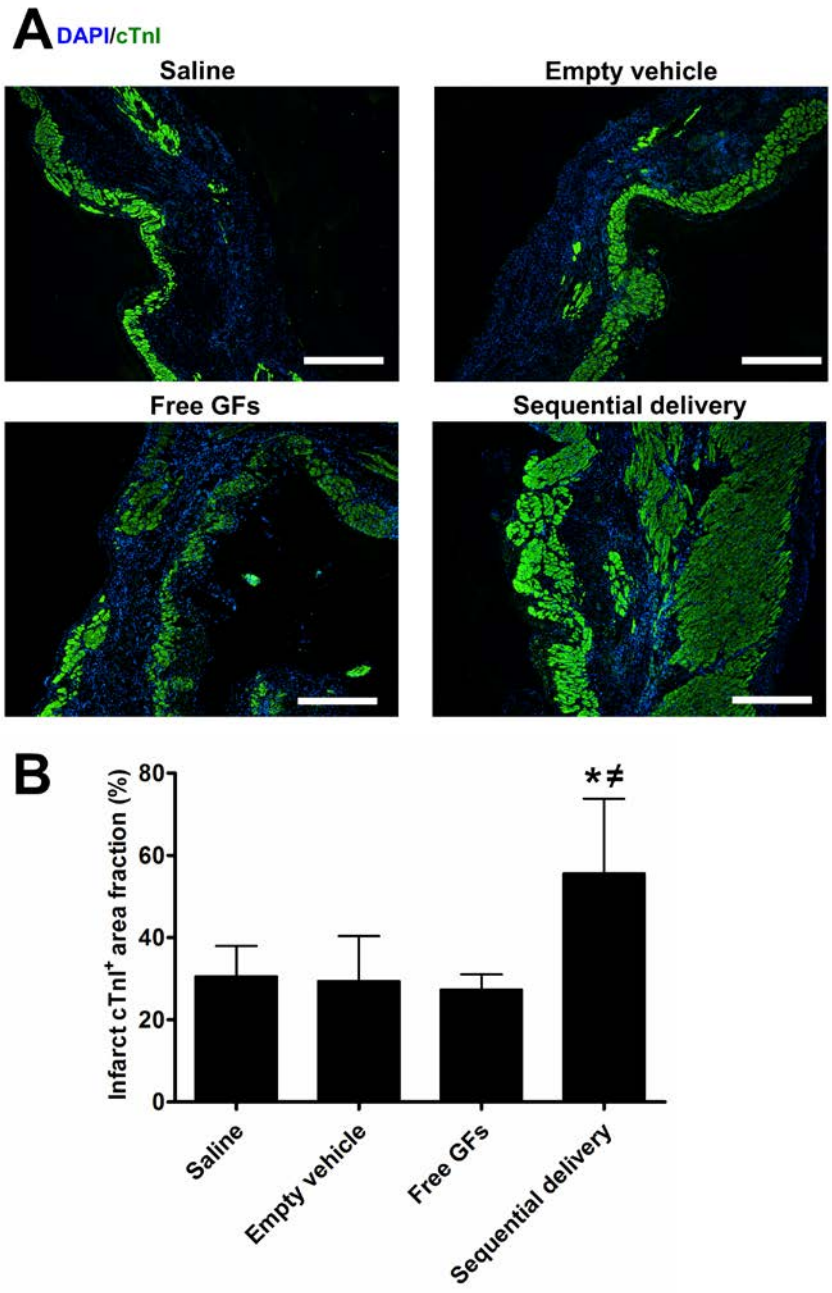

Figure 22. (A) At 4 weeks, cardiac troponin I (cTnI) staining (green) showed a less viable cardiac muscle in saline, empty vehicle, and free GFs groups, while sequential delivery group significantly preserved a larger area of viable cardiac muscle in the infarct zone. Scale bar=500μm. (B) **Quantitative analysis revealed that the sequential delivery group showed a significantly larger cTnI-positive area fraction in the infarct region compared to all groups. Data are presented as means ± SD (n=4-5 per group). * p<0.05 vs saline. ≠ p<0.05 vs free GFs.**

3.3.8 Sequential delivery reduces inflammation in the infarcted myocardium

Reducing inflammation triggered by MI is an important goal towards recovery and repair of the myocardium [66]. Local inflammation in the infarct zone was evaluated by staining for a pan-macrophage marker, CD68 (**Figure 23A)**. At 4 weeks, we observed that both free GFs ($p<0.05$) and sequential delivery ($p<0.001$) groups significantly reduced the presence of macrophages compared to saline (**Figure 23B**). Sequential delivery group showed many less macrophages than free GFs group, however no statistical difference was found between the two ($p>0.05$). Saline and empty vehicle groups showed a high presence of CD68-positive cells (**Figure 23A,B**). This result suggests a role for VEGF and/or PDGF in reducing macrophage infiltration into the infarct zone after MI possibly due to reduced tissue damage or down-regulation of pro-inflammatory cytokines.

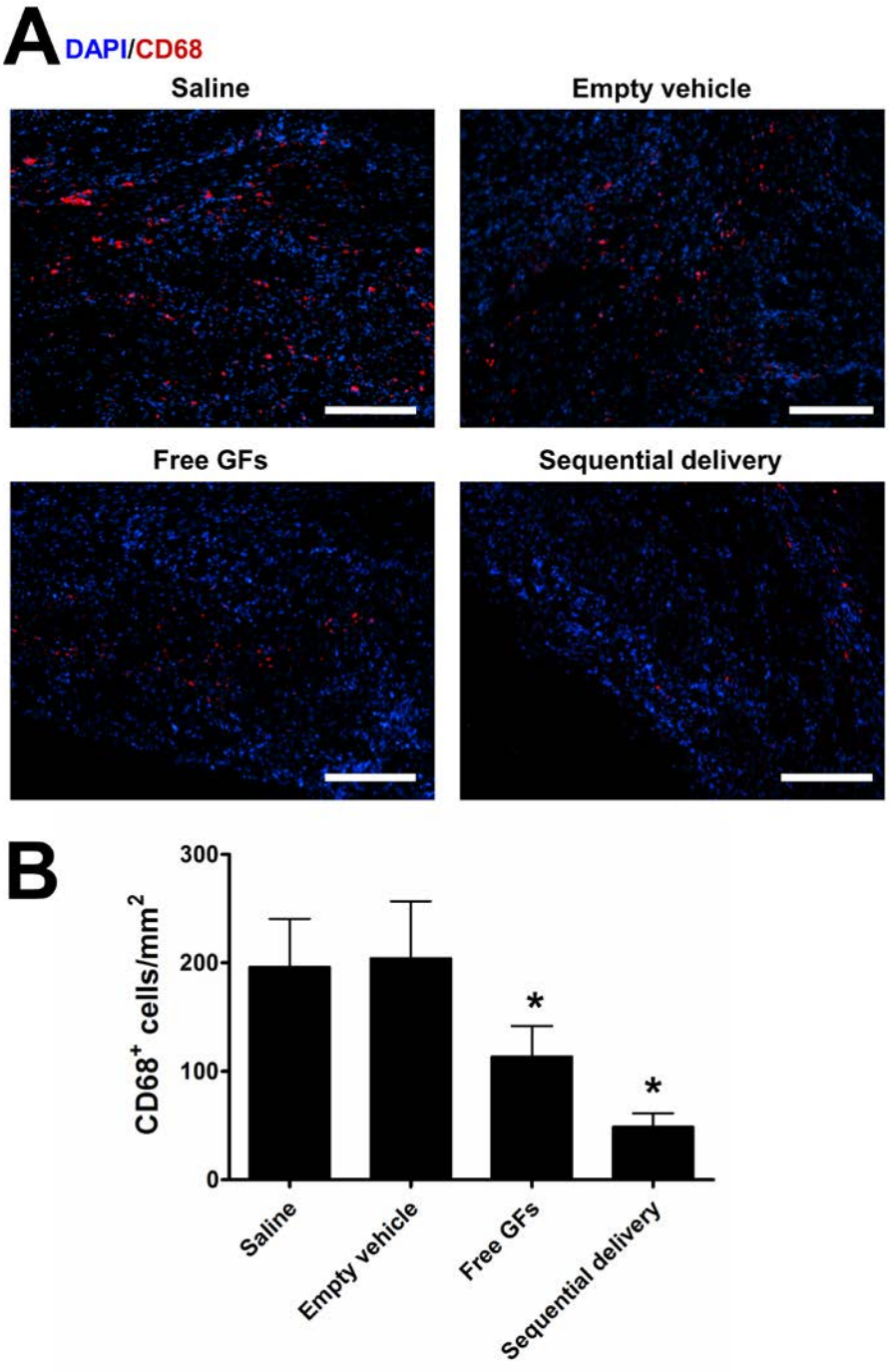

Figure 23. (A) Representative images of CD68 (red) staining show less positive cells in free GFs and sequential delivery groups at 4 weeks. Scale bar=250μm. (B) **Quantitative analysis showed large numbers of CD68-positive cells in saline and empty vehicle groups, while significantly less cells were found in free GFs group and even less in sequential delivery group. Data are presented as means ± SD (n=4-5 per group). * p<0.05 vs saline.**

3.4 DISCUSSION

With the aim of promoting tissue repair and functional recovery, restoring the blood supply to ischemic tissues through therapeutic angiogenesis remains an exciting route. VEGF and PDGF are potent angiogenic factors with relatively distinct roles [17]. One key to successful therapeutic angiogenesis is careful consideration of the spatiotemporal profiles of administered GFs. It has been shown that VEGF can inhibit PDGF signaling where VEGFR-2, activated by VEGF, complexes with PDGFR-β to block its signal transduction, thus compromising its role in pericyte recruitment and neovessel stabilization [39]. One study using synthetic modified RNA encoding human VEGF concluded that VEGF administration can effectively improve heart function when present for just 2 days after MI [299]. This strongly suggests that certain GFs are only needed in the early stage of angiogenesis, while others should be present in the later stages.

Administration of various angiogenic GFs has been studied for a long time [16, 20, 27]. However, most strategies showed limited therapeutic effect because they focus on delivering single GFs involved in the early stages of angiogenesis, while overlooking the importance of stabilizing the sprouting neovessels through the actions of late-stage GFs [17, 195, 208]. With a more comprehensive understanding of the mechanisms of angiogenesis, researchers realized the need to administer more than one GF in their therapeutic strategies [195]. However, these therapies still demonstrated low efficacy when important factors such as the spatiotemporal presentation and protection of GFs were not considered. For example, one study found that combinatorial plasmid gene transfer of VEGF and PDGF did not improve angiogenesis more than single plasmid treatments did in infarcted rat myocardium [302]. When the shortcomings of bolus injections were realized, investigators shifted their focus towards controlled delivery vehicles capable of sequential and spatiotemporal presentation of GFs. Factors such as GF

loading efficiency, spatiotemporal profiles, burst releases, control over release kinetics, GF bioactivity and bioavailability, and cost of manufacturing are challenges that should be addressed to create an effective delivery system [191, 195, 208, 210, 274]. Several systems demonstrated the ability to sequentially deliver two GFs, however they are not injectable, and thus difficult to apply towards treating heart diseases [40, 42, 303, 304]. Others were able to develop injectable platforms that displayed the benefit of sequential delivery using various GFs and in vivo models [41, 215, 305, 306].

In studies where an early-stage factor was presented first followed by a late-stage factor, improved angiogenic responses over single factors or non-sequential delivery were observed. For example, when presented simultaneously, PDGF-BB and Ang1 inhibited the VEGF and Ang2-mediated EC sprouting and pericyte detachment in vitro and microvessel formation in a subcutaneous implant in vivo model; yet presentation of PDGF-BB and Ang1 at a later stage enhanced the angiogenic process [40]. Similarly, when applied together, FGF-2 and PDGF-BB were shown to inhibit each other; however, sequential delivery of FGF-2 followed by PDGF-BB improved EC migration, EC and vascular pericyte colocalization, and functional angiogenesis in a subcutaneous implant model [43]. These results are in support of our in vitro findings regarding antagonism between VEGF and PDGF signaling. Therefore, in order to achieve a robust angiogenic response, therapies must take into consideration the multiple GFs involved, their spatiotemporal cues in the natural tissue microenvironment, and the translational potential of the delivery platform.

The delivery system described in this study is based on a combination of fibrin gel and a complex coacervate for sequential delivery of VEGF followed by PDGF. The coacervate contains heparin and a biocompatible polycation, PEAD, which closely and advantageously

imitates the native signaling environment involving extracellular matrix proteoglycans, ligands, and cell receptors [233, 285, 307, 308]. This vehicle can protect the GFs from rapid enzymatic degradation and potentiate their bioactivities [235].

We demonstrated that the fibrin gel-coacervate composite achieved early release of VEGF to trigger EC proliferation and sprouting and delayed release of PDGF to recruit pericytes that stabilize the newly formed vessels. Even though PDGF is still present in the early stage, our delivery system largely limited its overlap with VEGF presence and thus limited the antagonism between the two factors. Our in vitro assays demonstrated that PDGF coacervate significantly improved SMC proliferation and migration. We also showed the importance of sequential delivery of VEGF followed by PDGF towards EC proliferation by limiting PDGF-mediated inhibition of VEGF angiogenic effects, concurring with previous reports [39, 40, 43]. The benefit of sequential release was further demonstrated by improved microvasculature sprouting from rat aortic rings.

In vivo, we demonstrated using a rat MI model that the fibrin gel-coacervate system led to a robust angiogenic response with extensive formation of mature and functional blood vessels in the infarct zone. The significant increase in the number of vWF- and α-SMA positive vessels reflects the formation of new, stable, and mature vasculature. Our results further demonstrate a reduction in myocardial fibrosis, thus mitigating the loss in contractile function [66, 300]. Moreover, cardiomyocyte survival, essential for preserving contractile function, was improved as a result of sequential delivery of VEGF and PDGF. Several variables not investigated in this study may have played a role in the improvement of cardiomyocyte survival and angiogenesis. For example, VEGF has been shown to elevate the levels of nitric oxide (NO) [309, 310], which is a potent vasodilator and an endothelial survival factor that prevents apoptosis and improves

EC proliferation and migration [311]. Vasodilation soon after infarction may improve cardiomyocyte survival. VEGF also improves FGF-2-mediated angiogenesis [292]. Moreover, VEGF induces the release of SDF-1α which promotes cardiac stem cell and other progenitor cell mobilization to the infarct region [31]. In addition to its role in stabilizing neovessels, PDGF can also activate cardioprotective signaling pathways in cardiomyocytes [249]. Maintaining a viable cardiac muscle is essential to improving cardiac function after MI as demonstrated in studies attempting to stimulate proliferation of cardiomyocytes, prevent their apoptosis, and recruit cardiac progenitor cells to the heart [10, 102, 106, 312-315]. Moreover, we demonstrated that sequential delivery of VEGF and PDGF reduced the presence of macrophages in the infarct zone 4 weeks after MI. This reduction might be due to indirect VEGF and/or PDGF down-regulation of pro-inflammatory cytokines. It is also possible that the improved angiogenesis and better preservation of cardiac muscle observed in our study reduced tissue damage, which may have in turn reduced inflammation. The culmination of these many benefits was reflected on a functional level by improved cardiac contractility with approximately 66% improvement over untreated infarcted hearts at 4 weeks.

Many studies have investigated different types of delivery vehicles for spatiotemporal control over the release or expression of two or more GFs [40, 42, 43, 303-306, 316-319]. However, very few have been tested in an animal model of MI [41, 215, 320]. In a study testing sequential delivery of VEGF and PDGF to the infarcted myocardium, an increased systolic velocity-time integral, a measure of displacement of the myocardium during contraction, was reported, but surprisingly no significant improvement in ejection fraction or LV end-systolic dimension was observed compared to saline control or single GF delivery [41]. Our study demonstrates significantly improved cardiac function through the measurement of LV

contractility based on the FAC parameter. This functional improvement is corroborated by comprehensive histological and immunohistochemical analyses showing the beneficial effects of sequential delivery of VEGF and PDGF at the tissue level of the infarct region.

3.5 CONCLUSIONS

This study demonstrated that sequential controlled release of VEGF and PDGF can trigger the formation and stabilization of neovasculature, and improve cardiac function after MI in a rat model. The improvement was reported at 2 weeks and maintained at a similar level at 4 weeks. Improvements at the tissue level include increased mature blood vessel formation, cardiomyocyte survival, and decreased collagen deposition and inflammation in the infarct zone. These results suggest that VEGF and PDGF released spatiotemporally by the fibrin gel-coacervate delivery system can induce robust angiogenesis, reduce scar burden, and potentially halt the pathological progression post MI.

4.0 DEVELOPMENT OF A COMPREHENSIVE CARDIAC REPAIR APPROACH BY SPATIOTEMPORAL DELIVERY OF COMPLEMENTARY PROTEINS

After a heart attack, the infarcted myocardium is in urgent need for repair and regeneration to reestablish functionality and prevent death. Protein signaling plays a pivotal role in the natural tissue regeneration and repair process. With multiple pathologies developing after myocardial infarction (MI), treatment therapies should develop a comprehensive controlled release strategy that delivers therapeutic proteins spatiotemporally to prevent or reverse these pathologies. Here, we studied the combination of four complementary factors: tissue inhibitor of metalloproteinases 3 (TIMP-3) and interleukin-10 (IL-10) were embedded in a fibrin gel for early release, while basic fibroblast growth factor (FGF-2) and stromal cell-derived factor 1 alpha (SDF-1α) were embedded in heparin-based coacervates and distributed inside the same gel for a more sustained release. After optimizing this combination, we tested the efficacy of the spatiotemporal delivery of TIMP-3, FGF-2, and SDF-1α to the infarcted heart in a rat MI model. We report its significant ability to augment revascularization, myocardial elasticity, cardiomyocyte survival, and stem cell homing; reduce remodeling, dilation, inflammation, fibrosis, and extracellular matrix (ECM) degradation; and improve overall contractile function of the heart. Overall, our strategy indicates that addressing the multi-faceted pathological nature of MI is paramount to a successful repair and regeneration therapy.

4.1 INTRODUCTION

Myocardial infarction (MI) affects 7.6 million Americans. Approximately 720,000 Americans experience a heart attack each year, or one American every 44 seconds [2]. MI leads to the prolonged starvation of a portion of the heart muscle of blood flow, oxygen, and nutrients due to an occlusion in one of the two coronary arteries. This leads to defects in the contractile function of cardiomyocytes and alterations in the extracellular matrix (ECM) and the left ventricle (LV) geometry. The ischemic cardiac tissue starts experiencing necrosis and cell apoptosis, perivascular fibrosis, and fibrillar collagen deposition around myocytes. As a result of all these pathological changes, a scar tissue forms and a pathological remodeling of the ventricle starts, eventually leading to congestive heart failure. Current treatments for MI patients, such as reperfusion, β-blockers, and ACE inhibitors, do not suffice. They are able to delay further damage to the heart, but have not been successful at inducing significant cardiac repair and regeneration. Therefore, alternative and more comprehensive therapies that can reduce the damage of infarction, prevent or reverse the multiple pathologies developed by MI, regenerate the myocardium, and restore cardiac function are urgently needed.

In this work, we explored the efficacy of the controlled and timed release of a combination of complementary proteins, which are relatively distinct in their roles in cardiac function. Tissue inhibitor of metalloproteinases 3 (TIMP-3), interleukin-10 (IL-10), basic fibroblast growth factor (FGF-2), and stromal cell-derived factor 1 alpha (SDF-1α) are proteins with therapeutic potential in cardiac repair and regeneration (**Figure 24**). TIMP-3 inhibits the activity of matrix metalloproteinases (MMPs) which cleave ECM proteins [136]. Therefore, TIMP-3 might have an essential role in reducing ECM degradation early after infarction. IL-10 is an anti-inflammatory cytokine that has been shown to suppress infiltration of inflammatory

cells into the myocardium [67, 314]. FGF-2 plays a chief role in formation of neovasculature by inducing the proliferation, migration, and differentiation of vascular cells and enhancing the signaling of other angiogenic factors [16, 20]. SDF-1α is a potent chemotactic factor that can recruit stem cells to the infarct region [118, 119, 321]. TIMP-3 and IL-10 were intended to modulate, but not eliminate ECM degradation and inflammation soon after MI. FGF-2 and SDF-1α were intended to promote angiogenesis and recruit progenitor cells to the infarct region at the later stage of the repair process. Therefore, we designed a composite hydrogel comprised of fibrin gel and heparin-based coacervate to achieve the sequential release of TIMP-3 and IL-10 followed by FGF-2 and SDF-1α. To achieve this controlled release, TIMP-3 and IL-10 were encapsulated in fibrin gel to offer early release, while FGF-2 and SDF-1α were encapsulated in heparin-based coacervates and distributed in the same fibrin gel to offer a sustained release (**Figure 25A**). We have utilized the fibrin gel-coacervate composite previously to sequentially release proteins for therapeutic angiogenesis post-MI [322]. Coacervates can be formed by electrostatic interactions between a polycation and a polyanion [234, 235]. We utilize a synthetic polycation poly(ethylene argininylaspartate diglyceride) (PEAD), the natural polyanion heparin, and heparin-binding proteins to form protein-loaded coacervates that have been shown to encapsulate proteins with high efficiency and sustain their release for a long time [235, 293].

The endogenous biological system and tissue repair process are intrinsically very complex with many proteins involved, some of which interact with each other. Considering the four proteins of interest in our study and the combinations of controls that can result from them, it is cost-prohibitive to test all possible combinations and doses. To address this challenge, we used factorial design of experiments (DOE), a powerful statistical method, to reduce study

groups [323, 324]. Fractional factorial designs are commonly utilized in scientific studies and industrial applications. However, they have not been taken advantage of as commonly in biomedical research. These designs have been utilized previously to study drug combinations for treating Herpes simplex virus type 1 (HSV-1) and as a method to investigate the effects of different processing parameters for a tissue-engineering scaffold [325, 326]. Fractional factorial designs allow us to build statistical models using a small number of subjects. Such models can identify proteins important for therapeutic outcome, potential protein interactions, optimal protein doses, and optimal protein combinations.

Using a fractional factorial design, this initial combination of four proteins was optimized based on the contribution and dose of each protein to improve cardiac function after MI. The experimental results showed significant contributions of TIMP-3, FGF-2, and SDF-1α at improving cardiac function 4 weeks after MI. The optimized protein combination was then tested in an in-depth study for efficacy in cardiac repair and regeneration post-infarction. We demonstrate that the controlled and timed release of TIMP-3, FGF-2, and SDF-1α at optimized doses can significantly improve cardiac function and repair. Functional and histological evaluations were performed at 2 and/or 8 weeks after MI in a rat model. Improvements at the tissue level are reported through increased myocardial strain levels, angiogenesis, cardiomyocyte survival, stem cell homing, and reduced ventricular dilation, ECM degradation, inflammation, fibrosis, MMP activity, and cell apoptosis. We demonstrate, for the first time, that a more comprehensive therapy of controlled delivery of complementary proteins can mitigate the MI injury and set into motion a robust cardiac repair process, giving hope of driving the functional and structural recovery of the infarcted heart to a new level.

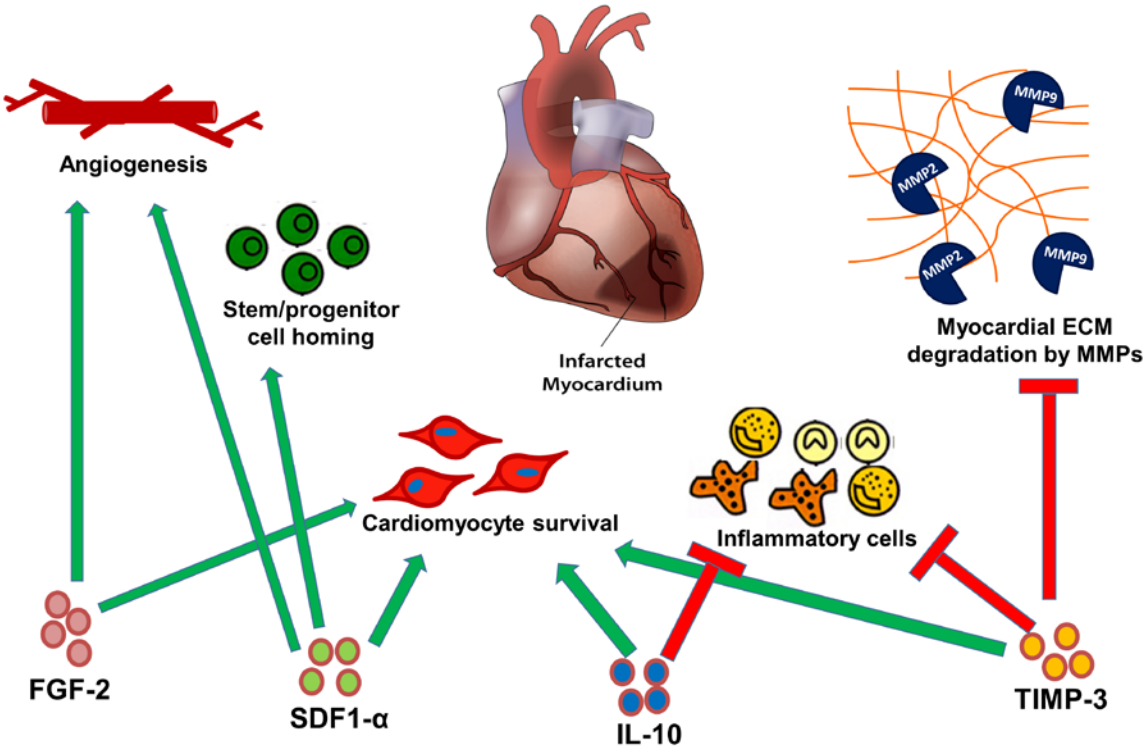

Figure 24. The four proteins FGF-2, SDF-1α, IL-10, and TIMP-3 have relatively distinct, but complementary cardiac functions. FGF-2 promotes angiogenesis by endothelial sprouting and pericyte recruitment and also cardiomyocyte survival. SDF1-α has the critical role of recruiting cardiac, endothelial, hematopoietic, and mesenchymal stem and progenitor cells to the infarcted area, while also promoting angiogenesis and cardiomyocyte survival. IL-10 reduces inflammation by inhibiting the infiltration of immune cells into the myocardium and also reduces cardiomyocyte death. TIMP-3 helps preserve the cardiac ECM structure by inhibiting the activity of MMPs and also promotes anti-inflammatory activities and cardiomyocyte survival.

4.2 MATERIALS AND METHODS

4.2.1 Release assay of complementary proteins

PEAD was synthesized as previously described [237]. The release assay was performed using 100ng of each of TIMP-3 (R&D Systems, Minneapolis, MN), IL-10, FGF-2, and SDF-1α (PeproTech, Rocky Hill, NJ). All solutions were prepared in 0.9% sterile saline. FGF-2 and SDF-1α coacervates were made by mixing 1µl of 100ng/µl for each of FGF-2 and SDF-1α with 2µl of 5mg/ml heparin first (Scientific Protein Labs, Waunakee, WI), then with 2µl of 25mg/ml of PEAD at PEAD:heparin:protein mass ratio of 250:50:1. This formed 6µl of FGF-2/SDF-1α coacervates. Fibrin gel-coacervate composite was made by mixing 80µl of 20mg/ml fibrinogen (Sigma-Aldrich, St. Louis, MO), 2µl of 5mg/ml heparin, 1µl of 100ng/µl for each of TIMP-3 and IL-10; then the 6µl FGF-2/SDF-1α coacervates were added, followed by 5µl of 1mg/ml aprotonin (Sigma-Aldrich, St. Louis, MO). Lastly, 5µl of 1mg/ml thrombin (Sigma-Aldrich, St. Louis, MO) was added to induce gelation, resulting in a 100µl fibrin gel-coacervate composite (**Figure 25A**). A 100µl of 0.9% saline was deposited on top of the gel composite to be collected at 1h, 16h, 1, 4, 7, 14, 28, and 42 days. The samples (n=3) were incubated at 37°C. After centrifugation at 12,100g for 10 min, supernatant was collected and stored at -80°C to detect amount of released proteins by sandwich enzyme-linked immunosorbent assay **(**ELISA) kits (PeproTech, Rocky Hill, NJ) (R&D Systems, Minneapolis, MN). The absorbance at 450/540nm was measured by a SynergyMX plate reader (Biotek, Winooski, VT). Standard solutions (n=3) that contained 100ng of each of the proteins in free-form in 100µl of 0.9% saline were prepared to create standard curves and determine total release.

4.2.2 Two-level half fractional factorial design

We formulated a two-level half fractional factorial design to select the combination of proteins and their doses that are the most effective at recovering cardiac function post MI. The two levels refer to upper and lower doses for each protein and were chosen based on previous experiments and literature review. The half fractional factorial design means half of the total runs were performed. For this design, we can estimate all main effects and some 2-factor interactions, which is quite reasonable in practice to evaluate the significance of each protein in the combination and find the corresponding optimal dose to use in the in-depth study [324].

Using the design formula $2^{(k-p)}$ with k = 4 factors, and p = 1 (for half fractional factorial), we studied 2^3= 8 dose groups. From our previous studies, preliminary results, and literature, we selected the most commonly used dose for each protein as the high doses and one-fifth of that as the low doses. The high doses for FGF-2, SDF-1α, IL-10, and TIMP-3 were 3, 3, 2, and 4μg respectively; while the lower doses are 0.6, 0.6, 0.4, and 0.8μg respectively (**Table 2**). Here, we refer to the protein dose as the amount of each protein embedded in the delivery vehicle. For example, for the average rat used in this study, a high dose 3 μg would correlate to approximately 15 μg /kg body weight (i.e. 3 μg/0.2kg rat). TIMP-3 and IL-10 were encapsulated in fibrin gel, while FGF-2 and SDF-1α were encapsulated in heparin-based coacervates and distributed in the same fibrin gel (**Figure 25A**). With n=3 per dose group and a sham group, we utilized 27 rats for this initial-stage study.

Using Minitab statistical software (State College, PA), this initial-stage design provided a data collection plan with 8 groups of varying protein doses to be tested (**Table 2**). Each group with varying protein doses was tested in a rat acute MI model. The key outcome measurement

of cardiac function was the LV ejection fraction (EF%) computed using cardiac magnetic resonance imaging (MRI) at 4 weeks post-MI. Ejection fractions were analyzed in Minitab software to provide estimates of the relative importance of each protein and its optimal dose in the context of improving cardiac function after MI. The results and analysis of this experiment allowed us to proceed to the in-depth study with a refined combination and doses of the proteins.

4.2.3 Rat acute myocardial infarction model

University of Pittsburgh Institutional Animal Care and Use Committee (IACUC) approval was obtained prior to beginning all animal studies. MI and injections were performed as previously described [297]. Briefly, 6-7 week old (175-225g) male Sprague-Dawley rats (Charles River Labs, Wilmington, MA) were anesthetized first then maintained with 2% isoflurane at 0.3L/min (Butler Schein, Dublin, OH), intubated, and connected to a mechanical ventilator to support breathing during surgery. The body temperature was maintained at 37°C by a hot pad. The ventral side was shaved and a small incision was made through the skin. Forceps, scissors, and q-tips were used to dissect through the skin, muscles, and ribs. Once the heart was visible, the pericardium was torn. MI was induced by permanent ligation of the left anterior descending (LAD) coronary artery using a 6-0 polypropylene suture (Ethicon, Bridgewater, NJ). Infarct was confirmed by macroscopic observation of a change in color from bright red to light pink in the area below the ligation suture. Five minutes after the induction of MI, different treatment and control solutions were injected intramyocardially at 3 equidistant points around the infarct zone using a 31-gauge needle (BD, Franklin Lakes, NJ).

For the factorial design optimization study, 100µl of fibrin gel-coacervate composite was prepared as follows: 18µl coacervate solution (PEAD:heparin:protein mass ratio at 50:10:1) containing respective doses of FGF-2 and SDF-1α as outlined in **Table 2**, 65µl of 20mg/ml fibrinogen, 10µl of solution containing heparin and respective doses of TIMP-3 and IL-10 as outlined in **Table 2**, 5µl of 1mg/ml aprotonin (Sigma-Aldrich, St. Louis, MO). Lastly, 2µl of 1.5mg/ml thrombin (Sigma-Aldrich, St. Louis, MO) was added and the total solution was injected shortly before gelation occurred, approximately 50 seconds after mixing (**Figure 28A**). The chest was closed and the rat was allowed to recover. After 4 weeks, all animals (n=27) were imaged using cardiac MRI and sacrificed.

For the in-depth study with refined protein combination and doses, four groups (n=56 rats) were studied: sham, saline, free proteins, and delivered proteins. Empty vehicle (empty fibrin gel-coacervate composite) was not tested as a control in this study as it has shown no difference to saline in our previous work [322]. The sham group (n=13) underwent the surgery in which the heart was exposed and pericardium was torn, then chest was closed and rat recovered. The saline group (n=14) underwent the surgery in which MI was induced and 100µl of 0.9% sterile saline was injected around the infarct region. The free proteins group (n=14) underwent the surgery in which MI was induced and 100µl of 0.9% sterile saline containing 3µg each of free TIMP-3, FGF-2, and SDF-1α was injected around the infarct region. The delivered proteins group (n=15) underwent the surgery in which MI was induced and 100µl of fibrin gel-coacervate composite was injected around the infarct region. The fibrin gel-coacervate composite was prepared briefly as follows: 18µl coacervate solution containing 3µg each of FGF-2 and SDF-1α, 67µl of 20mg/ml fibrinogen, 6µl of solution containing heparin and 3µg of TIMP-3, 5µl of 1mg/ml aprotonin (Sigma-Aldrich, St. Louis, MO). Lastly, 4µl of

1.5mg/ml thrombin (Sigma-Aldrich, St. Louis, MO) was added and the total solution was injected shortly before gelation occurred, approximately 40 seconds after mixing (**Figure 28**). All solutions were prepared in 0.9% sterile saline. The chest was closed and the rat was allowed to recover. At multiple time points, rats were imaged using echocardiography. At 8 weeks, a subset was imaged using cardiac MRI. After 2 (n=17) or 8 weeks (n=39), animals were sacrificed and hearts were harvested for histological, immunohistochemical, and western blot evaluations.

4.2.4 Echocardiography

At pre-MI, 1, 2, 5, and 8 weeks post-MI, rats (n=9-10 per group) were anesthetized then maintained with 1-1.5% isoflurane gas throughout the echocardiographic study. Rats were placed in the supine position, immobilized on a heated stage equipped with echocardiography, and the hair in the abdomen was removed. The body temperature was maintained at 37°C. Short-axis videos of the LV by B-mode were obtained using a high-resolution in small animal imaging system (Vevo 2100, Visual Sonics, Ontario, Canada) equipped with a high-frequency linear probe (MS400, 30 MHz) (FUJIFILM VisualSonics, Canada). End-systolic (ESA) and end-diastolic (EDA) areas were measured using NIH ImageJ and fractional area change (FAC) was calculated as: [(EDA-ESA)/EDA]×100% (**Figure 29A**). Percent improvements of one group over another were calculated as the difference between the % drops in FAC values of the first and second groups divided by the higher % drop of the two groups.

Myocardial strain level measurements: The ultrasound B-mode frames of LV short-axis view acquired at 8 weeks post-MI were analyzed (n=5 rats per group) using a strain analysis algorithm (VevoStrain^{TM}, Vevo2100). Five regions of interest (ROI) were selected along the LV

mid-wall including one ROI in the anterior lateral (infarcted area) and four ROIs in the anterior medial, septal, posterior, posterior lateral (unaffected areas) walls of the LV (**Figure 31A**). The peak strain in the infarcted area was normalized to the average peak strains of the four ROIs in unaffected LV walls during full cardiac cycles (from end-diastole to end-diastole). Both radial and circumferential strains were computed. The radial strain is defined as the percent change in myocardial wall thickness, and the circumferential strain is defined as the percent change in myocardial circumference.

4.2.5 Cardiac MRI

Cardiac MRI was used to measure LV volumes and ejection fraction from infarcted rat hearts at 4 weeks for the factorial design study (n=3 per group) or at 8 weeks for the in-depth follow-up study (n=5-8 per group). MRI was preformed using a Bruker Biospec 4.7-Tesla 40-cm scanner equipped with a 12-cm shielded gradient set, a 72mm transmit RF coil (Bruker Biospin, Billerica MA), and a 4-channel rat cardiac receive array (Rapid MR International, Columbus, OH). Rats were induced with isoflurane, intubated, and ventilated at 1mL/100g of body weight and maintained at 2% isoflurane in 2:1 O_2:N_2O gas mixture at 60 BPM. During the MRI procedure rats were continually monitored and rectal temperature was maintained at 37°C with warm air (SA Instruments, Stony Brook, NY). Following pilot scans, rats were imaged using a self-gated cine FLASH sequence (IntraGate) with the following parameters: TR/TE= 9.0/3.0 ms, 40x40mm FOV, 256x256 matrix, FA=10°, and 200 repetitions. 10-12 slices were collected to cover the area between the heart apex to the mitral valves with 1.5mm slice thickness with common navigator slice (**Appendix B**). End-systolic and end-diastolic phases were identified for each subject and the LV cavity manually traced using NIH ImageJ to determine LV end-

systolic (ESV) and end-diastolic (EDV) volumes (**Figure 30A**). These volumes were used to compute ejection fraction as EF% = [(EDV-ESV)/EDV]×100%. Percent improvements of one group over another were calculated as the difference between the % drops in EF values of the first and second groups divided by the higher % drop of the two groups.

4.2.6 Histological analysis

At 2 weeks (n=4-5 per group) and 8 weeks (n=5-7 per group) post-infarction, rats were sacrificed by injecting 2ml of saturated potassium chloride (KCl) solution (Sigma Aldrich, St. Louis, MO) in the LV to arrest the heart in diastole. Hearts were harvested, fixed in 2% paraformaldehyde (fisher Scientific, Fair Lawn, NJ) for 1-2 hours, deposited in 30% sucrose solution (w/v) overnight, frozen in O.C.T compound (Fisher Healthcare, Houston, TX), and stored at -20°C until cryosectioning. Specimens were cryosectioned at 8μm thickness from apex to the ligation level with 500μm intervals.

Hematoxylin and eosin (H&E) staining was performed for general evaluation. H&E stained slides were selected and the ventricular wall thickness in the infarct zone (n=3-4 per group at 2 wks, n=4-6 at 8 wks) was measured near the mid-section level of the infarct tissue using NIS Elements AR imaging software (Nikon Instruments, Melville, NY).

For assessment of interstitial fibrosis, Picrosirius red staining was used to stain collagen fibers and image under polarized light. The fraction area of collagen deposition in the cross-sectional area of the whole heart was measured by NIS Elements AR software near the mid-section level of the infarct tissue (n=3-5 per group at 2 wks, n=4-7 at 8 wks). An object count tool was used to include RGB pixels specific to the stained collagen fibers in the heart area by defining a proper threshold value.

4.2.7 Immunohistochemical analysis

For evaluation of inflammation, a rabbit polyclonal antibody F4/80 (1:100, Santa Cruz Biotechnology, Dallas, TX), a pan-macrophage surface marker, was used followed by an Alexa fluor 594 goat anti-rabbit antibody (1:200, Invitrogen, Carlsbad, CA). Slides were also co-stained by a mouse anti-rat CD163 (1:150, Bio-Rad Laboratories, Hercules, CA), an M2 macrophage phenotype marker, followed by an Alexa fluor 488 goat anti-mouse antibody (1:200, Invitrogen, Carlsbad, CA). Slides were last counterstained with 4',6-diamidino-2-phenylindole (DAPI) (Invitrogen, Carlsbad, CA). For quantification near the mid-section level of the infarct tissue, F4/80-positive and CD163-positive cells were counted in two opposite regions of the infarct border zone, averaged, and reported per mm^2 areas (n=3-4 rats per group at 2 wks).

For evaluation of cardiac muscle viability, a rabbit polyclonal cardiac troponin I (cTnI) antibody (1:200, US Abcam, Cambridge, MA) was used followed by an Alexa fluor 488 goat anti-rabbit antibody (1:200, Invitrogen, Carlsbad, CA). Slides were counterstained with DAPI. The fraction area of viable cardiac muscle in the cross-sectional area of the whole heart was measured by NIS Elements AR software near the mid-section level of the infarct tissue (n=3-5 per group at 2 wks, n=5-6 at 8 wks). An object count tool was used to include RGB pixels specific to the stained viable cardiac muscle in the heart area by defining a proper threshold value.

For evaluation of angiogenesis, endothelial cells (ECs) were detected by a rabbit polyclonal von Willebrand factor (vWF) antibody (1:200, US Abcam, Cambridge, MA) followed by an Alexa fluor 594 goat anti-rabbit antibody (1:200). Mural cells were detected by a FITC-conjugated anti-α-smooth muscle actin (α-SMA) monoclonal antibody (1:500, Sigma

Aldrich, St. Louis, MO). Slides were last counterstained with DAPI. For quantification near the mid-section level of the infarct tissue, vWF-positive vessels (defined as those with lumen) and α-SMA-positive vessels were counted in two opposite regions of the infarct border zone, averaged, and reported per mm^2 areas (n=3-4 rats per group at 2 wks, n=5-6 per group at 8 wks).

For evaluation of stem cell homing, stem/progenitor cells were detected by a rabbit polyclonal c-Kit antibody (1:100, Santa Cruz Biotechnology, Dallas, TX) followed by an Alexa fluor 488 goat anti-rabbit antibody (1:200). Slides were counterstained with DAPI. For quantification near the mid-section level of the infarct tissue, c-Kit-positive cells were counted in two opposite regions of the infarct border zone, averaged, and reported per mm^2 areas (n=5 rats per group at 8 wks).

4.2.8 Molecular markers expression by western blot

Rat hearts (n=15) were harvested and rapidly stored at −80°C for western blotting. For protein extraction, myocardial specimens weighing approximately 100mg were excised from the LV generating a composite material comprising a spectrum between normal, infarct, and borderzone tissue. The tissues were then homogenized at 0.2μg/ml in a modified lysis RIPA buffer (50mM Tris–HCl, 1% NP-40, 20mM DTT, 150mM NaCl, pH=7.4) with protease and phosphatase inhibitors. The complex was then centrifuged at 12,100g for 10 min, and the supernatant was collected and stored at −80°C until use.

For total protein content, the extracts above were quantified with Pierce 660nm Protein Assay (Thermo Fisher Scientific, Waltham, MA). The equivalent of 100μg protein was separated using 11.5% gel and then transferred onto a PVDF membrane (Bio-Rad Laboratories,

Hercules, CA). The membrane was blocked with 5% BSA in TBS with 0.05% Tween 20 for 1h, then incubated with following antibody solutions: AKT, p-AKT, ERK1/2, p-ERK1/2 (all at 1:300, Santa Cruz Biotechnology, Dallas, TX), cleaved caspase-3 (1:1,000, Cell Signaling Technology, Boston, MA), and GAPDH (1:5000, US Abcam, Cambridge, MA). The membranes were washed with TBS 3 times and incubated with secondary antibodies for 2h at room temperature. Signals were visualized using the ChemiDic^{TM} XRS + Imaging System (Bio-Rad Laboratories, Hercules, CA), and band densities were quantified using NIH ImageJ software (n=3 per group).

4.2.9 Myocardial protein secretion levels analysis by ELISA

The tissue lysates acquired in the western blot section (n=3-4 rats per group) were used for detecting the levels of insulin-like growth factor-I (IGF-I), vascular endothelial growth factor (VEGF), sonic hedgehog (Shh), and transforming growth factor-β1 (TGF-β1) in the LV myocardium. Sandwich ELISA kits for VEGF and IGF-I (PeproTech, Rocky Hill, NJ) were used per the manufacturer's instructions. Lysates were diluted 1:20 for VEGF and 1:50 for IGF-I. For Shh and TGF-β1, indirect ELISAs were run using rabbit polyclonal antibodies against Shh and TGF-β1 (both at 1:30, Santa Cruz Biotechnology, Dallas, TX) followed by a secondary biotinylated goat anti-rabbit IgG (1:100, Santa Cruz Biotechnology, Dallas, TX). Lysates were diluted 1:15 for Shh and 1:25 for TGF-β1. The absorbance at 450/540nm was measured by a SynergyMX plate reader. Results were corrected to account for differences in total protein content of samples.

4.2.10 MMP-2/9 activity assay

The tissue lysates acquired in the western blot section (n=3-4 rats per group) were used for detecting the activity of MMP-2/9 in the LV myocardium. The Calbiochem InnoZyme^{TM} Gelatinase activity assay fluorogenic kit (EMD Millipore, Bellerica, MA) was followed per the manufacturer's instructions. Briefly, lysate samples (diluted 1:2 in activation buffer) were incubated with a fluorogenic substrate solution that is highly selective for MMP-2 and MMP-9. Gelatinases in the sample lysates of the myocardium cleave the substrate, resulting in an increase in fluorescent signal measured at an excitation wavelength of 320nm and an emission wavelength of 405nm by a SynergyMX plate reader. The gelatinase control, activated similarly, was used at serial dilutions to create a standard curve for converting the fluorescence values of MMP activity to concentrations (ng/ml).

4.2.11 Statistical analysis

Results are presented as means ± standard deviations (SD). GraphPad Prism 5.0 software (La Jolla, CA) and Minitab software (State College, PA) were used for statistical analysis. Statistical differences between groups were analyzed by one-way ANOVA (multiple groups) or two-way repeated ANOVA (repeated echocardiographic measurements) with 95% confidence interval. Bonferroni multiple comparison test was performed for ANOVA post-hoc analysis. Statistical significance was set at $p<0.05$.

4.3 RESULTS

4.3.1 Fibrin gel-coacervate composite achieves sequential protein release

We have reported the use of the fibrin gel-coacervate composite previously for the early release of VEGF followed by the delayed release of PDGF to induce therapeutic angiogenesis in the infarcted heart [322]. In this study, we implement a more comprehensive strategy to prevent or reverse multiple pathologies developed after MI. We tested the fibrin gel-coacervate composite's ability for early release of TIMP-3 and IL-10 followed by delayed release of FGF-2 and SDF-1α. In order to obtain faster TIMP-3/IL-10 release, we embedded these two proteins in a fibrin gel directly, before gelation. We then embedded FGF-2 and SDF-1α within heparin-based coacervates distributed in the same fibrin gel to provide sustained release (**Figure 25A**).

The loading efficiencies were 85% for TIMP-3, 83% for IL-10, 97% for FGF-2, and 98% for SDF-1α, as quantified 1h after loading them into the composite. By day 1, approximately 40% of TIMP-3 and 50% of IL-10 have been released, reaching 90% and 97% total release respectively by one week (**Figure 25B**). As for FGF-2 and SDF-1α, we observed a longer sustained release that lasted for many weeks due to their encapsulation within the coacervates inside the gel. By one week, only 21% of FGF-2 and 28% of SDF-1α were released, reaching 55% and 48% total release respectively by 6 weeks (**Figure 25B**). This controlled release system achieved sequential release kinetics, where most of TIMP-3 and IL-10 amounts were released by 1 week compared to a sustained release of FGF-2 and SDF-1α that lasted at least 6 weeks. The in vivo release rates can be further influenced by one or more factors including fibrinolysis, enzymatic degradation by esterases and heparinases, hydrolytic degradation of PEAD, and dissociation of the coacervate in an ionic environment. Thus, in vivo

release is expected to be faster. Overall, the release kinetics attained with the fibrin gel-coacervate composite reflect the desired goal of providing TIMP-3 and IL-10 early after MI to reduce ECM degradation and inflammation, while providing FGF-2 and SDF-1α in a more sustained manner for triggering a robust neovasculature formation process and stem cell recruitment.

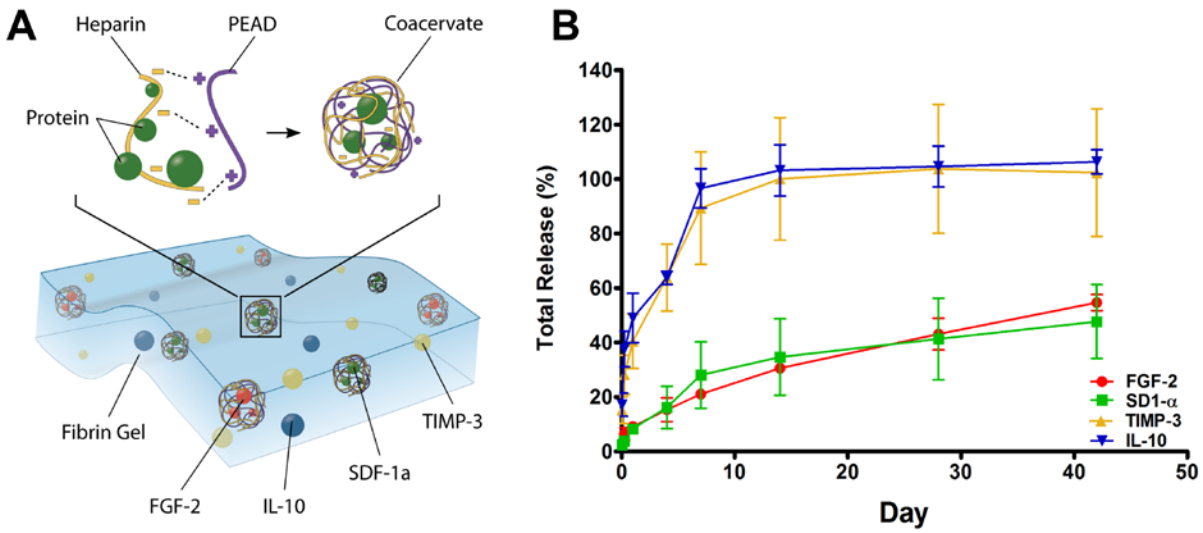

Figure 25. (A) The release system was comprised of a fibrin gel embedding TIMP-3 and IL-10 aimed for early release; and FGF-2/SDF-1α-loaded coacervates distributed within the same gel aimed for late release. The coacervate was formed through electrostatic interactions by combining FGF-2 and SDF-1α with heparin then with PEAD polycation. (B) The release system described achieved sequential quick release of TIMP-3 and IL-10 by 1 week followed by a sustained release of FGF-2 and SDF-1α up to 6 weeks. Data are presented as means ± SD (n=3).

4.3.2 Optimization of the protein combination and its doses

The use of TIMP-3, IL-10, FGF-2, or SDF-1α to promote cardiac repair post-MI is well supported by the literature [66, 88, 118, 119, 147, 177, 241, 314, 315, 327-332]. However, to our knowledge, they have never been tested in combination before. Therefore, the significance of each protein in the combination within the context of improving cardiac function and repair after MI is unknown. In addition, such a combination has not been evaluated using controlled delivery. Finally, there is no existing literature on the optimal dose for each protein in free or controlled release form. Therefore, we utilized a two-level half fractional factorial design to build a statistical model with a small number of runs, saving time, resources, and money [323, 324].

Table 2. Treatment groups according to two-level half fractional factorial design and the corresponding ejection fraction obtained by MRI.

Protein	FGF-2	SDF-1α	IL-10	TIMP-3	EF%	± SD
Dose group 1	3 µg	3 µg	2 µg	4 µg	**62.3**	**1.3**
Dose group 2	3 µg	3 µg	0.4 µg	0.8 µg	**56.8**	**1**
Dose group 3	3 µg	0.6 µg	2 µg	0.8 µg	**50.7**	**4.3**
Dose group 4	3 µg	0.6 µg	0.4 µg	4 µg	**59.4**	**3.6**
Dose group 5	0.6 µg	3 µg	2 µg	0.8 µg	**44.9**	**3.6**
Dose group 6	0.6 µg	3 µg	0.4 µg	4 µg	**58.9**	**3.4**
Dose group 7	0.6 µg	0.6 µg	2 µg	4 µg	**51.6**	**1.9**
Dose group 8	0.6 µg	0.6 µg	0.4 µg	0.8 µg	**41.1**	**2.9**
Sham					**70.2**	**2.1**

In this optimization study, we generated, using statistical software, a table organizing 8 groups with different upper and lower doses for each protein, to be tested for efficacy on ejection fraction (EF%) in a rat MI model (**Table 2**). MRI images were used to compute ESV, EDV, and EF values for all 27 rats in the study (**Appendix B**). The resulting mathematical model of the system provided valuable insight on the relative significance of each protein in the

combination on improving cardiac function and the optimal dose needed to benefit cardiac repair and regeneration. This factorial design has a resolution IV; meaning no main effects are aliased with any other main effect or 2-factor interactions, but some 2-factor interactions are aliased with other 2-factor interactions and main effects are aliased with 3-factor interactions. Aliasing means the loss of the ability to estimate some effects and/or interactions, which is the price paid for not running a full factorial design. However, a reasonable and common assumption in such designs is that higher-order interactions are assumed to be negligible because practically they are less likely to be important than lower-order interactions. The regression analysis assumes that the measurement and experimental errors in the data are normally distributed, random over time, and of equal variance at all levels of the response. These three assumptions were confirmed using analysis of residuals shown (**Appendix C**).

Results demonstrated the significant main effects of TIMP-3, FGF-2, and SDF-1α ($p<0.001$), while suggesting minimal effect of IL-10 ($p=0.273$) on improvement of cardiac function (**Figure 26**). This means that, within the context of improving EF% using controlled delivery of this combination, TIMP-3, FGF-2, and SDF-1α were beneficial for improving cardiac function while IL-10's effect was insignificant. Although IL-10 is a strong anti-inflammatory cytokine, its insignificant effect on improving cardiac function within the context of this protein combination might be due to the presence of TIMP-3, which has been shown to have anti-inflammation effects [63]. Therefore, we concluded that IL-10 should be removed from the protein combination when moving forward to execute the in-depth study with the refined parameters.

Factorial Regression: EF% versus FGF-2, SDF-1a, IL-10, TIMP-3

Analysis of Variance

Source	DF	Adj SS	Adj MS	F-Value	P-Value
Model	7	1255.86	179.409	20.59	0.000
Linear	4	1223.42	305.854	35.10	0.000
FGF-2	1	440.33	440.327	50.53	0.000
SDF-1a	1	173.88	173.882	19.96	0.000
IL-10	1	11.21	11.207	1.29	0.273
TIMP-3	1	598.00	598.002	68.63	0.000
2-Way Interactions	3	32.44	10.814	1.24	0.328
FGF-2*SDF-1a	1	0.20	0.202	0.02	0.881
FGF-2*IL-10	1	0.96	0.960	0.11	0.744
FGF-2*TIMP-3	1	31.28	31.282	3.59	0.076
Error	16	139.41	8.713		
Total	23	1395.27			

Model Summary

S	R-sq	R-sq(adj)	R-sq(pred)
2.95184	90.01%	85.64%	77.52%

Figure 26. Analysis of variance results show the relative significance of each of the 4 proteins: TIMP-3, IL-10, FGF-2, SDF-1α, and some of the 2-way interactions on improvement of ejection fraction (EF%).

TIMP-3 had the greatest main effect on improvement of EF% accounting for 43% of the total sum of squares (598/1395), followed by FGF-2 accounting for 32% (440/1395), then SDF-1α accounting for 12.5% (174/1395). Together, the main effects of these proteins dominate the system and account for 87.5% of the total sum of squares, suggesting that the combined individual effects of these 3 proteins are responsible for 87.5% of the change in EF%, while higher-order protein interactions and error account for 12.5% of that change (**Figure 26**).

As for the optimal protein doses, the most effective group of the 8 groups is group 1 restoring EF to 62%, which is closest to the average of 3 sham controls at 70% (**Table 2**). We observed, from the main effects plot, that all of the estimates for FGF-2, SDF-1α, and TIMP-3

had significant positive slopes, indicating that improvement of cardiac function, in this study, can be best achieved by using the higher doses of FGF-2, SDF-1α, and TIMP-3 (**Figure 27A**).

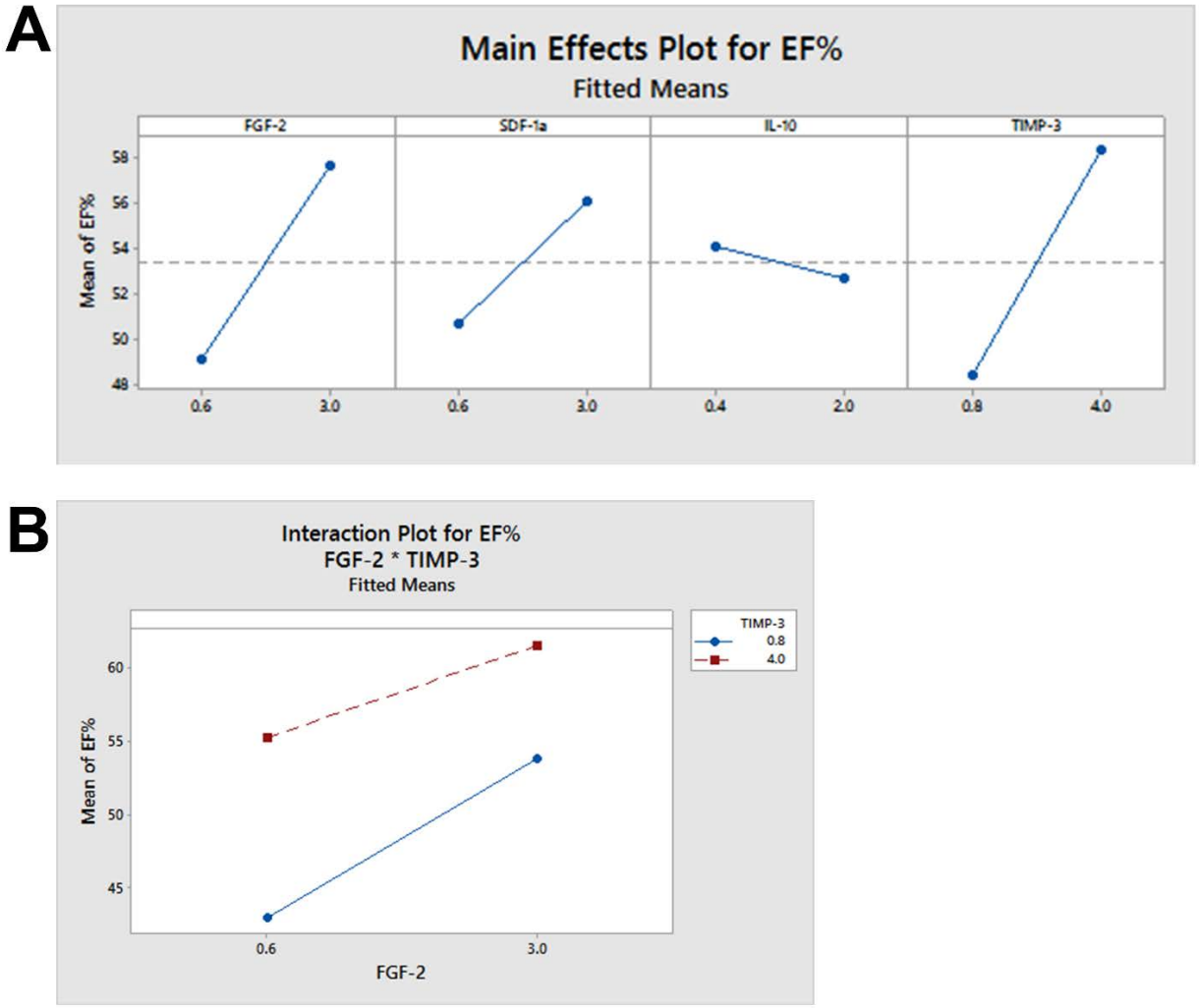

Figure 27. (A) The main effects plot shows the individual effect of each protein on EF% from respective lower to upper doses. (B) The interaction between TIMP-3 and FGF-2, nearly significant at p=0.076, suggests slight antagonism between the 2 proteins.

In addition to minimizing the required number of runs, another benefit of factorial experimentation is the ability to estimate 2-way interactions. Although, the effects of the 2-way protein interactions that this factorial design was able to estimate were all insignificant, the interaction between FGF-2 and TIMP-3 was worthy of consideration as it was nearly significant

at p=0.076 (**Figure 26**). The interaction plot suggests slight antagonism between the 2 proteins (**Figure 27B**). The improvement in EF% seen when FGF-2 is increased in dose is smaller when TIMP-3 is at the high dose than it is at the low dose (the slopes of the 2 lines are not equal) (**Figure 27B**). Physiologically, the 2 proteins might be fulfilling some similar functions and therefore their effects are overlapping when both are at the high dose.

Reducing the regression model to include only the 3 significant main effects and the interaction term (of TIMP-3 and FGF-2) leads to a new model to predict EF% (**Figure 28A**). The contour plot constructed from this model predicts an EF% of approximately 62% if we utilize FGF-2, SDF-1α, and TIMP-3 at 3μg each in the designed scheme within the fibrin gel-coacervate composite (**Figure 28B**). Taking these statistical results and the cost of each protein into consideration, we decided to move forward with FGF-2, SDF-1α, and TIMP-3 in the protein combination with a dose of 3μg for each, thereby keeping the upper doses of FGF-2 and SDF-1α, while reducing TIMP-3 dose slightly from 4μg to 3μg.

A

Factorial Regression: EF% versus FGF-2, SDF-1a, TIMP-3

Analysis of Variance

Source	DF	Adj SS	Adj MS	F-Value	P-Value
Model	4	1243.49	310.873	38.92	0.000
Linear	3	1212.21	404.070	50.58	0.000
FGF-2	1	440.33	440.327	55.12	0.000
SDF-1a	1	173.88	173.882	21.77	0.000
TIMP-3	1	598.00	598.002	74.86	0.000
2-Way Interactions	1	31.28	31.282	3.92	0.063
FGF-2*TIMP-3	1	31.28	31.282	3.92	0.063
Error	19	151.78	7.989		
Lack-of-Fit	3	12.37	4.123	0.47	0.705
Pure Error	16	139.41	8.713		
Total	23	1395.27			

Model Summary

S	R-sq	R-sq(adj)	R-sq(pred)
2.82640	89.12%	86.83%	82.64%

Regression Equation in Uncoded Units

EF% = 32.86 + 4.997 FGF-2 + 2.243 SDF-1a + 4.190 TIMP-3 - 0.595 FGF-2*TIMP-3

B

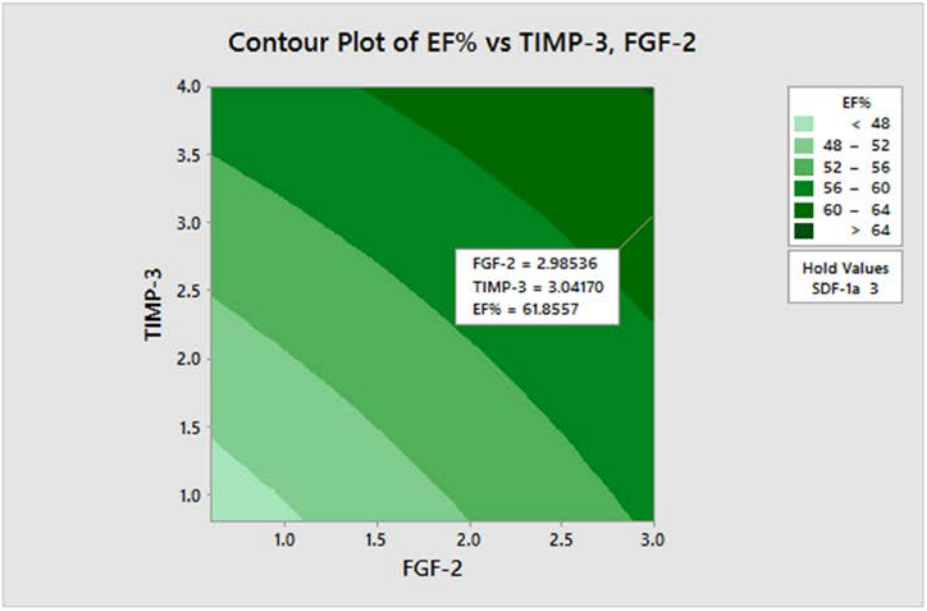

Figure 28. (A) Modified regression model, after removing IL-10. (B) A contour plot predicts the value of EF% upon choosing doses for TIMP-3 and FGF-2 among a range of values, while fixing SDF-1α dose at 3µg.

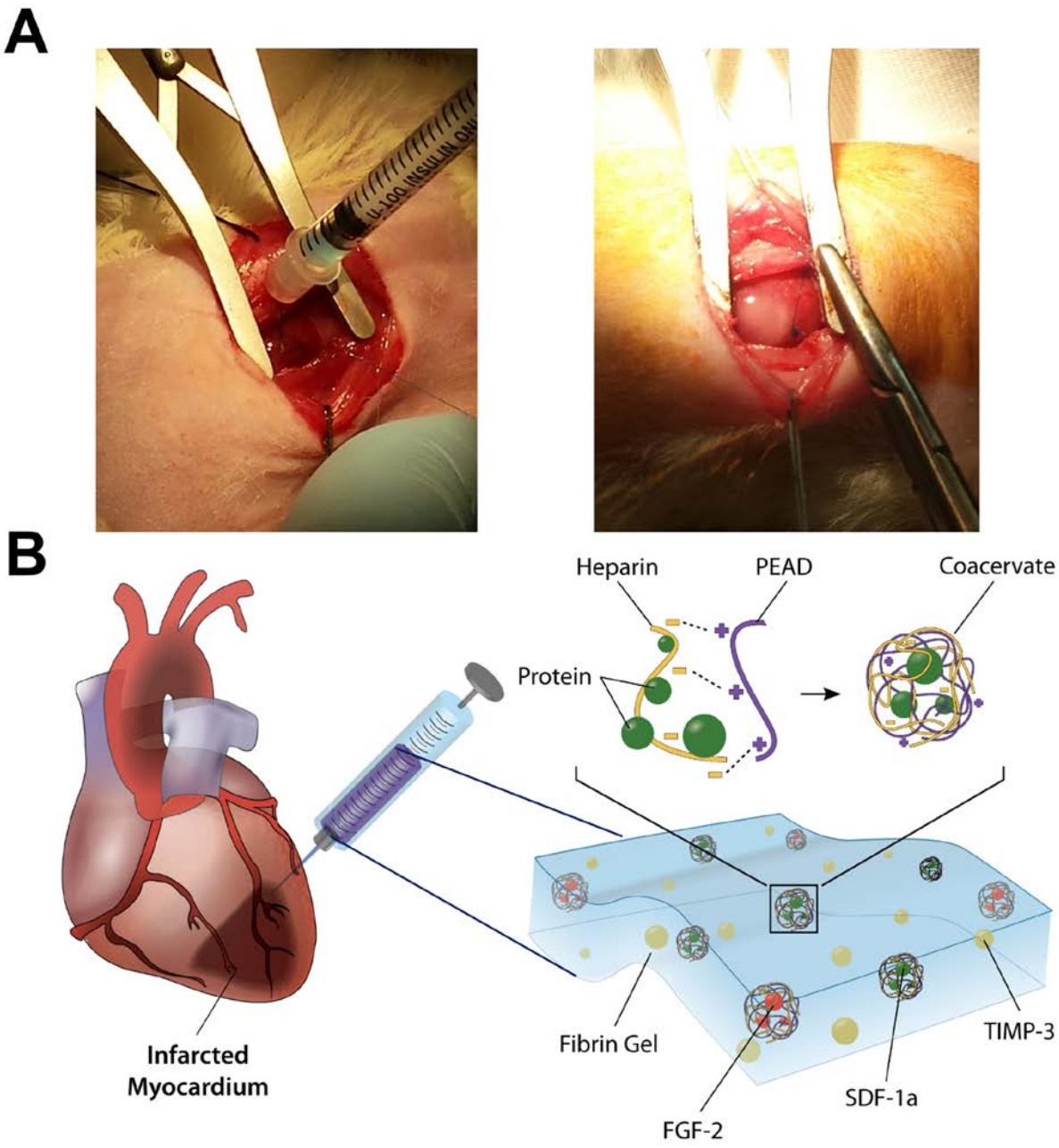

Figure 29. (A) In rat MI model, a 100µl fibrin gel-coacervate composite is injected intramyocardially shortly before gelation at 3 areas around the infarct zone. (B) The refined delivery approach includes injecting the infarcted heart with a fibrin gel-coacervate composite containing TIMP-3 within the fibrin gel, and FGF-2/SDF-1α-loaded coacervates distributed in the same gel, with proteins at 3µg each.

4.3.3 Spatiotemporal protein delivery improves cardiac function and reduces dilation

After refining the protein combination and doses, we evaluated the effect of spatiotemporal delivery of TIMP-3, FGF-2, and SDF-1α (3μg each) using the fibrin gel-coacervate composite in a rat MI model comparing sham, saline, free proteins, and delivered proteins (**Figure 29**). Empty vehicle (empty fibrin gel-coacervate composite) was not tested as a control in this study as it has shown no difference to saline in our previous work [322]. We evaluated changes in LV contractility as a measure of heart function. Fractional area change (FAC) was computed from ESA and EDA values of 2-D echocardiography videos (**Figure 30A**). Sham group maintained an FAC value of approximately 55% at all time points (**Figure 30B**). At 1 week post-infarction, FAC values of saline, free, and delivery groups dropped significantly, however, both delivery and free values were significantly higher than saline ($p<0.01$). This suggests that the 3-protein therapy, whether free or controlled-delivered, helped reduce the significant drop in heart function 1 week after MI. At 2 weeks, although free was still significantly higher than saline ($p<0.001$), both FAC values kept dropping, while delivery group started diverging and improving function significantly compared to both free and saline ($p<0.001$). At 5 weeks, free group was still significantly higher than saline ($p<0.05$), but only at a 36% FAC value compared to 32.5% for saline; whereas, the delivery group increased its improvement of cardiac function compared to both saline and free standing at 47% FAC value ($p<0.001$). At the terminal 8 weeks, the delivery group stood at 48% FAC value showing significant improvement compared to saline (30%) and free (32%) ($p<0.001$), while saline and free were statistically similar ($p>0.05$) (**Figure 30B**). The delivery group improved function approximately 74% over saline based on the terminal FAC values at 8 weeks.

The results were confirmed at 8 weeks by cardiac MRI measurements (**Figure 31**). ESA and EDA were traced and partial volumes were acquired using slice thickness, then added to compute ESV and EDV values (**Appendix B**) (**Figure 31A**). Ejection fraction (EF%) was computed from ESV and EDV relation. The delivery group (58%) showed a significantly higher EF% ($p<0.001$) compared to both saline (41%) and free (46%), which showed no significance between each other ($p>0.05$) (**Figure 31B**). Sham EF% stood at 69%, significantly higher than all groups ($p<0.001$). The delivery group improved function approximately 61% over saline based on the terminal EF values at 8 weeks. This shows that the spatiotemporal delivery of complementary proteins TIMP-3, FGF-2, and SDF-1α can significantly improve cardiac function at least 60% compared to no treatment, demonstrating the efficacy of the controlled release of these proteins in mitigating the MI injury and preventing the contractile dysfunction triggered by it.

In our evaluation of the therapy's effect on ventricular dilation, we assessed the changes in EDA and ESA values. When quantified, the saline and free groups showed significantly increasing ESA and EDA values at all time points after MI, with no statistical differences between them ($p>0.05$) (**Figure 30C,D**). The delivery group, on the other hand, showed sometimes significant reduction and other times a trend towards decreasing both EDA and ESA values at all times after MI compared to saline (**Figure 30C**). These results were confirmed at 8 weeks by cardiac MRI measurements (**Figure 31C,D**). The delivery group demonstrated a significantly smaller ESV compared to saline at 8 weeks ($p<0.01$) and a decreasing trend in EDV value (**Figure 31C**). These results suggest that the spatiotemporal delivery approach significantly reduces LV dilation, and thus in turn reduces the risk of cardiac rupture and heart failure. The ability of the controlled delivery group to improve cardiac function and reduce

ventricular dilation up to 8 weeks after infarction, stresses the importance of choosing complementary proteins and their spatiotemporal presentation per physiologic cues towards achieving effectiveness in treatment of the infarcted myocardium.

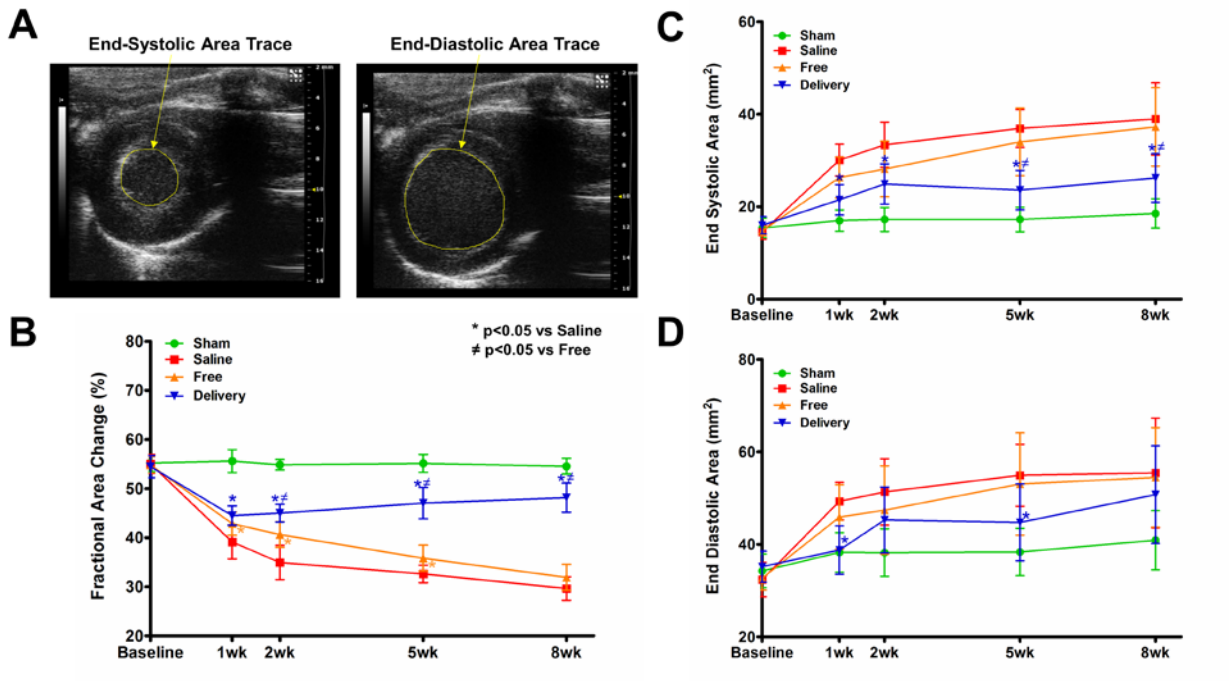

Figure 30. (A) Traces of end-systolic (ESA) and end-diastolic (EDA) areas from short-axis B-mode images of the left ventricle (LV) using echocardiography. (B) Fractional area change (FAC) values show differences between groups after MI at multiple time points, with significantly higher FAC value of the delivery group compared to saline and free from 2 weeks on. (C) Saline and free groups show increasing ESA values, which were reduced in delivery group. (D) Saline and free groups show increasing EDA values, which were reduced in delivery group. Data are presented as means ± SD (n=9-10 per group). * p<0.05 vs saline, ≠ p<0.05 vs free.

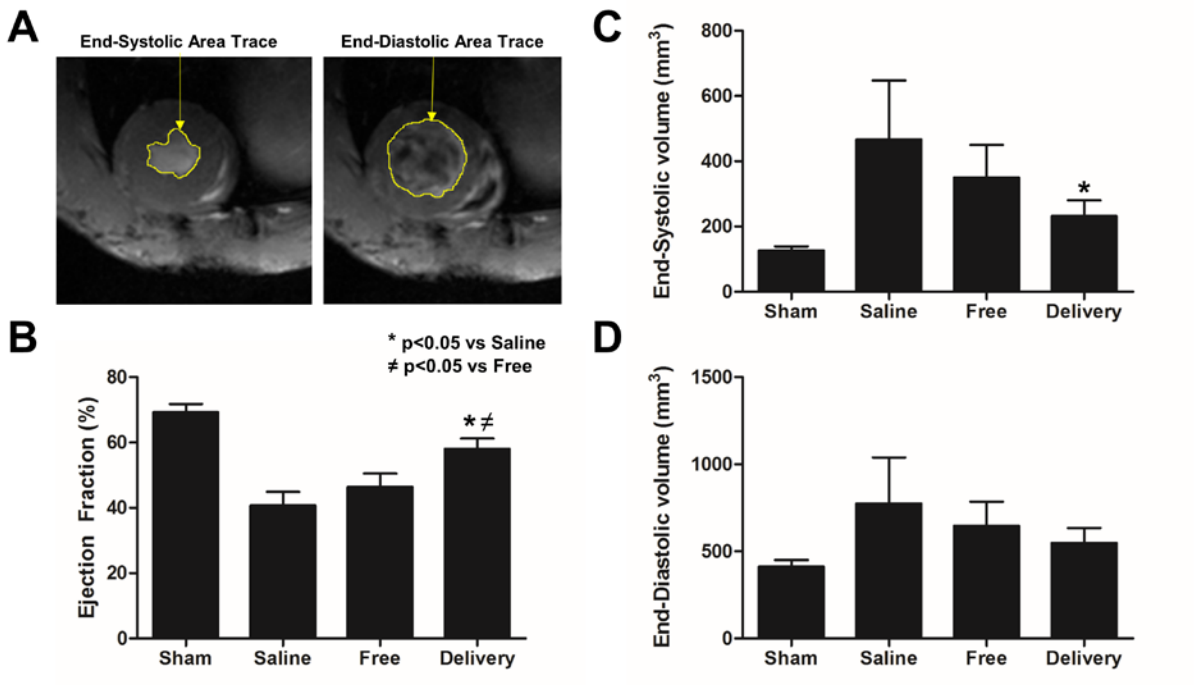

Figure 31. (A) Traces of end-systolic (ESA) and end-diastolic (EDA) areas from short-axis view images of the left ventricle (LV) using cardiac MRI. (B) Ejection fraction (EF%) values show differences between groups after MI at 8 weeks, with significantly higher EF% of the delivery group compared to saline and free. (C) Saline and free groups show increasing ESV value at 8 weeks, which was significantly reduced in delivery group. (D) Saline and free groups show increasing EDV value at 8 weeks, which was reduced in delivery group. Data are presented as means ± SD (n=5-8 per group). * p<0.05 vs saline, ≠ p<0.05 vs free.

4.3.4 Spatiotemporal protein delivery augments myocardial elasticity

We performed myocardial strain analysis at 8 weeks post-MI to evaluate the changes in the radial and circumferential strain levels of the myocardium after infarction and the effect of therapy on them. The radial strain, defined as the percent change in myocardial wall thickness, and the circumferential strain, defined as the percent change in myocardial circumference, were measured from short-axis view images of the LV from echocardiography using VevoStrain

analysis algorithm (**Figure 32A**). The strain of an infarcted sample was estimated by normalizing the estimated peak radial or circumferential strain in the infarcted area to that of the average of 4 non-infarct areas in LV walls during full cardiac cycles (**Figure 32A**). The free proteins group prevented some reduction in the radial and circumferential strains, but not to a significant level over saline ($p>0.05$) (**Figure 32B,C**). The delivery group, however, was able to significantly maintain the radial ($p<0.01$) and circumferential ($p<0.01$) myocardial strains at a higher level in comparison to the saline group, thereby keeping the levels very close to those of sham control (**Figure 32B,C**). This result indicates the efficacy of the spatiotemporal of complementary proteins TIMP-3, FGF-2, and SDF-1α in preserving the long-term LV myocardial elasticity after MI by preventing the LV wall from becoming stiffer which reduces its ability to contract and dilate properly.

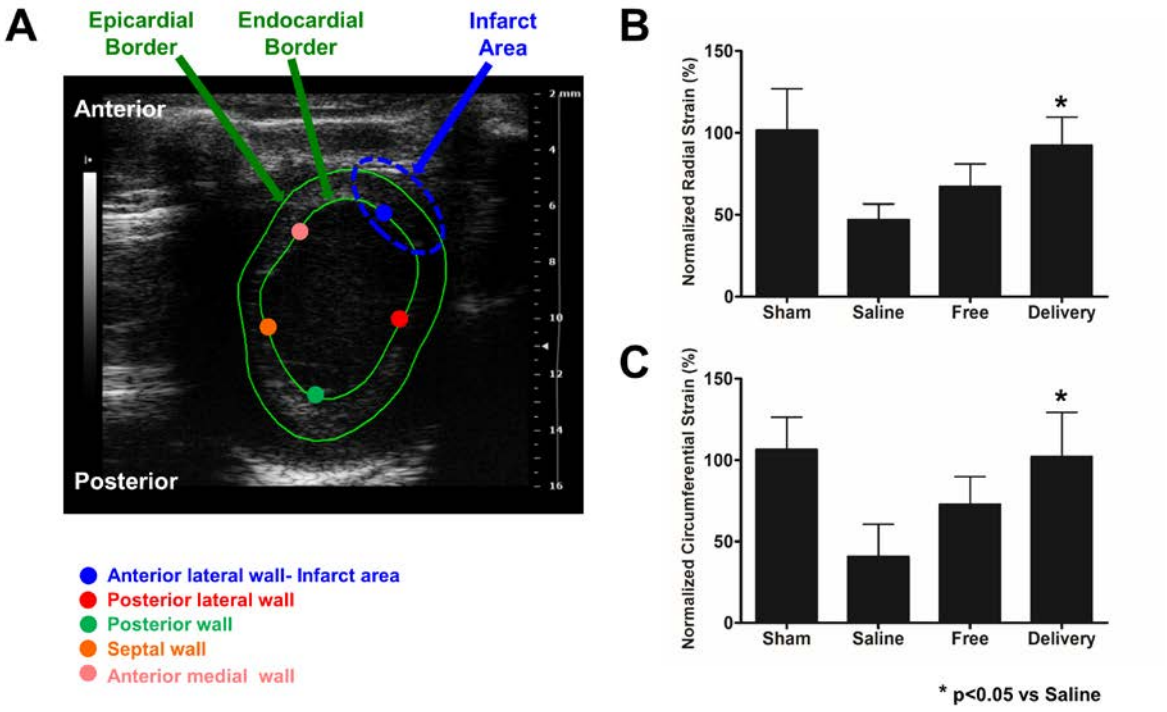

Figure 32. (A) Strain of an infarcted sample was estimated by normalizing the estimated peak radial or circumferential strain in the infarcted area to that of the average of 4 non-infarct areas in LV walls during a cardiac cycle. (B) Saline and free groups show decreasing radial strain at 8 weeks, which was significantly higher in delivery group. (C) Saline and free groups show decreasing circumferential strain at 8 weeks, which was significantly higher in delivery group. Data are presented as means ± SD (n=5 per group). * p<0.05 vs saline.

4.3.5 Spatiotemporal protein delivery reduces LV wall thinning and MMP activity

After functional evaluations, we performed investigations at the tissue level at 2 and/or 8 weeks. H&E stained hearts showed increased granulated scar tissue areas with thinner LV walls in the infarct and borderzone regions that exacerbated with time in infarcted groups but to a less extent in the delivery group (**Figure 33A**). The infarct scar tissue soon starts expanding from the infarct to non-infarct regions turning healthy tissue into collagenous granulated stiffer tissue,

clearly evident in non-treated samples (**Figure 33B**). LV wall thickness decreased considerably in saline and free groups as early as 2 weeks. In contrast, the delivery group significantly prevented LV wall thinning at 2 weeks compared to saline (**Figure 33C**). At 8 weeks, there were no statistical differences in LV wall thickness between saline, free, and delivery groups, although the delivery group clearly maintained a thicker wall average (**Figure 33C**).

At 8 weeks, we evaluated the activity of matrix metalloproteinases (MMPs) in the heart samples. MMP-2 and MMP-9 are important players implicated in many cardiovascular diseases and ECM degradation [141]. By allowing activated MMP-2/9 in our samples to cleave a fluorogenic specific substrate, we were able to detect the activity level of MMP-2/9 in the study groups. All infarct groups showed a high level of MMP activity (**Figure 34**). However, the delivery group showed significantly lower MMP activity compared to saline ($p<0.01$) and also lower activity than free group but not to a significant level ($p>0.05$) (**Figure 34**). The enhanced reduction of MMP activity by the delivery group is likely due to the controlled delivery of TIMP-3 within the fibrin gel-coacervate composite, where TIMP-3 can form tight complexes with MMP-2 and MMP-9 to prevent their activation, and thereby reducing ECM degradation and ventricular dilation and remodeling.

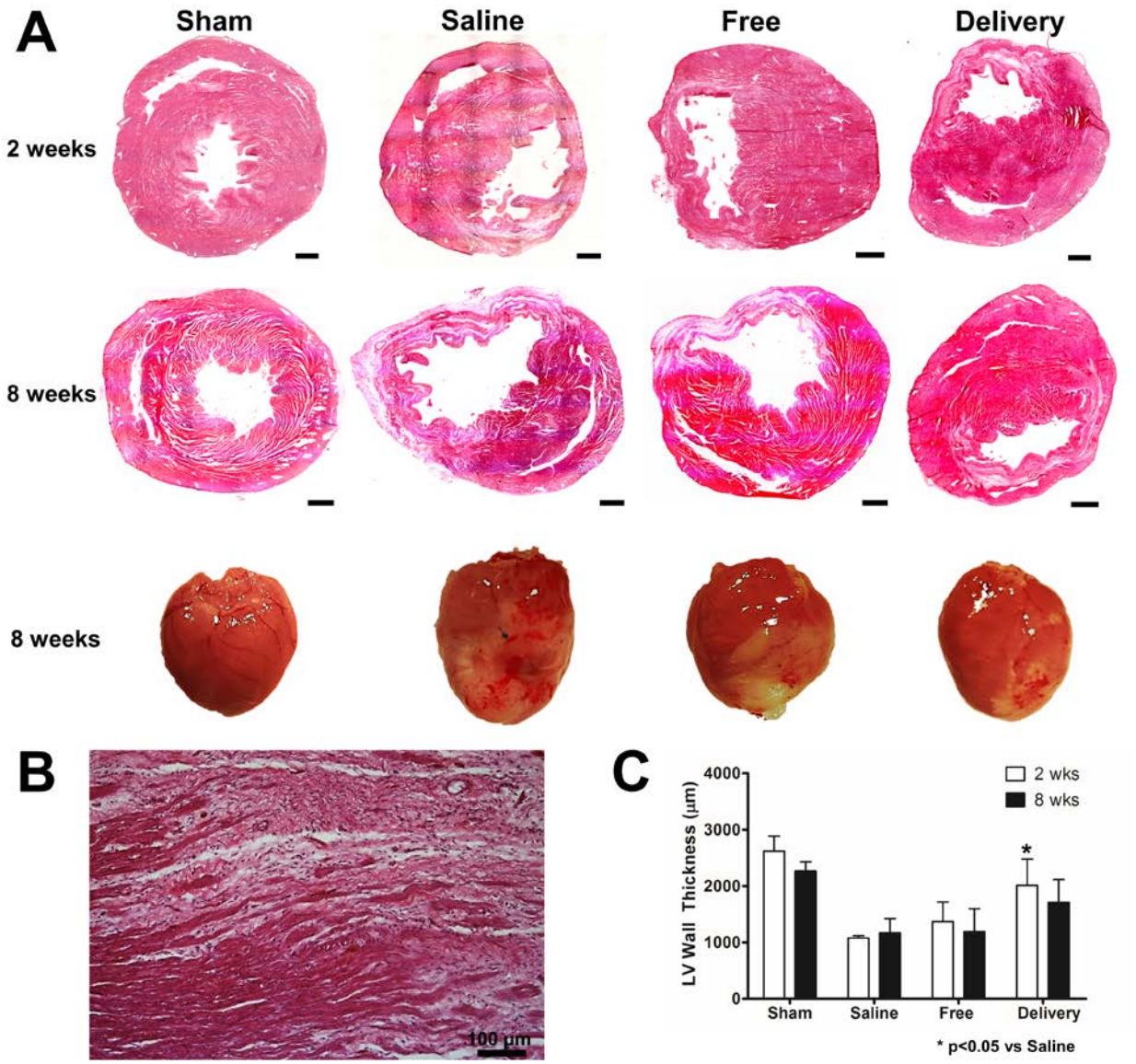

Figure 33. (A) Representative H&E images showed ventricular wall thinning with damaged cardiac muscle surrounded by scar tissue in saline and free proteins groups at 2 and 8 weeks. However, these damages were apparently alleviated in the delivery group. Scale bar=1000μm. (B) Transition between collagenous scar tissue and healthy tissue at the borderzone of a non-treated infarct sample. (C) Quantitative analysis shows generally reduced ventricular wall thinning by delivery group at 2 and 8 weeks over saline and free groups. Data are presented as means ± SD (n=3-4/group at 2 wks, n=4-6 at 8 wks). * p<0.05 vs saline.

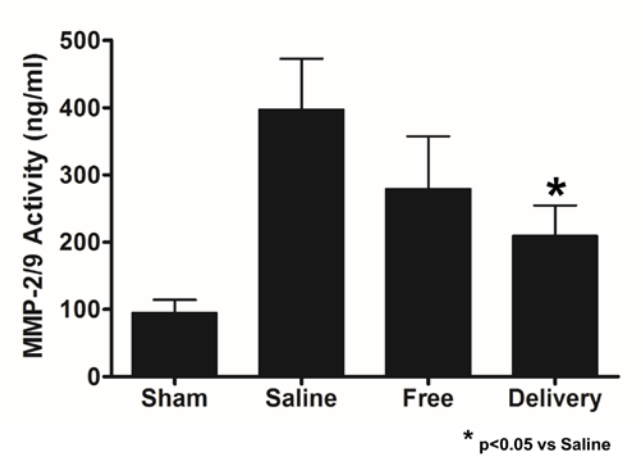

Figure 34. MMP-2/9 activity assay showed high levels of activity in infarct groups at 8 weeks, but was significantly reduced in the delivery group compared to saline. Data are presented as means ± SD (n=3-4 per group at 8 wks). * p<0.05 vs saline.

4.3.6 Spatiotemporal protein delivery reduces inflammation and increases M2 macrophages

Modulating the inflammatory response after MI in which certain harmful aspects of inflammation are prevented, can be very beneficial for the treatment of the infarcted myocardium. In this study, we assessed inflammation by co-staining for F4/80, a pan-macrophage cell surface marker, and CD163, an M2 macrophage marker (**Figure 35A**). Non-M2 macrophages, namely M1, have harmful effects promoting further inflammation, whereas M2 macrophages contribute to tissue repair and anti-inflammation [59]. At 2 weeks post-MI, both saline and free groups showed high numbers of non-M2 macrophages (red), while the delivery group showed a trend towards decreasing the presence of such macrophages ($p>0.05$) (**Figure 35A,B**). On the other hand, the delivery group significantly increased the presence of beneficial M2 macrophages (yellow/green showing co-staining of F4/80 and CD163) in

comparison to saline ($p<0.01$) (**Figure 35A,B**). Saline and free showed no statistical differences in their M2 macrophage numbers ($p>0.05$) (**Figure 35B**). The sham control showed minimal presence of macrophages. These results are suggestive of the efficacy of the spatiotemporal delivery of complementary proteins TIMP-3, FGF-2, and SDF-1α at reducing the detrimental effects that may result from an excessive inflammatory response post-MI and promoting healthy tissue repair through M2 macrophages.

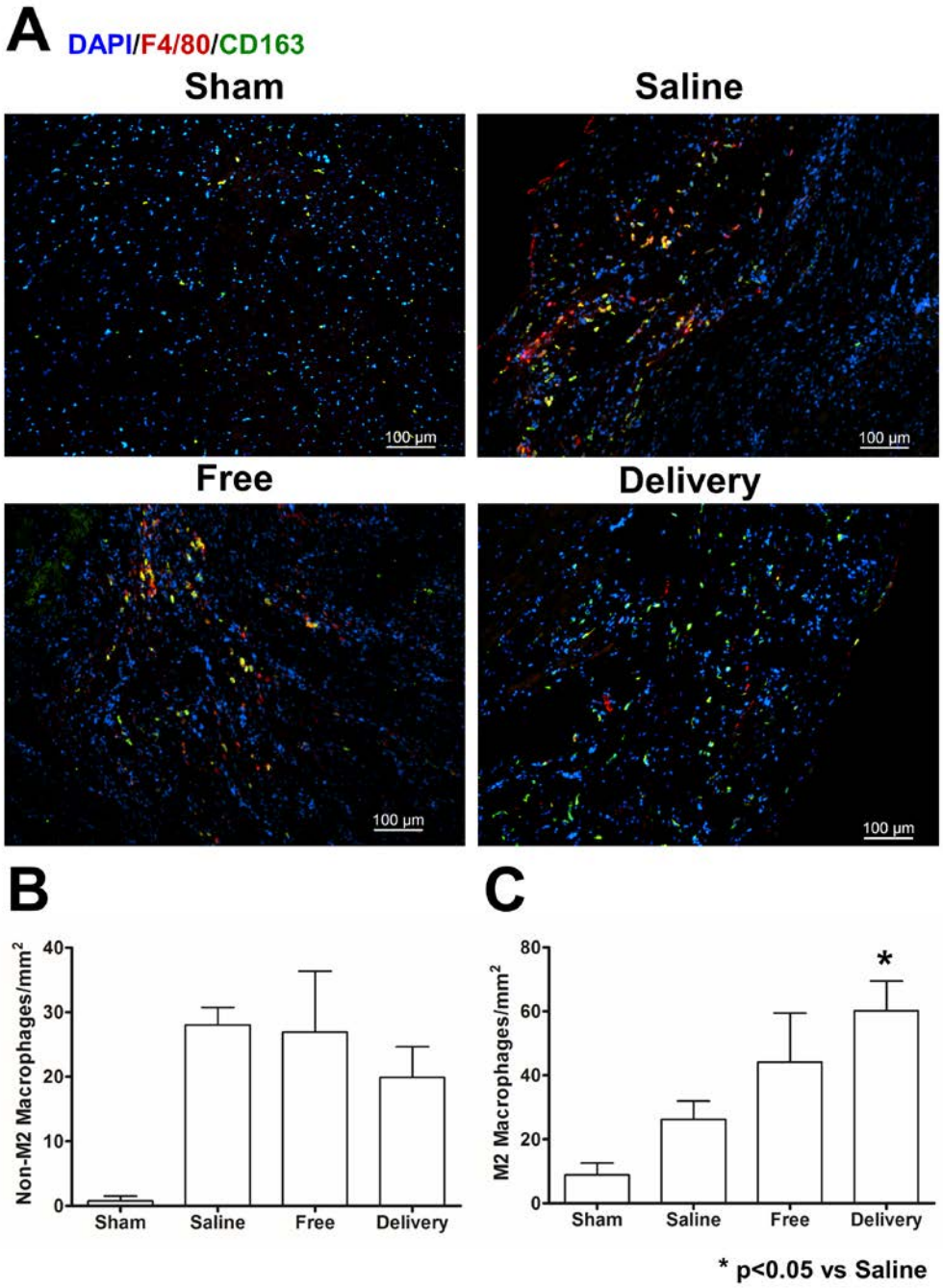

Figure 35. (A) Representative images of the different groups showing co-staining of F4/80 (red), a pan-macrophage marker, and CD163, an M2 macrophage marker (green) at 2 weeks. Co-localization of the 2 markers shows the color as yellow. (B) The delivery group shows a reduced number of non-M2 macrophages compared to saline and free, but not statistically significant. (C) The delivery group shows a significantly increased presence of M2 macrophages compared to saline. Data are presented as means ± SD (n=3-4 per group at 2 wks). * p<0.05 vs saline.

4.3.7 Spatiotemporal protein delivery supports cardiomyocyte survival and reduces apoptosis

The viability of the cardiac muscle is crucial for the proper function of the heart. Cardiomyocytes are responsible for imparting proper and synchronized contractile ability to the heart for pumping blood. As MI and the pathologies developing after it trigger a massive death of cardiomyocytes, it is extremely beneficial to support the survival of these cells, prevent their apoptosis, and trigger the regeneration of a viable myocardium. To examine the viability of the cardiac muscle, we stained for the live cardiomyocyte marker cardiac troponin I (cTnI) (green) (**Figure 36A**). We observed a major loss of viable myocardium in the saline group followed by the free group, then by the delivery group which apparently preserved the live cardiomyocytes to a larger extent at 2 weeks (**Appendix D.1**) and at 8 weeks (**Figure 36A**). Quantitative analysis of the area fraction of the viable cardiac muscle demonstrated a reduction in the amount of survived cardiomyocytes in all infarct groups at 2 weeks, with no statistical differences between them ($p>0.05$) (**Figure 36B**). At 8 weeks, the viability of the cardiac muscle was reduced more in the saline group (64% viable muscle), followed by the free group (75%) with no significant differences between them ($p>0.05$). In contrast, the delivery group was able to maintain the survival of the cardiac muscle (83%) significantly better than saline at 8 weeks ($p<0.01$) (**Figure 36B**).

A number of molecular pathways and markers play important roles in promoting survival or inducing apoptosis of the cardiomyocytes. The activated (phosphorylated) MAPK/ERK and Akt pathways have been shown to provide cardioprotective effects supporting the survival of cardiomyocytes after ischemia and preventing their apoptosis [76-78]. We used western blot to detect the expression levels of cleaved caspase-3, a pro-apoptosis mediator, and

pro-survival markers p-ERK1/2 and p-Akt in our groups at 8 weeks (**Figure 37**). As shown in our results, the intensity of the bands is clearly reduced in the delivery group for cleaved caspase-3 and increased in the cases of p-ERK1/2 and p-Akt (**Figure 37A**). This was confirmed by quantifying the intensity of the bands (**Figure 37B,C,D**). The free group was able to significantly increase p-ERK1/2 expression compared to saline ($p<0.01$) (**Figure 37B**). However, the delivery group significantly reduced the expression of cleaved caspase-3 and increased the expression of p-ERK1/2 and p-Akt compared to both saline ($p<0.001$) and free ($p<0.01$) groups (**Figure 37**). Taken together, these results demonstrate the effectiveness of the spatiotemporal delivery approach at supporting the long-term survival of cardiomyocytes, preventing their apoptosis, and providing overall cardioprotection after MI through activation of the Akt and ERK1/2 signaling pathways and the suppression of caspase-3 apoptotic mediation.

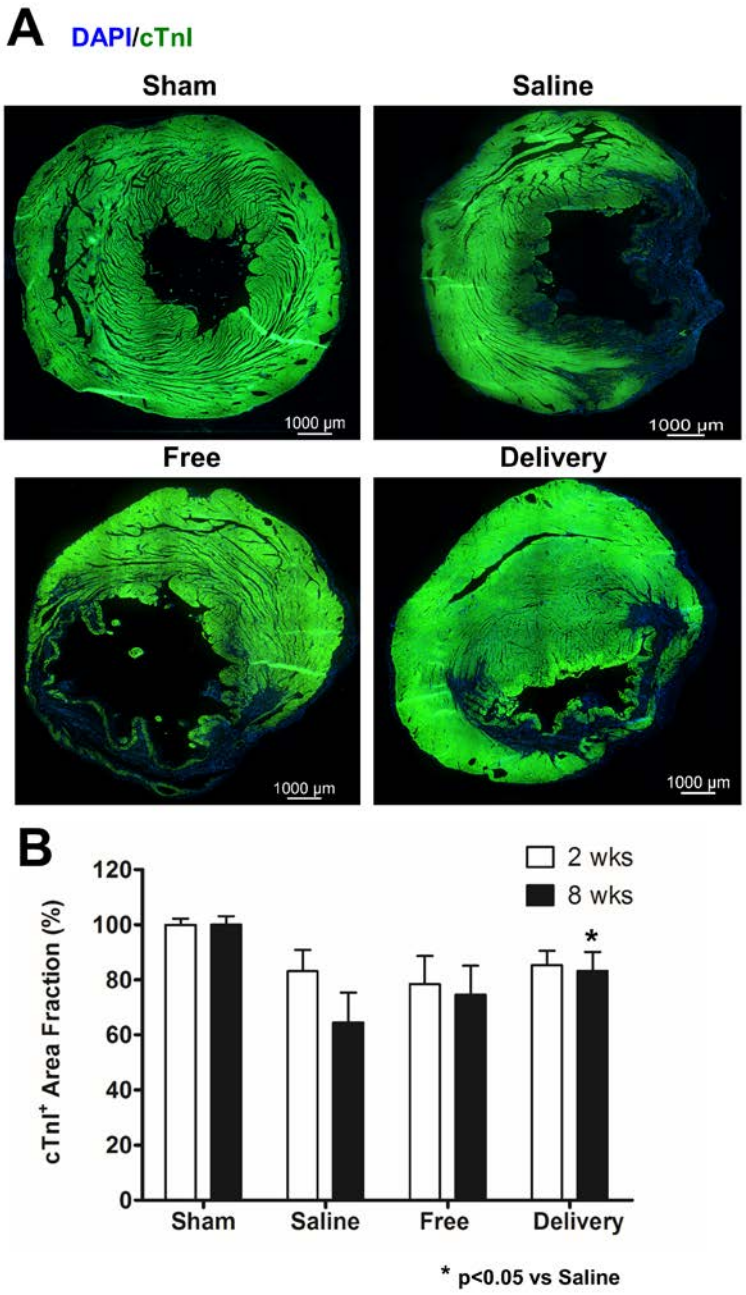

Figure 36. (A) Representative images of the different groups showing staining of viable cardiac muscle by cardiac troponin I (cTnI) (green). Reduced viable muscle can be observed in all infarct groups, with better preservation of the muscle in the delivery group at 8 weeks. (B) Quantitative analysis shows no differences between infarct groups at 2 weeks, but demonstrates the delivery group's significant preservation of cardiac muscle viability at 8 weeks compared to saline. Data are presented as means ± SD (n=3-5/group at 2 wks, n=5-6 at 8 wks). * p<0.05 vs saline.

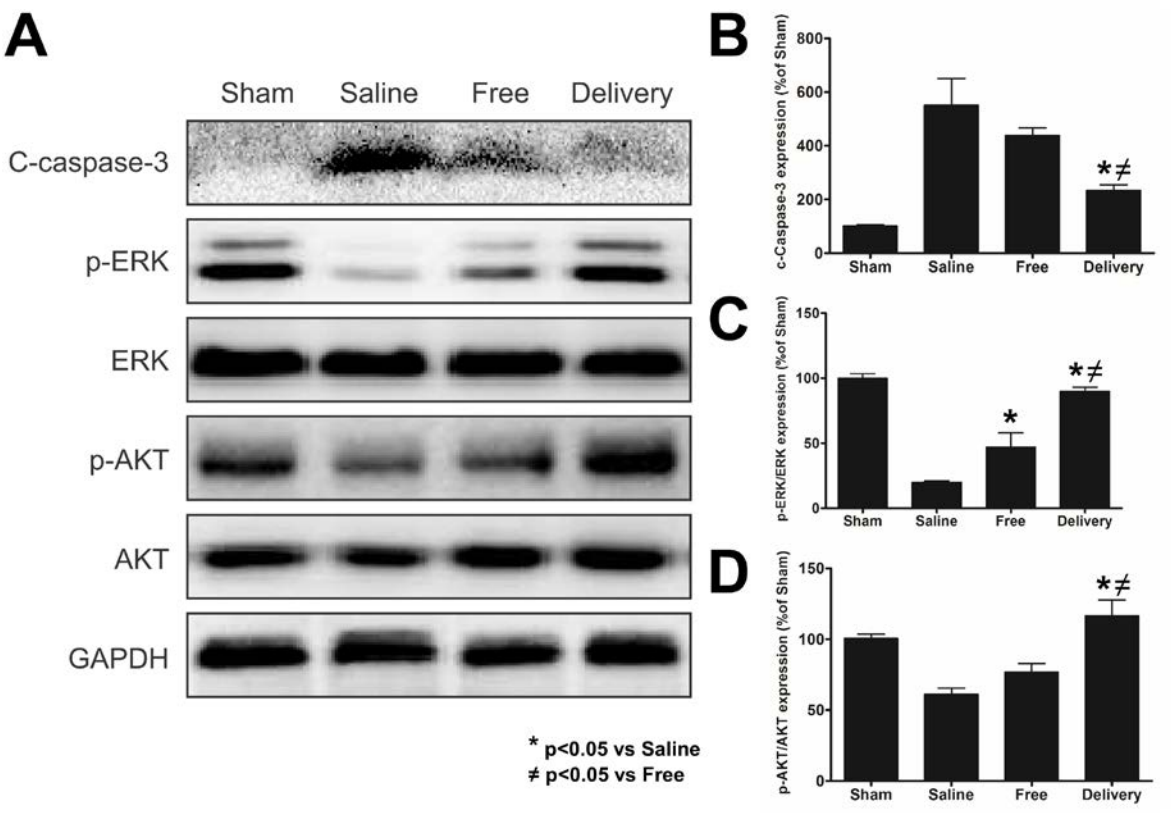

Figure 37. (A) Representative western blot images of the expression levels of p-ERK, p-Akt and cleaved caspase-3 in different study groups at 8 weeks. (B) The intensity band analysis of cleaved caspase-3 shows significant reduction of expression level in delivery group compared to saline and free groups. (C) The intensity band analysis of p-ERK1/2 shows significant increase of expression level in delivery group compared to saline and free groups, with free showing significance over saline as well. (D) The intensity band analysis of p-Akt shows significant of expression level in delivery group compared to saline and free groups. Data are presented as means ± SD (n=3/group at 8 wks). * p<0.05 vs saline, ≠ p<0.05 vs free.

4.3.8 Spatiotemporal protein delivery improves angiogenesis

The revascularization of the ischemic myocardium is key to tissue regeneration and functional recovery. New blood vessel formation can help restore the blood, nutrient, and oxygen flow to the damaged myocardial regions, and thereby enhance the survival of cardiomyocytes, reducing

the risk of chronic heart failure. To investigate the process of angiogenesis, we co-stained for vWF (red), an endothelial cell marker, and α-SMA (green), a pericyte marker (**Figure 38A**). Staining for α-SMA indicates maturity of a neovessel. At 2 weeks (**Appendix D.2**) and 8 weeks (**Figure 38A**), we observed a higher number of neovessels in the delivery group compared to saline and free. The sham control does not show neovessels as infarcted hearts do, but rather shows larger and more established blood vessels that are organized and not as frequent in one region as found in the borderzone of infarcts (**Figure 38A**). Quantitative analysis of infarct groups showed significantly higher number of vWF-positive vessels in delivery compared to saline at 2 weeks ($p<0.05$) (**Figure 38B**). At 8 weeks, the delivery group showed a significantly higher number of vWF-positive vessels than both saline and free groups ($p<0.01$) (**Figure 38B**).

For the quantitative analysis of the formation of mature neovessels (Co-localized stain of vWF and α-SMA), we found no significant differences in the number of vWF-α-SMA-positive vessels among the infarct groups at 2 weeks ($p>0.05$) (**Figure 38C**). However, at 8 weeks, the delivery group showed significantly higher presence of mature vWF-α-SMA-positive vessels than both saline and free groups ($p<0.001$) (**Figure 38C**). Our results demonstrate the ability of the spatiotemporal delivery approach to induce a robust angiogenesis process capable of forming stable and mature neovasculature that is likely to participate in perfusion. This enhanced revascularization in the delivery group is likely due to the sustained presence of the potent angiogenic factor FGF-2 being provided by the heparin-based coacervate within our composite gel.

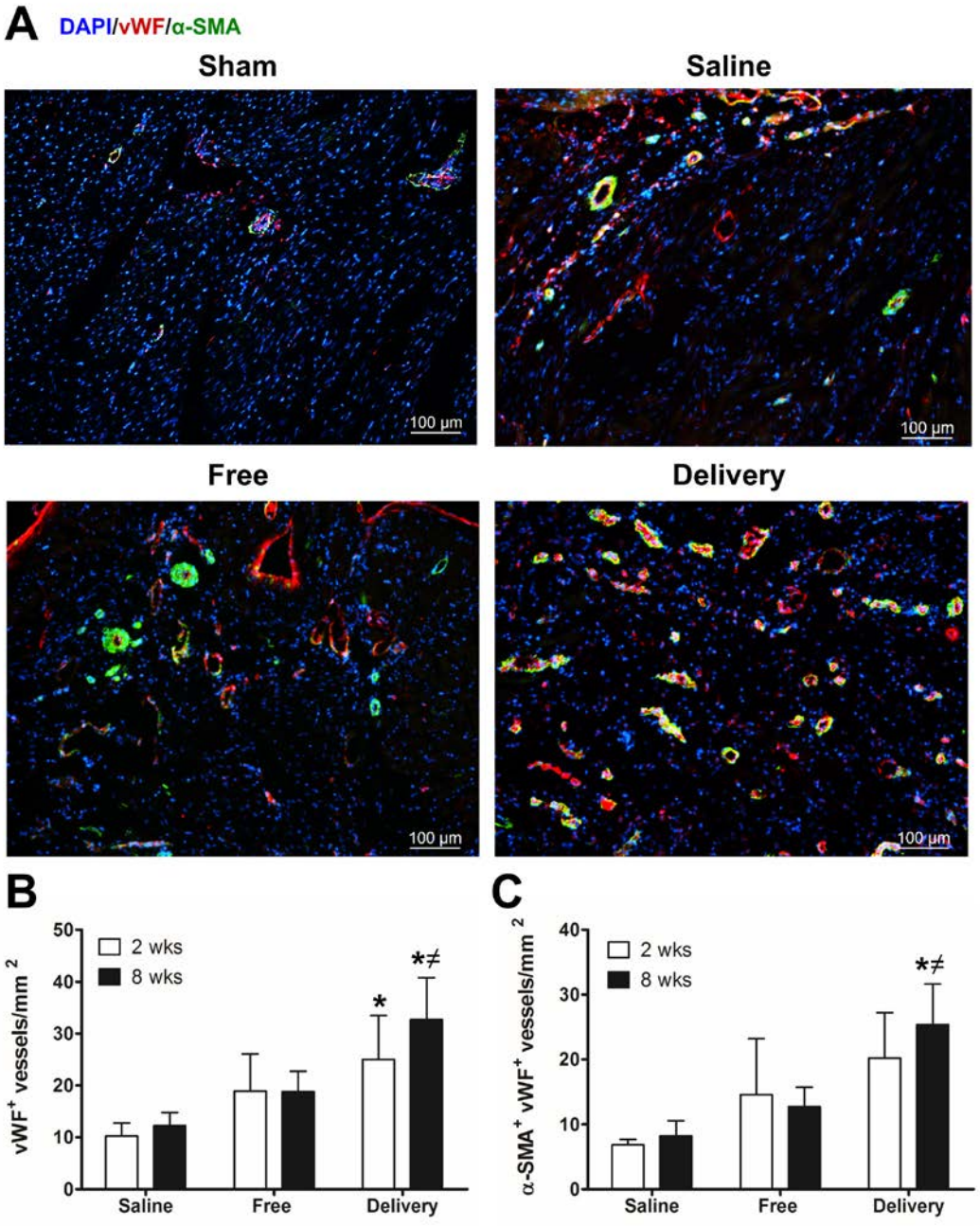

Figure 38. (A) Representative images of the different groups showing co-staining of vWF (red), an endothelial marker, and α-SMA (green), a pericyte marker at 8 weeks. (B) The delivery group shows a significantly greater number of vWF+ vessels compared to saline at 2 weeks and compared to saline and free at 8 weeks. (C) The delivery group shows a significantly greater number of vWF+ α-SMA+ vessels than saline and free groups at 8 weeks but not at 2 weeks. Data are presented as means ± SD (n=3-4/group at 2 wks, n=5-6 at 8 wks). * p<0.05 vs saline, ≠ p<0.05 vs free.

4.3.9 Spatiotemporal protein delivery increases stem cell homing to the myocardium

Stem cells, recruited to the infarcted myocardium, have the potential to differentiate into functional cells of cardiac lineages such as cardiomyocytes, vascular endothelial, and mural cells. Stem cells can also impart beneficial paracrine effects that activate repair and regeneration signaling [94]. To examine the homing of stem cells to the infarcted myocardium, we stained for c-Kit, a stem cell marker (**Figure 39A**). At 8 weeks after MI, saline and free groups showed no significant differences in the number of c-Kit-positive cells present at the borderzone ($p>0.05$) (**Figure 39B**). In contrast, the delivery group showed a significantly greater presence of c-Kit-positive cells at the borderzone compared to both saline and free groups ($p<0.01$) (**Figure 39B**). The sham control showed very few stem cells in the area where an infarct would have been induced, suggesting their limited presence in absence of an MI injury. These results indicate the efficacy of the spatiotemporal delivery approach at recruiting stem cells to the infarct region and potentially contribute in the regeneration of the myocardium. The enhanced and long-term presence of stem cells in the delivery group is likely due to the sustained availability of the powerful chemoattractant SDF-1α within our composite gel, being released by the coacervate.

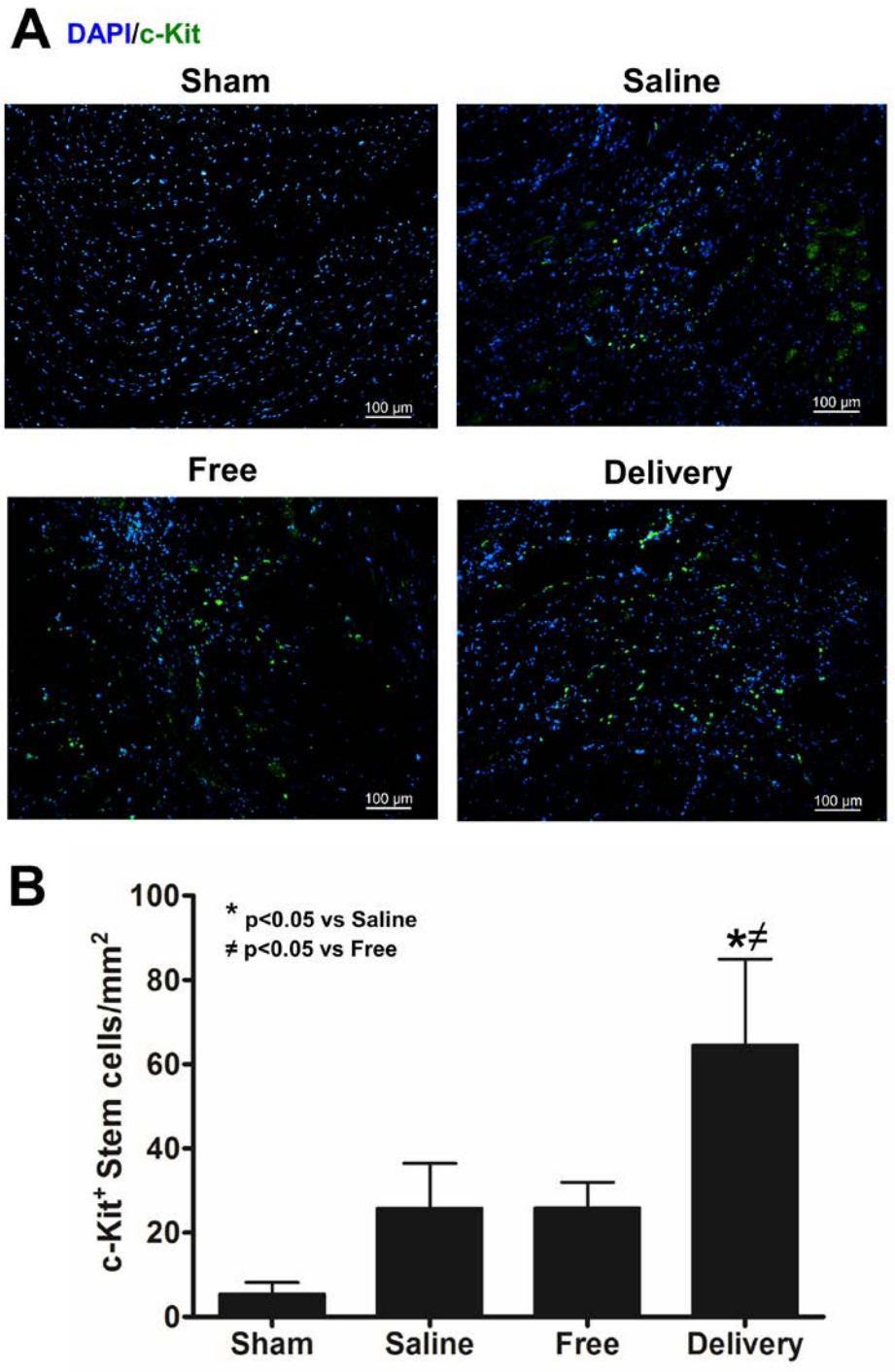

Figure 39. (A) Representative images of the different groups showing staining of c-Kit+ stem cells (green) at 8 weeks. (B) Quantitative analysis shows significantly greater number of c-Kit+ stem cells in delivery group compared to saline and free groups. Data are presented as means ± SD (n=5/group at 8 wks). * p<0.05 vs saline, ≠ p<0.05 vs free.

4.3.10 Spatiotemporal protein delivery reduces interstitial fibrosis after MI

Interstitial fibrosis develops at the infarct region and extends to non-infarct areas due to the excessive and uncontrollable collagen deposition that takes place in later stages after MI. This increased collagen deposition leads to increased stiffness in the myocardium, leading to contractile dysfunction. The extent of fibrosis was assessed using picrosirius red staining which stains collagen fibers with a metallic red color than are viewed under polarized light (**Figure 40A**). The saline group, and to a lesser degree the free group, showed extensive amount of fibrosis that extended from the infarct to non-infarct regions, while the delivery group showed far less fibrosis that seemed limited to the infarct area at 2 weeks (**Appendix D.3**) and at 8 weeks (**Figure 40A**). Collagen deposition was quantified as a positive fraction of the heart area and no statistical differences were found between the infarct groups at 2 weeks despite a clear reduction in the delivery group ($p>0.05$) (**Figure 40B**). At 8 weeks, collagen deposition increased in all infarct groups, but it was found to be significantly less in the delivery group (11%) compared to both saline (23%) ($p<0.01$) and free (18%) groups ($p<0.01$) (**Figure 40B**).

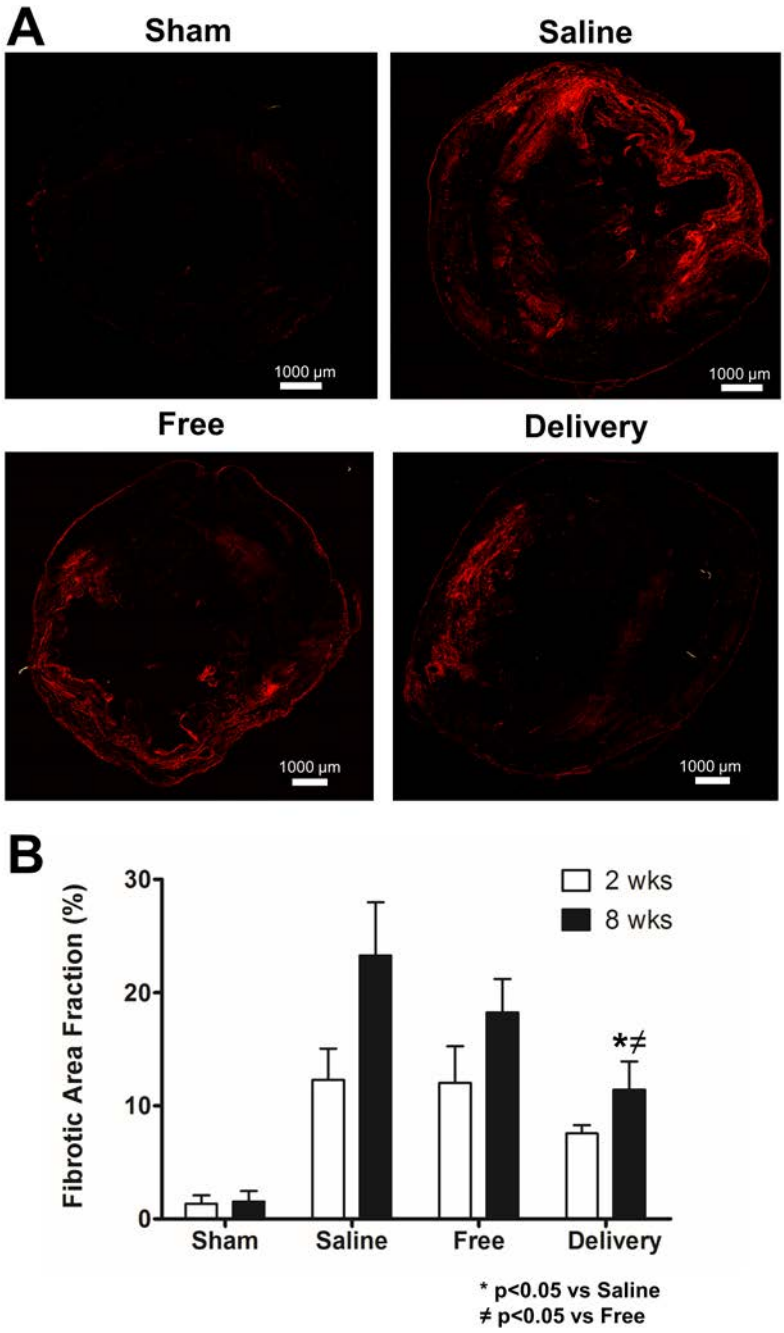

Figure 40. (A) Representative picrosirius red staining images show the dense collagen deposition along the LV wall and infarct zone in saline, followed by the free group, whereas it was limited to the infarct region in the delivery group at 8 weeks. (B) Quantitative analysis shows that collagen deposition was not different in infarct groups at 2 weeks but was significantly less in the delivery group compared to saline and free groups at 8 weeks. Data are presented as means ± SD (n=3-5/group at 2 wks, n=4-7 at 8 wks). * p<0.05 vs saline, ≠ p<0.05 vs free.

4.3.11 Spatiotemporal protein delivery regulates important protein levels

Certain proteins are involved in triggering cardiac repair mechanisms and others are implicated in advancing pathological changes post infarction. Therefore, regulation of the expression levels of such proteins represents an important aspect of effective therapies. The bioavailability and levels of proteins such as the ones in our complementary combination, TIMP-3, FGF-2, and SDF-1α, likely affect the signaling and levels of other proteins involved in the heart environment after MI. To investigate the effect of our spatiotemporal delivery approach on the levels of relevant proteins, we tested tissue lysates for the levels of insulin growth factor IGF-I, VEGF, Shh, and TGF-β1 at 8 weeks (**Figure 41**)**.** Quantitative analysis by ELISA showed significantly higher levels of IGF-I, an anti-apoptotic factor, in free ($p<0.01$) and delivery ($p<0.001$) groups compared to saline (**Figure 41A**). Moreover, the delivery group significantly increased the levels of VEGF, a potent angiogenic factor, and Shh, a master cardiac morphogen, over saline ($p<0.05$), while the free group was statistically similar to saline ($p>0.05$) (**Figure 41B,C**). Lastly, the free group significantly decreased the levels of TGF-β1, a pro-fibrotic factor, compared to saline, but the delivery group reduced TGF-β1 levels even more and was significantly less than both saline ($p<0.001$) and free ($p<0.05$) groups (**Figure 41D**). Taken together, these results suggest a high level of direct or indirect interaction between different proteins during response to tissue injury. The timed and controlled release of our complementary proteins augmented the presence of beneficial factors IGF-I, VEGF, and Shh that likely contributed to increased cardioprotection, revascularization, and signaling of repair mechanisms, while reduced levels of TGF-β1 likely contributed to reducing excessive collagen deposition and interstitial fibrosis [16, 27, 79, 165, 333, 334]. All these beneficial outcomes can aid in the prevention of heart failure and the restoration of heart function.

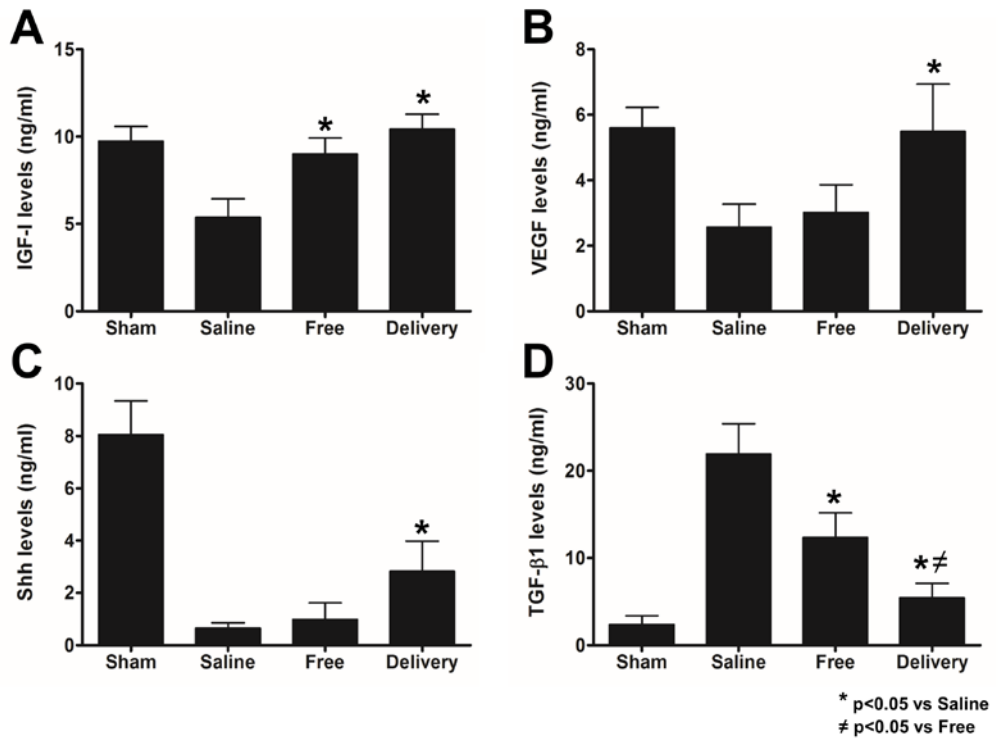

Figure 41. Levels of relevant proteins in tissue lysates at 8 weeks. (A) Free and delivery groups significantly increased IGF-I levels. (B) Delivery group significantly increased VEGF levels compared to saline. (C) Delivery group significantly increased Shh levels compared to saline. (D) Free group significantly decreased TGF-β1 levels compared to saline, but delivery group significantly decreased TGF-β1 levels compared to both saline and free. Data are presented as means ± SD (n=3-4/group at 8 wks). * p<0.05 vs saline, ≠ p<0.05 vs free.

4.4 DISCUSSION

As MI overwhelms the inflicted with multiple pathologies developing over time and progressing the heart towards dysfunction and failure, one can only imagine how complex and challenging an effective therapeutic approach, that fully repairs and regenerates the infarcted myocardium, would be to develop. Relevant therapeutic proteins, being crucial for cardiac cell signaling,

function, and behavior, represent very promising players to employ in MI treatment strategies. In order to ensure efficacy of a therapy, it is necessary to mimic the spatiotemporal presence of these proteins in the natural microenvironment during a proper tissue repair and regeneration process. This brings into spotlight the advantages of using an effective controlled delivery system that can release multiple proteins spatiotemporally after MI in order to induce cardiac repair and regeneration mechanisms.

In this work, we first explored the therapeutic potential of timed and controlled release of four proteins, which have relatively distinct but complementary roles in cardiac function, TIMP-3, IL-10, FGF-2, and SDF-1α, on improving cardiac function after MI in a rat model. To reduce inflammation and ECM degradation early after MI, TIMP-3 and IL-10 were encapsulated within a fibrin gel. To trigger a robust angiogenesis process and stem cell recruitment, FGF-2 and SDF-1α were encapsulated within heparin-based coacervates and distributed in the same fibrin gel. We have shown the efficacy of this fibrin gel-coacervate system for sequential release of VEGF and PDGF previously [322]. Fibrin gel, formed through the polymerization of fibrinogen by thrombin, is commercially available and has been used for protein and cell delivery [210]. We have also demonstrated in a number of studies the advantage of coacervate-delivered proteins for many biomedical applications, including cardiac repair [86, 241-244, 293, 322, 335, 336]. Our polyvalent complex coacervate is comprised of a synthetic polycation PEAD combined with heparin and a heparin-binding protein, enabling its sustained release over time due to PEAD degradation, changes in ionic environment, presence of enzymes, and other factors [235, 237]. Our results demonstrated the ability of the fibrin gel-coacervate composite to provide early release of TIMP-3 and IL-10 by one week, followed by a sustained release of FGF-2 and SDF-1α that lasted at least six weeks. The release kinetics

provided by this composite gel are deemed suitable for the desired spatiotemporal presence of the complementary proteins during the proper repair process.

Here, we utilized a two-level half fractional factorial design to refine and optimize the protein combination and its doses. This powerful statistical tool allowed us to perform a fraction of the total runs, providing cost-effectiveness and valuable information about the relative significance of each protein in the combination, some of the possible protein-protein interactions, and the optimal protein doses for improving cardiac function 4 weeks after MI in a rat model [323-325]. Our results demonstrated the significant contributions of TIMP-3, FGF-2, and SDF-1α to improving ejection fraction, while indicating minimal contribution of IL-10 towards that purpose. IL-10 is a potent anti-inflammation cytokine that is reported to improve cardiac function and angiogenesis, and reduce scar size and fibrosis after MI [66, 67, 314, 329, 337-339]. However, a study using IL-10 knock-out models deduced that it doesn't affect ventricular remodeling critically [68]. The insignificant effect of IL-10 reported in our study, within the context of the protein combination, might have been influenced by two factors. The first factor is that IL-10's role in improving cardiac function might have been diminished by the presence of TIMP-3, which itself has been reported to have anti-inflammation effects through its inhibition of TNF-α-converting enzyme (TACE), the enzyme activator of TNF-α [63, 64]. TNF-α is a pro-inflammatory factor, involved in inducing inflammatory cell invasion of the infarcted myocardium, MMP production, and cell apoptosis [62-64]. The second factor is that an appropriate level of inflammatory response is necessary after MI to phagocytose dead cells and their debris, and that the presence of IL-10 alongside TIMP-3, within the protein combination, might have rendered IL-10 redundant and did not add additional benefit towards improving cardiac function. This result prompted us to remove IL-10 from the protein

combination and proceed with TIMP-3, FGF-2, and SDF-1α at higher doses (3μg each) that proved more beneficial than lower doses at improving cardiac function.

After refining the protein combination and doses, we performed an in-depth in vivo study to test the efficacy of spatiotemporal release of TIMP-3, FGF-2, and SDF-1α from the fibrin gel-coacervate composite in a rat MI model and compared it to sham, saline, and free proteins groups. We demonstrated the delivery group's significant potential to improve cardiac function and trigger repair mechanisms after infarction bringing it close to the normal case of the sham control in many evaluations. In most cases, the delivery group showed significant differences compared to saline group, and to free proteins group in many cases. The free proteins group, although showing some potential and trends of improvement in different evaluations, was not able to induce significant repair as the delivery group did compared to saline. This was indicative of the importance of controlled and timed delivery of the complementary proteins TIMP-3, FGF-2, and SDF-1α. Many protein therapies failed to prove long-term efficacy for MI treatment because of the shortcomings of proteins applied in free form, including very short-half lives, low retention at the target site, high doses required, and lack of spatiotemporal cues. A study concluded that bolus injections of a cocktail of four important proteins: FGF-2, SDF-1α, IGF-I, and hepatocyte growth factor (HGF), did not improve cardiac function, reduce infarct size, or promote stable microvasculature [340]. The study's results might be attributed to the absence of controlled release because without properly protecting the therapeutic proteins and delivering them spatiotemporally, a therapy might prove ineffective at cardiac repair. Our delivery approach offers a solution to these challenges, by protecting the proteins within the fibrin gel-coacervate composite, localizing their presence at target tissue, and releasing them spatiotemporally.

The delivery group significantly improved the heart contractile function as early as 1 week after MI and lasted up to 8 weeks in comparison to saline and free proteins group, which had the cardiac function continuously drop over the period tested, measured by echocardiography and further confirmed by cardiac MRI at 8 weeks. We reported a cardiac function improvement of 60-75% above non-treated infarcted hearts. This effectively reduced the risk of MI progressing to heart failure. We also demonstrated significant reductions in ventricular dilation, ventricular wall thinning, myocardial wall stress and stiffness, and MMP activity. These assessments are interrelated and linked to adverse remodeling and early ECM degradation. The reductions we show in these evaluations might be highly attributed to the vital role of early TIMP-3 release from our delivery system. TIMP-3 is an ECM-bound enzyme that forms tight non-covalent and stable complexes with the non-activated latent form of MMPs (pro-MMP), blocking the MMP's catalytic domain and preventing its access to substrates [136, 137, 152]. This effectively inhibits activation of MMPs, responsible for cleaving and hydrolyzing many components of the ECM including elastin, fibronectin, collagen, and proteoglycans [136-138]. This feature of TIMP-3, being able to reduce ECM degradation, likely contributed to mitigating LV adverse remodeling, wall thinning, and dilation; thereby reducing the risk of cardiac rupture and contractile dysfunction. Other studies have shown the importance of TIMP-3 in cardiac diseases. Deficiency in TIMP-3 has been reported to lead to cardiac dilation, dysfunction, rupture, and mortality [147, 332, 341]. Cell-based TIMP-3 gene delivery improved heart function and reduced cardiac expression and activity of MMP-2 and -9 [151]. TIMP-3 delivered by collagen or hyaluronic gels was able to improve ejection fraction and reduce ventricular dilation and infarct size in rat and pig models [88, 177].

The delivery group in our study improved revascularization of the infarcted myocardium, triggering a robust angiogenesis process that led to the formation of mature neovessels with potential of participating in blood flow and perfusion. The triggers behind the formation of mature neovasculature in the borderzones of the infarct region can be linked mainly to FGF-2 and, to a lesser degree SDF-1α, present in our protein combination and delivered in a sustained manner by the coacervate. As a strong angiogenic factor, FGF-2 induces endothelial cell proliferation and sprouting leading to the formation of tube-like structures that evolve into neovessels with lumens [16, 20]. We have shown in our previous studies the ability of FGF-2 coacervate to induce persistent angiogenesis and cardiac repair [241, 242, 335]. Our protein signaling results show that the delivery group upregulates VEGF expression, which is an endothelial-specific factor that is important for angiogenesis and vasodilation [19, 291]. This result concurs with previous studies which demonstrated that FGF-2 upregulates VEGF and vice versa [23, 24]. FGF-2 also acts in synergy with PDGF signaling to improve neovessels' maturation and stability by pericytes [342]. In addition, SDF-1α can increase angiogenesis and myocardial repair by recruiting endothelial progenitor cells to the ischemic tissue and in response to VEGF signaling [31, 32]. TIMP-3 was also reported to increase VEGF levels from cardiac fibroblasts within the infarct area [88]. Moreover, increased expression of Shh, as found in this study due to the delivery group, has been shown to activate several signaling pathways and contribute to angiogenesis [343-345]. All these indications support our finding that spatiotemporal delivery of TIMP-3, FGF-2, and SDF-1α leads to the formation of new, mature, and stable blood vessels, necessary to the repair of MI injury.

As MI causes the death of millions of cardiomyocytes and puts millions more at risk, it is an indispensable task to support the survival of cardiomyocytes after MI and prevent their

apoptosis. Our delivery group showed remarkable ability to preserve the viability of the cardiac muscle, activate pro-survival molecular pathways ERK1/2 and Akt, inhibit apoptosis mediated by caspase-3, and increase expression of anti-apoptotic factor IGF-I. Many studies have proved the important role of activating the PI3K/Akt and Ras-Raf-MEK-ERK pathways to inhibit apoptosis and provide cardioprotection [76-78]. The complementary proteins in our system TIMP-3, FGF-2, and SDF-1α have all been reported to prevent cardiomyocyte apoptosis [85, 88, 151, 346-350]. Moreover, our delivery group induced higher expression levels of IGF-I and Shh. IGF-I is a well-studied potent cardioprotective and anti-apoptotic factor that activates the PI3K/Akt pathway and prevents cardiomyocyte apoptosis [351-354]. Shh also reduces cardiomyocyte apoptosis through increased expression of pro-survival markers and reduced expression of apoptotic markers, as we and other groups have shown [86, 343, 344].

Stem cell recruitment to the infarct region is another important aspect of an effective therapy because of the potential of stem cells to ultimately differentiate into cardiac and vascular cells and/or support the repair by paracrine signaling, thereby supporting the survival of remaining cardiomyocytes and regeneration of a viable myocardium that replaces the lost damaged one. Our delivery group showed significant ability at homing stem cells to the borderzones of the infarct. This is likely due to the sustained bioavailability of SDF-1α provided by the coacervate within our composite. SDF-1α is a powerful chemoattractant that can mobilize different types of progenitor cells such as endothelial progenitor cells (EPCs), hematopoietic stem cells (HSC), mesenchymal stem cells (MSCs), and cardiac stem cells (CSCs) to the infarcted myocardium [85]. Our group has shown that tissue-engineered scaffolds coated with SDF-1α coacervates improved migration and infiltration of EPCs and MSCs [355]. The stem/progenitor cells, when recruited by SDF-1α to the heart, can enhance angiogenesis

and cardiomyocyte survival and differentiation [117-119, 321, 330, 331]. FGF-2, present within our delivery system, and IGF-I, induced by our delivery combination, have been suggested to trigger differentiation of CSCs into functional cardiomyocytes [129, 130].

An excessive inflammatory response can have detrimental effects after MI. Large amounts of reactive oxygen species (ROS) produced by inflammatory cells invading the infarcted myocardium can cause massive cell death [55]. The spatiotemporal delivery approach employed in our study proved effective at reducing inflammation and promoting tissue repair. Our results revealed the reduction of non-M2 macrophages, which contain M1 macrophages that exacerbate inflammation and ECM degradation [59]. We also reported an increase in M2 macrophages which contribute to reconstruction of the ECM and anti-inflammatory effects [59]. TIMP-3, provided by our delivery approach, can exert anti-inflammatory effects by inhibiting TNF-α which increases in heart failure and triggers infiltration of inflammatory cells into the myocardium [62-64, 177]. Our strategy reduced the potentially deleterious impact of excessive inflammation by preventing the infiltration of harmful macrophages into the infarcted myocardium or possibly forcing a change in the phenotype of present ones to become of M2 phenotype involved in tissue repair.

The unregulated and excessive collagen deposition in the infarct, and later non-infarct regions, leads to interstitial fibrosis that increases myocardial stiffness and risk of contractile dysfunction. Fibrosis arises as a result of an imbalance in ECM structure and increased production of collagen by different cells, mainly myofibroblasts. Myofibroblasts contribute to adverse remodeling and are heavily influenced by the signaling of pro-fibrotic factors such as TGF-β [160, 163, 164]. In this study, our findings demonstrated that the spatiotemporal delivery of TIMP-3, FGF-2, and SDF-1α prevented the development of interstitial fibrosis and the

expansion of scar and granulation tissue to a large extent. All of these 3 complementary proteins play important roles in reducing fibrosis in the heart after MI injury [88, 212, 241, 356-359]. Our delivery group proved very effective at decreasing the levels of TGF-β1, a main promoter of fibrosis post-infarction [164]. Therapies that aimed to antagonize TGF-β and reduce fibrosis proved beneficial for the heart recovery [171-174]. These results likely helped in the preservation of myocardial elasticity as witnessed in our delivery group. Therefore, the efficacy of our spatiotemporal delivery approach at preventing the excessive deposition of fibrillary collagen reduced the risk of stiffening the ventricular wall, its loss of contractile ability, and progression to heart failure.

4.5 CONCLUSIONS

We developed an optimized combination therapy for the repair of the infarcted myocardium using complementary proteins TIMP-3, FGF-2, and SDF-1α. This therapy utilizes a composite of fibrin gel and heparin-based coacervates, where complementary proteins are embedded differently for achieving spatiotemporal release. TIMP-3 was embedded in the fibrin gel achieving early release, while FGF-2 and SDF-1α were encapsulated within heparin-based coacervates and distributed in the same gel achieving sustained release. We found this refined spatiotemporal delivery approach to significantly improve cardiac function up to 8 weeks after MI in rats. In addition, we reported significant improvements in myocardial elasticity, cardiomyocyte survival, angiogenesis, stem cell homing, activation of survival pathways, and important protein signaling. We also reported significant reductions in ventricular dilation and wall thinning, inflammation, MMP activity, fibrosis, and cell apoptosis. Taken together, we

believe that the more comprehensive a treatment strategy is, where multiple crucial proteins are employed and delivered in a spatiotemporal manner, the more the therapy will be successful and effective at cardiac repair. Therefore, the spatiotemporal delivery approach of complementary proteins TIMP-3, FGF-2, and SDF-1α may serve as a new therapy to ameliorate MI injury and set the infarcted myocardium on a path to full repair, regeneration, and functional recovery.

5.0 SUMMARY AND FUTURE DIRECTIONS

As our knowledge increases on the different roles and molecular pathways in which therapeutic proteins are involved, and the new developments in enabling spatiotemporal delivery of proteins through the design of effective controlled release systems, the enhanced options for treatment of myocardial infraction (MI) are expected to occur in the near future. In this dissertation, we demonstrated the strong potential of controlled delivery of different combinations of therapeutic proteins on the repair of the infarcted myocardium in a rat model.

In chapter 2, we investigated the ability of our heparin-based coacervate technology to co-release VEGF and HGF and the effect of the dual delivery on angiogenic in vitro assays. We were able to demonstrate the coacervate's high loading efficiency and sustained release of both factors for at least 3 weeks in vitro, and that coacervate-based dual delivery of VEGF and HGF triggered more profound angiogenic effects than free-form administration of the two factors and the controlled release of each one alone. In chapter 3, we designed a composite of fibrin gel and coacervate to achieve sequential release of VEGF and PDGF for the purpose of therapeutic angiogenesis after MI in a rat model. With VEGF encapsulated directly in fibrin gel and PDGF encapsulated within coacervates distributed in the same gel, an early release of VEGF was achieved compared to a more sustained and delayed release of PDGF. We demonstrated the effectiveness of this sequential delivery approach on inducing a more robust angiogenesis process, which led to the formation of mature and stable neovasculature in the infarct

borderzone. Sequential delivery of VEGF and PDGF reflected positively on a functional level with improved cardiac contractility, and on a tissue level with improved cardiac muscle viability and angiogenesis and reduced fibrosis and macrophage presence 4 weeks after infarction. In chapter 4, we aimed for a potentially comprehensive strategy to treat MI by investigating the spatiotemporal delivery of 4 complementary proteins: TIMP-3, IL-10, FGF-2, and SDF-1α. TIMP-3 and IL-10 were embedded in the fibrin gel directly for early release to reduce ECM degradation and inflammation, respectively, while FGF-2 and SDF-1α were encapsulated within coacervates inside the gel for sustained release that is favorable for angiogenesis and stem cell homing as these processes require prolonged signaling. We optimized this combination using factorial design of experiments and found that TIMP-3, FGF-2, and SDF-1α had significant effects on improving cardiac function, while IL-10 did not, prompting IL-10's removal from the combination. The optimized combination of TIMP-3, FGF-2, and SDF-1α delivered spatiotemporally by the fibrin-coacervate gel composite induced significant improvements in cardiac function, myocardial elasticity, cardiomyocyte survival, angiogenesis, stem cell homing, important protein signaling, and significant reductions in ventricular dilation, inflammation, fibrosis, MMP activity, apoptosis, and overall scar expansion.

In this dissertation, we were able to develop a potentially comprehensive strategy to treat MI based on a carefully designed therapeutic approach that provided 3 complementary and crucial proteins spatiotemporally to prevent a number of pathologies triggered by MI and set the infarcted myocardium on a path to repair and recovery. To better understand the improvement in the design of our therapeutic strategies over time, here we directly compare some of the important functional data between our approaches in chapters 3 and 4. In chapter 3, we focused on therapeutic angiogenesis through the sequential delivery of VEGF and PDGF to the infarcted

rat hearts. Using the echocardiography results, we estimated the functional improvement of this approach to be at 66% over untreated infarcted hearts at the terminal time point of 4 weeks after MI, showing a slight decline in function compared to the 68% improvement shown at 2 weeks. As for the other important functional assessment of ventricular dilation, we found no significant effect of the sequential delivery of VEGF and PDGF on dilation compared to untreated infarcted hearts with increasing dilation recorded throughout the period tested. In contrast, our potentially comprehensive approach, involving the spatiotemporal delivery of TIMP-3, FGF-2, and SDF-1α, developed in chapter 4 demonstrated significant advantages over the approach of chapter 3. At the functional level, we demonstrated our complementary approach preserved cardiac contractility significantly as early as 1 week after infarction with continuous improvement up to 8 weeks showing a 74% improvement over untreated infarcted rat hearts. This is an important advantage to see continuous improvement in function from 1 week to 8 weeks compared to the slight decline that we started to observe after 2 weeks in our chapter 3 approach. In regards to ventricular dilation, our results show significant reduction in LV dilation compared to untreated infarcted hearts up to 8 weeks. This is an additional advantage of the complementary approach in chapter 4 that we were not able to demonstrate with the previous approach of chapter 3, which showed no benefit on reducing dilation. We speculate that having TIMP-3 in our combination releasing early after MI helped preserve the structure of the heart and prevent ECM degradation, thereby significantly improving function and preventing dilation. In addition, having FGF-2 and SDF-1α, each with their unique roles in cardiac function, from angiogenesis, to stem cell homing, to supporting cardiomyocyte survival, and others drove the repair to a new level. Our results in chapter 4 indicate the advantage and improvement in our therapeutic strategy to repair the infarcted myocardium in a significantly more comprehensive

manner by addressing multiple MI pathologies through spatiotemporal delivery of multiple relevant proteins.

Future directions for the research performed in this dissertation include testing the efficacy of our complementary approach in a large animal model, possible expansion of the therapeutic strategy to include other therapeutic proteins and/or combine with stem cells, and investigating the ability to deliver the composite gel through minimally invasive technology. We believe that the next logical step for this research is evaluating our complementary therapeutic approach in a large animal model. This would require the investigation of proper scalability of the fibrin gel-coacervate composite formulation parameters and the protein doses. A multimodal approach that combines multiple therapeutic proteins with promising cardiac stem cells, for instance, might be an attractive strategy, whereby therapeutic agents can act on co-delivered cells and the target tissue cells at the same time. This might not only increase the efficacy of the repair process, but also increase the possibility of generating a new viable myocardial tissue synchronized and electromechanically coupled with the rest of the heart. Although pursuing such multimodal approaches might result in a longer regulatory process and delays in clinical translation, the potential for a significant enhancement in treatment outcome should make these sophisticated approaches intriguing with serious consideration for future therapies.

Localized therapy is very important to enhance efficacy in target tissues and reduce interaction with off-target tissues. It is also important to improve the translational potential of our therapy by enabling its delivery through minimally invasive approaches to reduce surgical time and costs, and patient morbidity. Therefore, we believe that to achieve localized delivery to the infarcted myocardium in a minimally invasive way, catheterization technology can be

utilized. However, catheter delivery of more advanced materials such as hydrogels is more challenging than the typical saline injections. Catheter-based access can be achieved through different routes such as intracoronary, intravenous, epicardial, transvascular, and endocardial. However, the retention of the cargo at the target tissue differs depending on the catheter approach. We believe that endocardial delivery might be the best approach to ensure high retention at the myocardial tissue. Endocardial delivery catheter devices would approach the myocardium from inside the ventricle with the help of support steerable designs and imaging systems to accurately target the infarct border zones. In order to ensure proper delivery of our gel-coacervate composite using catheter-based approaches, we need to optimize viscosity and gelation parameters so that gelation doesn't occur while the injectable material is still in the catheter or too late after injection where the therapeutic cargo would diffuse away from the target site. We would want the gelation to occur rather quickly in situ once the composite has been injected. Having features such as shear-thinning and stimuli-responsiveness might be promising to facilitate injectability and gelation of the composite gel at the right place and time. A successful localized therapy using catheter-based systems, would be of great value to reduce surgical invasiveness, time, and burden, while capitalizing on the gains of increased retention, cytocompatibility, and spatiotemporal release kinetics of therapeutic formulations. The development of such systems would significantly aid the clinical translation of cardiac repair approaches.

Because the heart physiology and pathology are inherently complex, it would be no surprise that more comprehensive therapeutic strategies with advanced delivery techniques, such as the one developed in this dissertation, may be needed to enable clinical translation of cardiac repair and regeneration therapies. As we expand our knowledge, decipher more

experimental data, and utilize more advanced technological tools, establishing a cure for ischemic heart disease could be within our reach in the foreseeable future.

APPENDIX A

RELEASE PROFILE OF VEGF AND PDGF FROM COACERVATE

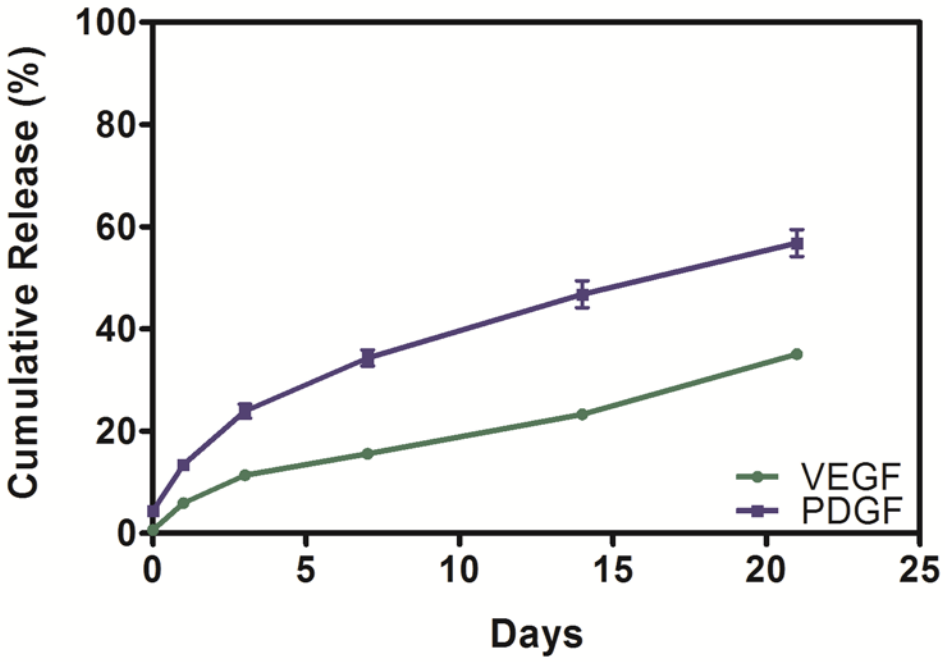

Supplementary Figure S1. Release of VEGF and PDGF from the coacervate. The coacervate was formed by mixing 100ng of each GF together, then with heparin, then with PEAD polycation. Release of each GF was detected by ELISA. The coacervate released 57% of PDGF compared to 35% of VEGF by 3 weeks. Data are presented as means ± SD (n=3).

APPENDIX B

MEASUREMENT OF ESV, EDV, AND EF USING MRI

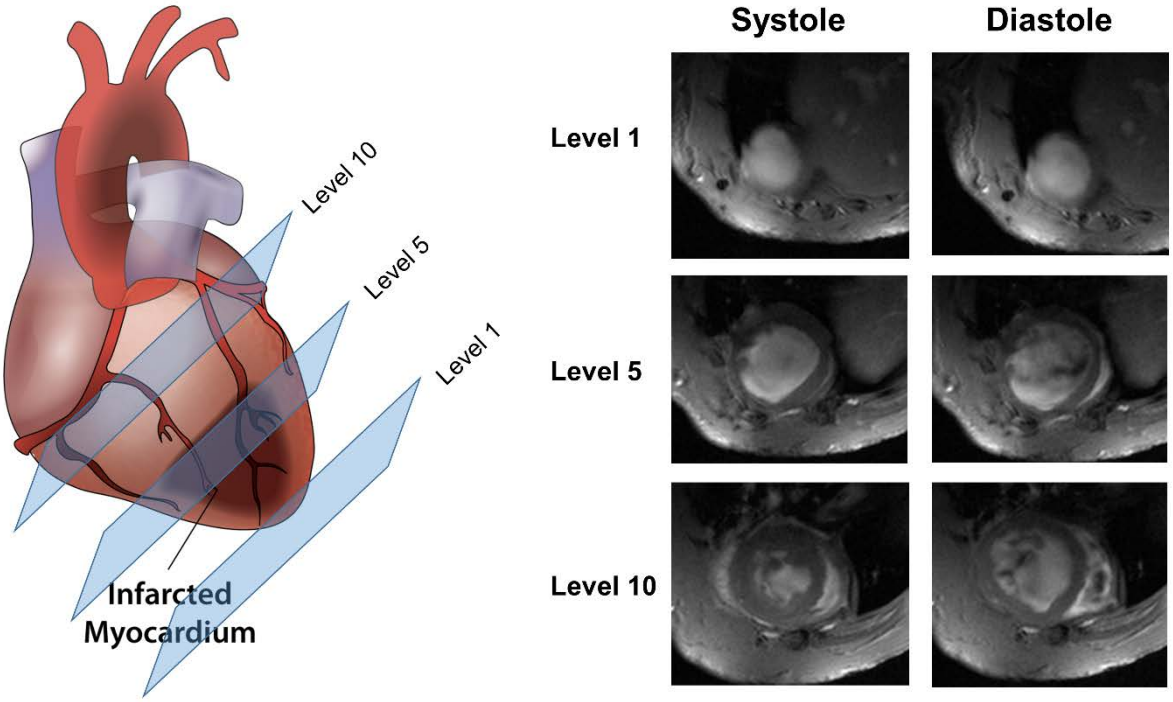

Supplementary Figure S2. MRI was performed with an average of 10 contiguous slices, at a thickness of 1.5 mm covering the distance from heart apex at level 1 to mitral valve at level 10 in the representative images. End-systolic and end-diastolic phases were identified for each subject and the LV cavity manually traced to determine LV end-systolic (ESV) and end-diastolic (EDV) volumes. Ejection fraction (EF%) was calculated from ESV and EDV values. The infarct reduces the contractility of the heart as seen at levels 1 and 5.

APPENDIX C

REGRESSION ANALYSIS OF FACTORIAL DESIGN MODEL

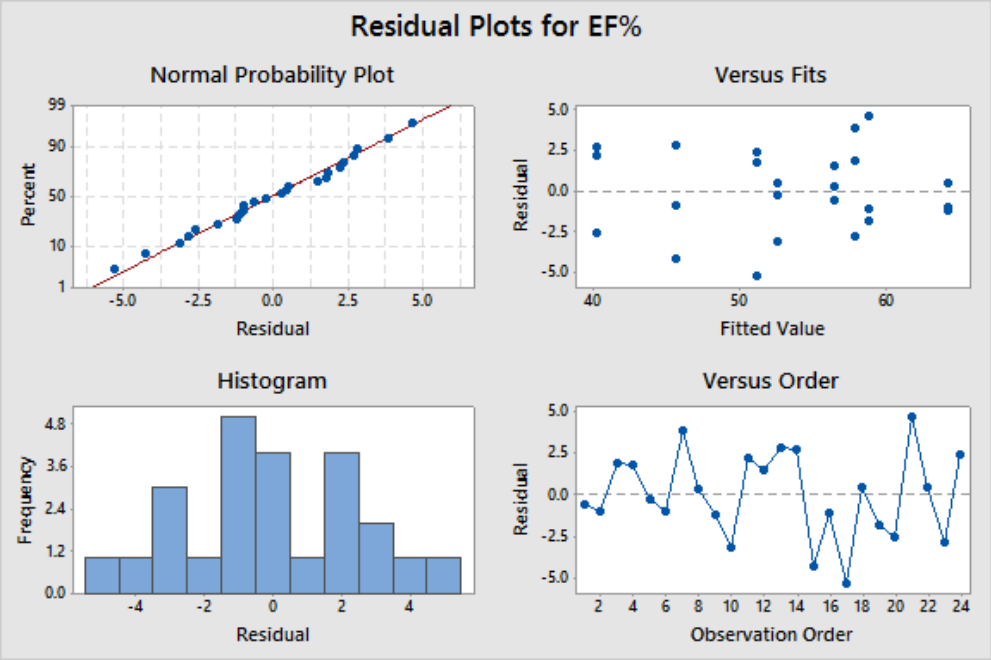

Supplementary Figure S3. Regression analysis assumes the measurement and experimental errors in the data meet three assumptions: (1) the errors are normally distributed as seen in the straight line of the normal probability plot, (2) the errors are independent of time as seen in the random pattern of the residuals over the observation order, (3) the spread of the residuals is roughly equivalent regardless of the level of the EF% response.

APPENDIX D

EFFECT OF DELIVERED COMPLEMENTARY PROTEINS ON CARDIOMYOCYTE SURVIVAL, ANGIOGENESIS, AND FIBROSIS AT 2 WEEKS AFTER MI

D.1 CARIAC MUSCLE VIABILITY AT 2 WEEKS AFTER MI

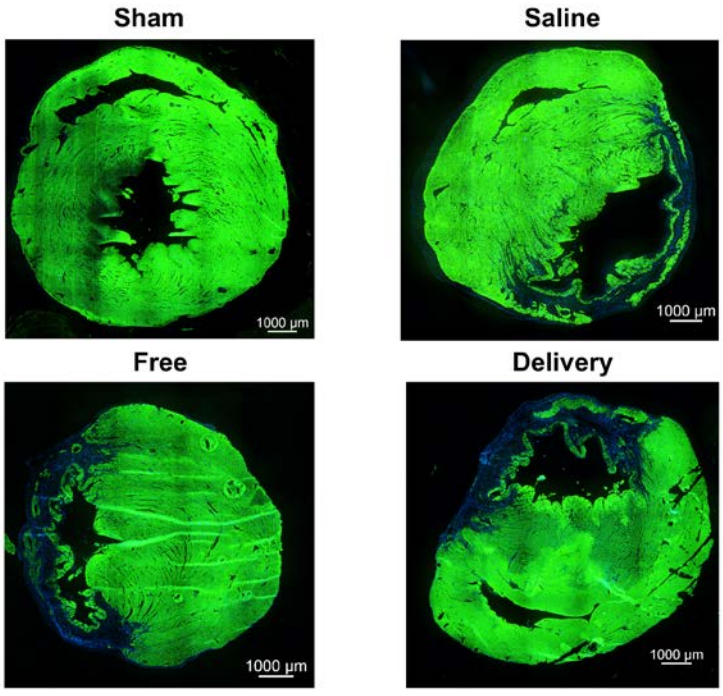

Supplementary Figure S4. Representative images of the different groups showing staining of viable cardiac muscle by cardiac troponin I (cTnI) (green) at 2 weeks after MI.

D.2 ANGIOGENESIS AT 2 WEEKS AFTER MI

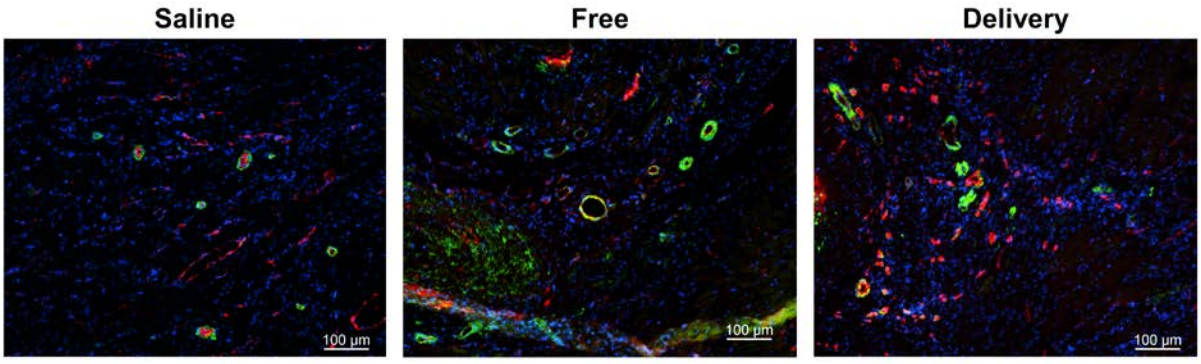

Supplementary Figure S5. Representative images of the infarct groups showing co-staining of vWF (red), an endothelial marker, and α-SMA (green), a pericyte marker at 2 weeks after MI.

D.3 FIBROSIS AT 2 WEEKS AFTER MI

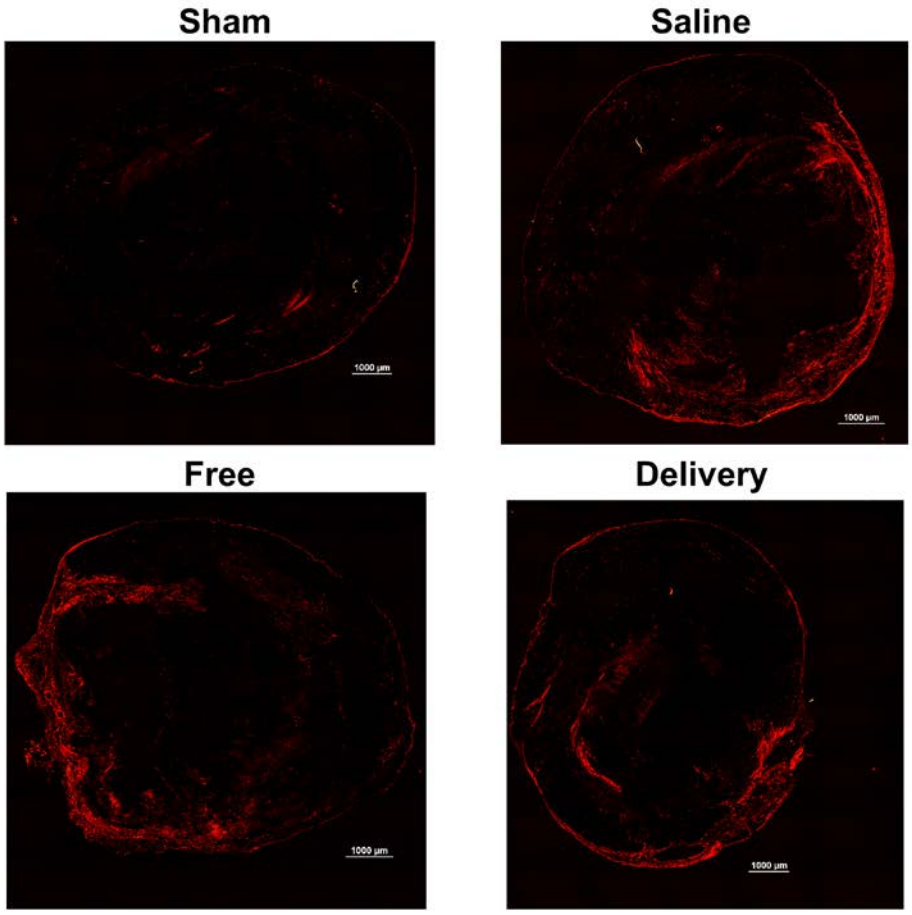

Supplementary Figure S6. Representative picrosirius red staining images show the extent of collagen deposition in the different groups at 2 weeks after MI.

BIBLIOGRAPHY

[1] Mendis S, Puska P, Norrving B, World Health Organization., World Heart Federation., World Stroke Organization. Global atlas on cardiovascular disease prevention and control. Geneva: World Health Organization in collaboration with the World Heart Federation and the World Stroke Organization; 2011.

[2] Go AS, Mozaffarian D, Roger VL, Benjamin EJ, Berry JD, Blaha MJ, et al. Heart disease and stroke statistics--2014 update: a report from the American Heart Association. Circulation 2014;129:e28-e292.

[3] Choi D, Hwang KC, Lee KY, Kim YH. Ischemic heart diseases: current treatments and future. J Control Release 2009;140:194-202.

[4] White HD, Chew DP. Acute myocardial infarction. Lancet 2008;372:570-84.

[5] Kurrelmeyer K, Kalra D, Bozkurt B, Wang F, Dibbs Z, Seta Y, et al. Cardiac remodeling as a consequence and cause of progressive heart failure. Clinical Cardiology 1998;21:14-9.

[6] Cohn JN, Ferrari R, Sharpe N. Cardiac remodeling--concepts and clinical implications: a consensus paper from an international forum on cardiac remodeling. Behalf of an International Forum on Cardiac Remodeling. J Am Coll Cardiol 2000;35:569-82.

[7] Alcon A, Cagavi Bozkulak E, Qyang Y. Regenerating functional heart tissue for myocardial repair. Cell Mol Life Sci 2012;69:2635-56.

[8] Hastings CL, Roche ET, Ruiz-Hernandez E, Schenke-Layland K, Walsh CJ, Duffy GP. Drug and cell delivery for cardiac regeneration. Adv Drug Deliv Rev 2015;84:85-106.

[9] Xin M, Olson EN, Bassel-Duby R. Mending broken hearts: cardiac development as a basis for adult heart regeneration and repair. Nat Rev Mol Cell Biol 2013;14:529-41.

[10] Braun T, Dimmeler S. Breaking the silence: stimulating proliferation of adult cardiomyocytes. Dev Cell 2009;17:151-3.

[11] Shiojima I, Sato K, Izumiya Y, Schiekofer S, Ito M, Liao R, et al. Disruption of coordinated cardiac hypertrophy and angiogenesis contributes to the transition to heart failure. J Clin Invest 2005;115:2108-18.

[12] Kerkela R, Karsikas S, Szabo Z, Serpi R, Magga J, Gao E, et al. Activation of hypoxia response in endothelial cells contributes to ischemic cardioprotection. Mol Cell Biol 2013;33:3321-9.

[13] Wang J, Hoshijima M, Lam J, Zhou Z, Jokiel A, Dalton ND, et al. Cardiomyopathy associated with microcirculation dysfunction in laminin alpha4 chain-deficient mice. J Biol Chem 2006;281:213-20.

[14] Leucker TM, Bienengraeber M, Muravyeva M, Baotic I, Weihrauch D, Brzezinska AK, et al. Endothelial-cardiomyocyte crosstalk enhances pharmacological cardioprotection. J Mol Cell Cardiol 2011;51:803-11.

[15] Winegrad S, Henrion D, Rappaport L, Samuel JL. Vascular endothelial cell-cardiac myocyte crosstalk in achieving a balance between energy supply and energy use. Adv Exp Med Biol 1998;453:507-14.

[16] Cochain C, Channon KM, Silvestre JS. Angiogenesis in the infarcted myocardium. Antioxid Redox Signal 2013;18:1100-13.

[17] Carmeliet P, Jain RK. Molecular mechanisms and clinical applications of angiogenesis. Nature 2011;473:298-307.

[18] Losordo DW, Dimmeler S. Therapeutic angiogenesis and vasculogenesis for ischemic disease. Part I: angiogenic cytokines. Circulation 2004;109:2487-91.

[19] Zachary I, Gliki G. Signaling transduction mechanisms mediating biological actions of the vascular endothelial growth factor family. Cardiovasc Res 2001;49:568-81.

[20] Formiga FR, Tamayo E, Simon-Yarza T, Pelacho B, Prosper F, Blanco-Prieto MJ. Angiogenic therapy for cardiac repair based on protein delivery systems. Heart Fail Rev 2012;17:449-73.

[21] Zachary I, Mathur A, Yla-Herttuala S, Martin J. Vascular protection: A novel nonangiogenic cardiovascular role for vascular endothelial growth factor. Arterioscler Thromb Vasc Biol 2000;20:1512-20.

[22] Kardami E, Detillieux K, Ma X, Jiang Z, Santiago JJ, Jimenez SK, et al. Fibroblast growth factor-2 and cardioprotection. Heart Fail Rev 2007;12:267-77.

[23] Seghezzi G, Patel S, Ren CJ, Gualandris A, Pintucci G, Robbins ES, et al. Fibroblast growth factor-2 (FGF-2) induces vascular endothelial growth factor (VEGF) expression in the endothelial cells of forming capillaries: an autocrine mechanism contributing to angiogenesis. J Cell Biol 1998;141:1659-73.

[24] Tomanek RJ, Holifield JS, Reiter RS, Sandra A, Lin JJ. Role of VEGF family members and receptors in coronary vessel formation. Dev Dyn 2002;225:233-40.

[25] Kano MR, Morishita Y, Iwata C, Iwasaka S, Watabe T, Ouchi Y, et al. VEGF-A and FGF-2 synergistically promote neoangiogenesis through enhancement of endogenous PDGF-B-PDGFRbeta signaling. J Cell Sci 2005;118:3759-68.

[26] Murakami M, Simons M. Fibroblast growth factor regulation of neovascularization. Curr Opin Hematol 2008;15:215-20.

[27] Segers VF, Lee RT. Protein therapeutics for cardiac regeneration after myocardial infarction. J Cardiovasc Transl Res 2010;3:469-77.

[28] Srinivas G, Anversa P, Frishman WH. Cytokines and myocardial regeneration: a novel treatment option for acute myocardial infarction. Cardiol Rev 2009;17:1-9.

[29] Gerritsen ME. HGF and VEGF: a dynamic duo. Circ Res 2005;96:272-3.

[30] Wang Y, Ahmad N, Wani MA, Ashraf M. Hepatocyte growth factor prevents ventricular remodeling and dysfunction in mice via Akt pathway and angiogenesis. J Mol Cell Cardiol 2004;37:1041-52.

[31] Tang JM, Wang JN, Zhang L, Zheng F, Yang JY, Kong X, et al. VEGF/SDF-1 promotes cardiac stem cell mobilization and myocardial repair in the infarcted heart. Cardiovasc Res 2011;91:402-11.

[32] Yamaguchi J, Kusano KF, Masuo O, Kawamoto A, Silver M, Murasawa S, et al. Stromal cell-derived factor-1 effects on ex vivo expanded endothelial progenitor cell recruitment for ischemic neovascularization. Circulation 2003;107:1322-8.

[33] Jay SM, Lee RT. Protein engineering for cardiovascular therapeutics: untapped potential for cardiac repair. Circ Res 2013;113:933-43.

[34] Pascual-Gil S, Garbayo E, Diaz-Herraez P, Prosper F, Blanco-Prieto MJ. Heart regeneration after myocardial infarction using synthetic biomaterials. J Control Release 2015;203C:23-38.

[35] Epstein SE, Kornowski R, Fuchs S, Dvorak HF. Angiogenesis therapy: amidst the hype, the neglected potential for serious side effects. Circulation 2001;104:115-9.

[36] Lee RJ, Springer ML, Blanco-Bose WE, Shaw R, Ursell PC, Blau HM. VEGF gene delivery to myocardium: deleterious effects of unregulated expression. Circulation 2000;102:898-901.

[37] Davis S, Yancopoulos GD. The angiopoietins: Yin and Yang in angiogenesis. Curr Top Microbiol Immunol 1999;237:173-85.

[38] Hellstrom M, Kalen M, Lindahl P, Abramsson A, Betsholtz C. Role of PDGF-B and PDGFR-beta in recruitment of vascular smooth muscle cells and pericytes during embryonic blood vessel formation in the mouse. Development 1999;126:3047-55.

[39] Greenberg JI, Shields DJ, Barillas SG, Acevedo LM, Murphy E, Huang J, et al. A role for VEGF as a negative regulator of pericyte function and vessel maturation. Nature 2008;456:809-13.

[40] Brudno Y, Ennett-Shepard AB, Chen RR, Aizenberg M, Mooney DJ. Enhancing microvascular formation and vessel maturation through temporal control over multiple pro-angiogenic and pro-maturation factors. Biomaterials 2013;34:9201-9.

[41] Hao X, Silva EA, Mansson-Broberg A, Grinnemo KH, Siddiqui AJ, Dellgren G, et al. Angiogenic effects of sequential release of VEGF-A165 and PDGF-BB with alginate hydrogels after myocardial infarction. Cardiovasc Res 2007;75:178-85.

[42] Richardson TP, Peters MC, Ennett AB, Mooney DJ. Polymeric system for dual growth factor delivery. Nat Biotechnol 2001;19:1029-34.

[43] Tengood JE, Ridenour R, Brodsky R, Russell AJ, Little SR. Sequential delivery of basic fibroblast growth factor and platelet-derived growth factor for angiogenesis. Tissue Eng Part A 2011;17:1181-9.

[44] Carnicer R, Crabtree MJ, Sivakumaran V, Casadei B, Kass DA. Nitric oxide synthases in heart failure. Antioxid Redox Signal 2013;18:1078-99.

[45] Wiemer G, Itter G, Malinski T, Linz W. Decreased nitric oxide availability in normotensive and hypertensive rats with failing hearts after myocardial infarction. Hypertension 2001;38:1367-71.

[46] Moroi M, Zhang L, Yasuda T, Virmani R, Gold HK, Fishman MC, et al. Interaction of genetic deficiency of endothelial nitric oxide, gender, and pregnancy in vascular response to injury in mice. J Clin Invest 1998;101:1225-32.

[47] Nakata S, Tsutsui M, Shimokawa H, Suda O, Morishita T, Shibata K, et al. Spontaneous myocardial infarction in mice lacking all nitric oxide synthase isoforms. Circulation 2008;117:2211-23.

[48] Dawson D, Lygate CA, Zhang MH, Hulbert K, Neubauer S, Casadei B. nNOS gene deletion exacerbates pathological left ventricular remodeling and functional deterioration after myocardial infarction. Circulation 2005;112:3729-37.

[49] Saraiva RM, Minhas KM, Raju SV, Barouch LA, Pitz E, Schuleri KH, et al. Deficiency of neuronal nitric oxide synthase increases mortality and cardiac remodeling after myocardial infarction: role of nitroso-redox equilibrium. Circulation 2005;112:3415-22.

[50] Burkard N, Williams T, Czolbe M, Blomer N, Panther F, Link M, et al. Conditional overexpression of neuronal nitric oxide synthase is cardioprotective in ischemia/reperfusion. Circulation 2010;122:1588-603.

[51] Scherrer-Crosbie M, Ullrich R, Bloch KD, Nakajima H, Nasseri B, Aretz HT, et al. Endothelial nitric oxide synthase limits left ventricular remodeling after myocardial infarction in mice. Circulation 2001;104:1286-91.

[52] Landmesser U, Engberding N, Bahlmann FH, Schaefer A, Wiencke A, Heineke A, et al. Statin-induced improvement of endothelial progenitor cell mobilization, myocardial

neovascularization, left ventricular function, and survival after experimental myocardial infarction requires endothelial nitric oxide synthase. Circulation 2004;110:1933-9.

[53] Wilson SS, Ayaz SI, Levy PD. Relaxin: a novel agent for the treatment of acute heart failure. Pharmacotherapy 2015;35:315-27.

[54] Frangogiannis NG. The mechanistic basis of infarct healing. Antioxid Redox Signal 2006;8:1907-39.

[55] Saparov A, Chen CW, Beckman SA, Wang Y, Huard J. The role of antioxidation and immunomodulation in postnatal multipotent stem cell-mediated cardiac repair. Int J Mol Sci 2013;14:16258-79.

[56] Yang JJ, Kettritz R, Falk RJ, Jennette JC, Gaido ML. Apoptosis of endothelial cells induced by the neutrophil serine proteases proteinase 3 and elastase. Am J Pathol 1996;149:1617-26.

[57] Bekkers SC, Yazdani SK, Virmani R, Waltenberger J. Microvascular obstruction: underlying pathophysiology and clinical diagnosis. J Am Coll Cardiol 2010;55:1649-60.

[58] Iba O, Matsubara H, Nozawa Y, Fujiyama S, Amano K, Mori Y, et al. Angiogenesis by implantation of peripheral blood mononuclear cells and platelets into ischemic limbs. Circulation 2002;106:2019-25.

[59] Lambert JM, Lopez EF, Lindsey ML. Macrophage roles following myocardial infarction. Int J Cardiol 2008;130:147-58.

[60] Heymans S, Luttun A, Nuyens D, Theilmeier G, Creemers E, Moons L, et al. Inhibition of plasminogen activators or matrix metalloproteinases prevents cardiac rupture but impairs therapeutic angiogenesis and causes cardiac failure. Nat Med 1999;5:1135-42.

[61] Christia P, Frangogiannis NG. Targeting inflammatory pathways in myocardial infarction. Eur J Clin Invest 2013;43:986-95.

[62] Bradham WS, Bozkurt B, Gunasinghe H, Mann D, Spinale FG. Tumor necrosis factor-alpha and myocardial remodeling in progression of heart failure: a current perspective. Cardiovasc Res 2002;53:822-30.

[63] Bradham WS, Moe G, Wendt KA, Scott AA, Konig A, Romanova M, et al. TNF-alpha and myocardial matrix metalloproteinases in heart failure: relationship to LV remodeling. Am J Physiol Heart Circ Physiol 2002;282:H1288-95.

[64] Wisniewska M, Goettig P, Maskos K, Belouski E, Winters D, Hecht R, et al. Structural determinants of the ADAM inhibition by TIMP-3: crystal structure of the TACE-N-TIMP-3 complex. J Mol Biol 2008;381:1307-19.

[65] Kurrelmeyer KM, Michael LH, Baumgarten G, Taffet GE, Peschon JJ, Sivasubramanian N, et al. Endogenous tumor necrosis factor protects the adult cardiac myocyte against ischemic-

induced apoptosis in a murine model of acute myocardial infarction. Proc Natl Acad Sci U S A 2000;97:5456-61.

[66] Krishnamurthy P, Rajasingh J, Lambers E, Qin G, Losordo DW, Kishore R. IL-10 inhibits inflammation and attenuates left ventricular remodeling after myocardial infarction via activation of STAT3 and suppression of HuR. Circ Res 2009;104:e9-18.

[67] Manukyan MC, Alvernaz CH, Poynter JA, Wang Y, Brewster BD, Weil BR, et al. Interleukin-10 protects the ischemic heart from reperfusion injury via the STAT3 pathway. Surgery 2011;150:231-9.

[68] Zymek P, Nah DY, Bujak M, Ren G, Koerting A, Leucker T, et al. Interleukin-10 is not a critical regulator of infarct healing and left ventricular remodeling. Cardiovasc Res 2007;74:313-22.

[69] Huang GN, Thatcher JE, McAnally J, Kong Y, Qi X, Tan W, et al. C/EBP transcription factors mediate epicardial activation during heart development and injury. Science 2012;338:1599-603.

[70] Murry CE, Reinecke H, Pabon LM. Regeneration gaps: observations on stem cells and cardiac repair. J Am Coll Cardiol 2006;47:1777-85.

[71] Lefer DJ, Granger DN. Oxidative stress and cardiac disease. Am J Med 2000;109:315-23.

[72] Takemura G, Fujiwara H. Role of apoptosis in remodeling after myocardial infarction. Pharmacol Ther 2004;104:1-16.

[73] Kajstura J, Cheng W, Reiss K, Clark WA, Sonnenblick EH, Krajewski S, et al. Apoptotic and necrotic myocyte cell deaths are independent contributing variables of infarct size in rats. Lab Invest 1996;74:86-107.

[74] Black SC, Huang JQ, Rezaiefar P, Radinovic S, Eberhart A, Nicholson DW, et al. Co-localization of the cysteine protease caspase-3 with apoptotic myocytes after in vivo myocardial ischemia and reperfusion in the rat. J Mol Cell Cardiol 1998;30:733-42.

[75] Cheng W, Kajstura J, Nitahara JA, Li B, Reiss K, Liu Y, et al. Programmed myocyte cell death affects the viable myocardium after infarction in rats. Exp Cell Res 1996;226:316-27.

[76] Kis A, Yellon DM, Baxter GF. Second window of protection following myocardial preconditioning: an essential role for PI3 kinase and p70S6 kinase. J Mol Cell Cardiol 2003;35:1063-71.

[77] Tsang A, Hausenloy DJ, Mocanu MM, Yellon DM. Postconditioning: a form of "modified reperfusion" protects the myocardium by activating the phosphatidylinositol 3-kinase-Akt pathway. Circ Res 2004;95:230-2.

[78] Wang Y. Mitogen-activated protein kinases in heart development and diseases. Circulation 2007;116:1413-23.

[79] Sluijter JP, Condorelli G, Davidson SM, Engel FB, Ferdinandy P, Hausenloy DJ, et al. Novel therapeutic strategies for cardioprotection. Pharmacol Ther 2014;144:60-70.

[80] Harada M, Qin Y, Takano H, Minamino T, Zou Y, Toko H, et al. G-CSF prevents cardiac remodeling after myocardial infarction by activating the Jak-Stat pathway in cardiomyocytes. Nat Med 2005;11:305-11.

[81] Cai Z, Manalo DJ, Wei G, Rodriguez ER, Fox-Talbot K, Lu H, et al. Hearts from rodents exposed to intermittent hypoxia or erythropoietin are protected against ischemia-reperfusion injury. Circulation 2003;108:79-85.

[82] Fiordaliso F, Chimenti S, Staszewsky L, Bai A, Carlo E, Cuccovillo I, et al. A nonerythropoietic derivative of erythropoietin protects the myocardium from ischemia-reperfusion injury. Proc Natl Acad Sci U S A 2005;102:2046-51.

[83] Moon C, Krawczyk M, Ahn D, Ahmet I, Paik D, Lakatta EG, et al. Erythropoietin reduces myocardial infarction and left ventricular functional decline after coronary artery ligation in rats. Proc Natl Acad Sci U S A 2003;100:11612-7.

[84] Ye L, Du XL, Xia JH, Jiang P, Wang JT, Fan HM, et al. [An experimental study of recombinant human erythropoietin on the treatment of acute myocardial infarction in rats]. Zhonghua Yi Xue Za Zhi 2006;86:2776-80.

[85] Bromage DI, Davidson SM, Yellon DM. Stromal derived factor 1alpha: a chemokine that delivers a two-pronged defence of the myocardium. Pharmacol Ther 2014;143:305-15.

[86] Johnson NR, Wang Y. Controlled delivery of sonic hedgehog morphogen and its potential for cardiac repair. PLoS One 2013;8:e63075.

[87] Sivaraman B, Ramamurthi A. Growth Factor Delivery Matrices for Cardiovascular Regeneration. In: Suuronen EJ, Ruel M, editors. Biomaterials for Cardiac Regeneration: Springer International Publishing; 2015. p. 159-214.

[88] Uchinaka A, Kawaguchi N, Mori S, Hamada Y, Miyagawa S, Saito A, et al. Tissue inhibitor of metalloproteinase-1 and -3 improves cardiac function in an ischemic cardiomyopathy model rat. Tissue Eng Part A 2014;20:3073-84.

[89] Boon RA, Iekushi K, Lechner S, Seeger T, Fischer A, Heydt S, et al. MicroRNA-34a regulates cardiac ageing and function. Nature 2013;495:107-10.

[90] Hu S, Huang M, Li Z, Jia F, Ghosh Z, Lijkwan MA, et al. MicroRNA-210 as a novel therapy for treatment of ischemic heart disease. Circulation 2010;122:S124-31.

[91] Communal C, Colucci WS. The control of cardiomyocyte apoptosis via the beta-adrenergic signaling pathways. Arch Mal Coeur Vaiss 2005;98:236-41.

[92] Palojoki E, Saraste A, Eriksson A, Pulkki K, Kallajoki M, Voipio-Pulkki LM, et al. Cardiomyocyte apoptosis and ventricular remodeling after myocardial infarction in rats. Am J Physiol Heart Circ Physiol 2001;280:H2726-31.

[93] Butany J, Nair V, Naseemuddin A, Nair GM, Catton C, Yau T. Cardiac tumours: diagnosis and management. Lancet Oncol 2005;6:219-28.

[94] Malliaras K, Terrovitis J. Cardiomyocyte proliferation vs progenitor cells in myocardial regeneration: The debate continues. Glob Cardiol Sci Pract 2013;2013:303-15.

[95] Muralidhar SA, Mahmoud AI, Canseco D, Xiao F, Sadek HA. Harnessing the power of dividing cardiomyocytes. Glob Cardiol Sci Pract 2013;2013:212-21.

[96] Anversa P, Nadal-Ginard B. Myocyte renewal and ventricular remodelling. Nature 2002;415:240-3.

[97] Rubart M, Field LJ. Cardiac regeneration: repopulating the heart. Annu Rev Physiol 2006;68:29-49.

[98] Heallen T, Zhang M, Wang J, Bonilla-Claudio M, Klysik E, Johnson RL, et al. Hippo pathway inhibits Wnt signaling to restrain cardiomyocyte proliferation and heart size. Science 2011;332:458-61.

[99] von Gise A, Lin Z, Schlegelmilch K, Honor LB, Pan GM, Buck JN, et al. YAP1, the nuclear target of Hippo signaling, stimulates heart growth through cardiomyocyte proliferation but not hypertrophy. Proc Natl Acad Sci U S A 2012;109:2394-9.

[100] Eulalio A, Mano M, Dal Ferro M, Zentilin L, Sinagra G, Zacchigna S, et al. Functional screening identifies miRNAs inducing cardiac regeneration. Nature 2012;492:376-81.

[101] Porrello ER. microRNAs in cardiac development and regeneration. Clin Sci (Lond) 2013;125:151-66.

[102] Kuhn B, del Monte F, Hajjar RJ, Chang YS, Lebeche D, Arab S, et al. Periostin induces proliferation of differentiated cardiomyocytes and promotes cardiac repair. Nat Med 2007;13:962-9.

[103] Lorts A, Schwanekamp JA, Elrod JW, Sargent MA, Molkentin JD. Genetic manipulation of periostin expression in the heart does not affect myocyte content, cell cycle activity, or cardiac repair. Circ Res 2009;104:e1-7.

[104] Lemmens K, Doggen K, De Keulenaer GW. Role of neuregulin-1/ErbB signaling in cardiovascular physiology and disease: implications for therapy of heart failure. Circulation 2007;116:954-60.

[105] Liu X, Gu X, Li Z, Li X, Li H, Chang J, et al. Neuregulin-1/erbB-activation improves cardiac function and survival in models of ischemic, dilated, and viral cardiomyopathy. J Am Coll Cardiol 2006;48:1438-47.

[106] Bersell K, Arab S, Haring B, Kuhn B. Neuregulin1/ErbB4 signaling induces cardiomyocyte proliferation and repair of heart injury. Cell 2009;138:257-70.

[107] Galindo CL, Ryzhov S, Sawyer DB. Neuregulin as a heart failure therapy and mediator of reverse remodeling. Curr Heart Fail Rep 2014;11:40-9.

[108] Engel FB, Hsieh PC, Lee RT, Keating MT. FGF1/p38 MAP kinase inhibitor therapy induces cardiomyocyte mitosis, reduces scarring, and rescues function after myocardial infarction. Proc Natl Acad Sci U S A 2006;103:15546-51.

[109] Ellison GM, Vicinanza C, Smith AJ, Aquila I, Leone A, Waring CD, et al. Adult c-kit(pos) cardiac stem cells are necessary and sufficient for functional cardiac regeneration and repair. Cell 2013;154:827-42.

[110] Hsieh PC, Segers VF, Davis ME, MacGillivray C, Gannon J, Molkentin JD, et al. Evidence from a genetic fate-mapping study that stem cells refresh adult mammalian cardiomyocytes after injury. Nat Med 2007;13:970-4.

[111] Tamura Y, Matsumura K, Sano M, Tabata H, Kimura K, Ieda M, et al. Neural crest-derived stem cells migrate and differentiate into cardiomyocytes after myocardial infarction. Arterioscler Thromb Vasc Biol 2011;31:582-9.

[112] Smith RR, Barile L, Cho HC, Leppo MK, Hare JM, Messina E, et al. Regenerative potential of cardiosphere-derived cells expanded from percutaneous endomyocardial biopsy specimens. Circulation 2007;115:896-908.

[113] Loffredo FS, Steinhauser ML, Gannon J, Lee RT. Bone marrow-derived cell therapy stimulates endogenous cardiomyocyte progenitors and promotes cardiac repair. Cell Stem Cell 2011;8:389-98.

[114] Malliaras K, Li TS, Luthringer D, Terrovitis J, Cheng K, Chakravarty T, et al. Safety and efficacy of allogeneic cell therapy in infarcted rats transplanted with mismatched cardiosphere-derived cells. Circulation 2012;125:100-12.

[115] Mirotsou M, Jayawardena TM, Schmeckpeper J, Gnecchi M, Dzau VJ. Paracrine mechanisms of stem cell reparative and regenerative actions in the heart. J Mol Cell Cardiol 2011;50:280-9.

[116] Doppler SA, Deutsch MA, Lange R, Krane M. Cardiac regeneration: current therapies-future concepts. J Thorac Dis 2013;5:683-97.

[117] Penn MS, Pastore J, Miller T, Aras R. SDF-1 in myocardial repair. Gene Ther 2012;19:583-7.

[118] Saxena A, Fish JE, White MD, Yu S, Smyth JW, Shaw RM, et al. Stromal cell-derived factor-1alpha is cardioprotective after myocardial infarction. Circulation 2008;117:2224-31.

[119] Segers VF, Tokunou T, Higgins LJ, MacGillivray C, Gannon J, Lee RT. Local delivery of protease-resistant stromal cell derived factor-1 for stem cell recruitment after myocardial infarction. Circulation 2007;116:1683-92.

[120] Abdel-Latif A, Bolli R, Zuba-Surma EK, Tleyjeh IM, Hornung CA, Dawn B. Granulocyte colony-stimulating factor therapy for cardiac repair after acute myocardial infarction: a systematic review and meta-analysis of randomized controlled trials. Am Heart J 2008;156:216-26 e9.

[121] Takano H, Ueda K, Hasegawa H, Komuro I. G-CSF therapy for acute myocardial infarction. Trends Pharmacol Sci 2007;28:512-7.

[122] Urbanek K, Rota M, Cascapera S, Bearzi C, Nascimbene A, De Angelis A, et al. Cardiac stem cells possess growth factor-receptor systems that after activation regenerate the infarcted myocardium, improving ventricular function and long-term survival. Circ Res 2005;97:663-73.

[123] Smart N, Risebro CA, Melville AA, Moses K, Schwartz RJ, Chien KR, et al. Thymosin beta4 induces adult epicardial progenitor mobilization and neovascularization. Nature 2007;445:177-82.

[124] Urao N, Okigaki M, Yamada H, Aadachi Y, Matsuno K, Matsui A, et al. Erythropoietin-mobilized endothelial progenitors enhance reendothelialization via Akt-endothelial nitric oxide synthase activation and prevent neointimal hyperplasia. Circ Res 2006;98:1405-13.

[125] Bergmann MW, Haufe S, von Knobelsdorff-Brenkenhoff F, Mehling H, Wassmuth R, Munch I, et al. A pilot study of chronic, low-dose epoetin-{beta} following percutaneous coronary intervention suggests safety, feasibility, and efficacy in patients with symptomatic ischaemic heart failure. Eur J Heart Fail 2011;13:560-8.

[126] Taniguchi N, Nakamura T, Sawada T, Matsubara K, Furukawa K, Hadase M, et al. Erythropoietin prevention trial of coronary restenosis and cardiac remodeling after ST-elevated acute myocardial infarction (EPOC-AMI): a pilot, randomized, placebo-controlled study. Circ J 2010;74:2365-71.

[127] Hsueh YC, Wu JM, Yu CK, Wu KK, Hsieh PC. Prostaglandin E(2) promotes post-infarction cardiomyocyte replenishment by endogenous stem cells. EMBO Mol Med 2014;6:496-503.

[128] Taghavi S, George JC. Homing of stem cells to ischemic myocardium. Am J Transl Res 2013;5:404-11.

[129] Padin-Iruegas ME, Misao Y, Davis ME, Segers VF, Esposito G, Tokunou T, et al. Cardiac progenitor cells and biotinylated insulin-like growth factor-1 nanofibers improve endogenous and exogenous myocardial regeneration after infarction. Circulation 2009;120:876-87.

[130] Rosenblatt-Velin N, Lepore MG, Cartoni C, Beermann F, Pedrazzini T. FGF-2 controls the differentiation of resident cardiac precursors into functional cardiomyocytes. J Clin Invest 2005;115:1724-33.

[131] Graham HK, Horn M, Trafford AW. Extracellular matrix profiles in the progression to heart failure. European Young Physiologists Symposium Keynote Lecture-Bratislava 2007. Acta Physiol (Oxf) 2008;194:3-21.

[132] Jugdutt BI. Ventricular remodeling after infarction and the extracellular collagen matrix: when is enough enough? Circulation 2003;108:1395-403.

[133] Weber KT, Anversa P, Armstrong PW, Brilla CG, Burnett JC, Jr., Cruickshank JM, et al. Remodeling and reparation of the cardiovascular system. J Am Coll Cardiol 1992;20:3-16.

[134] Gaertner R, Jacob MP, Prunier F, Angles-Cano E, Mercadier JJ, Michel JB. The plasminogen-MMP system is more activated in the scar than in viable myocardium 3 months post-MI in the rat. J Mol Cell Cardiol 2005;38:193-204.

[135] Romanic AM, Burns-Kurtis CL, Gout B, Berrebi-Bertrand I, Ohlstein EH. Matrix metalloproteinase expression in cardiac myocytes following myocardial infarction in the rabbit. Life Sci 2001;68:799-814.

[136] Visse R, Nagase H. Matrix metalloproteinases and tissue inhibitors of metalloproteinases: structure, function, and biochemistry. Circ Res 2003;92:827-39.

[137] Sternlicht MD, Werb Z. How matrix metalloproteinases regulate cell behavior. Annu Rev Cell Dev Biol 2001;17:463-516.

[138] Vu TH, Werb Z. Matrix metalloproteinases: effectors of development and normal physiology. Genes Dev 2000;14:2123-33.

[139] Deschamps AM, Spinale FG. Pathways of matrix metalloproteinase induction in heart failure: bioactive molecules and transcriptional regulation. Cardiovasc Res 2006;69:666-76.

[140] Fedak PW, Altamentova SM, Weisel RD, Nili N, Ohno N, Verma S, et al. Matrix remodeling in experimental and human heart failure: a possible regulatory role for TIMP-3. Am J Physiol Heart Circ Physiol 2003;284:H626-34.

[141] Etoh T, Joffs C, Deschamps AM, Davis J, Dowdy K, Hendrick J, et al. Myocardial and interstitial matrix metalloproteinase activity after acute myocardial infarction in pigs. Am J Physiol Heart Circ Physiol 2001;281:H987-94.

[142] Lindsey ML, Escobar GP, Mukherjee R, Goshorn DK, Sheats NJ, Bruce JA, et al. Matrix metalloproteinase-7 affects connexin-43 levels, electrical conduction, and survival after myocardial infarction. Circulation 2006;113:2919-28.

[143] Ducharme A, Frantz S, Aikawa M, Rabkin E, Lindsey M, Rohde LE, et al. Targeted deletion of matrix metalloproteinase-9 attenuates left ventricular enlargement and collagen accumulation after experimental myocardial infarction. J Clin Invest 2000;106:55-62.

[144] Janssens S, Lijnen HR. What has been learned about the cardiovascular effects of matrix metalloproteinases from mouse models? Cardiovasc Res 2006;69:585-94.

[145] Trescher K, Bernecker O, Fellner B, Gyongyosi M, Schafer R, Aharinejad S, et al. Inflammation and postinfarct remodeling: overexpression of IkappaB prevents ventricular dilation via increasing TIMP levels. Cardiovasc Res 2006;69:746-54.

[146] Takawale A, Fan D, Basu R, Shen M, Parajuli N, Wang W, et al. Myocardial recovery from ischemia-reperfusion is compromised in the absence of tissue inhibitor of metalloproteinase 4. Circ Heart Fail 2014;7:652-62.

[147] Fedak PW, Smookler DS, Kassiri Z, Ohno N, Leco KJ, Verma S, et al. TIMP-3 deficiency leads to dilated cardiomyopathy. Circulation 2004;110:2401-9.

[148] Ikonomidis JS, Hendrick JW, Parkhurst AM, Herron AR, Escobar PG, Dowdy KB, et al. Accelerated LV remodeling after myocardial infarction in TIMP-1-deficient mice: effects of exogenous MMP inhibition. Am J Physiol Heart Circ Physiol 2005;288:H149-58.

[149] Kassiri Z, Defamie V, Hariri M, Oudit GY, Anthwal S, Dawood F, et al. Simultaneous transforming growth factor beta-tumor necrosis factor activation and cross-talk cause aberrant remodeling response and myocardial fibrosis in Timp3-deficient heart. J Biol Chem 2009;284:29893-904.

[150] Roten L, Nemoto S, Simsic J, Coker ML, Rao V, Baicu S, et al. Effects of gene deletion of the tissue inhibitor of the matrix metalloproteinase-type 1 (TIMP-1) on left ventricular geometry and function in mice. J Mol Cell Cardiol 2000;32:109-20.

[151] Tian H, Huang ML, Liu KY, Jia ZB, Sun L, Jiang SL, et al. Inhibiting matrix metalloproteinase by cell-based timp-3 gene transfer effectively treats acute and chronic ischemic cardiomyopathy. Cell Transplant 2012;21:1039-53.

[152] Yu WH, Yu S, Meng Q, Brew K, Woessner JF, Jr. TIMP-3 binds to sulfated glycosaminoglycans of the extracellular matrix. J Biol Chem 2000;275:31226-32.

[153] Opie LH, Commerford PJ, Gersh BJ, Pfeffer MA. Controversies in ventricular remodelling. Lancet 2006;367:356-67.

[154] Reinhardt D, Sigusch HH, Hensse J, Tyagi SC, Korfer R, Figulla HR. Cardiac remodelling in end stage heart failure: upregulation of matrix metalloproteinase (MMP) irrespective of the underlying disease, and evidence for a direct inhibitory effect of ACE inhibitors on MMP. Heart 2002;88:525-30.

[155] Tziakas DN, Chalikias GK, Parissis JT, Hatzinikolaou EI, Papadopoulos ED, Tripsiannis GA, et al. Serum profiles of matrix metalloproteinases and their tissue inhibitor in patients with

acute coronary syndromes. The effects of short-term atorvastatin administration. Int J Cardiol 2004;94:269-77.

[156] Peterson JT. The importance of estimating the therapeutic index in the development of matrix metalloproteinase inhibitors. Cardiovasc Res 2006;69:677-87.

[157] Covell JW. Factors influencing diastolic function. Possible role of the extracellular matrix. Circulation 1990;81:III155-8.

[158] Cleutjens JP, Kandala JC, Guarda E, Guntaka RV, Weber KT. Regulation of collagen degradation in the rat myocardium after infarction. J Mol Cell Cardiol 1995;27:1281-92.

[159] Porter KE, Turner NA. Cardiac fibroblasts: at the heart of myocardial remodeling. Pharmacol Ther 2009;123:255-78.

[160] van den Borne SW, Diez J, Blankesteijn WM, Verjans J, Hofstra L, Narula J. Myocardial remodeling after infarction: the role of myofibroblasts. Nat Rev Cardiol 2010;7:30-7.

[161] Zhang Y, Kanter EM, Laing JG, Aprhys C, Johns DC, Kardami E, et al. Connexin43 expression levels influence intercellular coupling and cell proliferation of native murine cardiac fibroblasts. Cell Commun Adhes 2008;15:289-303.

[162] Pellman J, Lyon RC, Sheikh F. Extracellular matrix remodeling in atrial fibrosis: mechanisms and implications in atrial fibrillation. J Mol Cell Cardiol 2010;48:461-7.

[163] Rohr S. Myofibroblasts in diseased hearts: new players in cardiac arrhythmias? Heart Rhythm 2009;6:848-56.

[164] Daskalopoulos EP, Janssen BJ, Blankesteijn WM. Myofibroblasts in the infarct area: concepts and challenges. Microsc Microanal 2012;18:35-49.

[165] Frantz S, Hu K, Adamek A, Wolf J, Sallam A, Maier SK, et al. Transforming growth factor beta inhibition increases mortality and left ventricular dilatation after myocardial infarction. Basic Res Cardiol 2008;103:485-92.

[166] Cunnington RH, Wang B, Ghavami S, Bathe KL, Rattan SG, Dixon IM. Antifibrotic properties of c-Ski and its regulation of cardiac myofibroblast phenotype and contractility. Am J Physiol Cell Physiol 2011;300:C176-86.

[167] Aisagbonhi O, Rai M, Ryzhov S, Atria N, Feoktistov I, Hatzopoulos AK. Experimental myocardial infarction triggers canonical Wnt signaling and endothelial-to-mesenchymal transition. Dis Model Mech 2011;4:469-83.

[168] Carthy JM, Garmaroudi FS, Luo Z, McManus BM. Wnt3a induces myofibroblast differentiation by upregulating TGF-beta signaling through SMAD2 in a beta-catenin-dependent manner. PLoS One 2011;6:e19809.

[169] Laeremans H, Rensen SS, Ottenheijm HC, Smits JF, Blankesteijn WM. Wnt/frizzled signalling modulates the migration and differentiation of immortalized cardiac fibroblasts. Cardiovasc Res 2010;87:514-23.

[170] Sun Y, Weber KT. Angiotensin converting enzyme and myofibroblasts during tissue repair in the rat heart. J Mol Cell Cardiol 1996;28:851-8.

[171] Sun Y, Zhang JQ, Zhang J, Ramires FJ. Angiotensin II, transforming growth factor-beta1 and repair in the infarcted heart. J Mol Cell Cardiol 1998;30:1559-69.

[172] Yu CM, Tipoe GL, Wing-Hon Lai K, Lau CP. Effects of combination of angiotensin-converting enzyme inhibitor and angiotensin receptor antagonist on inflammatory cellular infiltration and myocardial interstitial fibrosis after acute myocardial infarction. J Am Coll Cardiol 2001;38:1207-15.

[173] Turner NA, Porter KE, Smith WH, White HL, Ball SG, Balmforth AJ. Chronic beta2-adrenergic receptor stimulation increases proliferation of human cardiac fibroblasts via an autocrine mechanism. Cardiovasc Res 2003;57:784-92.

[174] Porter KE, Turner NA, O'Regan DJ, Balmforth AJ, Ball SG. Simvastatin reduces human atrial myofibroblast proliferation independently of cholesterol lowering via inhibition of RhoA. Cardiovasc Res 2004;61:745-55.

[175] Shiroshita-Takeshita A, Brundel BJ, Burstein B, Leung TK, Mitamura H, Ogawa S, et al. Effects of simvastatin on the development of the atrial fibrillation substrate in dogs with congestive heart failure. Cardiovasc Res 2007;74:75-84.

[176] Beltrami CA, Finato N, Rocco M, Feruglio GA, Puricelli C, Cigola E, et al. Structural basis of end-stage failure in ischemic cardiomyopathy in humans. Circulation 1994;89:151-63.

[177] Eckhouse SR, Purcell BP, McGarvey JR, Lobb D, Logdon CB, Doviak H, et al. Local hydrogel release of recombinant TIMP-3 attenuates adverse left ventricular remodeling after experimental myocardial infarction. Sci Transl Med 2014;6:223ra21.

[178] Muraoka N, Ieda M. Direct reprogramming of fibroblasts into myocytes to reverse fibrosis. Annu Rev Physiol 2014;76:21-37.

[179] Ieda M, Fu JD, Delgado-Olguin P, Vedantham V, Hayashi Y, Bruneau BG, et al. Direct reprogramming of fibroblasts into functional cardiomyocytes by defined factors. Cell 2010;142:375-86.

[180] Inagawa K, Miyamoto K, Yamakawa H, Muraoka N, Sadahiro T, Umei T, et al. Induction of cardiomyocyte-like cells in infarct hearts by gene transfer of Gata4, Mef2c, and Tbx5. Circ Res 2012;111:1147-56.

[181] Jayawardena TM, Egemnazarov B, Finch EA, Zhang L, Payne JA, Pandya K, et al. MicroRNA-mediated in vitro and in vivo direct reprogramming of cardiac fibroblasts to cardiomyocytes. Circ Res 2012;110:1465-73.

[182] Song K, Nam YJ, Luo X, Qi X, Tan W, Huang GN, et al. Heart repair by reprogramming non-myocytes with cardiac transcription factors. Nature 2012;485:599-604.

[183] Efe JA, Hilcove S, Kim J, Zhou H, Ouyang K, Wang G, et al. Conversion of mouse fibroblasts into cardiomyocytes using a direct reprogramming strategy. Nat Cell Biol 2011;13:215-22.

[184] Mathison M, Gersch RP, Nasser A, Lilo S, Korman M, Fourman M, et al. In vivo cardiac cellular reprogramming efficacy is enhanced by angiogenic preconditioning of the infarcted myocardium with vascular endothelial growth factor. J Am Heart Assoc 2012;1:e005652.

[185] Bers DM. Cardiac excitation-contraction coupling. Nature 2002;415:198-205.

[186] Pieske B, Kretschmann B, Meyer M, Holubarsch C, Weirich J, Posival H, et al. Alterations in intracellular calcium handling associated with the inverse force-frequency relation in human dilated cardiomyopathy. Circulation 1995;92:1169-78.

[187] Schwinger RH, Bohm M, Schmidt U, Karczewski P, Bavendiek U, Flesch M, et al. Unchanged protein levels of SERCA II and phospholamban but reduced Ca2+ uptake and Ca(2+)-ATPase activity of cardiac sarcoplasmic reticulum from dilated cardiomyopathy patients compared with patients with nonfailing hearts. Circulation 1995;92:3220-8.

[188] Piper HM, Kasseckert S, Abdallah Y. The sarcoplasmic reticulum as the primary target of reperfusion protection. Cardiovasc Res 2006;70:170-3.

[189] Silverman HS, Stern MD. Ionic basis of ischaemic cardiac injury: insights from cellular studies. Cardiovasc Res 1994;28:581-97.

[190] Ducceschi V, Di Micco G, Sarubbi B, Russo B, Santangelo L, Iacono A. Ionic mechanisms of ischemia-related ventricular arrhythmias. Clin Cardiol 1996;19:325-31.

[191] Lee K, Silva EA, Mooney DJ. Growth factor delivery-based tissue engineering: general approaches and a review of recent developments. J R Soc Interface 2011;8:153-70.

[192] Ozawa CR, Banfi A, Glazer NL, Thurston G, Springer ML, Kraft PE, et al. Microenvironmental VEGF concentration, not total dose, determines a threshold between normal and aberrant angiogenesis. J Clin Invest 2004;113:516-27.

[193] Wu DT, Bitzer M, Ju W, Mundel P, Bottinger EP. TGF-beta concentration specifies differential signaling profiles of growth arrest/differentiation and apoptosis in podocytes. J Am Soc Nephrol 2005;16:3211-21.

[194] Schneider IC, Haugh JM. Mechanisms of gradient sensing and chemotaxis: conserved pathways, diverse regulation. Cell Cycle 2006;5:1130-4.

[195] Chen FM, Zhang M, Wu ZF. Toward delivery of multiple growth factors in tissue engineering. Biomaterials 2010;31:6279-308.

[196] Singh M, Berkland C, Detamore MS. Strategies and applications for incorporating physical and chemical signal gradients in tissue engineering. Tissue Eng Part B Rev 2008;14:341-66.

[197] Affolter M, Weijer CJ. Signaling to cytoskeletal dynamics during chemotaxis. Dev Cell 2005;9:19-34.

[198] Bailly M, Wyckoff J, Bouzahzah B, Hammerman R, Sylvestre V, Cammer M, et al. Epidermal growth factor receptor distribution during chemotactic responses. Mol Biol Cell 2000;11:3873-83.

[199] Ho WC, Uniyal S, Zhou H, Morris VL, Chan BM. Threshold levels of ERK activation for chemotactic migration differ for NGF and EGF in rat pheochromocytoma PC12 cells. Mol Cell Biochem 2005;271:29-41.

[200] Kang CE, Gemeinhart EJ, Gemeinhart RA. Cellular alignment by grafted adhesion peptide surface density gradients. J Biomed Mater Res A 2004;71:403-11.

[201] Ruhrberg C, Gerhardt H, Golding M, Watson R, Ioannidou S, Fujisawa H, et al. Spatially restricted patterning cues provided by heparin-binding VEGF-A control blood vessel branching morphogenesis. Genes Dev 2002;16:2684-98.

[202] Humphrey JD, Dufresne ER, Schwartz MA. Mechanotransduction and extracellular matrix homeostasis. Nat Rev Mol Cell Biol 2014;15:802-12.

[203] Tomasek JJ, Gabbiani G, Hinz B, Chaponnier C, Brown RA. Myofibroblasts and mechano-regulation of connective tissue remodelling. Nat Rev Mol Cell Biol 2002;3:349-63.

[204] Hahn C, Schwartz MA. Mechanotransduction in vascular physiology and atherogenesis. Nat Rev Mol Cell Biol 2009;10:53-62.

[205] Grinnell F, Ho CH, Lin YC, Skuta G. Differences in the regulation of fibroblast contraction of floating versus stressed collagen matrices. J Biol Chem 1999;274:918-23.

[206] Kolodney MS, Elson EL. Correlation of myosin light chain phosphorylation with isometric contraction of fibroblasts. J Biol Chem 1993;268:23850-5.

[207] Cukierman E, Pankov R, Stevens DR, Yamada KM. Taking cell-matrix adhesions to the third dimension. Science 2001;294:1708-12.

[208] Tayalia P, Mooney DJ. Controlled growth factor delivery for tissue engineering. Adv Mater 2009;21:3269-85.

[209] Shuman JA, Zurcher JR, Sapp AA, Burdick JA, Gorman RC, Gorman JH, 3rd, et al. Localized targeting of biomaterials following myocardial infarction: a foundation to build on. Trends Cardiovasc Med 2013;23:301-11.

[210] Vasita R, Katti DS. Growth factor-delivery systems for tissue engineering: a materials perspective. Expert Rev Med Devices 2006;3:29-47.

[211] Tessmar JK, Gopferich AM. Matrices and scaffolds for protein delivery in tissue engineering. Adv Drug Deliv Rev 2007;59:274-91.

[212] Fujita M, Ishihara M, Morimoto Y, Simizu M, Saito Y, Yura H, et al. Efficacy of photocrosslinkable chitosan hydrogel containing fibroblast growth factor-2 in a rabbit model of chronic myocardial infarction. J Surg Res 2005;126:27-33.

[213] Lin X, Fujita M, Kanemitsu N, Kimura Y, Tambara K, Premaratne GU, et al. Sustained-release erythropoietin ameliorates cardiac function in infarcted rat-heart without inducing polycythemia. Circ J 2007;71:132-7.

[214] Ehrbar M, Djonov VG, Schnell C, Tschanz SA, Martiny-Baron G, Schenk U, et al. Cell-demanded liberation of VEGF121 from fibrin implants induces local and controlled blood vessel growth. Circ Res 2004;94:1124-32.

[215] Ruvinov E, Leor J, Cohen S. The promotion of myocardial repair by the sequential delivery of IGF-1 and HGF from an injectable alginate biomaterial in a model of acute myocardial infarction. Biomaterials 2011;32:565-78.

[216] Song M, Jang H, Lee J, Kim JH, Kim SH, Sun K, et al. Regeneration of chronic myocardial infarction by injectable hydrogels containing stem cell homing factor SDF-1 and angiogenic peptide Ac-SDKP. Biomaterials 2014;35:2436-45.

[217] Sonnenberg SB, Rane AA, Liu CJ, Rao N, Agmon G, Suarez S, et al. Delivery of an engineered HGF fragment in an extracellular matrix-derived hydrogel prevents negative LV remodeling post-myocardial infarction. Biomaterials 2015;45:56-63.

[218] Bastings MM, Koudstaal S, Kieltyka RE, Nakano Y, Pape AC, Feyen DA, et al. A fast pH-switchable and self-healing supramolecular hydrogel carrier for guided, local catheter injection in the infarcted myocardium. Adv Healthc Mater 2014;3:70-8.

[219] Kadner K, Dobner S, Franz T, Bezuidenhout D, Sirry MS, Zilla P, et al. The beneficial effects of deferred delivery on the efficiency of hydrogel therapy post myocardial infarction. Biomaterials 2012;33:2060-6.

[220] Salimath AS, Phelps EA, Boopathy AV, Che PL, Brown M, Garcia AJ, et al. Dual delivery of hepatocyte and vascular endothelial growth factors via a protease-degradable hydrogel improves cardiac function in rats. PLoS One 2012;7:e50980.

[221] Panyam J, Labhasetwar V. Dynamics of endocytosis and exocytosis of poly(D,L-lactide-co-glycolide) nanoparticles in vascular smooth muscle cells. Pharm Res 2003;20:212-20.

[222] Kokai LE, Tan H, Jhunjhunwala S, Little SR, Frank JW, Marra KG. Protein bioactivity and polymer orientation is affected by stabilizer incorporation for double-walled microspheres. J Control Release 2010;141:168-76.

[223] Cross DP, Wang C. Stromal-derived factor-1 alpha-loaded PLGA microspheres for stem cell recruitment. Pharm Res 2011;28:2477-89.

[224] Formiga FR, Pelacho B, Garbayo E, Abizanda G, Gavira JJ, Simon-Yarza T, et al. Sustained release of VEGF through PLGA microparticles improves vasculogenesis and tissue remodeling in an acute myocardial ischemia-reperfusion model. J Control Release 2010;147:30-7.

[225] Formiga FR, Pelacho B, Garbayo E, Imbuluzqueta I, Diaz-Herraez P, Abizanda G, et al. Controlled delivery of fibroblast growth factor-1 and neuregulin-1 from biodegradable microparticles promotes cardiac repair in a rat myocardial infarction model through activation of endogenous regeneration. J Control Release 2014;173:132-9.

[226] Chang MY, Yang YJ, Chang CH, Tang AC, Liao WY, Cheng FY, et al. Functionalized nanoparticles provide early cardioprotection after acute myocardial infarction. J Control Release 2013;170:287-94.

[227] Lee J, Tan CY, Lee SK, Kim YH, Lee KY. Controlled delivery of heat shock protein using an injectable microsphere/hydrogel combination system for the treatment of myocardial infarction. J Control Release 2009;137:196-202.

[228] Al Kindi H, Paul A, You Z, Nepotchatykh O, Schwertani A, Prakash S, et al. Sustained release of milrinone delivered via microparticles in a rodent model of myocardial infarction. J Thorac Cardiovasc Surg 2014;148:2316-23.

[229] Galagudza M, Korolev D, Postnov V, Naumisheva E, Grigorova Y, Uskov I, et al. Passive targeting of ischemic-reperfused myocardium with adenosine-loaded silica nanoparticles. Int J Nanomedicine 2012;7:1671-8.

[230] Suarez S, Grover GN, Braden RL, Christman KL, Almutairi A. Tunable protein release from acetalated dextran microparticles: a platform for delivery of protein therapeutics to the heart post-MI. Biomacromolecules 2013;14:3927-35.

[231] Tolli MA, Ferreira MP, Kinnunen SM, Rysa J, Makila EM, Szabo Z, et al. In vivo biocompatibility of porous silicon biomaterials for drug delivery to the heart. Biomaterials 2014;35:8394-405.

[232] Oh KS, Song JY, Yoon SJ, Park Y, Kim D, Yuk SH. Temperature-induced gel formation of core/shell nanoparticles for the regeneration of ischemic heart. J Control Release 2010;146:207-11.

[233] Johnson NR, Wang Y. Coacervate delivery systems for proteins and small molecule drugs. Expert Opin Drug Deliv 2014;11:1829-32.

[234] Black KA, Priftis D, Perry SL, Yip J, Byun WY, Tirrell M. Protein Encapsulation via Polypeptide Complex Coacervation. ACS Macro Letters 2014;3:1088-91.

[235] Chu H, Johnson NR, Mason NS, Wang Y. A [polycation:heparin] complex releases growth factors with enhanced bioactivity. J Control Release 2011;150:157-63.

[236] Zern BJ, Chu H, Wang Y. Control growth factor release using a self-assembled [polycation:heparin] complex. PLoS One 2010;5:e11017.

[237] Chu H, Gao J, Wang Y. Design, synthesis, and biocompatibility of an arginine-based polyester. Biotechnol Prog 2012;28:257-64.

[238] Rodriguez-Cabello JC, Arias FJ, Rodrigo MA, Girotti A. Elastin-like polypeptides in drug delivery. Adv Drug Deliv Rev 2015.

[239] Kimmerling KA, Furman BD, Mangiapani DS, Moverman MA, Sinclair SM, Huebner JL, et al. Sustained intra-articular delivery of IL-1RA from a thermally-responsive elastin-like polypeptide as a therapy for post-traumatic arthritis. Eur Cell Mater 2015;29:124-39; discussion 39-40.

[240] Bhattacharyya J, Bellucci JJ, Weitzhandler I, McDaniel JR, Spasojevic I, Li X, et al. A paclitaxel-loaded recombinant polypeptide nanoparticle outperforms Abraxane in multiple murine cancer models. Nat Commun 2015;6:7939.

[241] Chu H, Chen CW, Huard J, Wang Y. The effect of a heparin-based coacervate of fibroblast growth factor-2 on scarring in the infarcted myocardium. Biomaterials 2013;34:1747-56.

[242] Chu H, Gao J, Chen CW, Huard J, Wang Y. Injectable fibroblast growth factor-2 coacervate for persistent angiogenesis. Proc Natl Acad Sci U S A 2011;108:13444-9.

[243] Johnson NR, Wang Y. Controlled delivery of heparin-binding EGF-like growth factor yields fast and comprehensive wound healing. J Control Release 2013;166:124-9.

[244] Johnson NR, Kruger M, Goetsch KP, Zilla P, Bezuidenhout D, Wang Y, et al. Coacervate Delivery of Growth Factors Combined with a Degradable Hydrogel Preserves Heart Function after Myocardial Infarction. ACS Biomaterials Science & Engineering 2015.

[245] Paulis LE, Geelen T, Kuhlmann MT, Coolen BF, Schafers M, Nicolay K, et al. Distribution of lipid-based nanoparticles to infarcted myocardium with potential application for MRI-monitored drug delivery. J Control Release 2012;162:276-85.

[246] Wang B, Cheheltani R, Rosano J, Crabbe DL, Kiani MF. Targeted delivery of VEGF to treat myocardial infarction. Adv Exp Med Biol 2013;765:307-14.

[247] Zhang S. Fabrication of novel biomaterials through molecular self-assembly. Nat Biotechnol 2003;21:1171-8.

[248] Davis ME, Hsieh PC, Takahashi T, Song Q, Zhang S, Kamm RD, et al. Local myocardial insulin-like growth factor 1 (IGF-1) delivery with biotinylated peptide nanofibers improves cell therapy for myocardial infarction. Proc Natl Acad Sci U S A 2006;103:8155-60.

[249] Hsieh PC, Davis ME, Gannon J, MacGillivray C, Lee RT. Controlled delivery of PDGF-BB for myocardial protection using injectable self-assembling peptide nanofibers. J Clin Invest 2006;116:237-48.

[250] Kim JH, Jung Y, Kim SH, Sun K, Choi J, Kim HC, et al. The enhancement of mature vessel formation and cardiac function in infarcted hearts using dual growth factor delivery with self-assembling peptides. Biomaterials 2011;32:6080-8.

[251] Webber MJ, Han X, Murthy SN, Rajangam K, Stupp SI, Lomasney JW. Capturing the stem cell paracrine effect using heparin-presenting nanofibres to treat cardiovascular diseases. J Tissue Eng Regen Med 2010;4:600-10.

[252] Johnson NR, Ambe T, Wang Y. Lysine-based polycation:heparin coacervate for controlled protein delivery. Acta Biomater 2014;10:40-6.

[253] Ori A, Wilkinson MC, Fernig DG. A systems biology approach for the investigation of the heparin/heparan sulfate interactome. J Biol Chem 2011;286:19892-904.

[254] Li H, Johnson NR, Usas A, Lu A, Poddar M, Wang Y, et al. Sustained release of bone morphogenetic protein 2 via coacervate improves the osteogenic potential of muscle-derived stem cells. Stem Cells Transl Med 2013;2:667-77.

[255] Chu H, Wang Y. Therapeutic angiogenesis: controlled delivery of angiogenic factors. Ther Deliv 2012;3:693-714.

[256] Li WW, Talcott KE, Zhai AW, Kruger EA, Li VW. The role of therapeutic angiogenesis in tissue repair and regeneration. Adv Skin Wound Care 2005;18:491-500; quiz 1-2.

[257] Risau W. Mechanisms of angiogenesis. Nature 1997;386:671-4.

[258] Foundation TA. Market Study and Analysis of Angiogensis-dependent Diseases. Third Edition ed: Cambridge; 2001.

[259] Bussolino F, Di Renzo MF, Ziche M, Bocchietto E, Olivero M, Naldini L, et al. Hepatocyte growth factor is a potent angiogenic factor which stimulates endothelial cell motility and growth. J Cell Biol 1992;119:629-41.

[260] Ferrara N. Role of vascular endothelial growth factor in physiologic and pathologic angiogenesis: therapeutic implications. Semin Oncol 2002;29:10-4.

[261] Rosen EM, Goldberg ID. Scatter factor and angiogenesis. Adv Cancer Res 1995;67:257-79.

[262] Ruvinov E, Leor J, Cohen S. The effects of controlled HGF delivery from an affinity-binding alginate biomaterial on angiogenesis and blood perfusion in a hindlimb ischemia model. Biomaterials 2010;31:4573-82.

[263] Taniyama Y, Morishita R, Aoki M, Nakagami H, Yamamoto K, Yamazaki K, et al. Therapeutic angiogenesis induced by human hepatocyte growth factor gene in rat and rabbit hindlimb ischemia models: preclinical study for treatment of peripheral arterial disease. Gene Ther 2001;8:181-9.

[264] Yancopoulos GD, Davis S, Gale NW, Rudge JS, Wiegand SJ, Holash J. Vascular-specific growth factors and blood vessel formation. Nature 2000;407:242-8.

[265] Golocheikine A, Tiriveedhi V, Angaswamy N, Benshoff N, Sabarinathan R, Mohanakumar T. Cooperative signaling for angiogenesis and neovascularization by VEGF and HGF following islet transplantation. Transplantation 2010;90:725-31.

[266] Sulpice E, Ding S, Muscatelli-Groux B, Berge M, Han ZC, Plouet J, et al. Cross-talk between the VEGF-A and HGF signalling pathways in endothelial cells. Biol Cell 2009;101:525-39.

[267] Van Belle E, Witzenbichler B, Chen D, Silver M, Chang L, Schwall R, et al. Potentiated angiogenic effect of scatter factor/hepatocyte growth factor via induction of vascular endothelial growth factor: the case for paracrine amplification of angiogenesis. Circulation 1998;97:381-90.

[268] Xin X, Yang S, Ingle G, Zlot C, Rangell L, Kowalski J, et al. Hepatocyte growth factor enhances vascular endothelial growth factor-induced angiogenesis in vitro and in vivo. Am J Pathol 2001;158:1111-20.

[269] Chalupowicz DG, Chowdhury ZA, Bach TL, Barsigian C, Martinez J. Fibrin II induces endothelial cell capillary tube formation. J Cell Biol 1995;130:207-15.

[270] Aranda E, Owen GI. A semi-quantitative assay to screen for angiogenic compounds and compounds with angiogenic potential using the EA.hy926 endothelial cell line. Biol Res 2009;42:377-89.

[271] Yamagishi S, Yonekura H, Yamamoto Y, Katsuno K, Sato F, Mita I, et al. Advanced glycation end products-driven angiogenesis in vitro. Induction of the growth and tube formation of human microvascular endothelial cells through autocrine vascular endothelial growth factor. J Biol Chem 1997;272:8723-30.

[272] Ashikari-Hada S, Habuchi H, Kariya Y, Itoh N, Reddi AH, Kimata K. Characterization of growth factor-binding structures in heparin/heparan sulfate using an octasaccharide library. J Biol Chem 2004;279:12346-54.

[273] Wang X, Wenk E, Hu X, Castro GR, Meinel L, Wang X, et al. Silk coatings on PLGA and alginate microspheres for protein delivery. Biomaterials 2007;28:4161-9.

[274] Silva AK, Richard C, Bessodes M, Scherman D, Merten OW. Growth factor delivery approaches in hydrogels. Biomacromolecules 2009;10:9-18.

[275] Carmeliet P. Angiogenesis in life, disease and medicine. Nature 2005;438:932-6.

[276] Baumgartner I, Rauh G, Pieczek A, Wuensch D, Magner M, Kearney M, et al. Lower-extremity edema associated with gene transfer of naked DNA encoding vascular endothelial growth factor. Ann Intern Med 2000;132:880-4.

[277] Detmar M, Brown LF, Schon MP, Elicker BM, Velasco P, Richard L, et al. Increased microvascular density and enhanced leukocyte rolling and adhesion in the skin of VEGF transgenic mice. J Invest Dermatol 1998;111:1-6.

[278] Sengupta S, Gherardi E, Sellers LA, Wood JM, Sasisekharan R, Fan TP. Hepatocyte growth factor/scatter factor can induce angiogenesis independently of vascular endothelial growth factor. Arterioscler Thromb Vasc Biol 2003;23:69-75.

[279] Boros P, Miller CM. Hepatocyte growth factor: a multifunctional cytokine. Lancet 1995;345:293-5.

[280] Makarevich P, Tsokolaeva Z, Shevelev A, Rybalkin I, Shevchenko E, Beloglazova I, et al. Combined transfer of human VEGF165 and HGF genes renders potent angiogenic effect in ischemic skeletal muscle. PLoS One 2012;7:e38776.

[281] Chapanian R, Amsden BG. Combined and sequential delivery of bioactive VEGF165 and HGF from poly(trimethylene carbonate) based photo-cross-linked elastomers. J Control Release 2010;143:53-63.

[282] Vailhe B, Vittet D, Feige JJ. In vitro models of vasculogenesis and angiogenesis. Lab Invest 2001;81:439-52.

[283] Nissanov J, Tuman RW, Gruver LM, Fortunato JM. Automatic vessel segmentation and quantification of the rat aortic ring assay of angiogenesis. Lab Invest 1995;73:734-9.

[284] Gerritsen ME, Tomlinson JE, Zlot C, Ziman M, Hwang S. Using gene expression profiling to identify the molecular basis of the synergistic actions of hepatocyte growth factor and vascular endothelial growth factor in human endothelial cells. Br J Pharmacol 2003;140:595-610.

[285] Pellegrini L. Role of heparan sulfate in fibroblast growth factor signalling: a structural view. Curr Opin Struct Biol 2001;11:629-34.

[286] Deveza L, Choi J, Yang F. Therapeutic angiogenesis for treating cardiovascular diseases. Theranostics 2012;2:801-14.

[287] Hwang H, Kloner RA. Improving regenerating potential of the heart after myocardial infarction: factor-based approach. Life Sci 2010;86:461-72.

[288] Zachary I, Morgan RD. Therapeutic angiogenesis for cardiovascular disease: biological context, challenges, prospects. Heart 2011;97:181-9.

[289] Betsholtz C. Insight into the physiological functions of PDGF through genetic studies in mice. Cytokine Growth Factor Rev 2004;15:215-28.

[290] Eklund L, Olsen BR. Tie receptors and their angiopoietin ligands are context-dependent regulators of vascular remodeling. Exp Cell Res 2006;312:630-41.

[291] Ferrara N, Gerber HP, LeCouter J. The biology of VEGF and its receptors. Nat Med 2003;9:669-76.

[292] Maulik N, Thirunavukkarasu M. Growth factors and cell therapy in myocardial regeneration. J Mol Cell Cardiol 2008;44:219-27.

[293] Awada HK, Johnson NR, Wang Y. Dual delivery of vascular endothelial growth factor and hepatocyte growth factor coacervate displays strong angiogenic effects. Macromol Biosci 2014;14:679-86.

[294] Awada HK, Hwang MP, Wang Y. Towards comprehensive cardiac repair and regeneration after myocardial infarction: Aspects to consider and proteins to deliver. Biomaterials 2016;82:94-112.

[295] Aplin AC, Fogel E, Zorzi P, Nicosia RF. The aortic ring model of angiogenesis. Methods Enzymol 2008;443:119-36.

[296] Go RS, Owen WG. The rat aortic ring assay for in vitro study of angiogenesis. Methods Mol Med 2003;85:59-64.

[297] Dobner S, Bezuidenhout D, Govender P, Zilla P, Davies N. A synthetic non-degradable polyethylene glycol hydrogel retards adverse post-infarct left ventricular remodeling. J Card Fail 2009;15:629-36.

[298] Freeman I, Kedem A, Cohen S. The effect of sulfation of alginate hydrogels on the specific binding and controlled release of heparin-binding proteins. Biomaterials 2008;29:3260-8.

[299] Zangi L, Lui KO, von Gise A, Ma Q, Ebina W, Ptaszek LM, et al. Modified mRNA directs the fate of heart progenitor cells and induces vascular regeneration after myocardial infarction. Nat Biotechnol 2013;31:898-907.

[300] Sutton MG, Sharpe N. Left ventricular remodeling after myocardial infarction: pathophysiology and therapy. Circulation 2000;101:2981-8.

[301] Tsai HM. von Willebrand factor, shear stress, and ADAMTS13 in hemostasis and thrombosis. ASAIO J 2012;58:163-9.

[302] Hao X, Mansson-Broberg A, Blomberg P, Dellgren G, Siddiqui AJ, Grinnemo KH, et al. Angiogenic and cardiac functional effects of dual gene transfer of VEGF-A165 and PDGF-BB after myocardial infarction. Biochem Biophys Res Commun 2004;322:292-6.

[303] Chen RR, Silva EA, Yuen WW, Mooney DJ. Spatio-temporal VEGF and PDGF delivery patterns blood vessel formation and maturation. Pharm Res 2007;24:258-64.

[304] Davies NH, Schmidt C, Bezuidenhout D, Zilla P. Sustaining neovascularization of a scaffold through staged release of vascular endothelial growth factor-A and platelet-derived growth factor-BB. Tissue Eng Part A 2012;18:26-34.

[305] Shin SH, Lee J, Lim KS, Rhim T, Lee SK, Kim YH, et al. Sequential delivery of TAT-HSP27 and VEGF using microsphere/hydrogel hybrid systems for therapeutic angiogenesis. J Control Release 2013;166:38-45.

[306] Sun Q, Silva EA, Wang A, Fritton JC, Mooney DJ, Schaffler MB, et al. Sustained release of multiple growth factors from injectable polymeric system as a novel therapeutic approach towards angiogenesis. Pharm Res 2010;27:264-71.

[307] Capila I, Linhardt RJ. Heparin-protein interactions. Angew Chem Int Ed Engl 2002;41:391-412.

[308] Mulloy B, Forster MJ. Conformation and dynamics of heparin and heparan sulfate. Glycobiology 2000;10:1147-56.

[309] Morbidelli L, Chang CH, Douglas JG, Granger HJ, Ledda F, Ziche M. Nitric oxide mediates mitogenic effect of VEGF on coronary venular endothelium. Am J Physiol 1996;270:H411-5.

[310] van der Zee R, Murohara T, Luo Z, Zollmann F, Passeri J, Lekutat C, et al. Vascular endothelial growth factor/vascular permeability factor augments nitric oxide release from quiescent rabbit and human vascular endothelium. Circulation 1997;95:1030-7.

[311] Cooke JP, Losordo DW. Nitric oxide and angiogenesis. Circulation 2002;105:2133-5.

[312] Bergmann O, Bhardwaj RD, Bernard S, Zdunek S, Barnabe-Heider F, Walsh S, et al. Evidence for cardiomyocyte renewal in humans. Science 2009;324:98-102.

[313] Abbott JD, Huang Y, Liu D, Hickey R, Krause DS, Giordano FJ. Stromal cell-derived factor-1alpha plays a critical role in stem cell recruitment to the heart after myocardial infarction but is not sufficient to induce homing in the absence of injury. Circulation 2004;110:3300-5.

[314] Dhingra S, Sharma AK, Arora RC, Slezak J, Singal PK. IL-10 attenuates TNF-alpha-induced NF kappaB pathway activation and cardiomyocyte apoptosis. Cardiovasc Res 2009;82:59-66.

[315] Takehara N, Tsutsumi Y, Tateishi K, Ogata T, Tanaka H, Ueyama T, et al. Controlled delivery of basic fibroblast growth factor promotes human cardiosphere-derived cell engraftment to enhance cardiac repair for chronic myocardial infarction. J Am Coll Cardiol 2008;52:1858-65.

[316] Choi DH, Subbiah R, Kim IH, Han DK, Park K. Dual growth factor delivery using biocompatible core-shell microcapsules for angiogenesis. Small 2013;9:3468-76.

[317] Drinnan CT, Zhang G, Alexander MA, Pulido AS, Suggs LJ. Multimodal release of transforming growth factor-beta1 and the BB isoform of platelet derived growth factor from PEGylated fibrin gels. J Control Release 2010;147:180-6.

[318] Jiang B, Akar B, Waller TM, Larson JC, Appel AA, Brey EM. Design of a composite biomaterial system for tissue engineering applications. Acta Biomater 2014;10:1177-86.

[319] Tengood JE, Kovach KM, Vescovi PE, Russell AJ, Little SR. Sequential delivery of vascular endothelial growth factor and sphingosine 1-phosphate for angiogenesis. Biomaterials 2010;31:7805-12.

[320] Zhang H, Yuan YL, Wang Z, Jiang B, Zhang CS, Wang Q, et al. Sequential, timely and controlled expression of hVEGF165 and Ang-1 effectively improves functional angiogenesis and cardiac function in vivo. Gene Ther 2013;20:893-900.

[321] Zhang G, Nakamura Y, Wang X, Hu Q, Suggs LJ, Zhang J. Controlled release of stromal cell-derived factor-1 alpha in situ increases c-kit+ cell homing to the infarcted heart. Tissue Eng 2007;13:2063-71.

[322] Awada HK, Johnson NR, Wang Y. Sequential delivery of angiogenic growth factors improves revascularization and heart function after myocardial infarction. J Control Release 2015;207:7-17.

[323] Mee R. A Comprehensive Guide to Factorial Two-Level Experimentation. New York: Springer; 2009.

[324] Wu C-F, Hamada M. Experiments : planning, analysis, and parameter design optimization. New York: Wiley; 2000.

[325] Jaynes J, Ding X, Xu H, Wong WK, Ho CM. Application of fractional factorial designs to study drug combinations. Stat Med 2013;32:307-18.

[326] Saraf A, Baggett LS, Raphael RM, Kasper FK, Mikos AG. Regulated non-viral gene delivery from coaxial electrospun fiber mesh scaffolds. J Control Release 2010;143:95-103.

[327] Garbern JC, Minami E, Stayton PS, Murry CE. Delivery of basic fibroblast growth factor with a pH-responsive, injectable hydrogel to improve angiogenesis in infarcted myocardium. Biomaterials 2011;32:2407-16.

[328] Laham RJ, Sellke FW, Edelman ER, Pearlman JD, Ware JA, Brown DL, et al. Local perivascular delivery of basic fibroblast growth factor in patients undergoing coronary bypass surgery: results of a phase I randomized, double-blind, placebo-controlled trial. Circulation 1999;100:1865-71.

[329] Yu Y, Zhang ZH, Wei SG, Chu Y, Weiss RM, Heistad DD, et al. Central gene transfer of interleukin-10 reduces hypothalamic inflammation and evidence of heart failure in rats after myocardial infarction. Circ Res 2007;101:304-12.

[330] Kanki S, Segers VF, Wu W, Kakkar R, Gannon J, Sys SU, et al. Stromal cell-derived factor-1 retention and cardioprotection for ischemic myocardium. Circ Heart Fail 2011;4:509-18.

[331] Penn MS. Importance of the SDF-1:CXCR4 axis in myocardial repair. Circ Res 2009;104:1133-5.

[332] Hammoud L, Lu X, Lei M, Feng Q. Deficiency in TIMP-3 increases cardiac rupture and mortality post-myocardial infarction via EGFR signaling: beneficial effects of cetuximab. Basic Res Cardiol 2011;106:459-71.

[333] Lavine KJ, Ornitz DM. Fibroblast growth factors and Hedgehogs: at the heart of the epicardial signaling center. Trends Genet 2008;24:33-40.

[334] Pan JY, Zhou SH. The hedgehog signaling pathway, a new therapeutic target for treatment of ischemic heart disease. Pharmazie 2012;67:475-81.

[335] Chen WC, Lee BG, Park DW, Kim K, Chu H, Kim K, et al. Controlled dual delivery of fibroblast growth factor-2 and Interleukin-10 by heparin-based coacervate synergistically enhances ischemic heart repair. Biomaterials 2015;72:138-51.

[336] Johnson NR, Wang Y. Coacervate delivery of HB-EGF accelerates healing of type 2 diabetic wounds. Wound Repair Regen 2015;23:591-600.

[337] Holladay CA, Duffy AM, Chen X, Sefton MV, O'Brien TD, Pandit AS. Recovery of cardiac function mediated by MSC and interleukin-10 plasmid functionalised scaffold. Biomaterials 2012;33:1303-14.

[338] Burchfield JS, Iwasaki M, Koyanagi M, Urbich C, Rosenthal N, Zeiher AM, et al. Interleukin-10 from transplanted bone marrow mononuclear cells contributes to cardiac protection after myocardial infarction. Circ Res 2008;103:203-11.

[339] Stumpf C, Seybold K, Petzi S, Wasmeier G, Raaz D, Yilmaz A, et al. Interleukin-10 improves left ventricular function in rats with heart failure subsequent to myocardial infarction. Eur J Heart Fail 2008;10:733-9.

[340] Hwang H, Kloner RA. The combined administration of multiple soluble factors in the repair of chronically infarcted rat myocardium. J Cardiovasc Pharmacol 2011;57:282-6.

[341] Fan D, Takawale A, Basu R, Patel V, Lee J, Kandalam V, et al. Differential role of TIMP2 and TIMP3 in cardiac hypertrophy, fibrosis, and diastolic dysfunction. Cardiovasc Res 2014.

[342] Cao R, Brakenhielm E, Pawliuk R, Wariaro D, Post MJ, Wahlberg E, et al. Angiogenic synergism, vascular stability and improvement of hind-limb ischemia by a combination of PDGF-BB and FGF-2. Nat Med 2003;9:604-13.

[343] Ahmed RP, Haider KH, Shujia J, Afzal MR, Ashraf M. Sonic Hedgehog gene delivery to the rodent heart promotes angiogenesis via iNOS/netrin-1/PKC pathway. PLoS One 2010;5:e8576.

[344] Kusano KF, Pola R, Murayama T, Curry C, Kawamoto A, Iwakura A, et al. Sonic hedgehog myocardial gene therapy: tissue repair through transient reconstitution of embryonic signaling. Nat Med 2005;11:1197-204.

[345] Pola R, Ling LE, Silver M, Corbley MJ, Kearney M, Blake Pepinsky R, et al. The morphogen Sonic hedgehog is an indirect angiogenic agent upregulating two families of angiogenic growth factors. Nat Med 2001;7:706-11.

[346] Cao R, Eriksson A, Kubo H, Alitalo K, Cao Y, Thyberg J. Comparative evaluation of FGF-2-, VEGF-A-, and VEGF-C-induced angiogenesis, lymphangiogenesis, vascular fenestrations, and permeability. Circ Res 2004;94:664-70.

[347] Karsan A, Yee E, Poirier GG, Zhou P, Craig R, Harlan JM. Fibroblast growth factor-2 inhibits endothelial cell apoptosis by Bcl-2-dependent and independent mechanisms. Am J Pathol 1997;151:1775-84.

[348] Tian H, Cimini M, Fedak PW, Altamentova S, Fazel S, Huang ML, et al. TIMP-3 deficiency accelerates cardiac remodeling after myocardial infarction. J Mol Cell Cardiol 2007;43:733-43.

[349] Hu X, Dai S, Wu WJ, Tan W, Zhu X, Mu J, et al. Stromal cell derived factor-1 alpha confers protection against myocardial ischemia/reperfusion injury: role of the cardiac stromal cell derived factor-1 alpha CXCR4 axis. Circulation 2007;116:654-63.

[350] Huang C, Gu H, Zhang W, Manukyan MC, Shou W, Wang M. SDF-1/CXCR4 mediates acute protection of cardiac function through myocardial STAT3 signaling following global ischemia/reperfusion injury. Am J Physiol Heart Circ Physiol 2011;301:H1496-505.

[351] Buerke M, Murohara T, Skurk C, Nuss C, Tomaselli K, Lefer AM. Cardioprotective effect of insulin-like growth factor I in myocardial ischemia followed by reperfusion. Proc Natl Acad Sci U S A 1995;92:8031-5.

[352] Chao W, Matsui T, Novikov MS, Tao J, Li L, Liu H, et al. Strategic advantages of insulin-like growth factor-I expression for cardioprotection. J Gene Med 2003;5:277-86.

[353] Li Q, Li B, Wang X, Leri A, Jana KP, Liu Y, et al. Overexpression of insulin-like growth factor-1 in mice protects from myocyte death after infarction, attenuating ventricular dilation, wall stress, and cardiac hypertrophy. J Clin Invest 1997;100:1991-9.

[354] Suleiman MS, Singh RJ, Stewart CE. Apoptosis and the cardiac action of insulin-like growth factor I. Pharmacol Ther 2007;114:278-94.

[355] Lee KW, Johnson NR, Gao J, Wang Y. Human progenitor cell recruitment via SDF-1alpha coacervate-laden PGS vascular grafts. Biomaterials 2013;34:9877-85.

[356] Cheng Z, Ou L, Zhou X, Li F, Jia X, Zhang Y, et al. Targeted migration of mesenchymal stem cells modified with CXCR4 gene to infarcted myocardium improves cardiac performance. Mol Ther 2008;16:571-9.

[357] Kwon JS, Kim YS, Cho AS, Cho HH, Kim JS, Hong MH, et al. Regulation of MMP/TIMP by HUVEC transplantation attenuates ventricular remodeling in response to myocardial infarction. Life Sci 2014;101:15-26.

[358] Tang J, Wang J, Song H, Huang Y, Yang J, Kong X, et al. Adenovirus-mediated stromal cell-derived factor-1 alpha gene transfer improves cardiac structure and function after experimental myocardial infarction through angiogenic and antifibrotic actions. Mol Biol Rep 2010;37:1957-69.

[359] Yan P, Chen KJ, Wu J, Sun L, Sung HW, Weisel RD, et al. The use of MMP2 antibody-conjugated cationic microbubble to target the ischemic myocardium, enhance Timp3 gene transfection and improve cardiac function. Biomaterials 2014;35:1063-73.